THE CREEP PROPERTIES OF A SERIES OF ZINC-RICH ZINC-ALUMINIUM ALLOYS

ARSHAD AHMED MIR

Doctor of Philosophy

THE UNIVERSITY OF ASTON IN BIRMINGHAM

Feburary 1998

THE UNIVERSITY OF ASTON IN BIRMINGHAM

THE CREEP PROPERTIES OF A SERIES OF ZINC-RICH ZINC-ALUMINIUM ALLOYS

ARSHAD AHMED MIR PhD 1998

THESIS SUMMARY

The compressive creep behaviour of six sand cast zinc-rich alloys: No3 and No5, corresponding to BS 1004A and BS 1004B, respectively, alloy No2, ILZRO.16 and two newer alloys ACuZinc5 and ACuZinc10 was investigated. The total creep contraction of the alloys was found to be well correlated using an empirical equation. On the basis of this equation, a parametrical relationship was derived which allowed the total creep contraction to be related to the applied stress, the temperature and the time of test, so that a quantitative assesment of compressive creep of the alloys could be made under different testing conditions. The primary creep and secondary creep rates were found for the alloys at different temperatures and stresses. Generally, the primary creep contraction was found to increase with copper content, whereas secondary creep rates decreased in the order No3, No5, ACuZinc10, ACuZinc5 and No2. ILZRO.16 was tested only at the highest stress and two higher temperatures. The results showed that ILZRO.16 had higher creep resistance than all the other alloys. Thus, based on the above empirical equation, alloy No2 was found to have a substantially better total creep resistance than alloys No3 and No5, and slightly better than ACuZinc5 and ACuZinc10 for strains up to 1%. Both ACuZinc alloys had higher creep strength than commercial alloys No3 and No5. Alloy No5 had much higher creep resistance than alloy No3 under all conditions. The superior creep resistance of alloy No2 was considered to be due to the presence of small precipitates of ε-phase in the zinc matrix and a regular eutectic morphology. The stress exponents and activation energies for creep under different testing conditions were found to be consistent with some established creep-controlling mechanisms; i.e. dislocation climb for alloy No3, dislocation climb over second phase particles for alloys No5, No2, ACuZinc5 and ACuZinc10, controlled by lattice diffusion in the zinc-rich phase. The lower creep resistance of alloy No3 was mainly due to the lower creep strength of copper-free primary η particles having greater volume than eutectic in the microstructure. Alloys No5, ACuZinc5 and ACuZinc10 showed much better creep resistance than alloy No3, based on the precipitation-hardening due to the presence of small ε-phase precipitates. The primary ε dendrites in both ACuZinc alloys however were not much beneficial in improving the creep resistance of the alloys.

The load-relaxation behaviour of all six alloys was also investigated under different conditions. The initial load loss was high, diminishing gradually with time, but not ceasing. The amount of load loss increased rapidly with test temperature, and almost all of the relaxation curves approximated to a logarithmic decay of load with time. The load-relaxation strength of the alloys was correlated by using a general load-relaxation equation. This equation was used to compute the retained loads for longer service times which showed that ILZRO.16 had the best load-relaxation strength, followed by ACuZinc10, ACuZinc5, No2 and No5 at temperatures $\geq 0.5\ T_m$. At temperatures lower than $0.5\ T_m$, both ACuZinc alloys showed less resistance than alloy No2. Activation energies for load-relaxation of the alloys were also found to be in the range of activation energies for lattice diffusion in pure zinc, indicating that the relaxation rate was being controlled by diffusion in the zinc-rich phase. The resistance to load loss generally increased with increasing copper content, particularly at higher temperatures.

Key Words: **Compressive Creep, Sand castings, Zinc-rich Alloys, Load-Relaxation.**

DEDICATION

To my parents, wife, sons Sheharyar and Haseeb and the rest of family for their support.

ACKNOWLEDGEMENTS

All praise to the Almighty, who bestowed upon me the potential and ability to make this research a reality.

I would like to express my deep heart felt feelings of appreciation and gratitude to my supervisor Dr. S. Murphy for his continuous and tireless guidance and encouragement throughout the duration of this work, without whom this research work would not have been possible. He was always available for extending his assistance and advice as and when required.

Thanks are also due to Dr. K. Sawalha, and the staff of the Mechanical and Electrical Engineering Department of Aston University, particularly D. Farmer, J. Jeffs, J. Foden, P.A. Pizer and James Duggins for their valuable assistance.

I am also grateful for the financial support of the Goverment of Pakistan during this study.

LIST OF CONTENTS

LIST OF TABLES

LIST OF FIGURES

CHAPTER 1

1.0 INTRODUCTION

The commercial zinc-based alloys No3 and No5 were the first major zinc alloys developed, and are widely used as useful engineering materials for parts or frames in industrial machinery, scientific equipment and domestic appliances. More specifically, they are used in automotive applications, mechanical components, body hardwares and trimmings, lighting fixtures and many other different applications. They have a good combination of mechanical and physical properties; particularly the relatively low melting temperatures, their ability to be cast in the highest speed die-casting machines and fluidity characteristics, which make them successful competitors against other non-ferrous alloys since their introduction. However, their low creep strength, particularly in applications subjected to moderately elevated temperatures, limits their use.

Efforts were made to develop creep-resistant alloys which might be used in the structural applications where conventional zinc alloys could not be used. This led to the development of improved creep-resistant zinc-based alloys ACuZinc5, ACuZinc10 and ILZRO.16. Along with creep, other properties of ACuZinc alloys including yield strength, ultimate tensile strength, hardness and wear resistance, which are claimed to be better than conventional zinc alloys (No3 and No5) and ZA alloys, i.e. ZA.8, ZA.12 and ZA.27.

Creep is the time-dependent strain which takes place under a given constant load or stress and temperature. Creep does not occur only at high temperatures as is often believed, but has been observed in metals down to 1.2 K. It is a unique deformation mechanism for metals and alloys, particularly at elevated temperatures because the deformation may become so large that a component can no longer perform its function. Creep tests are commonly performed by applying constant stress or load to uniaxial specimens, and creep data is obtained in the form of strain as a function of time. This creep data is used to find out creep related parameters, such as primary creep extension or contraction, the secondary creep rate, time to 1% creep strain and stress to fracture at a given time.

It is an important design requirement to find out the compressive and tensile creep of components used in commercial applications, particularly at moderately elevated

temperatures. Therefore, the important feature of this research was to determine the relative compressive creep resistances of the commercial zinc-based alloys, i.e., No3, No5 and No2, in comparison with the newer zinc-rich alloys, ACuZinc5, ACuZinc10 and ILZRO.16, and also to provide a complete characterisation of their compressive creep behaviour. Research has been carried out to determine the tensile creep strength of these zinc-based alloys in the past, but so far no attempt had been made to investigate the compressive creep behaviour of these alloys. Since compressive creep is also important in zinc alloys applications, especially when they are used in automotives where compression is common, it was therefore considered of great interest to study the compressive creep properties of these alloys in detail. A compressive creep machine was required to undertake the creep tests on these alloys. Therefore, the design and fabrication of compressive creep machine was the first critical and important part of this research work.

The other important aspect of this research is the load-relaxation experimentation of these alloys. Castings of zinc alloys are widely used for automotive components, where screwed steel fasteners are commonly used to fix castings together or mount a casting onto another structure. These fasteners are tightened to a predetermined torque to develop the required tensile preload in the fastener. If these castings are kept at above ambient temperatures, creep may produce a partial loss of the preload due to relaxation processes in the castings. Experiments were therefore carried out to determine the extent of load relaxation in zinc alloys. The main objective of these tests was to compare the load relaxation behaviour of different zinc-rich alloys under similar test conditions.

The overall aim of this research was to establish a better understanding of compressive creep and load relaxation characteristics of zinc-rich alloys in terms of their creep kinetics and metallographic structure. It will also be greatly helpful in further development and application of these zinc-based alloys.

CHAPTER 2

2.0 LITERATURE SURVEY

2.1 Creep & Stages of Creep

There are different definitions of creep in the literature.

According to Conrad[1], " Creep is the time-dependent deformation of materials which occurs under constant stress and temperature. Creep is not restricted to high temperature as is often believed but has been observed in metals down to 1.2K."

Dowling[2] defines creep in the following way:

" Creep is deformation that accumulates with time. Depending on the magnitude of the applied stress and its time of application, the deformation may become so large that a component can no longer perform its function."

Creep of metals and alloys is usually determined by a test in which a constant stress or load is applied to a specimen at a given elevated temperature, and the creep strain is measured graphically as a function of time.[3]

Figure 2.1- curve (a) shows a typical creep curve which exhibits various stages of creep.

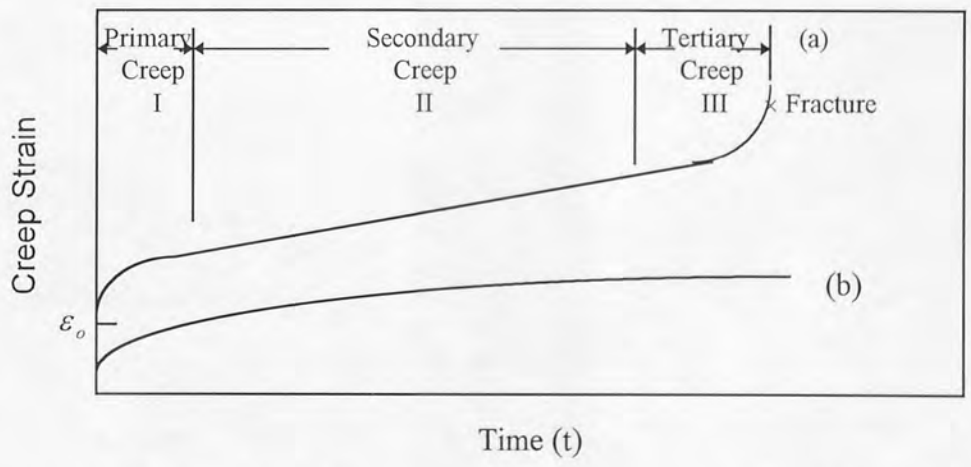

Figure 2.1. (a) Typical creep curve, showing primary, secondary and tertiary regions (b) logarithmic creep curve.

Creep involves plastic deformation, due to which the cross-sectional area of the specimen changes continuously, and it is difficult to conduct a creep test at a constant stress, the tests are therefore usually performed at a constant load.[3]

Compressive creep is similar to the tensile creep except the load or stress applied is in compression. Compressive creep is common in industrial applications, and during the study of materials, it is therefore important to investigate the effects of compressive

creep. It has been observed that the criterion of failure in compressive loading is likely to be tensile or shearing failure in all materials except the most plastic materials[4]. If the test specimen is relatively long, i.e. L/D > 3 where L is the length and D is diameter of the specimen, failure will probably occur by buckling, as shown in *Figure 2.2(a)*. If the length of test piece is small (L/D < 3), the plastic specimen will barrel *Figure 2.2(b)*. If the material of the test piece is not plastic, or if it has low shear strength, then failure may occur by shearing along a plane direction, as can be seen[4] in *Figure 2.2(c)* since the component of the associated shear stress of a uniaxial compressive stress is always half the intensity of the compressive stress. The effects of creep in compression are likely to be similar to those in tension for reasonably plastic materials except that failure is much less likely in compression creep tests. Temperature change affects the compressive properties in the similar way as it does the tensile properties except that malleability will not decrease as rapidly as ductility when the temperature is raised towards the melting temperature of the material.

Generally, there are three stages in a creep curve, in addition to a stage which is considered as preliminary: an almost instantaneous strain obtained immediately on the application of the load on the specimen.

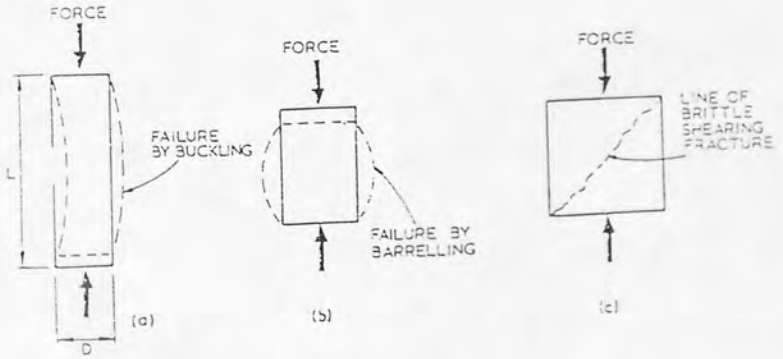

Figure 2.2. Failure modes in compression; (a) instability (b) bulging under frictional restraint (barreling) (c) brittle shearing.

The three stages of creep are:

1. **Primary Creep:** It is the creep strain that occurs at a diminishing rate until it reaches a constant rate. It is also called transient creep.

2. **Secondary or Steady-state Creep:** The creep strain that shows a minimum and almost constant rate.

3. **Tertiary Creep:** This stage in the typical creep curve occurs just prior to failure (stress rupture). It has a highly accelerated strain rate and is always present whenever stress rupture occurs. However, for many creep tests, the time available is limited and the tests are terminated before the occurrence of tertiary creep.

Generally, the creep curve of metallic alloys in compression is similar to that in tension, and has the same three characteristics, i.e. a decelerating primary stage, a secondary stage having steady-state creep rate, and a third or tertiary stage which has an accelerating rate. However, there is a major difference between compressive and tensile creep beyond the initiation of tertiary creep stage, since in the latter case, the creep rate accelerates continuously until the fracture of the specimen; whereas, in compressive creep, the creep rate generally goes through successive stages of acceleration and deceleration, and fracture does not occur.[5] Sully[5] observed two main differences between the results of compression and tensile creep tests. Firstly, the initial or primary creep extension was larger in the compression test than in the tension test. Secondly, the creep results from relatively brittle materials have shown that these materials may initiate failure under axial tensile load due to the presence of stress concentrations, such as casting defects and grinding cracks, etc. On the other hand, these defects have relatively little effect on the materials which are under compressive stress, and therefore the compression creep test is a better measure of the intrinsic creep resistance of these materials.

Creep curves of a wide variety of forms are obtained from the creep tests, but they all include the essential stages of the typical (idealised) creep curve. It is believed that the shape of the creep curve always depends on the stress (load) applied or temperature level, e.g. the creep curve may consist of only two stages at very low stresses for a fixed temperature. At low stresses, Stage2 (secondary or steady-state creep) with almost constant creep rate, lasts for a very long time and neither failure nor tertiary stage with accelerated creep rate may occur at all. It is also shown that the secondary creep rate is very small at low stresses.[6] Contrary behaviour occurs at higher stresses, where failure occurs after a short period of time. In this case, steady-state creep may be non-existent, or of very short duration because the tertiary creep or failure may be observed almost immediately after the primary creep.[6] Another important characteristic of creep

phenomenon is that the longer the creep test, the smaller the total creep extension that is obtained.[7]

2.2 The Creep Diagram & The Main Types of Creep

The creep diagram is a temperature-stress graph which shows the types of creep in its different regions. *Figure 2.3* shows such a creep diagram.[8]

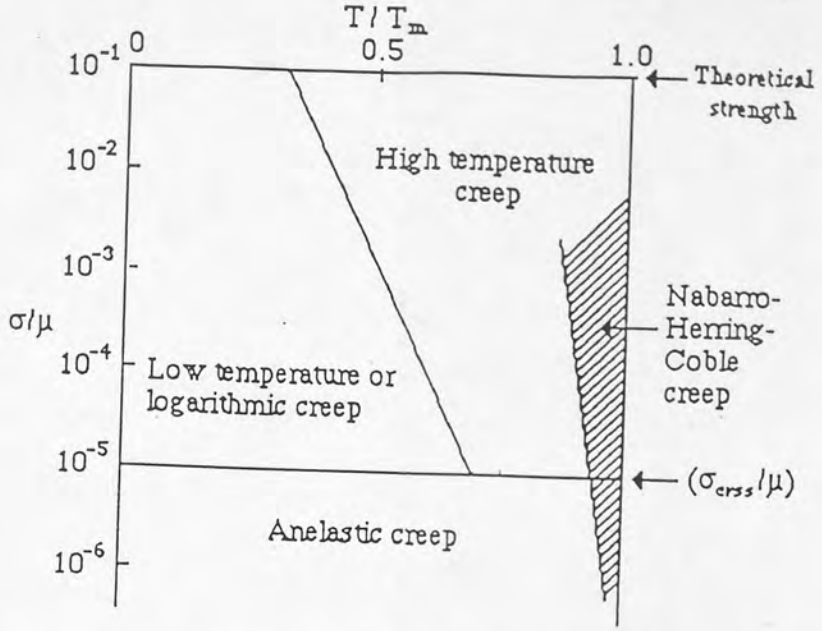

Figure 2.3. The creep diagram: the conditions of temperature and stress which produce the main types of creep.[8]

There are three main types of creep which can be observed during creep tests. These types depend on the applied stress and the test temperature. In the creep diagram, the temperature and stress have been plotted as T/T_m and σ/μ, where T_m is the melting point of metal, σ the applied stress, T the test temperature and μ is the shear modulus instead of simply as T and σ, so that a metal of low melting point or low elastic modulus can be treated equally with a metal of high melting point or high elastic modulus. When temperature and stress are normalised by dividing by T_m and μ, it is observed that different types of creep fall roughly in the same regions on the creep diagram, even though the metals and alloys tested for creep differ widely in their melting points and elastic constants.

The upper limit of the diagram is the theoretical shear stress which represents the stress required to lift planes of atoms in the crystal bodily over neighbouring planes and produce permanent deformation.[9] The bottom limit of the diagram is set by the critical resolved shear stress (σ_{crss}). There is extensive motion of dislocations and dislocation

multiplication for stresses above σ_{crss} but below this stress, the amounts of dislocation and multiplication are slight, and therefore, little plastic deformation takes place. A great amount of plastic deformation occurs only if the critical resolved shear stress σ_{crss} is exceeded.[8]

2.2.1 Logarithmic or Low-Temperature Creep

If a sample is deformed by a stress which is more than the critical resolved shear stress and the test temperature is relatively low, i.e. below about 0.5 of the absolute melting temperature of metal, it will be difficult for edge dislocations to move perpendicular to their slip planes. The applied stress causes deformation by producing dislocation multiplication and moving dislocations over long distances. Recovery does not take place due to lack of thermal activation at low temperatures and causes unrelieved work hardening, which makes motion of dislocations on slip planes more difficult, and eventually causes the dislocation multiplication to stop, and reduces the creep rate almost to zero.[10] Since diffusion is slow at low temperatures, therefore, the motion of dislocations in directions other than parallel to their slip planes is also slow.

It can be predicted that creep, which is of a transient nature, occurs in the low-temperature region of the creep diagram. In this region of the creep diagram, thermal stress fluctuations help in the process of deformation and therefore creep strain is produced. However, with the increase of deformation, the stress fluctuations also increase the hardening of the sample. As a result, the more a sample is deformed, its further deformation becomes more difficult. Therefore, the rate of creep deformation decreases with increasing time[3] and contribution of low-temperature creep to total creep strain is also comparatively small. This type of creep is called low-temperature creep or logarithmic creep *(Figure 2.1 - curve(b)* because the strain depends logarithmically on time.

It has been proved experimentally[8] that low-temperature creep is of a transient nature because the creep rate decreases to zero as the inverse of the time. The creep equation determined from measurements at low temperatures is given by:[8]

$$\varepsilon = \varepsilon_e + \varepsilon_p + \varepsilon_o \log (1 + \nu t) \qquad (2.1)$$

This equation gives the creep rate as:

$$\dot{\varepsilon} = \frac{\varepsilon_o \nu}{1 + \nu t} \qquad (2.2)$$

where, ε_e is the elastic strain, ε_p the instantaneous plastic strain, and ε_o and ν are constants which depend on stress and the test temperature.

Logarithmic creep has been observed in polycrystalline aluminium and copper below 200K, some hexagonal metals at low temperatures, and some other materials such as rubber and glass.[11]

Some form of transient creep always occurs at all temperatures but it is not necessary to obey the logarithmic law.[11] Since with decreasing temperature, activated processes also become slower, therefore, during a creep test at lower temperature, a smaller activation rate is measured.

2.2.2 High-Temperature Creep

Creep is considered principally a high-temperature phenomenon in most engineering materials. It is recognised that the melting point of the alloy or metal under creep test is important and the temperature at which creep becomes significant, is related to the melting point.[12]

Creep deformation can be observed at low temperatures but it is not very important for all practical purposes when test temperature is between zero and $0.3T_m$, where T_m is the melting point of the material in degrees Kelvin. On the other hand, when the test temperature is raised above $0.3T_m$ (according to some researchers $0.4T_m$[10] or $0.5T_m$[13]), creep deformation becomes significant.[12] At high temperatures, the dislocations acquire a new degree of freedom. The dislocations can climb as well as glide and they are no longer restricted to move only in their original slip planes.[14] Since slip occurs on new slip planes, the rate of work hardening is reduced.[10]

Ahmadieh and Mukherjee[15] derived the following equation for high-temperature diffusion-controlled transient creep:

$$\varepsilon = \varepsilon_o + \dot{\varepsilon}_s t + (\beta - 1) \Big/ K[1 - \exp(-K \dot{\varepsilon}_s t)] \qquad (2.3)$$

where ε_o is the instantaneous strain on loading, $\dot{\varepsilon}_s$ the secondary creep rate, $K\dot{\varepsilon}_s$ the rate constant, and β is the ratio of initial to secondary creep rates. The experimental

creep data on stainless steel, Al, Ag, Cu, Pt, low carbon Ni, Mo, plain carbon steel, and W were found to correlate well with the proposed creep equation.[15]

2.3 Creep Mechanisms at High Temperature

The secondary or steady-state creep stage is the most important of all the three creep stages, and the mechanisms or theories of high-temperature creep are therefore concerned primarily with the steady-state part of the creep-curve.

2.3.1 Dislocation Creep Mechanisms

At high temperatures, dislocations attain a new degree of freedom. At this temperature, they can climb as well as glide and are therefore no longer constrained to move only in their slip planes. Mechanisms which are based on this climb-plus-glide sequence are called climb-controlled or recovery-controlled creep. The main difference of these mechanisms from those of plastic flow at lower temperatures (which may also be thermally-activated) is the rate-controlling process[14], because in climb-controlled mechanisms, the creep rate is controlled by the diffusion of vacancies between dislocations[8] instead of the activated glide of the dislocation itself at lower temperatures. Therefore, vacancies also play an important part in the climb motion of edge dislocations and mixed dislocations.

2.3.1.1 Climb-Controlled Glide Model

The dislocation-climb theory for steady-state creep was first proposed by Weertman[16] in 1955. The theory was based on the climb of edge dislocations. In his first attempt to develop dislocation-climb theory, Weertman used Mott's mechanism of dislocation - climb.[17] This theory was a major advancement in the rationalisation of the mechanical behaviour of metals at high temperatures[18], however, it was limited only to pure metals or simple alloys.[16]

According to this theory, the rate-controlling process during steady-state creep is the diffusion of vacancies between dislocations which create vacancies and those which destroy them. The proposed creep equation is:[16]

$$\text{Creep rate} = \text{const}\,(\sigma^{\alpha} / kT) \exp(-Q / kT) \qquad (2.4)$$

where σ is the applied stress, α a constant (α = 3 to 4), k Boltzmann's Constant, T the absolute temperature and Q is the activation energy of self-diffusion. This process

usually exhibits an activation energy equal to that for lattice self-diffusion (Q_d) at temperatures above $0.5T_m$, but there are number of cases where values of activation energy for creep (Q_c) of ~ $0.5\text{-}0.6Q_d$ have been observed over a limited range of temperature below $0.65T_m$.[19]

This equation is valid only from the critical shear stress to a stress which is equal to 0.1 to 1.0 N/m^2 (10^8 to 10^9 dynes/cm^2) in the stress range of creep diagram. It has been observed that at higher stresses, the creep rate increases much more rapidly with stress.[16]

Later, Weertman[20] proposed another dislocation-climb model for steady-state creep which was slightly different from the first model. According to this second model, the production of immobile dislocations was not required.

In both models, the relation between creep rate and stress can be expressed by power laws. However, for polycrystals, the first model gives a power of 3 and the second model a power of 4.5. But later, it was revealed that only the second model was in reasonable agreement with experimental results.[20,21] Weertman considered a case where dislocation loops were emitted from fixed and more or less uniformly distributed sources and were confined to their glide planes. The leading dislocations were eventually arrested at obstacles and, after a sufficient number of dislocation loops had been emitted, the back stress (elastic in nature) prevented further source operation.[22] For a constant stress, this situation would rapidly lead to a discontinuation of dislocation motion and therefore, of deformation. However, the leading dislocations of the pile-ups would continue to climb and annihilate. After the annihilation, a new dislocation loop might be emitted from the source[21] and therefore, creep would continue. On this basis, Weertman expressed the creep rate ($\dot{\varepsilon}$) by the following equation:[23]

$$\dot{\varepsilon} = \frac{3\pi^2\sigma^2 D}{2\sqrt{2}\mu^2 b^2} Sinh\left(\frac{\sqrt{3}\sigma^{2.5} b^{1.5}}{8\mu^{1.5}\sqrt{M}kT}\right) \qquad (2.5)$$

where σ is the measured stress, b the length of the Burgers vector, D the self-diffusion coefficient, $D = D_A D_B / D_A C_B + D_B C_A$, where C_A and C_B are the fractional concentrations of the alloy species and D_A and D_B are their diffusion constants, μ the shear modulus, M the density of Frank-Read sources on one slip system, k Boltzmann's

constant and T is the absolute temperature. This equation reduces to the power law equation at low stresses:[23]

$$\dot{\varepsilon} = \frac{3\sqrt{6}\pi^2\sigma^{4.5}D}{2^5\sqrt{b}\sqrt{M}\mu^{3.5}kT} \qquad (2.6)$$

This equation predicts a stress exponent of 4.5. The model has been proved experimentally and is valid for various alloy systems.[23] The main characteristic of this model is that it correlates quite well with most of the mechanical data on high-temperature creep[18] and therefore, considered as one of the major mechanisms which operate at high temperatures. However, the stress exponent (n) depends on the content of alloys over the stress levels where the power law is valid. The results show that the value of the exponent decreases from 4.5 for pure metals towards close to 3 by increasing the alloy content.[23] The same trend was also reported for many solid solution alloys due to the increase of stress.[24]

This suggests that there is a transition in creep behaviour from climb-control at low stresses to control by viscous glide at high-stress levels.[24]

2.3.1.2 Viscous Glide Model

During the process of dislocation-climb, it has been experienced that dislocations glide and climb alternately. Since dislocation-climb and viscous-glide are two sequential processes, the measured steady-state creep rate is controlled by the slower process.[24] This has led to the development of a model based on viscous glide, which applies only to solid solution alloys[25], and the deformation is governed by one of the micro-creep mechanisms proposed by Weertman. This mechanism suggests that there is the possibility of a transition to control by viscous glide as the stress is increased. An experimental work[26] on creep of Al - 3 % Mg alloy has revealed that there is a sharp transition from control by dislocation-climb to control by viscous-glide as the stress is increased beyond 1.2×10^{-4} G [24], where G is the shear modulus.

Nam et al[27] have studied the transition creep behaviour of Al-3 % Mg solid solution alloy at 573K (0.62 T_m). According to their investigation, the transition stress of the stress exponent can be a function of grain size.

According to the viscous-glide mechanism, the creep rate is given by the following equation:[23]

$$\dot{\varepsilon} = \frac{0.35\sigma^3}{\mu^2 A^2} \qquad (2.7)$$

where A is a constant which depends upon the solute-dislocation interaction that is viscously retarding dislocation glide[9], and it can be evaluated from the particular micro-creep mechanism.

Jones and Sellars[28] also derived an expression for creep rate based on viscous-glide of dislocations which is given below:

$$\dot{\varepsilon} = \frac{0.06\sigma^3}{G^2 A} \qquad (2.8)$$

2.3.1.3 Dislocation-Jog Model

A jog is defined as a point where a dislocation jumps from one plane to another. The jogs on a screw dislocation are always edge jogs. If the screw dislocation is forced to move, it is observed that jogs can not maintain their positions in the dislocation by glide in their own slip planes, and it is possible only by climb of the jogs.

There are two types of jogs:[21]

(i) Vacancy-emitting jogs, and

(ii) Vacancy-absorbing jogs.

The jog-dragging process and the climb-controlled process are considered as two quite different concepts of creep mechanism.[22] The dislocation-jog model is also considered a high-temperature steady-state creep mechanism[29,30], where the jog-dragging-screw dislocations control the creep rate.[31] The jogs on dislocations will be saturated with vacancies, whereas the rate of emission and absorption of vacancies will fix the rate of movement of the dislocations, and this in turn, will depend on the rate of vacancy diffusion.[22] Therefore, there are two regimes of creep; (i) when the jog density is less than the density of vacancies (except at very high stresses), and in this case, the creep rate is controlled by vacancy self-diffusion, and (ii) when the jog density is greater than the density of vacancies where the creep rate is controlled by interstitial self-diffusion.[32]

For dislocation-jog mechanism, the secondary creep rate is given by[29]:

$$\dot{\varepsilon}_s = 2\pi\rho_s D\alpha\left(\frac{b}{a_o}\right)^3 Sinh\left(\frac{\sigma b^2 \lambda}{2kT}\right) \qquad (2.9)$$

where ρ_s is the mobile screw dislocation density, D the self-diffusion coefficient, α the number of atoms in a cell, b the Burgers vector, a_o the lattice parameter, λ the average spacing between jogs and k is Boltzmann's constant.

Assuming that the number of both types of jog (vacancy-emitting and vacancy-absorbing) are equal, the creep rate is given by the following expression[21]:

$$\dot{\varepsilon} = BD_s \rho Sinh \frac{\sigma b^2 l}{kT} \qquad (2.10)$$

where ρ is the density of the mobile dislocations, l is the distance between the jogs and the numerical constant B ~ 20.

2.3.1.4 Recovery-Creep Model

The recovery-creep model was first proposed by Bailey[33] and later by Orowan.[34] The model was subsequently elaborated by other researchers.[35] The earlier models of recovery creep did not describe details of the deformation process, but the more recent formulations by McLean[36] and Lagneborg[37,38] have considered the recovery mechanism in some detail.

McLean formulated the recovery-creep process quantitatively by means of the classical expression:[36]

$$\dot{\varepsilon} = \dot{\varepsilon}_o \exp\left[-\frac{bA(h\varepsilon - rt)}{kT}\right] \qquad (2.11)$$

where ε_o is the initial creep rate, b the Burgers vector, A the activation area, h the strain-hardening coefficient, r the recovery rate and t is the time.

The refined recovery-creep model based upon the earlier theories of recovery-creep, proposed by Lagneborg[37], takes into account the variation in strain-hardening and the recovery with dislocation density, which the simple recovery-creep models do not consider. This refined model provides an improved description of the strain versus time relation in the primary and secondary stages, gives information regarding the dislocation density versus time variation and also the constant dislocation density that is reached in the secondary stage of creep.

According to this refined model[37], the steady-state creep rate is given by:

$$\dot{\varepsilon}_s = \frac{2M\tau\rho_s^{\,2}}{C} \qquad (2.12)$$

where M is the mobility of climbing dislocations, τ the dislocation-line tension, ρ_s the steady-state dislocation density and C is a constant which relates ε and ρ.

Lagneborg[38] formulated another modified recovery-creep model. It describes the time- and stress-dependence of the creep rate in the primary and secondary stages. According to this modified model, the secondary creep rate is given by:[38]

$$\dot{\varepsilon}_s \sim 2b\bar{l}M\tau\left(\frac{\sigma}{\alpha Gb}\right)^4 \qquad (2.13)$$

where $\bar{l}$ is mean free path of dislocation motion and M is the mobility of climbing dislocations.

This expression is in close agreement with empirical laws.

2.3.1.5 Nabarro-Herring-Coble Creep

Nabarro-Herring-Coble Creep is a special kind of steady-state creep which can occur at high temperature in specimens of very small size or of very fine grain material[8]. This type of creep occurs at stress levels which are too low for dislocation processes to be significant. Nabarro-Herring-Coble Creep can be observed in the Creep Diagram[8] *(Figure 2.3)*.

Creep can occur at high temperature when an appreciable number of vacancies are transported from one side of a grain to another under stress for a specimen of fine-grained structure. The mass transport of atoms and vacancies has been indicated in *Figure 2.4a*. The stress-directed flow of atoms and vacancies changes the shape of the grain which becomes longer in the tensile direction *(Figure 2.4b)*. This type of creep was first proposed by Nabarro[39], and subsequently Herring[40] developed an analysis from which the creep rate produced by this mechanism, can be calculated. The Nabarro-Herring creep is perhaps the best understood of all creep theories.

The original theory developed by Nabarro and Herring considered that diffusion occurs only through the crystal lattice, however, material can also be transferred along grain-boundaries.[22] Grain-boundaries can accommodate or release atoms or, in other words,

generate or annihilate vacancies. It has been observed that the energy required to form a vacancy at the top or bottom surface of the grain *(Figure 2.4a)* is different from the energy needed to form a vacancy at a side surface if a tensile stress is applied to the grain vertically. When there is a net flow of vacancies in one direction, an equal net flow of atoms occurs in the opposite direction. Therefore, atoms are removed from the side faces of the grain and transferred to the top and bottom faces. As a result, the grain changes its dimensions, as shown in *Figure 2.4b.*[8]

For diffusion creep, if the rate-controlling step is the diffusion over distances of the order of the grain size (d), while the applied stress (σ) is the driving force, then, according to Nabarro and Herring[39,40], the creep rate is given by the following expression:

$$\dot{\varepsilon} = \frac{\alpha_v \sigma \Omega D_v}{kTd^2} \qquad (2.14)$$

where Ω is the atomic volume, D_v the diffusion coefficient in the grains, k Boltzmann's constant and α_v is a dimensionless numerical factor (constant), the magnitude of which depends on the grain geometry, but it is usually of the order of ten.[19] In a uniaxial tensile or compressive test, α is about five.[31] In contrast to dislocation creep, Nabarro - Herring creep varies with stress linearly and occurs at $T \approx 0.8\ T_m$.[11]

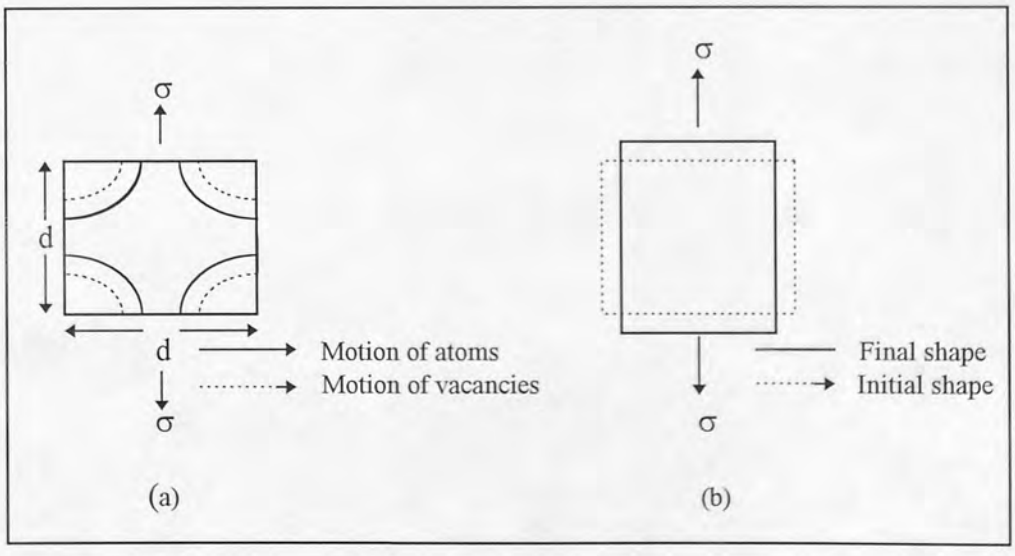

Figure 2.4. Nabarro-Herring creep. (a) Mass motion of atoms and vacancies across a small grain of dimension d under an applied stress. (b) Change in shape of a grain under the mass motion shown in (a).

According to Nabarro and Herring theory, diffusion occurs only through the crystal lattice. However, Coble[41] revealed that the diffusion path was not only confined to the interior of a grain and could occur along grain-boundaries. The temperature range over which vacancy-diffusion creep is significant may be extended to much lower temperature, i.e. $T \approx 0.5\ T_m$, if the vacancies flow down the grain-boundaries instead of the grains. In this case, the creep rate is also proportional to stress, but inversely proportional to the cube of the grain size, and is given by:[41]

$$\dot{\varepsilon} = \frac{\alpha_{gb}\sigma\Omega\delta D_{gb}}{kTd^3} \qquad (2.15)$$

where $\dot{\varepsilon}$ is Coble or grain-boundary diffusion creep, D_{gb} the grain-boundary self-diffusion coefficient, α_{gb} a constant which has a value of around forty[41] and δ is the effective thickness of a grain-boundary.

If temperature (≈ 0.5 to $0.6\ T_m$) and stresses are low, diffusion creep (lattice or along grain-boundaries) becomes a significant mechanism of creep in a number of high-technology operations, e.g. it has been observed in magnesium-based canning materials used in gas-cooled reactors.[11]

Later, Burton and Greenwood[42] analysed the creep rate by the stress-directed diffusion of vacancies along surfaces or grain boundaries of crystals having cylindrical and cubic shape, by using the Coble mechanism.

The formulae derived for the creep rates are as follows:

(a) for an axially stressed cylinder:

$$\dot{\varepsilon} = 64D_g\omega\sigma\Omega/kTLD^2[1+(4L/3D)] \qquad (2.16)$$

where T is temperature, L the length of cylinder, D the diameter, D_g the coefficient of self-diffusion, ω the grain boundary width, Ω the atomic volume, and k is Boltzmann's constant.

(b) for a cube uniaxially stressed perpendicular to a pair of faces:

$$\dot{\varepsilon} = 16D_g\omega\sigma\Omega/kTL^3 \qquad (2.17)$$

2.4 Grain Boundary Sliding

If the test temperature of creep is raised approximately to $0.5T_m$, significant sliding is observed along the grain boundaries. At this temperature, the grain boundaries are considered as a source of weakness rather than strength.[43]

Grain boundary sliding was studied by a number of investigators. The study of grain boundary sliding in aluminium by Hanson and Wheeler[44] from the early work on this subject is considered especially important because it paved the way for the later research. They investigated the movement of grain boundaries in polycrystalline aluminium which was strained slowly at 250°C. The sliding is generally limited to the immediate vicinity of the grain boundary for small displacements in bicrystals. However, when creep strain is increased, the width of sliding zone increases with time.

According to McLean and Farmer[45], the grain boundary displacement is directly proportional to the total elongation of the specimen during the creep test. To estimate the contribution of the grain boundary sliding to the total strain during creep, scratch mark experiments are usually used.[46]

The proportionality between grain boundary displacement and total creep strain gives a constant[43], i.e. $\varepsilon_{gb} / \varepsilon_t = \text{constant}$ (2.18)

where ε_{gb} = Grain boundary displacement,

and ε_t = Total creep strain

The ratio $\varepsilon_{gb}/\varepsilon_t$ increases if temperature is increased and stress is decreased. However, below a critical stress, the ratio decreases if stress is further decreased.[43]

Fazan et al[47] found that $\varepsilon_{gb}/\varepsilon_t$ remained constant and independent of temperature for a constant stress. It was observed that for alloys, this ratio increased with decrease in stress more rapidly than for the pure metals, which meant that at lower stresses, alloys had greater values of $\varepsilon_{gb}/\varepsilon_t$.

According to Gibbs[48], the total tensile strain of a polycrystalline aggregate is equal to the mean strain of individual grains in the aggregate, i.e. $\varepsilon_t = \varepsilon_{gb}$, provided the number of grains per unit length is unchanged.

The contribution of grain boundary sliding to the total strain is shown in *Table 2.1*[49,50] for zinc alloys and some other materials.

Since different procedures were used to calculate the results, it was therefore difficult to make direct comparison of results, but the general trend was the same in every test, i.e. the contribution of grain boundary sliding to the total strain observed was maximum in region II (superplasticity) and decreased at both high (region III) and low (region I) strain rate values.[49]

It was observed by Valiev and Kaibyshev[51] that the amount of grain boundary sliding (GBS) was strongly dependent on the angle between the axis of the creep specimen and the sliding boundary trace on the surface. It was noted that in region I, sliding was mainly at the transverse boundaries, whereas in the other two regions (region II and III), the largest amount of sliding was observed at boundaries situated at 45° to the axis of the specimen. In all three regions, the boundaries which showed the highest sliding, were also the most active in boundary migration.

Table 2.1 : Contribution of Grain Boundary Sliding to the Total Axial Strain.

	$\varepsilon_{gb}/\varepsilon_t$ (%)			
Material	**Region I**	**Region II**	**Region III**	**Ref.**
Zn-22% Al	30	60	30	49
Pb-Tl		50	33	"
Mg-Al eutectic	12	64	29	"
Pb-Sn eutectic		70		"
Pb-Sn eutectic	21	56	20	"
Mg-1.5% Mn-0.3% C	33	41-49	30	"
Al-9% Zn-1.0% Mg		63	26	"
Zn-0.4% Al	42	48	28	"
Zn-22% Al	10 ±5	11 ± 5	6 ± 3	50

2.5 Correlation of Creep Data

When creep tests are performed to find out how some parameters, such as time needed to produce a certain creep strain, vary with stress and temperature for any material, a simple graphical representation of a creep curve is adequate. However, for many practical and theoretical purposes, a simple graphical representation of a creep curve does not fulfil the requirements, and it is often desirable to develop equations which show the strain accumulation with time. In this way, graphical representation can be replaced by analytical procedures which allow the creep curves to be presented in terms

of a set of parameters. Other equations can also then be formulated which describe how these parameters vary with temperature, stress or material details. Therefore, the creep characteristics of a material can be expressed in terms of one or more constitutive equations which relate stress-strain-time and temperature.

2.5.1 Stress-Dependence of Secondary Creep Rate

The influence of stress on the creep rate is an important experimental variable. The secondary creep rate of a polycrystalline material may vary over a wide range of stress. The possible rate controlling processes and the variables that control the creep rate are usually considered significant in the following stress ranges.

(i) Low Stress Creep Range:

The relation between the steady-state creep rate and stress is usually linear at very low stresses[39,52], and is given as follows:[53]

$$\dot{\varepsilon}_s = K\sigma \qquad (2.19)$$

where K is a constant and σ is the applied stress.

It is generally believed that creep in this stress range is due to a process of stress-directed diffusion (Nabarro-Herring-Coble Creep)[39,41], and not due to dislocation motion.

(ii) Intermediate Stress Creep Range:

In a range of intermediate stresses, the stress dependence of secondary creep rate is usually described using the following power law equation:[21]

$$\dot{\varepsilon}_s = A\sigma^n \qquad (2.20)$$

where A is a constant and n is the stress exponent. Both A and n are independent of stress within the region considered but A, and to some extent n, depends on the test temperature[13], though in some cases it is not sensitive to the testing temperature, e.g. for arc-melted tungsten-3.6 w/o rhenium-0.33 w/o zirconium carbide at high temperatures of 1900-2400 K.[54] It has been found that the value of n ranges from 1 to 7 for annealed metals and alloys and does not seem to depend on crystal structure of the material.[55-57] Depending on the material and test conditions, generally, the stress exponent (n) ranges between 4 and 6 for pure metals and between 2 and 4 for alloys[15], but there are some exceptions to these ranges, e.g. for γ-Fe, n = 1 at 1360°C[58], and for

Pb, n lies between two and four.[16] Some iron-aluminium alloys also show values of n ranging between 4.6 and 6.8.[59]

At intermediate stresses, the creep behaviour of solid solution alloys depends upon several factors, which include the solute concentration, the solute-solvent size difference and the test temperature.[60]

For metals, the variations in n appear to have no systematic relationship with crystal structure[18,24], stacking-fault energy, grain size or any other known factor.

2.5.2 Temperature-Dependence of Secondary Creep Rate

Experimental results show that creep is a thermally activated process, and normally the temperature sensitivity of the creep rate is presented in terms of an Arrhenius-type equation with a characteristic activation energy (Q_c), which is considered as the rate controlling mechanism:[21,53]

$$\dot{\varepsilon}_s = K \exp(-Q_c / RT) \qquad (2.21)$$

where K is a constant for a given creep stress and creep strain, and may be slightly dependent on temperature. The exponential factor shows the rate at which a controlling mechanism allows the process to carry on, where Q_c is the activation energy for creep. R is the universal gas constant and T is the test temperature in Kelvin.

It has been proved experimentally that the activation energy for creep is often independent of strain.[61-65] Under some test conditions, Q_c is found to be a function of temperature and stress.[21,63] For temperatures above ~ 0.5 T_m[8,21,53], the activation energy for creep does not change with temperature and stress and closely approaches the activation energy for self diffusion. e.g. the activation energy for creep of aluminium has been found to be nearly equal to the activation energy (Q_d = 34 kcal/mol) for self-diffusion.[53] Therefore, it is believed that the most likely mechanism of creep in that region may be dislocation climb[20] or nonconservative motion of jogs in screw dislocations.[29] However, it has been shown by Poirier[66] that the region where activation energies for creep and self diffusion coincide is limited, which usually starts only about 0.6 or 0.7 T_m and does not always extend to the melting point of the material. To prove his point, Poirier made a detailed re-examination of all published data of creep for five pure metals. It was observed that the results of four metals showed that the values of Q_c and Q_d were not similar above 0.5 T_m.[66]

At lower temperatures, the activation energy decreases when temperature is decreased.[21] Between 0.3 and 0.4 T_m (Range II in *Figure. 2.5*), the activation energy for creep is normally less than that for self diffusion, and the rate controlling process of creep is believed to be associated with cross-slip of screw dislocations.[67] Below range II, the activation energy for creep decreases almost linearly with temperature decrease and the mechanism of creep in this range is due to dislocation intersection processes.[68] If both stress and temperature are considered as major factors which influence the creep rate, especially at low temperatures, then both stress and temperature dependence terms can be incorporated in one equation for secondary creep rate, as given below:

$$\dot{\varepsilon}_s = C \sigma^n \exp(-Q_c / RT) \qquad (2.22)$$

or

$$\dot{\varepsilon}_s = C'(\mathrm{Sinh}\, \alpha\sigma)^n \exp(-Q_c / RT) \qquad (2.23)$$

From the results of creep tests, the activation energy for creep can be determined from a plot of $\ln \dot{\varepsilon}_s$ versus 1/T for a constant secondary creep rate.

2.5.3 Time-Dependence of Creep Strain

The time-dependence of the creep strain in the primary and secondary stages is based on Andrade's $(\text{time})^{1/3}$ law.[13,21,69] This equation is given as follows:[13]

$$\varepsilon = \varepsilon_o + \beta t^m + \dot{\varepsilon}_s\, t \qquad (2.24)$$

where ε_o is the instantaneous strain, β and m are constants independent of time, t the time, and $\dot{\varepsilon}_s$ is the secondary creep rate.

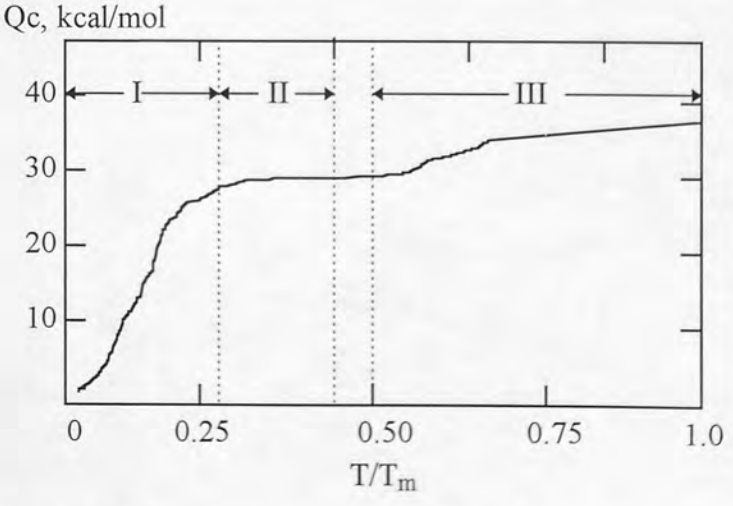

Figure 2.5. Activation energy for creep of pure polycrystalline aluminium as a function of temperature.[21]

For many metals and alloys, the value of m has been found in the range of 0.03 to nearly 1.0, and it depends on both temperature and stress.[13] Within certain limits, this relation satisfies experimental results obtained on a large number of metals and alloys (with fcc, bcc, hcp structures) and ceramic oxides.[70]

Brinson and Argent[71], and Davies et al[72] have shown the agreement with this relation *(Equation 2.24)* of creep strain and time. However, this expression has been found to predict an infinite initial creep rate and it can not produce a true steady-state.[21,64] To overcome these deficiencies of creep-time relationship, the following exponential expression is used which was found adequate over wide ranges of deformation.[13,64]

$$\varepsilon = \varepsilon_o + \varepsilon_t(1 - e^{-rt}) + \dot{\varepsilon}_s \, t \qquad (2.25)$$

where ε_o is the strain observed upon loading, ε_t the limiting transient strain during the primary stage of creep, and r is the ratio of transient creep rate to the transient creep strain. The initial creep rate is given by $r\,\varepsilon_t + \dot{\varepsilon}_s$.

Equation 2.25 has been used successfully in describing the time dependence of creep strain for ferritic and stainless steel within the temperature range of 0.4 to 0.6 T_m[13], and many other metals and alloys. Although the relation gives an adequate description for most of the creep life, a general deviation over the first 10-15% of the primary creep also occurs, due to which the actual creep rates are larger than those predicted.[73-75]

An important finding of these investigations was that the initial creep rate, the duration and shape of the primary stage and the steady-state creep rate, all showed the same stress-dependence which suggested that the mechanism controlling the creep rate was the same throughout the primary and secondary stages.[73,75] When the test temperatures are close to the melting point of the material, the creep curves become essentially linear at low stresses and this has been found to be the case for Al, Au, Cu and δ-Fe at 0.96 to 0.99 T_m. In these cases, primary creep does not exist and the creep curve is described by the following relation: [13]

$$\varepsilon = \varepsilon_o + \dot{\varepsilon}_s \, t \qquad (2.26)$$

Evans et al [76-78] have recently proposed a new creep life prediction method, i.e. the θ - projection concept, in order to quantify the changes in the creep curve shape with stress

and temperature. This concept envisages normal creep curves as the sum of a decreasing primary and an accelerating tertiary region, whereas a steady-state does not exist. There is also an increase in creep strain with time which may be described by the following expression: [76]

$$\varepsilon_c = \theta_1\left(1 - e^{-\theta_2 t}\right) + \theta_3\left(e^{\theta_4 t} - 1\right) \qquad (2.27)$$

where θ_1 and θ_3 are scaling terms defining the extent of the primary and tertiary stage of creep with respect to strain, and θ_2 and θ_4 are rate parameters which govern the curvatures of the primary and tertiary components, respectively.

Equation (2.27) presents the creep curve as an addition of decelerating and accelerating exponential functions of time in which θ plays the important role of governing the shape of the creep curve.

Since by using different θ relationships, the minimum creep rate can be calculated for any stress and temperature, it is therefore very easy to compute the values of n and Q_c for a wide range of stress and temperature. It has been observed during θ analysis for copper that both n and Q_c decrease gradually with decreasing stress and temperature[78], which quantifies the dependence of creep curve shape on stress and temperature.

Although it has been claimed that θ - projection concept offers numerous theoretical and practical advantages, it can only be used to describe the creep curves under a constant stress[76], and at present only a few reports are available to confirm the applicability and validity of the concept.

2.6 Experimental Zinc-based Zn-Al Alloys

A total of six zinc-rich Zn-Al alloys were used for compressive creep and load-relaxation experiments, which include alloys No3, No5, No2, ILZRO.16 and two recently developed[79,80] ACuZinc alloys, i.e. ACuZinc5 and ACuZinc10.

2.6.1 The Background and General Properties of Zn-Al Alloys

Zinc-rich alloys were first developed and utilised in some pressure die-castings as a substitute for tin and lead alloys because tin was expensive and lead had low strength.[81] One of the earliest zinc-rich alloys developed for use had 5% Cu, 6% Sn, 0.5% Al and the balance zinc.[81] Although the early die-castings of zinc alloys seemed satisfactory, it

was observed that in many cases rapid deterioration set in after a few months of service and results were not according to the expectations. It was found that these problems were mostly due to intercrystalline corrosion in these alloys because of some impurities such as lead, tin and cadmium; but the overageing was due to the high copper content.[81,82]

With the advancement in casting technology and availability of high-purity zinc (99.99%), the New Jersey Zinc Company introduced two pressure die-casting zinc alloys, i.e. Zamak 3 and 5 (known as Mazak 3 and 5 in the United Kingdom)[1] between 1930-40.[82] Both alloys can be used to produce widely-used engineering materials having reliable properties, when properly alloyed, cast and applied. These alloys have a unique combination of properties which allows the rapid, economic casting of strong, accurate and durable parts and hence, have dominated the market since their introduction.

The zinc-based alloys have many advantages over other non-ferrous die-casting materials, such as aluminium, magnesium and copper alloys because zinc alloys can be more easily cast, and are stronger and more ductile. They also require less finishing, can be held to lower tolerances and can be casted in thinner sections. The die life for zinc die-castings is also longer than that for other die-casting materials due to low casting temperatures required for zinc-based alloys. The production rate (shots/hour) is also much higher than other alloy systems.[83] They are used in a variety of applications, ranging from the simplest drawer handle to the most complex precision automotive part.[84] The nominal compositions of the die cast alloys are given in *Table 2.2.* [80,83,85] Alloys No3 and No5, however, have poor resistance to creep in applications where sustained loads are applied at temperatures above 100°C[84], and therefore do not always meet the design requirements.

ILZRO[2] therefore started research to develop a die-casting alloy that would have higher creep strength without sacrificing the other excellent properties of alloys No3 and No5. In the mid 1960 s, ILZRO developed a cold-chamber pressure die-casting alloy with some additions of titanium. This alloy was named as ILZRO.14, which was later on

[1] *Mazak 3 and 5 corresponds to the specification of BS1004A and BS1004B respectively, in British Standards (1972). They have been designated as alloys No3 and No5 in this text.*

[2] *ILZRO: International Lead Zinc Research Organisation.*

superseded by ILZRO.16. This is a special-purpose creep-resistant alloy which also meets the requirements of structural applications and its creep strength is markedly superior to that of alloys No3 and No5 at all testing conditions. For example, it was observed that when an aged sample of No3 was tested at room temperature, it showed about the same creep resistance as an aged sample of ILZRO.16 tested at 177°C.[86] It is shown that higher creep resistance of ILZRO.16 is due to its alloying constituents of chromium and titanium. These elements form a fine eutectic inter-growth of intermetallic compounds with zinc, e.g. $TiZn_{15}$ in Ti alloys[87,88], which creates an effective barrier to grain growth, but it is considered that the most important factor is that it increased the structural stability and creep resistance by eliminating a substantial number of high energy, mobile grain boundaries.[87,88]

However, the other mechanical properties of ILZRO.14 and ILZRO.16 at room temperature are inferior to those of alloys No3 and No5[83,86] and unlike alloys No3 and No5, they can not be die-cast in a hot-chamber die-casting machine in which the injection plunger sleeve and gooseneck are continuously immersed in molten zinc in the machine part or furnace. Due to the low aluminium content of ILZRO.14 and 16, it would slowly dissolve iron if left in contact with the steel plunger sleeve and cast iron goose-neck. Therefore, both alloys must be cast in cold-chamber die-casting machines. The typical mechanical properties of the alloys are given in *Table 2.3*.

High aluminium zinc-based (ZA) alloys were also developed in the process of exploring zinc-rich alloys. The first alloy having 12% aluminium was proposed by ILZRO in 1962 and was named ILZRO.12. Later, aluminium content was reduced to 11%, which together with other changes gave improved properties. This improved alloy is now known as ZA.12. In the late 1970s, Noranda Corporation under contract for ILZRO developed two additional alloys, ZA.8 and ZA.27. The chemical composition of these three alloys according to ASTM B 669-82 ingot specification is shown in *Table 2.2*.[83]

The advantages of ZA alloys include good mechanical properties, excellent bearing characteristics, ease of finishing and also pollution-free melting.[82,83] Due to these advantages, these alloys are used as alternatives to other well-developed alloy systems, such as aluminium-based alloys, brasses, bronzes and cast-irons.[84] Originally, these alloys were developed as sand and gravity casting alloys, but later on they were used in a

Table 2.2 : Chemical Composition of zinc-based alloys (% by weight).

Alloy	Al	Cu	Mg	Ti	Cr	Zn
No3	3.5-4.3	0.25 max.	0.02-0.05	-	-	Balance
No5	3.5-4.3	0.75-1.25	0.03-0.08	-	-	"
No2	3.5-4.3	2.5-3.0	0.02-0.05	-	-	"
ACuZinc5	2.8-3.3	5.0-6.0	0.025-0.05	-	-	"
ACuZinc10	3.0-4.0	10.0-11.0	0.025-0.05	-	-	"
ILZRO.16	0.01-0.04	1.0-1.5	0.02 max.	0.15-0.25	0.10-0.20	"
ZA.8	8.0-8.8	0.8-1.3	0.015-0.03	-	-	"
ZA.12	10.5-11.5	0.5-1.2	0.015-0.03	-	-	"
ZA.27	25.0-28.0	2.0-2.5	0.01-0.02	-	-	"

wide range of casting processes including pressure die casting. They can be die-cast in cold-chamber machines, but ZA.8, due to its low aluminium content and lower melting point can even be used in conventional hot-chamber machines. From all three ZA alloys, ZA.27 has the highest strength and hardness, followed by ZA.12 and ZA.8. There is no significant effect of casting techniques on the tensile strength of ZA.27, whereas the hardness and tensile properties of ZA.8 and ZA.12 are significantly higher in die-cast condition.

Murphy et al[89] investigated the effect of elevated temperatures in the range of 20°C to 260°C on the tensile properties of the die-cast alloys No3, ZA.8 and ZA.27. They found variations in ultimate tensile strength, proof stress and elongation with temperature. It was observed that ZA.27 had the highest strength, about 60% greater than that of alloy No3, followed by ZA.8 which had 30% higher strength than No3.The ultimate tensile strength and proof stress of the alloys decreased with increasing temperature and the rate of decrease was proportional to the aluminium content, whereas ZA.27 showed quite a sharp decrease with temperature. Elongation results gave a very pronounced temperature dependence.

Table 2.3 : Typical mechanical properties of zinc-based alloys.

Mechanical Property	No3	No5	No2	ILZRO.16
Ultimate Tensile Strength (MPa)	283	328	358.5	227.5 - 234.4
Yield Strength 0.2% offset (MPa)	195	—	—	137.9 - 144.8
Elongation (%)	10	7	7	5 - 6
Hardness (BHN)	82	91	100	75 - 77
Shear Strength (MPa)	213.7	262	317	—

Below 100°C , the ductility of ZA.27 increased very slowly, then at an increasing rate with rise in temperature up to the maximum temperature tested, exhibiting an expected characteristic of superplasticity of the alloy. Alloy No3 showed different behaviour from ZA.27 because initially there was a rapid rise in elongation, but this increase was the highest between 150-200°C and decreased thereafter. The elongation in ZA.8 behaved in a similar way to that of ZA.27 in the temperature range of 20 to 150°C, then it was the highest at about 200°C and decreased in a similar manner to that of alloy No3.[89]

Later, a similar research work was carried out in a more limited temperature range of up to 150°C on alloys No3, No5 and ZA. alloys by Loong.[90] His results for alloys No3, ZA.8 and ZA.27 were in close agreement with those of Durman[84] for the same alloys. It was found[90] that the tensile strength of alloys No5 and ZA.12 were between those of No3 and ZA.8, and of ZA.8 and ZA.27, respectively. The elongations in ZA.12 and alloy No5 were also very similar to that of ZA.27 and ZA.8, respectively. There was a general reduction in tensile strength and hardness, and an improvement in ductility with

aging of the alloys. Alloy No3 showed a greater improvement in ductility with aging than the other alloys.

Recently, in the General Motors Research Laboratory, two high copper zinc-based alloys, namely ACuZinc5 and ACuZinc10 were developed[79] after an investigation of 40 alloy compositions in the range 0-12 wt.% copper, 0-15 wt.% aluminium with the balance zinc and some impurities. The chemical composition of both ACuZinc alloys is given in *Table2.2.*[79,85] It has been found[79] that the strength of ACuZinc5 was 20% and 50% higher than ZA.8 and alloy No3, respectively. Properly designed die-cast components of ACuZinc5 have strength properties comparable to that of low-carbon steel, brass and many other engineering materials.[85] The tensile properties for as-cast ACuZinc5, alloy No3 and ZA.8 are shown in *Table 2.4.* [79]

Table 2.4 : Typical Tensile Properties of As-Die-Cast Hot-Chamber Zinc Alloys.

Alloy	0.2% YS (MPa)	UTS (MPa)	Total Elongation (%)
ACuZinc5	338	407	5.0
Alloy No3	187	262	19.3
ZA.8	254	334	2.7

It was also observed that the tensile strength of the ACuZinc alloys was governed by the type of primary phase, while yield strength was controlled by the matrix surrounding the primary phase.[79]

In the hot-chamber zinc-rich alloys, ACuZinc5 is harder than alloy No3 and ZA.8. It is also harder than machined brass (SAE CA360), which is considered as an alternative material in an application when alloy No3 die-castings do not have adequate wear resistance. ACuZinc5 has a Brinell hardness of 118, which is 38 Brinell points harder than 380Al, 36 points harder than alloy No3.[85] From cold-chamber zinc alloys, ACuZinc10 is harder than ZA.12 and ZA.27, as well as 380Al, a common cold-chamber aluminium die-casting alloy. The ductility of die cast ACuZinc10 is also about twice that of the die-cast ZA.8 alloy.

The higher strength and hardness of ACuZinc alloys is due to the presence of the primary ε-phase (Cu-rich) which is harder and stronger than other (α and η) phases, and

acts as a reinforcement in the matrix of ACuZinc alloys. The average values of hardness and strength of the primary ε phase of ACuZinc10, and the matrix, are shown in *Table 2.5.*[79]

Table 2.5 : The Average Hardness and Strength of the Primary ε -Phase and the Matrix (η phase + eutectic) in pressure die-cast ACuZinc10.

	Microhardness (DPH) 300	Compressive Yield Strength (MPa)	Ultimate Tensile Strength (MPa)
ε Phase	135-175	459	587
η phase + eutectic	110-120	327	278

Hanna and Rashid[91] also determined the wear characteristics and friction behaviour of various zinc alloys by a block-on-ring test and compared them with those of ACuZinc alloys. It was observed that ACuZinc alloys had lower mass wear rates and lower coefficients of friction than ZA.27, No3 and pure zinc. The wear rate and coefficient of friction of ZA.27 were two to three times higher, and those of No3 were three to four times higher than ACuZinc5. The relatively higher wear resistance of the ACuZinc alloys is attributed largely to the hard, copper-bearing, ε-phase.[91] The die castability of ACuZinc5 was found to be similar to that of No3 and better than that of ZA.8. The surface finish of the ACuZinc die castings was equal to or better than that of the production components. The polished sections of identical components which were made, using conditions optimized for alloy No3, showed that ACuZinc5 components had far less porosity than the production components of alloy No3.[80]

2.6.1.1 The Effect of Alloying Elements on General Properties of Alloys

The main alloying elements of zinc-based alloys, beside aluminium, are copper and magnesium. It was found that the effect of increasing Cu had the most effect between 0 and 1%[92] on creep properties of alloys No5, ZA.8 and ZA.12. Copper additions up to 2 or 2.5% significantly increase the tensile strength and hardness of the alloys. However, due to excess copper, ductility is reduced, and more than 1% Cu can cause dimensional growth on aging, due to a four-phase reaction. In both ACuZinc alloys, the improved strength, hardness, ductility and wear properties are attributed to the Cu-rich epsilon phase.[79,80] Magnesium additions are also very effective in small amounts of up to 0.01% in increasing the hardness and tensile strength, but at the expense of ductility. It is shown

that the effect of 0.01% magnesium on tensile strength of alloys is similar to that of a 2% copper addition.[92] Magnesium is also useful in preventing intergranular corrosion, which may occur when low levels of impurities, such as, lead, tin and cadmium are present.[92]

2.6.2 The Creep Characteristics of Zn-Al Alloys

The creep behaviour of commercial zinc alloys has been studied over the years, and most of the published creep data for these alloys are derived from the actual creep tests and/or simple limited extrapolation of experimental creep data.

The tensile creep data of alloy No3 at 25°C for different times ranging from instantaneous to ten years is shown in *Figure 2.6.*[83] This creep data was obtained from tests continued for up to five years, but the data for ten years was obtained by extrapolation of the five-year tests. From this data, it was possible to compute the permissible design stress at 25°C for an allowable design strain of up to approximately 0.8% in a desired service life of up to ten years. The effect of temperature up to 100°C on the allowable design stress for both alloys No3 and No5 is shown in *Figures 2.7 and 2.8*, respectively.[83] In these figures, secondary creep rates are expressed as % creep strain in 10,000 hours. These figures show that alloy No5 is more creep-resistant than No3 under all test conditions. It can also be observed that the difference in the secondary creep rates increases if stress is increased, indicating a different stress-dependence behaviour of these alloys.

A rough empirical equation was developed which could be used to obtain the permissible stress at any temperature:[83]

$$S_T = \frac{S_{25^\circ C} \times 28}{T} \qquad (2.28)$$

where S_T is permissible stress at any temperature from 25°C to 100°C, $S_{25^\circ C}$ the permissible stress at 25°C and T is the given temperature in °C.

ILZRO.16 was developed particularly to meet the demand for an alloy having high creep resistance at elevated temperatures where other zinc alloys can not be used. Creep data for ILZRO.16 at various test conditions are presented in *Figure 2.9.*[83] The creep resistance of ILZRO.16 is compared graphically with that of alloy No3 in *Figure 2.10*,

and it is clear that the creep strength of ILZRO.16 was markedly superior to that of alloy No3 under all testing conditions.[83]

The creep properties of ZA.8, ZA.12 and ZA.27 were investigated by the Noranda Corporation[84]. It was found on the basis of design stress that all three alloys showed approximately the same creep resistance at room temperature, whereas, the creep resistance of ZA.27 at 100°C was much lower than that at 20°C. The results indicated that the projected design stress of ZA.27 was reduced from approximately 69 MPa at room temperature to 5.6 MPa at 100°C, and it was expected that alloys ZA.8 and ZA.12 would also behave similarly. However, a later investigation by Murphy et al[93] on alloys No3, ZA.8, ZA.12 and ZA.27 at 120 °C proved different. Using the time to a total creep elongation of 1% as a measure, it was found[93] that ZA.8 had the best creep resistance, closely followed by ZA.12, whereas ZA.27 was slightly better than alloy No3. ZA.8 had significantly higher creep strength than alloys No3 and ZA.27.

Durman[84] also investigated the tensile creep behaviour of alloys No3, ZA.8 and ZA.27 under different test conditions. On the basis of calculated design stresses at different allowable creep strains (0.2 ~1%), it was concluded[84] that ZA.8 had a substantially better total creep resistance than the alloys No3 and ZA.27. ZA.27 was marginally better than the alloy No3 for allowable creep strains higher than 0.5%, but inferior for smaller strains, due to its higher primary creep than that of alloy No3.

2.7 Creep in the Ternary and Higher Alloys

Although experience has shown that Zn-Al binary alloys possess good forming and mechanical properties, these alloys have a low resistance to creep due to their superplastic characteristics. Due to poor creep strength, these alloys have limited commercial use.

In order to improve their creep strength, many researchers have studied the effect of alloying additions on Zn-Al alloys. Naziri and Pearce[94] checked the effect of copper additions up to 1% on creep properties of slightly hyper-eutectoid alloys (20% Al). They found that copper additions did not have a significant effect above about 150°C. However, it was observed that at room temperature, the addition of up to 1% copper continuously improved the creep resistance of the alloy and for 1% addition, the improvement was by a factor of 140.

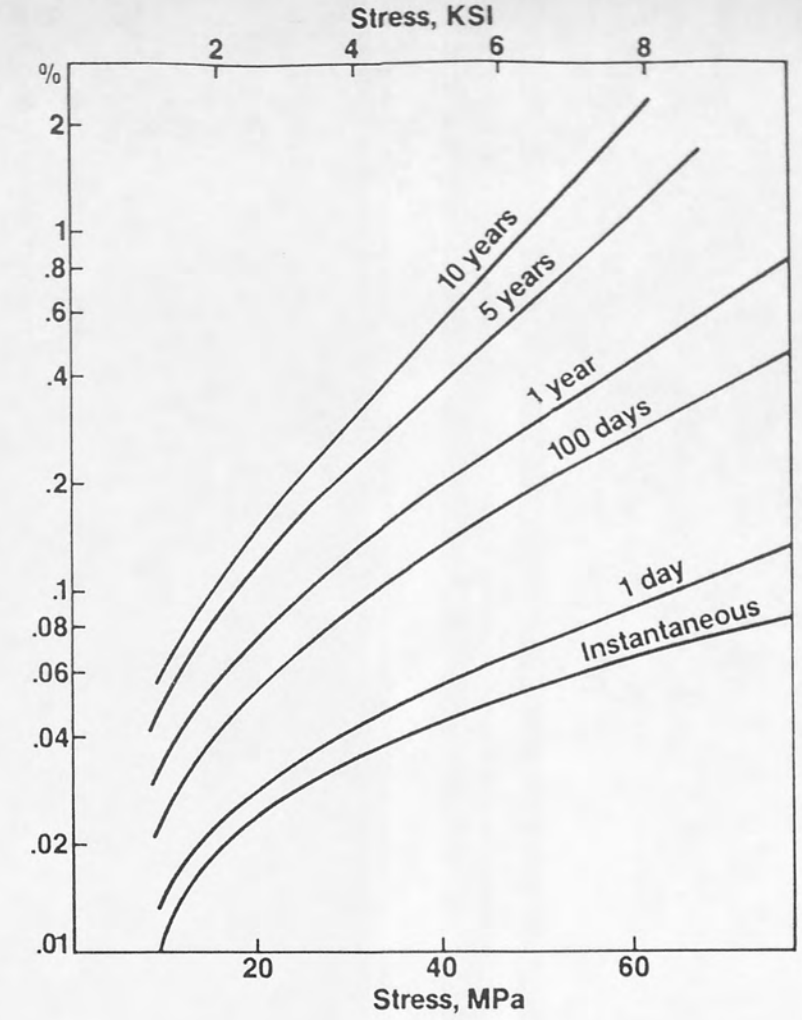

Figure 2.6. Tensile creep properties of alloy No3 at 25°C (% allowable strain in indicated time versus allowable stress).[83]

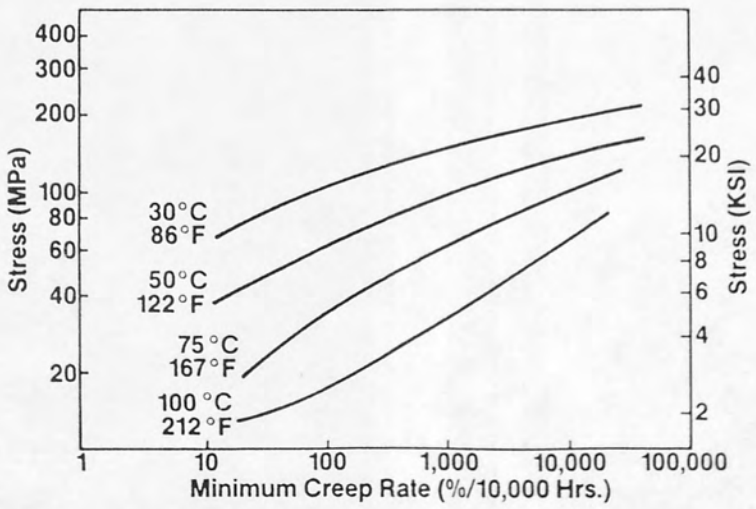

Figure 2.7. Tensile creep properties of alloy No3 at various temperatures.[83]

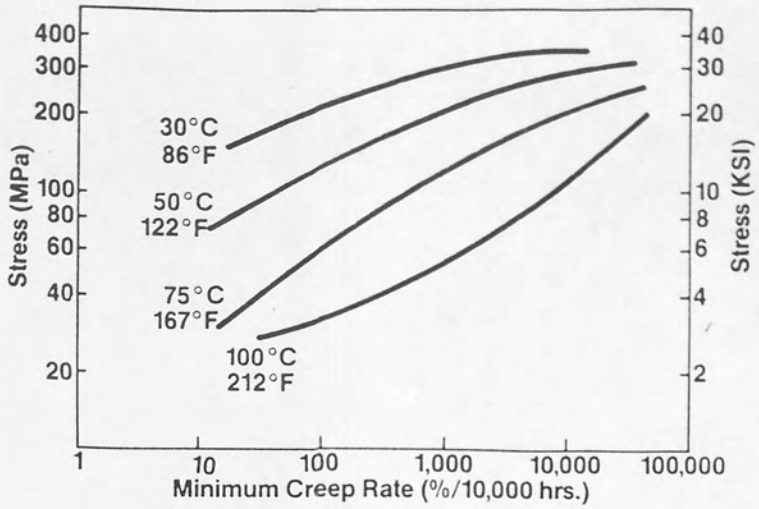

Figure 2.8. Tensile creep properties of alloy No5 at various temperatures.[83]

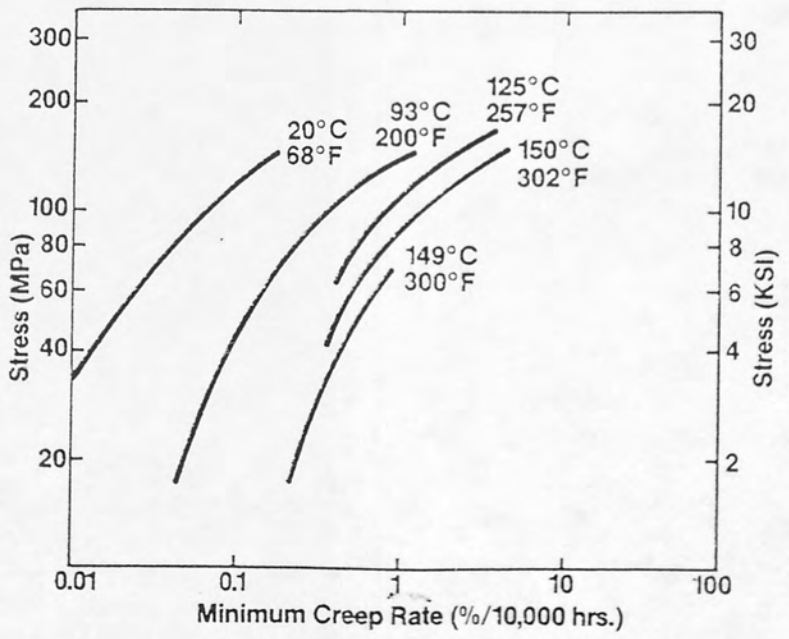

Figure 2.9. Tensile creep properties of ILZRO.16 at various temperatures.[83]

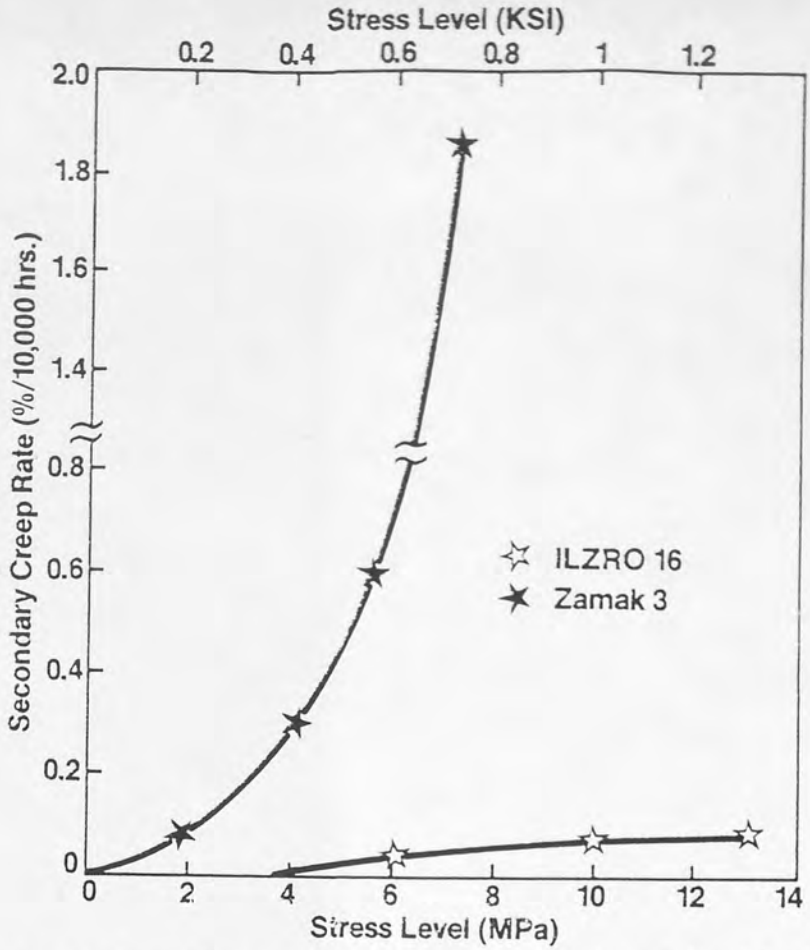

Figure 2.10. Secondary creep rate as a function of stress level for ILZRO.16 and alloy No3.

Later, Nuttall[95] investigated the creep properties of three eutectoid-based ternary Zn-Al alloys, one with 4% Cu, the second with 0.2% Mn and third with 1% Si. The alloy containing 1% silicon cracked on hot rolling or swaging and little further research work was carried out on this alloy. However, the steady-state creep resistance of the other two alloys was measured at a stress of 35 MPa after various heat treatments. The results indicated that the room temperature creep resistance of the alloys was significantly increased due to the copper additions of up to 1%, but there was no improvement in the creep resistance of alloys when the copper content was increased from 1 to 4%. The creep resistance of a manganese-containing alloy was observed to be substantially better than that of any of the alloys containing copper. In the as-quenched condition, the steady-state creep rate of Zn-Al-0.2Mn was 8.1×10^{-6} h^{-1} as compared to 9.0×10^{-5} h^{-1} for Zn-Al-1Cu and 8.0×10^{-5} h^{-1} for Zn-Al-4Cu.

Other researchers like Mulvania et al[96] also tried to modify the composition of eutectoid alloys in an attempt to improve the creep resistance by adding single elements; titanium, chromium, manganese, copper and magnesium. They found that generally the

creep resistance of alloys was improved by alloying at room temperature. It was observed that manganese, titanium and chromium had little effect in improving the creep strength. However, additions of magnesium and copper show a significant improvement in creep resistance of alloys. Copper additions up to 0.5% enhanced the creep resistance, but additional copper was not beneficial. It was also noted that an addition of 0.018%Mg produced the highest creep strength overall and showed a much greater improvement than 0.06% Mg. The optimum combination of high creep strength and low superplastic flow stress was observed in an alloy with 0.42% Cu and 0.002% Mg, which had a creep resistance equivalent to that of a commercial zinc die-casting.

Savaskan and Murphy[93,97,98] investigated the creep behaviour of one eutectoid and two near-eutectoid alloys, containing 3 and 4% Cu in both as-cast and heat treated conditions, over a range of stress and temperature. The results showed that the alloys containing 3 and 4% Cu, in both as-cast and heat treated conditions, had much lower secondary creep rates than the binary alloys; and the as-cast alloy, in turn, had substantially lower secondary creep rates than heat treated alloys of the same composition. In the as-cast condition, the alloy with 4% Cu exhibited a lower creep rate than that with 3% Cu among the ternary alloys. However, these results were reversed in heat treated condition. This was due to the overall copper content which increased the creep resistance of as-cast alloys, whereas, in the case of heat treated alloys, it was attributed to the matrix copper content.

Savaskan and Murphy in their first two works[97,98] also showed that the secondary creep rates of these alloys in both as-cast and heat treated conditions could be correlated, using an equation of the form:

$$\dot{\varepsilon}_s = A \sigma^n \exp(-Q_c / RT) \qquad (2.29)$$

where n = 3, and a mean value of Q_c = 87 kJ/mole.

Later, Murphy et al[93] modified the *Equation (2.29)* and correlated the creep data more satisfactorily by the following empirical equation:

$$f(e) = C t \sigma^n \exp(-Q_c / RT) \qquad (2.30)$$

where f (e) is some function of creep deformation, C a constant, t the time, σ the stress, n the stress exponent, Q_c the activation energy for creep, T the absolute temperature and

R is the universal gas constant. They found a stress exponent of 3.33 for alloys tested in the stress range of 10 to 60 MPa. The activation energies for as-cast alloys were similar, with a mean value of 122 kJ/mole. For heat-treated alloys, the activation energies were found in the range 60-107 kJ/mole.

Recently, Hanna and Rashid[79,80] investigated the creep properties of two new ternary pressure die-cast Zn-Al alloys, i.e. ACuZinc5 and ACuZinc10 over a wide range of stress and temperature, and compared the results with those of pressure die-cast alloy No3 and ZA. alloys. They determined the creep resistance of several zinc-rich alloys including ACuZinc in the as-cast condition. The test temperatures were 21°C and 150°C, and the applied stresses were 40 and 200 MPa. At all temperature and stress levels, the secondary creep rate of both ACuZinc alloys was much lower than that of the other zinc-rich alloys. It was observed that the creep strain rate of ACuZinc alloys was five to seven times lower than the commercial zinc die-casting alloys.[80] The times required for total creep strains of 0.5 and 1%, and the time to fracture were also found for pressure die-cast ACuZinc and other zinc-rich alloys (pressure die-cast) at 40 MPa and 150°C from experimental data and it was shown that time to 1% strain was 33 h for ACuZinc10, 12.5 h for ACuZinc5, 7 h for ZA.27 and 5 h for alloy No3. Similarly, time to fracture of ACuZinc alloys was many times higher than other commercial zinc-based alloys.[80]

The results showed that ACuZinc5 had a much lower creep rate than alloy No3 and ZA8 and ACuZinc10 exhibited significantly lower creep rate than alloys No3 and ZA27. Therefore, these alloys have substantially better creep resistance than alloy No3 or ZA. alloys under different testing conditions. ACuZinc10 was found to has better creep resistance than ACuZinc5.

The creep strain versus time plots at room temperature and stress of 200 MPa are shown for hot- and cold-chamber alloys in *Figures 2.11 and 2.12*, respectively.

The creep behaviour of ACuZinc5 was also investigated[85] at 150 °C and a stress of 60 MPa. The results were compared with those of alloys No3 and ZA.8. The creep strain of ZA.8 was much lower than alloy No3, and that of ACuZinc5 was lower than ZA.8. The time to fracture for ACuZinc5 was about three times greater than ZA.8.

It has been observed that higher creep strength of ACuZinc alloys is due to the presence of Cu-rich epsilon (ε) phase, which occupies about half of the microstructure in ACuZinc10 and 30% in ACuZinc5.[79] Therefore, these improved zinc alloys can be used

for structural applications as net shape zinc die-castings at elevated temperatures where higher creep, wear and strength properties are required.[79]

From experimental data, the design stresses which produce a total creep strain of 0.2% in 10,000 h were determined to be 55 MPa for ACuZinc10 at 50°C compared to 22 MPa for ZA.27 and only 8 MPa for alloy No3.[96]

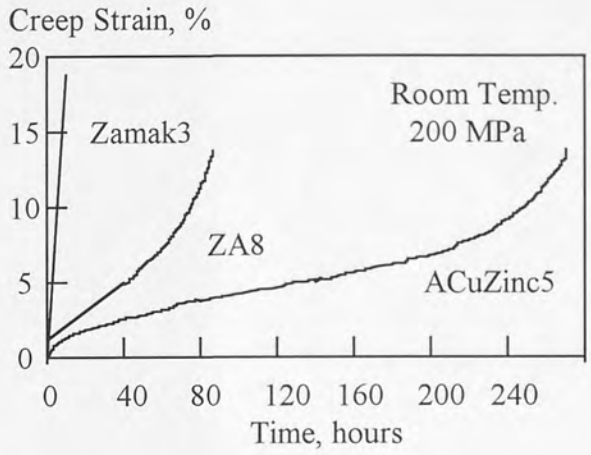

Figure 2.11. Creep strain versus time plots for hot-chamber alloys at room temperature at a stress of 200 MPa.[79]

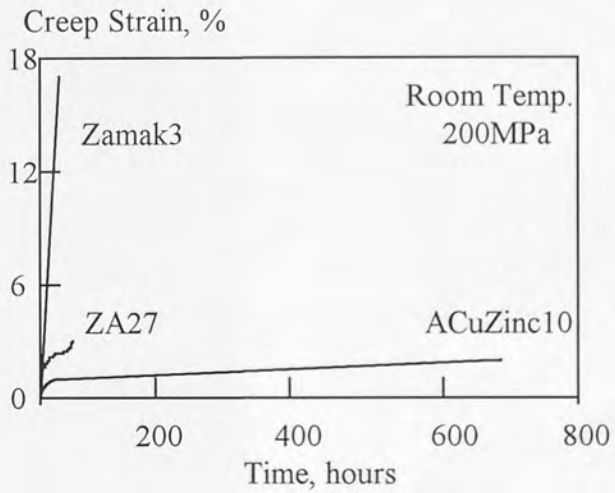

Figure 2.12. Creep strain versus time plots for cold-chamber alloys at room temperature at a stress of 200 MPa.[79]

2.8 The Binary Zn-Al System

The binary phase diagram of the Zn-Al system is one of the most investigated equilibrium diagrams over a period of more than 80 years.[99] Many phase diagrams have been published during this period but are now obsolete except the liquidus curves and temperatures of three phase equilibria. The most attention was given to determine; (i) the solidus curve, (ii) the solid solubility of Zn in Al, which includes the boundary of the

closed miscibility gap above 275°C, and also (iii) the solid solubility of Al in Zn. The major dispute among the researchers for many years was the possibility of a peritectic reaction in Zn-Al system.

The earliest investigators[100-102] proposed equilibrium diagrams of Zn-Al system which showed the following similarities: (i) these diagrams exhibited an intermediate phase of variable composition around 78% Zn, generally denoted as β, and formed by a peritectic reaction of the melt (at about 443°C) with the aluminium-based solid solution α containing about 70% Zn, (ii) a eutectic of β and also the zinc-based solid solution η at 95% Zn, at temperature 380°C, and (iii) a eutectoid decomposition of β, whereas the eutectoid point was situated at 270-280°C. Later, Owen and Pickup[103] and Elwood[104,105], studied the system by high temperature X-ray camera method, but could not confirm the existence of a peritectic reaction.

Fink and Willey[106], by using resistivity and microscopic techniques, concluded that the peritectic reaction was not present. Later, Gayler and Sutherland[107], on the basis of thermal, microscopic and dilometric evidence, reached the same conclusion. The thermal arrest which was found by them at 443°C was due to a rapid change in composition of the α' solution along the solidus.

The Zn-Al phase diagram compiled by Hansen and Anderko[108], is shown in *Figure 2.13*. The figure has been drawn from the results of Elwood and earlier workers, and does not show the peritectically-formed intermediate β phase.

Figure 2.13. Zinc-Aluminium phase diagram compiled by Hansen and Anderko.[108]

The consecutive work of Presnyakov et al[109] and Goldak and Parr[110] has produced a binary diagram of *Figure 2.14,* which is considered as perhaps the most accurate representation of the Zn-Al system proposed in recent years. The diagram accounts for all the experimental facts.

Presnyakov et al studied the Zn-Al system in detail to find out whether a peritectic reaction existed. The alloys were prepared from 99.99% aluminium and 99.96% zinc by crucible melting and cast into graphite moulds. They studied a small portion of the phase diagram in great detail and discovered a very narrow two-phase field. From this investigation, they concluded that; (i) the peritectic reaction, in fact, existed at about 443°C, (ii) another phase, known as β phase, distinct from the α phase, existed and also involved a discontinuity in the solubility, and (iii) a second eutectoid decomposition of the α' phase into α + β occurred at about 340°C, with the eutectoid point at about 70% Zn.

Later, Goldak and Parr confirmed the work of Presnyakov et al explicitly by a high temperature X-ray diffractometer study of the Zn-Al system in the region 40-75 wt. Zn. In this study, aluminium and zinc of 99.999% purity were used for the preparation of alloys. The alloys consisted of 70% zinc and 30% aluminium. As specimens of the highest possible purity were required during this investigation, the levitation-melting technique was adopted.

The phase diagram of Presnyakov et al, confirmed by Goldak and Parr is considered probably the most accurate representation of the binary diagram for Zn-Al system to date. In this phase diagram, α is the Al-rich terminal solid solution, α' is the part of it which lies on Zn-rich side of the monotectoid, β is the Zn-rich eutectoid phase and η is the Zn-rich terminal solid solution. The invariant transformations observed in solidification are given as below:

a peritectic, liquid + α → β at approximately 70% Zn, 443°C; and

an eutectic, liquid → β + η at 94.9% Zn, 382°C.

The solid solubility of zinc in aluminium at different temperatures has been determined and given in *Table 2.6.*[111]

Table 2.6 : The solid solubility of zinc in aluminium at different temperatures

Temperature (°C)	Solubility (% wt.)
77	2.5
127	6.2
177	11.5
227	18.0
275	31.6
327	43.5
340	49.0-69.5
351.5	61.3
443	70.0

In the temperature range of 340°C to 351°C, the Al-rich solid solutions break down into two phases α and α', which are both an fcc solid solution of zinc in aluminium having different percentages of zinc. At 340°C, this gap of miscibility extends from 49 to 69.5% zinc and regularly shrinks on heating to reach the single point at 351°C. It can be observed that $\alpha' + \beta$ is a very narrow field nearly equal to 1 wt.% wide[110], extending from an eutectoid point at 69.5% Zn to the peritectic point at 443°C.

At the zinc end, the solidus and liquidus slopes down to the eutectic sharply. When an alloy consists of two metal components, the phases are essentially solid solutions. This is because metals always have some degree of mutual solubility; sometimes this is very small.[112] Aluminium is soluble in zinc in small amounts, approximately 1.1 percent aluminium at 380°C, which decreases to 0.65% at eutectoid temperature (275°C) and 0.42% Al at 227°C.[111]

At 340°C, f.c.c. β phase has a lattice parameter decreasing from 4.0400Å at 70% Zn to 4.0300Å at 76% Zn.[109] It decomposes by an eutectoid reaction into $\alpha + \eta$ at 275°C with the eutectoid point at 78% Zn. At 25°C, the lattice parameter of pure aluminium is 4.0414Å[113] and it decreases almost linearly to 4.0000Å at 65% Zn in α region.[105] Zinc has a hexagonal close packed (h.c.p.) crystal structure with the following lattice parameters:[113]

a = 2.6595Å, c = 4.9368Å when it is pure,

and a = 2.6650Å, c = 4.9870Å when saturated with aluminium.

2.9 The Binary Zn-Cu System

The phase diagram of the binary Zn-Cu system is presented in *Figure 2.15.*[114] This diagram can be regarded as very well established. It differs only slightly from that

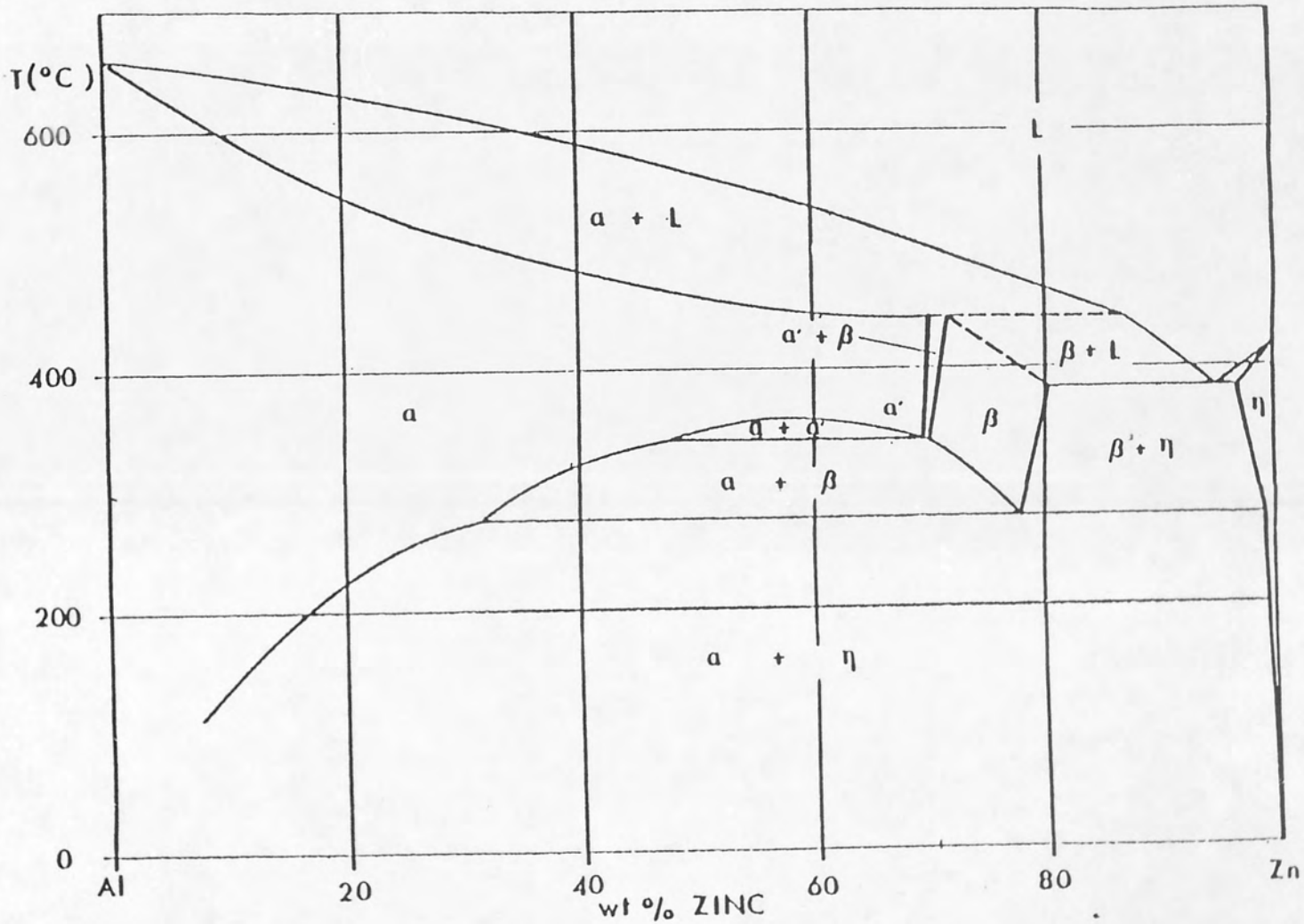

Figure 2.14. Accepted phase diagram of binary Zinc-Aluminium system.

compiled by Hansen and Anderko.[108] Five peritectic reactions are shown in this figure. Four intermediate phases, i.e. β, γ, δ and ε also exist in the system, and except for δ phase, they have broad ranges of solid solubility.

The solubility of copper in zinc decreases with decreasing temperature which can be observed from *Figure 2.15*, and given in *Table 2.7*.[108]

Table 2.7 : The Solid Solubility of Copper in Zinc

Temperature (°C)	Solubility (wt.%)
100	0.3
200	0.9
300	1.65
400	2.50
424	2.70

Ageing of a supersaturated solid solution of η phase precipitates the ε phase. The crystal structure of both phases is essentially the same, i.e. c.p.h., but the c/a ratio is very different. The lattice spacings are given as below:[84]

ε : a = 2.735Å c = 4.285Å, c/a = 1.57 at 21% at.% Cu

η : a = 2.668Å c = 4.870Å, c/a = 1.83 at 1.55% at.% Cu

2.10 The Ternary Zn-Al-Cu System

This system has been studied intensively in past 70 years. Fletcher and Thomas[115] investigated the Cu-rich areas of the system thoroughly. Willey[116] compiled the isothermal sections of the Zn-Al-Cu system at different temperatures.

Strawbridge et al[117] showed that the solid solubility of copper in aluminium increased with increasing zinc. They reported an increase in the solubility from 2.8% Cu with 0% Zn to about 3.4% Cu with 8% Zn, at 460°C.

The low copper part of the Zn-Al-Cu ternary system was also studied by Murphy.[118] The isothermal section of the system at 350°C is shown in *Figure 2.16*, taken from his work. It is clear from this figure that there is considerable solid solubility of copper in the α and β phases, different from that reported earlier by Koster and Moeller, because they found only 1.5% Cu in α in equilibrium with the θ and T′, but in this recent work[118] 3.3% Cu was found in the α phase. In his work, Murphy also found that solid

solubility of copper increased with zinc content to a maximum of 4.5% copper at a zinc content of 70.9%.

The isothermal section at 290°C by Murphy is shown in *Figure 2.17*, which shows that with the development of a wide $\alpha + \beta$ field in the Zn-Al system, a broad $\alpha + \beta + T'$ field is introduced in the ternary diagram. The copper content in the α and β solid solutions have decreased to 2.5%, and all two-phase fields have narrowed. The $\beta + T'$ two phase field, in particular, is found to be extremely narrow, which indicates an imminent Class II four-phase reaction, given as follows:

$$\beta + T' \Leftrightarrow \alpha + \varepsilon$$

whereas, the α phase in equilibrium with θ and T' has increased considerably with the amount of copper in the solid solution, as found at 350°C.

Figure 2.18 shows the isothermal section at 280°C at which the four-phase reaction is complete, and two three-phase fields, i.e. $\alpha + T' + \varepsilon$ and $\alpha + \beta + \varepsilon$ have been separated by a narrow phase field.

At 270°C, two important changes were observed, as shown in *Figure 2.19*. In this case, β phase has been replaced by the $(\alpha + \varepsilon + \eta)$ phase field, furthermore, the phase field $(\alpha+\varepsilon)$ has narrowed, indicating another four phase reaction just below 270°C, and given as:

$$\alpha + \varepsilon \Leftrightarrow T' + \eta$$

In *Figure 2.20*, at 250°C, the three phase field $(\alpha + T' + \eta)$ resulting from the above reaction covers a large part of the diagram.

It was also observed by Murphy that β phase had already decomposed at 275°C. Since the binary diagram of the Zn-Al system *(Figure 2.14)* shows that this decomposition takes place at 275°C, he therefore concluded that β phase decomposes at a higher temperature in the ternary system and the Class II four phase reaction, actually has occurred:

$$\beta + \varepsilon \Leftrightarrow \alpha + \eta$$

with the $\alpha + \beta + \eta$ phase field contracts to the binary edge. The reaction sequences in both binary and ternary systems have been summarised by Murphy and shown in *Figure 2.21*.

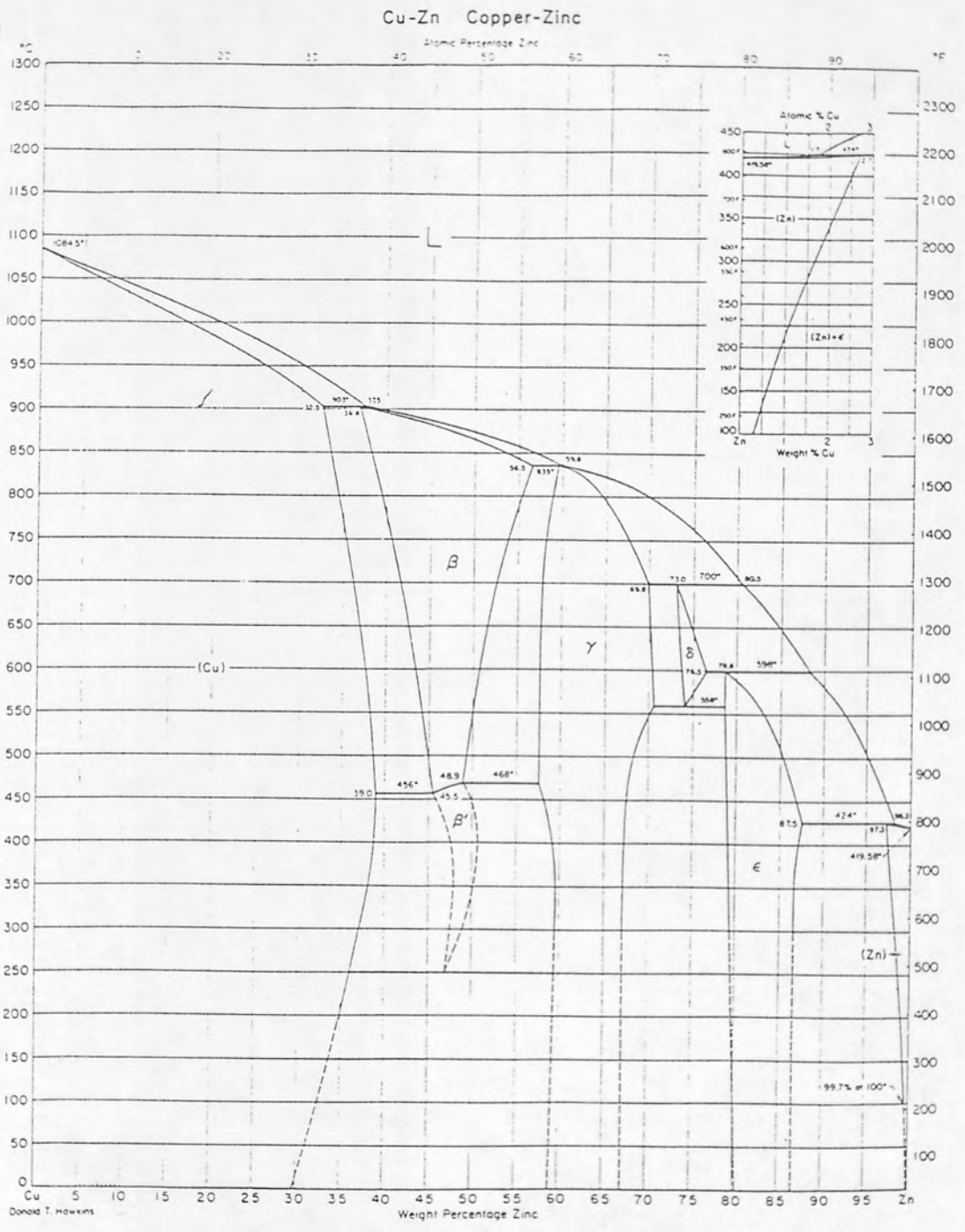

Figure 2.15. The equilibrium phase diagram of the binary Zn-Cu system.

The structure of the T′ phase was investigated by Murphy[119] in detail, using electron diffraction, X-ray diffraction and electron-probe microanalysis. He established that T′ had a rhombohedral superlattice structure with a = 8.676Å and α = 27.41°, and it was based on an assembly of five small CsCl-type cells, joined corner to corner along[111] direction.

The rhombohedral symmetry was due to the presence of a vacant lattice site in the middle of the central CsCl cell. The additional random vacancies were indicated by composition, density and structural measurements; and a possible distribution scheme was presented, as shown in *Table 2.8.*[119] In order to reduce the electron/atom site ratio, it is highly probable that zinc is substituted for aluminium, but it is unlikely to be much lower than 1.72.

Table 2.8 : Fractional Occupancy of the T′ Lattice Sites.

	Site									
	A	B	C	D	E	F	G	H	I	J
Al	0.90		0.75		0.90		0.90		0.75	
Cu		0.90		0.70				0.70		0.90
Zn			0.25		0.10		0.10		0.25	

Figure 2.16. Isothermal section of Zn-Al-Cu system at 350°C after Murphy.[118]

Figure 2.17. Isothermal section of Zn-Al-Cu system at 290°C after Murphy.[118]

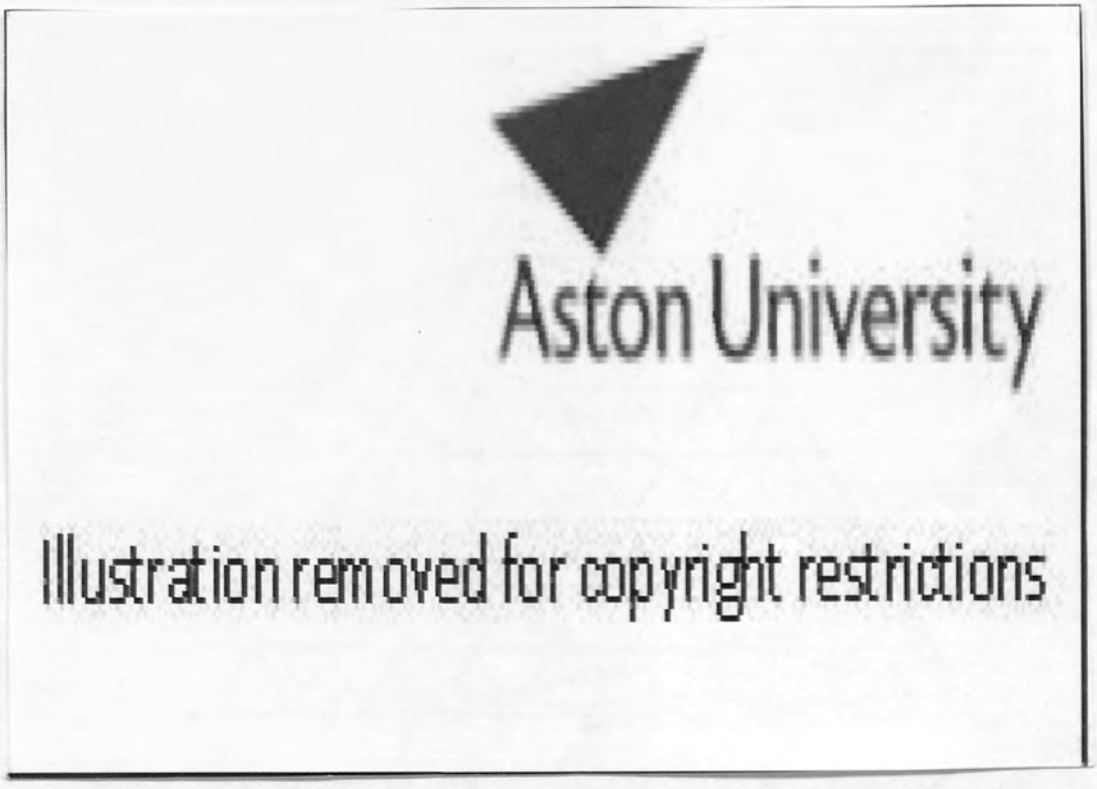

Figure 2.18. Isothermal section of Zn-Al-Cu system at 280°C after Murphy.[118]

Figure 2.19. Isothermal section of Zn-Al-Cu system at 270°C after Murphy.[118]

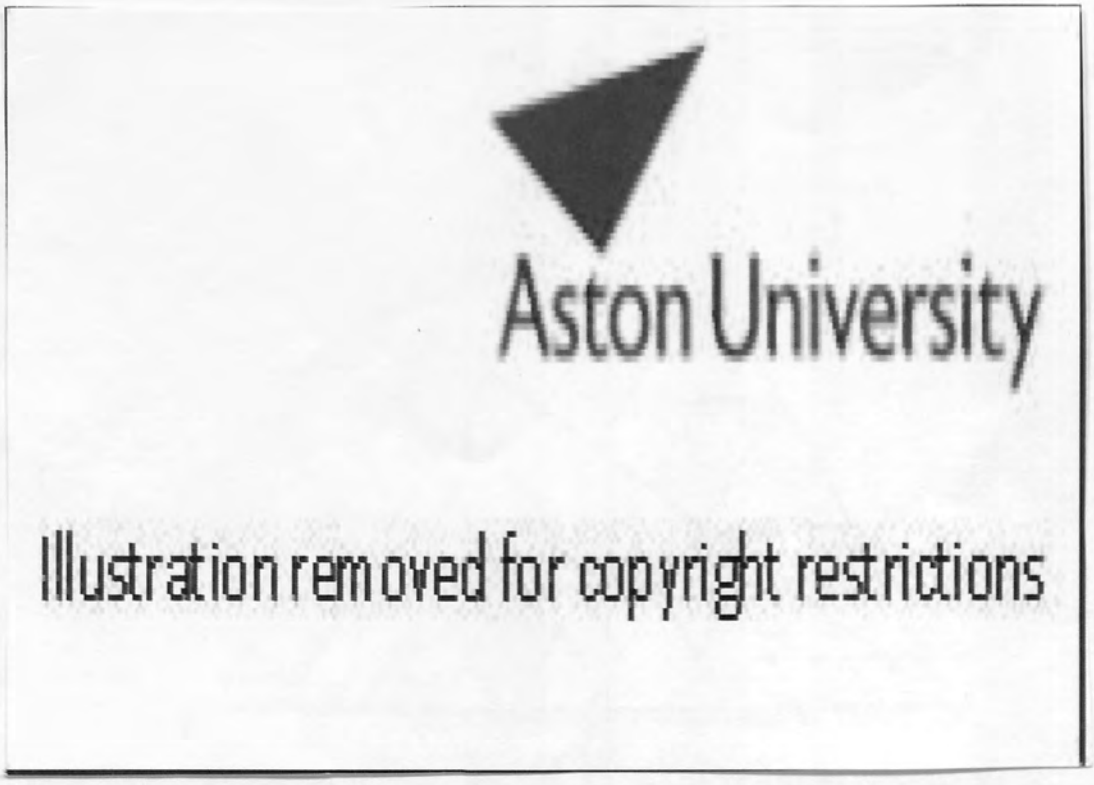

Figure 2.20. Isothermal section of Zn-Al-Cu system at 250°C after Murphy.[118]

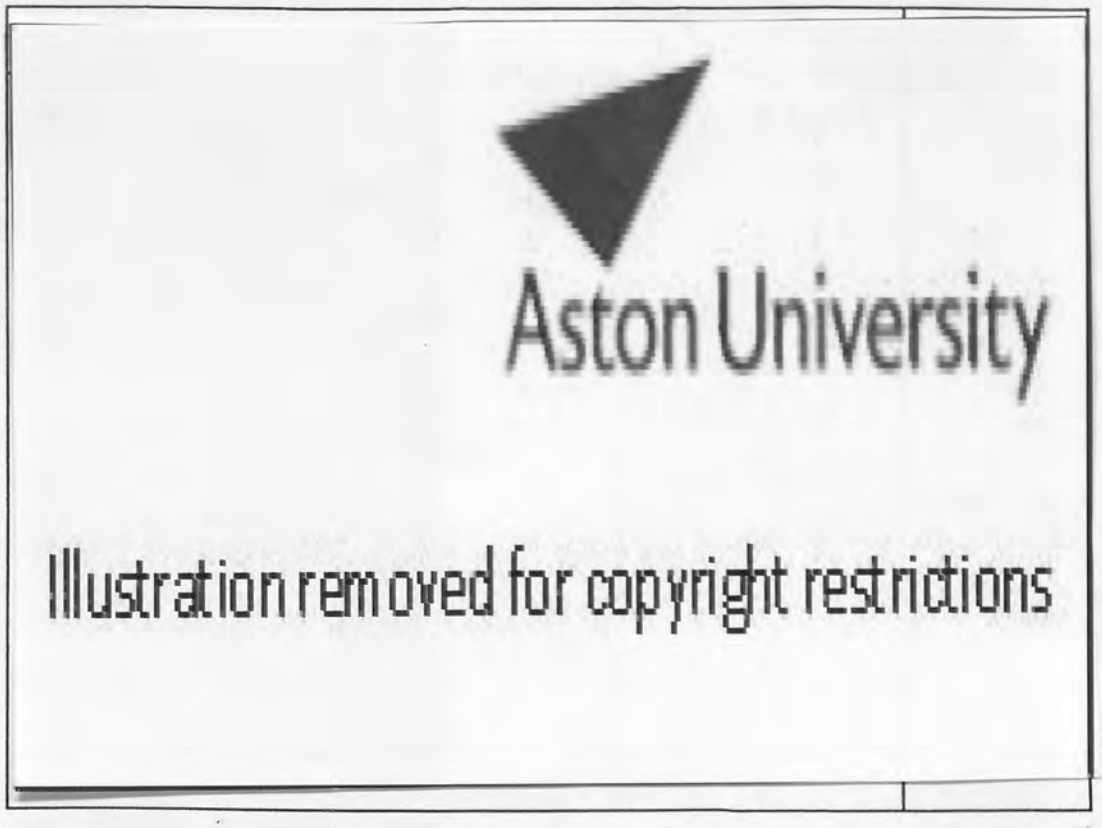

Figure 2.21. Solid-state reactions in the low-copper part of the Zn-Al-Cu system according to Murphy.[118]

2.11 Load-Relaxation

Load-relaxation is the time and temperature dependent decrease of load in a material due to conversion of elastic into inelastic (plastic) strain.[120] Therefore, during this process, the total strain is kept constant while the load applied initially decreases with time.[13] A common example of this phenomenon is the relaxation of load (stress) in the bolts of joints in a 'hot' environment. The rim of a gas-turbine disc which works with a cooling system, is another case where relaxation may cause a marked redistribution of stress.[121]

The phenomenon is related to creep and seems to exhibit the characteristics of logarithmic creep.[13] The data obtained from load relaxation tests can be used to develop stress-relief heat treatments for reducing residual stresses, and also for the design of such mechanical elements as joints, bolted flanges, press-fit elements, gaskets and springs.[120,122] The data obtained is also an important source to evaluate the constitutive relations governing a material's inelastic behaviour.[120]

A greater creep rate is expected during constant stress creep than during stress (load) relaxation which involves creep under a decreasing stress.[13]

It has been observed that load or stress relaxation is a problem in rivet and screw joints, particularly in automobile components where the temperature is usually high. It is also considered important in other stressed components, such as wheel rims and consoles for spring brackets in cars which are used in a warm climate.[123]

2.11.1 Load-Relaxation Properties of Zinc-Based Alloys

The load-relaxation behaviour of zinc-rich Zn-Al alloys was studied only in recent years. Murphy and Haines[124] investigated the load relaxation characteristics of commercial zinc alloys, i.e. No3, No5, No2 and ZA.8.

During the load-relaxation tests, they used a new device to continuously monitor preload loss in these zinc-based pressure die castings. A load cell was used to monitor load loss in an ISO metric 6 × 1 steel screw set into castings made from these alloys, and tightened to give an initial preload of 5900 N (1320 lbf). Each casting was held at a constant temperature in an oil bath and the tests were conducted for periods of up to 100 hours. The test temperature range was 22-80°C.

All test specimens were produced using a single impression die on the same hot-chamber machine, where a central hole in the boss of the casting was formed during die casting using a tapered core. The residual load was measured continuously and plotted as a function of test time for all alloys. In all experiments, the initial load loss was high, diminishing gradually with time, but not ceasing. The amount of load loss increased rapidly with test temperature, and all curves approximated to a logarithmic decay of preload with time. There was some variation in the initial part of the curves.

The results showed[124] that commercial zinc alloys had clear differences in the comparative resistance to preload loss. Generally, alloy No2 had the best resistance, with alloy No5 next and No3 worst at all testing conditions. The variation of 50 hour load was plotted as a function of copper content for three hypoeutectic alloys. There was little difference in behaviour at room temperature, but at higher temperatures of 60 and 80°C, a linear dependence of retained load on copper content was displayed. ZA.8 showed different behaviour from other alloys. It had poor resistance in comparison with the higher zinc alloys at low temperatures, but improved its relative position as the test temperature was increased to become comparable to alloy No2 at 80°C.

Later, Murphy and Goodwin[125] examined the preload loss of steel fasteners set into zinc alloy pressure die-castings. The load loss was continuously monitored over a period of 150 hours using a calibrated load cell. The tests were conducted at 50°C and 80°C on alloys No3, No5 and ZA.8.

Commercial high-strength zinc-coated steel screws were used for the majority of the tests. The base design was an ISO-metric M 6 × 1 steel fastener of 10mm engagement length set in a roll-threaded casting which had a boss diameter of 12.7mm, and torqued to give an initial preload of 6000 N.

The following variations were engineered in the base configuration and tested:

- Changing the engagement length from 10 to 25 mm.
- Thread pitch was varied from 0.75 mm to 1.25 mm.
- Reducing the external diameter of the boss from 12.7 mm to 10.0 mm.
- Changing the way the casting thread was produced replacing a roll-threaded casting by, (i) a casting having a thread made by a cutting action tap, and (ii) a casting where the thread was provided by a self-tapping screw.

The results showed[125] that for the common combination of an M 6 × 1 steel screw set into a 10mm hole pre-threaded by a roll-forming tap in alloy No3 pressure die casting, an initial load of 6000 N decays to about 17% of its initial value over the first 150 hours at 80°C, with very little change thereafter. Alloy No5 which contains a small copper content, retains more than 25% of its initial load after the same time, and ZA.8 retains about 30%. At lower test temperature of 50°C, the proportions of retained load are approximately 35% for No3, 55% for No5 and 60% for ZA.8.

It has been found that change in engagement length had significant effect on the retained load. Improvements in long-term retained loads of 100% for No3, and 60% for No5 and ZA.8 at 80°, while 55% for No3 and 30% for No5 and ZA.8 at 50°C were observed by increasing the engagement length by 50% from 10 to 15mm. Further increases were beneficial for certain materials, but might lead to unacceptable weight penalties for small improvements.

The thread pitch had a smaller but still important effect on load relaxation. When the pitch of a 6mm screw was changed from 0.75 to 1.25mm, it increased the long-term

retained load by an average of 22%, although alloy No3 showed no improvement and alloy No5 a 46% improvement at 80°C.

The effect of reducing the external diameter of the boss was not large. The research[141] revealed that most of the load relaxation was due to thread-related effects rather than compressive stress on the boss, and doubling the compressive stress resulted in an average load reduction of only 20%, with alloy No3 least sensitive to this variable. Another important factor was the way the thread was formed in the hole. It was found that a cut-threaded casting gave on average a long-term preload retention, 42% and 33% better than the standard roll-threaded casting at 80°C and 50°C, respectively, while the use of self-tapping screws gave worse results when compared with ordinary metric screws in roll-threaded holes. It was also observed that these reductions were modest, particularly at the higher temperature where an average reduction of just 7% was measured.

By taking the average long-term retained loads for all of the load relaxation tests, it was found that an increase of 41% could be obtained by replacing alloy No3 with No5, and 59% by substituting ZA.8. These improvements were similar for both test temperatures.

CHAPTER 3

3.0 COMPRESSIVE CREEP MACHINE

3.1 Design of Creep Machine

The compressive creep machine is shown in *Figure 3.1*. The machine is of the standard weighted lever-arm type, with a lever arm ratio of 10:1. The machine has been designed for compressive creep testing of zinc-based alloys to find out their compressive creep behaviour.The machine consists of:

(1) Three vertical supporting columns with a lever, which is placed on the top of these columns.

(2) Three plates of mild steel fixed between two front columns with support flanges. The first plate has been used to support the hydraulic-jack. The second plate is fixed between the other two plates, and its prime purpose is to hold another structure which is ultimately used to compress the test specimen. The oil-bath is placed on a third plate, which can be moved up and down by a rotating square-threaded rod manually.

(3) A hydraulic-jack, which plays an important role in the smooth application of load on the specimen. Initially, the hydraulic-jack sustains the applied load,and then transfers it to the specimen very smoothly at the start of the experiment.

(4) The structure, made of four steel plates, which is used to compress the test specimen.

(5) Two linear-bearings which are fixed at the centres of two steel plates. These bearings assist in the alignment of the loading arrangement.

(6) Two small steel plates, having highly-finished surfaces between which the specimen is compressed.

(7) An oil-bath, which is used to heat the specimen up to the required constant temperature and maintain it until the termination of the test. The operating temperature of the oil-bath is 45 to 300°C and the extended temperature range with additional cooling is -100 to 300°C.

(8) The temperature controller, a part of the oil-bath, that has a temperature control accuracy of ± 0.03°C.

(9) A hand-pump connected to the hydraulic-jack.

(10) A load-scale and appropriate loading-weights.

(11) A steel rod of dia. 35mm, passing through the hydraulic-jack. One end of this rod is connected to the lever through a universal joint, while the other end is joined to a smaller rod of dia. 8mm using another universal joint.

Figure 3.1. Designed compressive creep machine with oil-bath.

(12) Two universal joints which are helpful in the alignment of the steel rods.

(13) A silver-steel tension rod having a diameter of 8mm. This rod having threads on both sides, passes through the linear-bearings and the specimen, and assists in the alignment of the loading-arrangement.

(14) A transducer, used for the measurement of creep strain and could work up to the maximum test temperature of 160°C.

(15) A square-threaded rod, used to move the oil-bath up and down according to the test requirement.

(16) A top plate.

(17) The strain-recording equipment.

(18) A small circular plate of high-strength steel having highly smooth surface, and is used to hold the test sample from its lower end.

(19) A nut of size M6 × 1 (ISO), tightened below the small circular plate, at the lower end of the small steel rod of 8mm diameter.

Most of the fabrication and machining work of creep machine has been accomplished in the Manufacturing and Production Engineering Laboratory of Aston University.

Some parts of the machine were purchased from the market which included:

(i) The hydraulic-jack with hand-pump.

(ii) The oil-bath.

(iii) The Silicone oil (Sil 300), which is used in oil-bath to heat the creep specimen up to the required test temperature.

(iv) A transducer.

(v) Nuts, bolts, and washers, used during the assembly of the machine.

(vi) Two linear-bearings.

(vii) A Personal Computer, with measurement and control software called 'Windmill'.

3.1.1 Heating Equipment (Oil-Bath)

Heating equipment (oil-bath) is a very important part of the creep machine. The main purpose of oil-bath is to heat the test specimen up to the required test temperature and also maintain this temperature up to the end of the experiment.

The oil-bath has been manufactured by Haake (Germany) and its technical specifications are according to German Standard DIN 58966. The size of oil-bath is 380×300×425mm,

while the bath can be filled up to 200mm of depth, which is about 80% of total depth. The total weight of bath is 17 k. The operating temperature of the oil-bath is 45 to 300°C and extended temperature range with additional cooling is -100 to 300°C. The heating capacity is 3000 W. The oil used is Sil 300, having flash point of 280°C which is much higher than the maximum test temperature of 160°C.

The required test temperature can be adjusted from the digital temperature setting mode, and the temperature display is also in digital form.

This oil-bath has been selected for the creep machine because of :

(i) Its high accuracy of temperature control.

(ii) Heating capacity.

(iii) The oil used fulfils the test temperature requirements due to its higher flash point.

(iv) The maximum operating temperature of bath is much higher than the highest test temperature.

3.1.2 Strain-Recording Equipment

The strain-recording equipment consists of a transducer, the strain indicator and the computer, and is shown in *Figure 3.2.*

The initial value of creep deformation was set before the application of load on the test sample. At the start of the experiment when the load was applied on the test specimen, creep began to occur, due to which the transducer core moved axially. Since this core was directly connected to the strain indicator, the creep strain (mm) was shown by the indicator. The values of creep deformation were shown according to the time intervals selected in the 'Windmill' computer software. This software has been purchased so that creep strain can be recorded precisely.

The 'Windmill' programme was modified according to the creep testing requirements. For this purpose, at the start of the test, the time interval between two readings of creep strain was very small, i.e. 5 seconds, which increased gradually and eventually the last time interval was one hour. The computer showed the creep data in the form of strain (mm) versus time (s).

The data file of each creep test was saved on the computer hard-disk, and copied to the floppy disk for further creep analysis.

3.1.3 Testing of Creep Machine

After assembly, the creep machine was tested to check its performance. For this purpose, the first two experiments were carried out on test specimens of ZA.8 and ACuZinc10. These tests were performed at a stress of 100 MPa at 100°C. The creep deformation was recorded on the plotter, which was already being used for tensile creep machines. The plotter was later replaced by the strain-indicator and computer, and the digital results compared with the plotter record. This showed that there were no errors in the settings of the data acquisition and analysis programme.

Another creep test was done on a mild-steel specimen at 100 MPa and 160°C. The resulting graph of this test exhibited almost no creep in the sample.

The results of these initial tests showed that the machine was working according to the required standards and the resulting graphs could be used for further creep analysis of these zinc-based alloys.

Figure 3.2. The strain-recording equipment.

CHAPTER 4

4.0 EXPERIMENTAL WORK

4.1 Experimental Alloys

4.1.1 Commercial Zinc-based Alloys

Three commercial zinc alloys, i.e. No3, No5 and No2 were used for both compressive creep and load-relaxation tests. Alloys No3 and No5 and pure aluminium were provided by Britannia Alloys and Chemicals Ltd. U.K. in the form of ingots with guaranteed composition, while alloy No2 was prepared at the foundry of Aston University.

To prepare alloy No2, high purity (99.99%) zinc and aluminium (99.985%) were used. The calculated amount of zinc and aluminium was melted in a standard box-type gas-air furnace at about 500°C. Since alloy No2 has also a copper content of about 2.8%, a calculated weight of hardener (50% Cu and 50% Al) was therefore added to the melt, and then vigorously stirred. Alloy No2 has a very small amount of magnesium (0.02 ~ 0.05%), and to avoid the loss of magnesium, it was added to the melt at as low a temperature as possible. The mixture was again vigorously stirred. The resultant alloy (No2) was then poured into a sand mould to prepare the required casting.

4.1.2 ACuZinc Alloys and ILZRO.16

Two ACuZinc (ACuZinc5 and ACuZinc10) alloys and ILZRO.16 were also used in the main compressive creep work and load-relaxation experiments. ILZRO.16 was provided by Britannia Alloys and Chemicals Ltd. U.K. in ingot form, whereas, ACuZinc5 and ACuZinc10 were prepared in the same way as alloy No2, except that the temperature was higher (600°C) for ACuZinc alloys.

4.1.3 Casting of Alloys

There are four major factors which should be considered during the development of moulding and casting methods. These four factors are:[126]

1. Size of Moulding.
2. Composition of alloys.
3. Mechanical properties of materials.
4. Production and economic factors.

Different methods are employed to cast the zinc-based alloys studied here which include sand casting, investment casting, die-casting, permanent-mould casting.

Sand-casting was used to cast all six alloys used in this research work because it allows a wide choice of alloys, size and design of castings and low tooling costs. Another reason was that these zinc alloys were not tested in the past for compression creep in sand-cast form.

4.1.3.1 Sand Casting

Among all gravity casting processes, sand casting is the most widely used. The traditional moulding material is a natural sand where the silica grains are coated with a film of clay. If the right proportion of moisture is present, this mixture can be squeezed or packed against a pattern and will take up and retain a complex shape.

Since sand is not a good conductor of heat, sand castings cool slowly and the resultant metallurgical structure of these castings is coarse-grained.

4.1.3.2 Preparation of Mould

The mould of the required shape and dimensions is very important for the production of sand castings, and different techniques are used for this purpose[127]. Since not too many castings of zinc alloys were required during this work, hand moulding was employed to prepare them.

The steps followed during the preparation of the mould are given below:

1. Fabrication of a metal-pattern 100mm long and 18mm in diameter. The pattern consisted of two identical parts. The split pattern was easier to mould, and it could be easily extracted after the sand was properly packed around it. The pattern was fabricated very carefully because the accuracy and quality of the pattern governs to a great extent the reproduction of a satisfactory mould, and thus the production of a casting of the correct dimensions.
2. The bottom half of the pattern was placed in the bottom half of the flask on a mould-board. Two bronze chills were also placed on each side of the bottom half of the pattern to help in preventing shrinkage cavities and promote soundness in the castings.
3. The bottom half of the mould was prepared by filling the bottom half of the flask with moulding sand. The sand used was Bromsgrove Red silica containing a small amount of Bentonite clay (about 12%) with the right proportion of moisture to activate the clay. For conventional moulding, a typical range of moisture content recommended is 3-3.5%.[143] It was very important to maintain this amount of moisture, because it controls all the strength properties of the sand mix and can markedly affect the quality of the

sand-castings. Therefore, during the mould preparation, the moisture content was maintained within the range of 3-3.5%.

The sand mix was now ready to ram. The ramming was done carefully and uniformly by using a wooden dolly, to achieve a greater degree of sand compaction. After ramming, the excess sand was struck off the flask with a trowel.

4. The bottom half of mould was rolled over and the top half of the pattern and flask placed in position.

5. The parting-powder (Talc powder) was applied on the prepared bottom half of the mould. This powder was very fine, clay-free and used to separate easily the top and bottom halves of mould. It was also helpful in smooth extraction of pattern from the mould.

6. The top half of the mould was prepared in the same manner as the bottom half. The flask was separated, the patterns were removed and the flask closed. Since most metals contract during the solidification[127] (average contraction about 5%), risers were utilised to supply molten metal to the casting and avoiding the formation of shrinkage cavities. The risers were cut with a tapered pipe. To be effective, the size of the risers was kept sufficient to provide extra metal, and ensured that it stayed molten until the casting itself had solidified. The risers also remained open to atmospheric pressure. The runners were prepared using a brass pipe to cut away the sand.

7. The successful production of clean and sound sand castings depends on the way by which the molten metal is fed into the mould cavity, and the arrangements made to accommodate the shrinkage that normally occurs on solidification.

8. Another important point to be considered was the proper gating system. The metal falls vertically inside the mould due to top-gating, with the consequent risk of splashing and sand erosion. To avoid this, the metal may be introduced at the lowest point of the mould, i.e. bottom-gating and to prevent the adverse temperature gradients produced by this procedure, ingates were provided which became inoperative in turn as the molten metal rose in the mould. Heart and Square was used for cutting the ingates. After which, the flask was closed.

All loose sand particles were removed from both top and bottom halves. The mould was closed in such a way that the flasks were perfectly registered without any crushing of mould or cross-jointing of the flasks. The top and bottom halves of flask were clamped together, using locating pins attached to one box.

9. The alloy was melted in the required amount in a standard box type gas air furnace, which can work up to a maximum temperature of 1100-1200°C. For the measurement of

furnace temperature, a standard Pyrotenax Chromel/Alumel thermocouple having a digital indicator, was used. It could work within an accuracy of ± 2°C. Standard fire-bricks were used as the lining of furnace. The air was provided from a blower and gas was supplied from the main supply-line.

10. The molten master alloy was transferred from the furnace via clay graphite pots (standard A4 size) to the ingot mould. The molten alloy was then poured into the mould in the required amount. Lifting tongs were used to take out the molten alloy from furnace , while pouring tongs were used to pour the material into mould. After pouring the molten alloy, it was left for about half an hour to cool.

11. After cooling, the casting was broken out of its mould and flask manually, and it was ready for the remaining processes, i.e. cleaning and fettling.

4.2 Compressive Creep Testing

The compressive creep tests were performed mainly with the conventional zinc alloys, No3, No5, and No2 and two ACuZinc alloys, i.e. ACuZinc5 and ACuZinc10. Some creep experiments were also done with ILZRO.16. These tests were carried out at temperatures of 70°C, 100°C, 130°C and 160°C with a stress range of 20 MPa to 100 MPa. This temperature and stress range was chosen to test these alloys for creep at lower and comparatively higher temperatures and stresses. Most of the tests were done in duplicate to better establish the creep behaviour of the alloys. A few tests were performed in triplicate, if duplicate experiments were not enough to determine the creep behaviour of the alloys.

4.2.1 The Creep Test Specimen

The test piece used in the compressive creep experiments is shown in *Figure 4.1 (a)*. The test specimens for all creep experiments were machined from the castings in the Manufacturing and Production Engineering Laboratory of Aston University. The specimens were of cylindrical shape, having the following finished dimensions:

length = 30mm, diameter = 13mm, and bore (plain) = 8mm

First of all, a length (rod) of casting was cut in such a way that two or three test pieces could be prepared from it. The diameter of this rod was then rough machined on a lathe, and reduced nearly to the required diameter of the specimen, i.e. about 14mm. To achieve an 8mm bore in the rod, a 6mm drill was initially used followed by an 8mm drill in order to prevent material destruction. After which, the outer diameter of test piece

was reduced to 13mm by fine machining on the lathe, which was the last step in the preparation of the specimen.

The machining operation during the production of these test pieces was carefully controlled so as to reduce surface finish variations to a minimum.

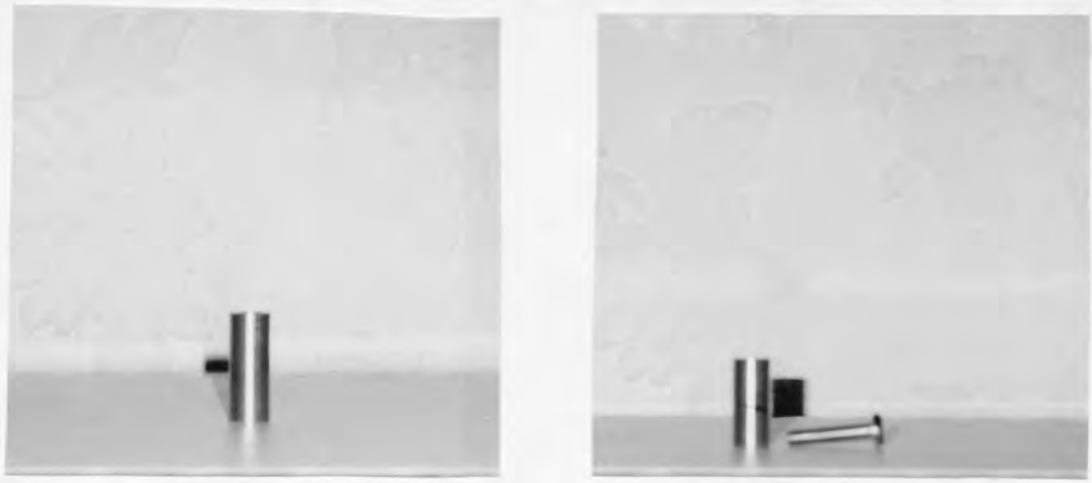

(a) *(b)*

Figure 4.1. Test pieces used for (a) creep testing (b) load-relaxation testing with screw.

4.2.2 Compressive Creep Machine and Strain-Recording Equipment

A standard weighted lever arm compressive creep machine, designed by the present author and his colleague, was used for creep tests.

The complete design and description of the creep machine and its accessories including the strain-recording equipment, is given in Chapter 3.

4.2.3 Creep Test Procedure

First of all, the test specimen was loaded and the transducer core fixed into the small rod passing through the test piece. Then the oil-bath was set at the required test temperature and switched on. The temperature of the specimen inside the oil-bath was measured by a digital potentiometer, using chromel/alumel thermocouples which were attached to the test piece, in order to check and avoid any temperature gradients along the gauge length of the test piece.

Before the start of the experiment, a reasonable time (about 1 hour) was allowed for the temperature of oil-bath and test piece to stabilise, and temperature changes were limited to a maximum of $\pm$ 1°C for the whole period of the test. The oil-bath was raised to the

required level manually through a square-threaded rod, and it was confirmed that the test piece and the structure of steel plates along it were dipped in oil.

In order to obtain the required stress level on the test piece, a suitable weight was calculated by taking into account the lever arm ratio. The calculated weight was put on the hanging weight pan, and the hydraulic-jack was used to hold this weight. When the required test temperature was attained after some time, the load was applied on the test piece through hydraulic-jack by loosening its knob. The resulting creep deformation was recorded by the strain-recording equipment, and displayed by the computer.

The procedure of recording creep contraction was very simple and straightforward. Before the start of experiment, the reading on the strain-indicator would be in the range $\pm$ 0.01, and this range was obtained by rotating the transducer core in the clockwise or anti-clockwise direction. As soon as the load was applied to the test piece, the creep strain could be observed on the strain-indicator in digital form. The values of creep strain (mm) versus time (s) were also shown by the computer through a measurement and control software called 'Windmill', which was designed particularly for these types of tests. The strain-indicator and computer were used to obtain the accurate and precise creep strain measurements. The experiments were conducted to a minimum creep deformation of 1%. The strain measurements of each creep test were then saved as a separate file on floppy-disk, and used for further creep analysis of these alloys. Since most of the experiments were carried out in duplicate, the mean values were therefore used to investigate the creep behaviour of the alloys.

4.2.4 Precautions during Creep Tests

The following precautions were essential to acquire reliable data from the creep tests:

1. The load applied should not be variable during the whole test period.
2. The temperature variations of oil-bath should be within $\pm$ 1°C.
3. The test piece loading train must be aligned properly, otherwise the resulting creep strain will not be reliable.
4. Thermocouples should be firmly in contact with the surface of the specimen, so that its temperature can be detected accurately.

4.3 Load-Relaxation Testing

All six zinc-based alloys were also used for load-relaxation testing. The load-relaxation tests were carried out at three different temperatures, i.e. 80°C, 100°C and 120°C, using an initial preload of 6000 N. All load-relaxation tests were duplicated to better establish the behaviour of these alloys. Some tests were done more than twice where the duplicate experiments were not enough to establish the load-relaxation behaviour of alloys.

4.3.1 The Load-Relaxation Test Specimen

The test specimen used for load-relaxation tests is shown in *Figure 4.1 (b)*, which is also of cylindrical shape, having the following size:

length = 30mm, diameter = 13mm, and bore (threaded) = 6mm.

The threads (M6 × 1) were according to ISO standards.

The specimens for load-relaxation experiments were also produced in the Manufacturing and Production Engineering Laboratory of Aston University. They were fabricated in the same manner as creep test specimens. The only difference in creep and load-relaxation test pieces was that of bore type and size, i.e. in a creep test piece, the bore was 8mm and plain, whereas in the load-relaxation specimen, the bore was 6mm with threads. These threads were cut with a thread-cutting tap. The test pieces for both types of experiments were fabricated very carefully, so that variations in the size could be minimised.

4.3.2 Load-Relaxation Testing Equipment

The equipment used for load-relaxation tests consists of oil-bath, load-monitoring device, and a data-acquisition system.

The oil-bath is used to heat the specimen and maintain the desired temperature throughout the test. The oil-bath has a capacity of 30 liters, and can work up to the maximum temperature of 150°C. The oil used was Vitrea (32). A stirrer was used to circulate the oil and thus achieve a uniform temperature throughout the bath. A temperature controller is attached to the oil-bath which shows the temperature of oil in digital form, and also controls the test temperature with an accuracy of ± 0.1°C. At one time, up to seven specimens can be tested in the oil-bath. The oil-bath is shown in *Figure 4.2*.

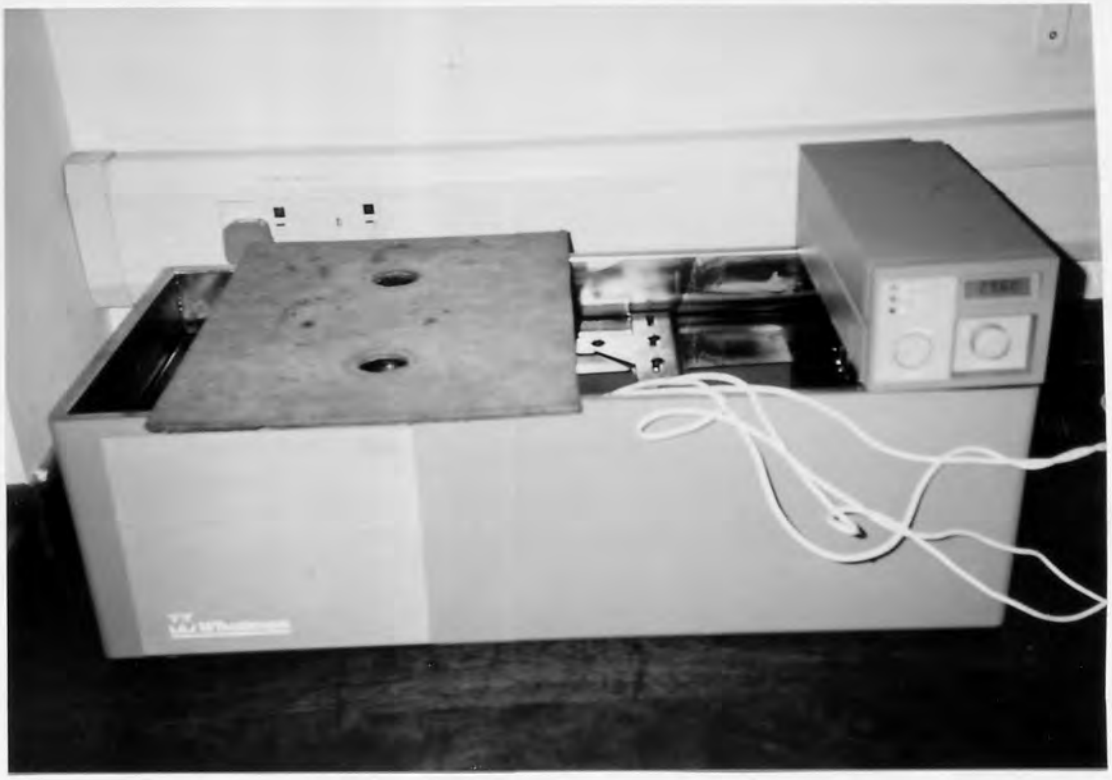

Figures 4.2. The oil-bath used in load-relaxation experiments.

The load-monitoring device was used for the continuous monitoring of load in the commercial fasteners used. It consists of a short tension rod to which the head of the fastener is attached, which reacts the tensile stress in the fastener through a compression load cell. When the casting was screwed onto the fastener, it simulated the effect of inserting a screw into a hole. The load cell (doughnut shaped) was a purchased item, used to measure the force exerted on the screw thread of a casting. It was a small, high capacity load cell, having a range of 0.15 to 13600 k. Its operating temperature range is -54°C to 121°C. The casting material was stainless steel and it was said to be safe for 50% overload. The load cell is shown in *Figure 4.3.*

The data acquisition (logging) system is used to record the results of load relaxation tests. The system called Translog 500, is a comprehensive hardware and software package for the retrieval, recording, alarm monitoring and computation of data from transducers of many kinds. It was manufactured by RDP Electronics Ltd. U.K. It has modular construction which is easily expandable. The system has digital filtering for high resolution and can scan very fast, i.e. up to 100 channels/second. Calibration facilities including push button zero setting and auto-scaling in engineering units has been provided.[1]

[1] *All informations about data acquisition system (Translog 500) has been provided by RDP Electronics Ltd.*

The system has a host computer data logging programme, which can be used with any computer having the necessary RS232 serial interface, and can be linked with spreadsheets such as Lotus 123. It is very user friendly with simple English word commands. 32 software comparators each with High (HI) and Low (LO) set-points can be used to monitor transducer channels and operate relays. There are input/output modules for set point or programmed commands. Variable speed logging is another useful feature provided by the programme. This allows the user to program the data-logging speed to suit the application, e.g. at the start of a logging RUN, it is often necessary to take lots of data readings, and then slowing down as the RUN progresses.

Data-logging may be directed to floppy disk, hard disk, ram disk, or printer, and data storage is only limited by the disk capacity. The system is suitable for short and long-term data-logging.

4.3.3 Load-Relaxation Test Procedure

A M6 × 1 (ISO standard) threaded screw was locked into the tension rod, and the load monitor assembled. The test piece was then threaded onto the screw up to 16mm depth, which was the desired engagement of screw. The entire monitoring assembly was dipped into the hot oil at a constant required test temperature, and left for about 3 hours to equilibrate.

To start the experiment, the tension rod and screw were loaded by turning the fine-pitch nut at the top of the rod. This process was continued until the initial load of approximately 6000 N which was recorded by the load cell , could be achieved. This whole process completed in a very short time, i.e. 15 ~ 20 s.

The data-acquisition (logging) system was started as tightening commenced. The preload loss was then continuously monitored by the load cell for a period of up to about 160 hours, after which the test was terminated. Up to four tests were carried out simultaneously, and the test temperature was kept constant with a variation of ± 0.5°C. The results of experiments were recorded by data-acquisition system, and displayed on a computer in the form of load (N) relaxed versus time (s).

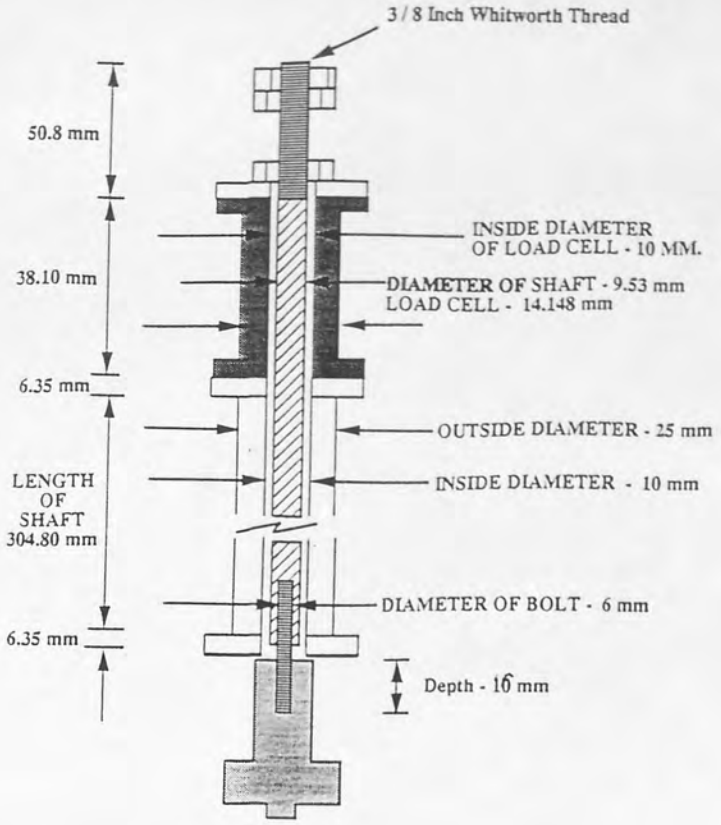

Figure 4.3. The load monitoring cell.

All load-relaxation tests were carried out in duplicate, and if results were not satisfactory, i.e. appreciable scatter was found in the results, some additional tests were also performed at those particular test conditions. The average values of the results were calculated and the mean values taken to represent the load-relaxation behaviour of the alloys.

4.4 Metallography

4.4.1 Scanning Electron Microscopy (SEM)

Samples from each alloy in the as-cast condition and after the creep tests, were examined by scanning electron microscopy to study the structures and the effects of compressive creep on microstructures. To observe the structures of alloys in the as-cast condition, samples were cut from as-cast components. These were mounted in bakelite, and ground on silicon carbide papers, followed by polishing using diamond abrasive to a final finish of 1μm to obtain a scratch-free mirror surface. Similarly, to study the effects of creep deformation on microstructure of alloys, samples were cut from the cross-section and longitudinal side of the creep-tested specimen. These samples were prepared in the same manner as those of the as-cast alloys.

To obtain better resolution and to take advantage of the big difference between atomic numbers of two main constituent elements (Zn and Al) of the alloys, backscattered electron scanning electron microscopy was adopted as the general investigation method, since by using backscattered electrons, contrast could be achieved from the difference in average atomic number (Z) of various phases in the sample. Higher Z regions have more nuclear charge, and hence give rise to a great number of backscattered and smaller number of absorbed electrons than low-Z regions. For this purpose, the scanning electron microscope, Cambridge Instruments SEM fitted with a special large area, backscattered electron detector was used.

4.4.2 Optical Microscopy

Samples of alloys No2, ACuZinc5 and ACuZinc10 after the creep tests were also prepared for optical microscopy. The procedure of preparation was similar to SEM except after the final finish of 1μm, 2% Nital was used as an etchant for a varying length of time depending on the alloy. After etching, the samples were ready to examine by optical microscopy, and an optical microscope was used for this purpose.

CHAPTER 5

5.0 EXPERIMENTAL RESULTS

5.1 Chemical composition of the Experimental Alloys

The chemical composition of the alloys was determined by atomic-absorption spectroscopy and the results are given in *Table 5.1.*

Table 5.1. Chemical composition of the experimental alloys (wt. %).

Alloy	Al	Cu	Mg	Ti	Cr	Zn
No3	4.23	0.008	0.05	-	-	Balance
No5	3.96	0.84	0.04	-	-	"
No2	4.21	2.79	0.03	-	-	"
ACuZinc5	3.07	5.20	0.04	-	-	"
ACuZinc10	3.51	9.33	0.03	-	-	"
ILZRO16	0.002	1.36	-	0.21	0.14	"

5.2 Compressive Creep Results of Alloys

For all compressive creep experiments of the alloys, the results are presented in the form of graphs plotted as creep strain (ε) versus time (s).

In all cases, the curves showed the same general form, i.e. a primary creep stage which exhibited a steadily decreasing strain rate, followed by a linear steady-state region (secondary creep). Since most of the creep experiments were conducted to produce a minimum creep strain of 1-1.5%, which was usually reached in the secondary creep region, the tests were not generally allowed to proceed into the tertiary creep region. However, some curves showed a tertiary region when the alloys were tested for longer times at higher stress and temperature, e.g. alloy No3 at 100 MPa and 160°C, and No5 at 100 MPa and 160°C or 60 MPa and 130°C.

In some tests, 1% creep strain was reached rather early in the creep process, due to which the exact secondary creep rate was difficult to calculate, the experiments were therefore extended in those cases until well defined secondary creep regions were obtained.

Since a large number of experiments were done to investigate the compressive creep behaviour of alloys, it was therefore difficult to include the creep curves of all tests.

However, some examples of creep curves were selected to show the characteristic time-creep strain (%) behaviour of the alloys tested, as seen in *Figures 5.1 to 5.6*. The comparisons of the creep strains (%) for alloys under different testing conditions, are also shown in *Figures 5.7 to 5.9*. From these curves, it was observed that in general, alloy No3 had the least primary creep and No2 the greatest. Also, the secondary creep regions of alloy No3, were comparatively shorter than alloys No5, No2, ACuZinc5 and ACuZinc10. Alloys No5, No2, ACuZinc5 and ACuZinc10 had prolonged secondary creep regions, and generally for No2 it was the greatest. Secondary creep rates (ε_s) were calculated from the steady-state parts of the creep curves, using linear regression analysis. The slope of the regression was taken to be the value of the secondary creep rate and the intercept of the slope on the strain ordinate at zero time, the primary creep strain including instantaneous creep strain. In addition to secondary creep rates and primary creep contractions, the times to produce a creep strain of 1%, 0.7%, 0.5% and 0.2% were also calculated from these curves. The creep data of alloys No3, No5, No2, ACuZinc5 and ACuZinc10 are tabulated in Appendix A for each test condition.

ILZRO.16 was tested only at high stress and temperatures, and the results at these test conditions showed that ILZRO.16 was the most creep-resistant among all six alloys tested. The creep data of ILZRO.16 at these test conditions can be seen in Appendix A. Generally, ACuZinc5 had higher creep strength than ACuZinc10.

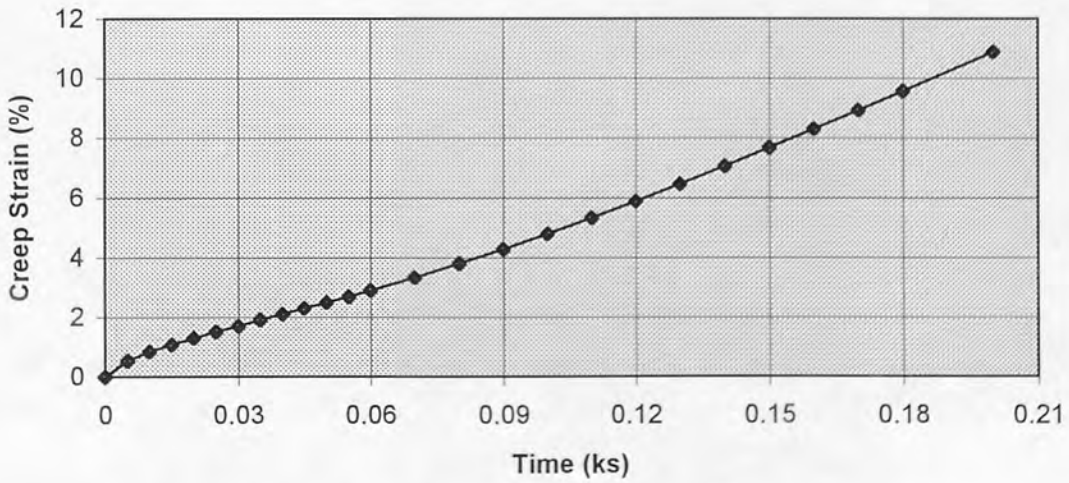

Figure 5.1. Creep curve of alloy No3 at 100 MPa and 160° C.

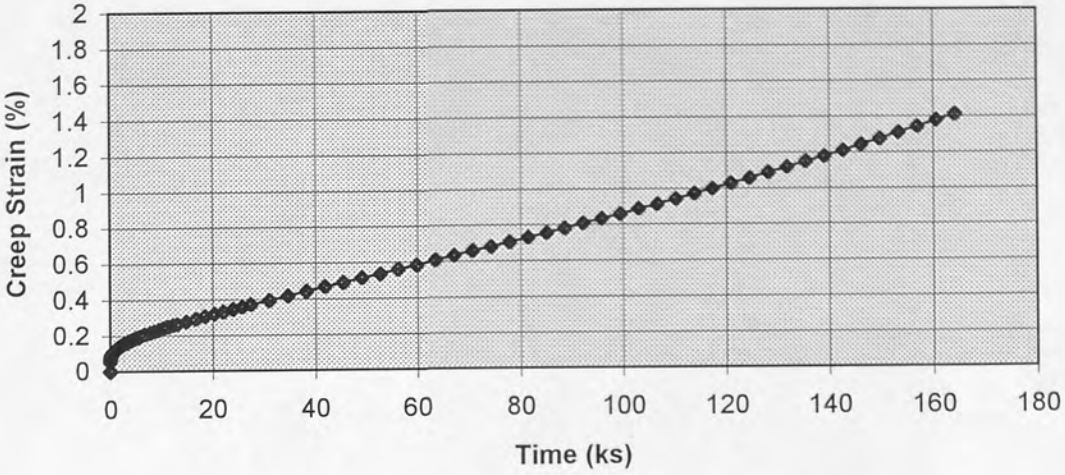

Figure 5.2. Creep curve of alloy No5 at 40 MPa and 130° C.

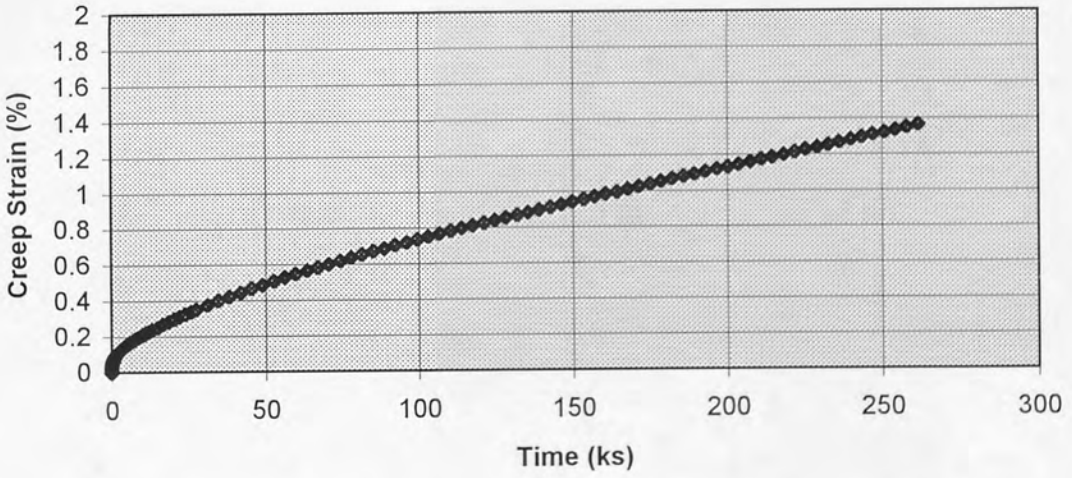

Figure 5.3. Creep curve of alloy No2 at 40 MPa and 130° C.

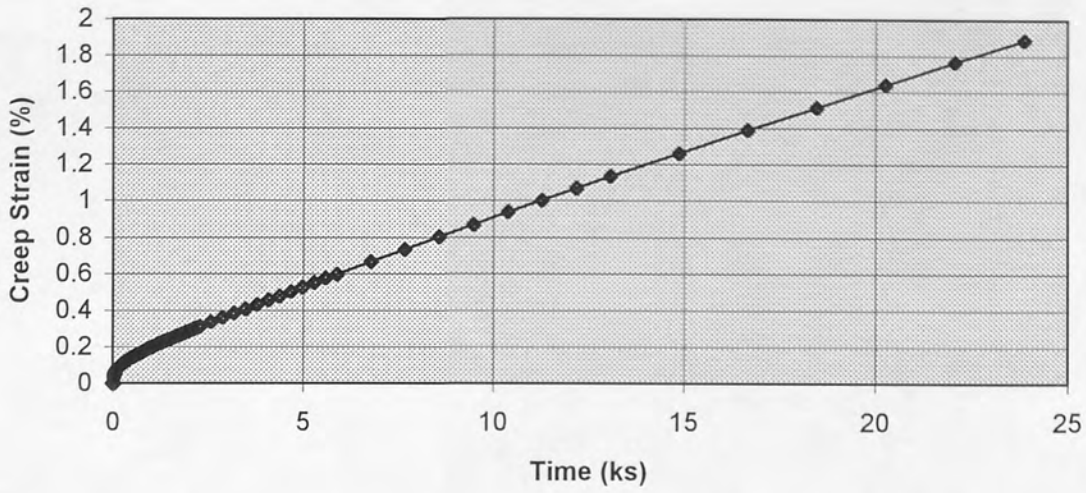

Figure 5.4. Creep curve of ACuZinc5 at 40 MPa and 160° C.

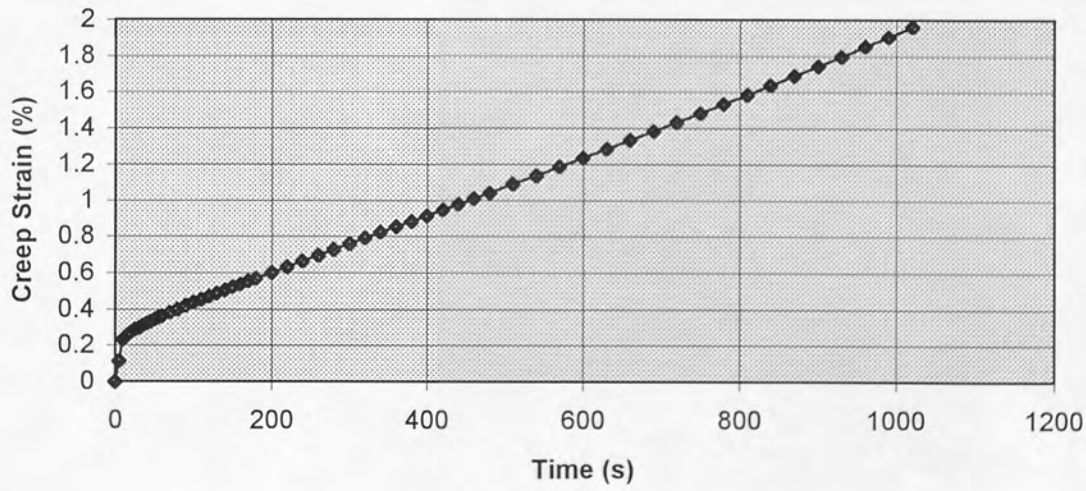

Figure 5.5. Creep curve of ACuZinc10 at 100 MPa and 160° C.

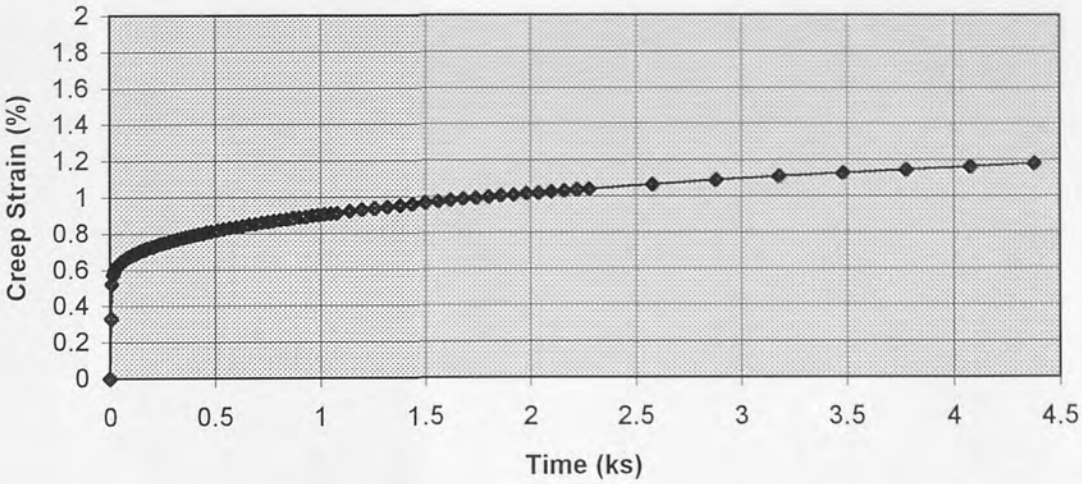

Figure 5.6. Creep curve of ILZRO.16 at 100 MPa and 160° C.

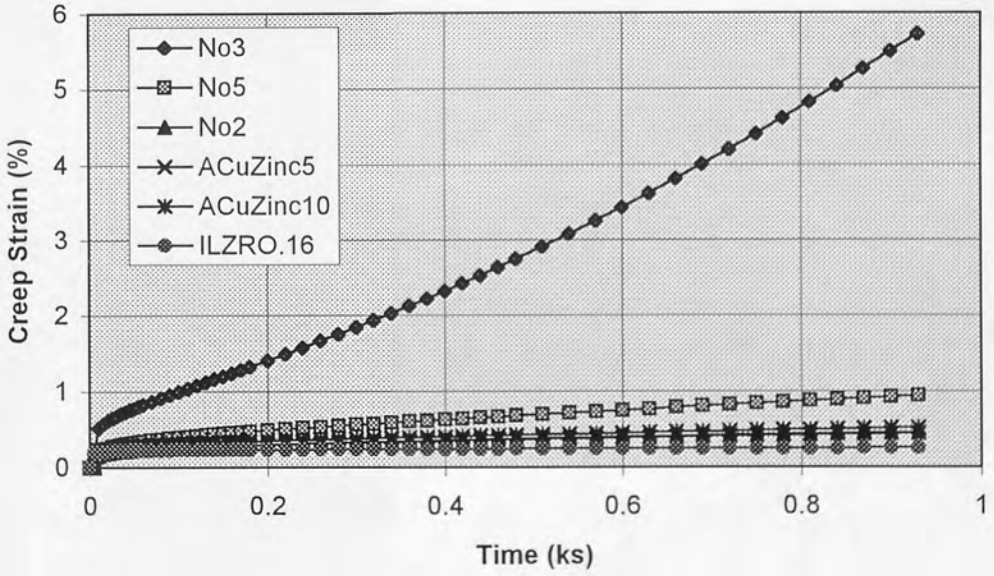

Figure 5.7. Comparison of creep curves for alloys at 100 MPa and 130° C.

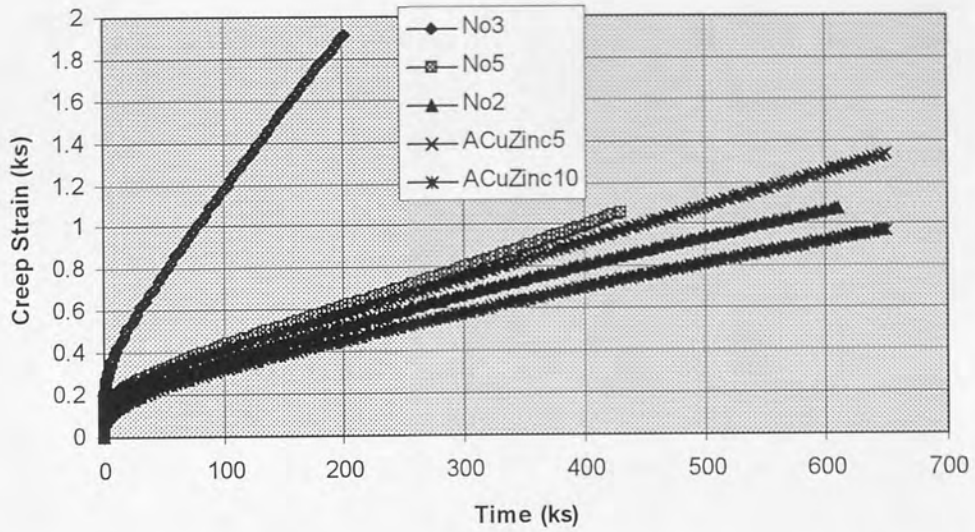

Figure 5.8. Comparison of creep curves for alloys at 60 MPa and 100° C.

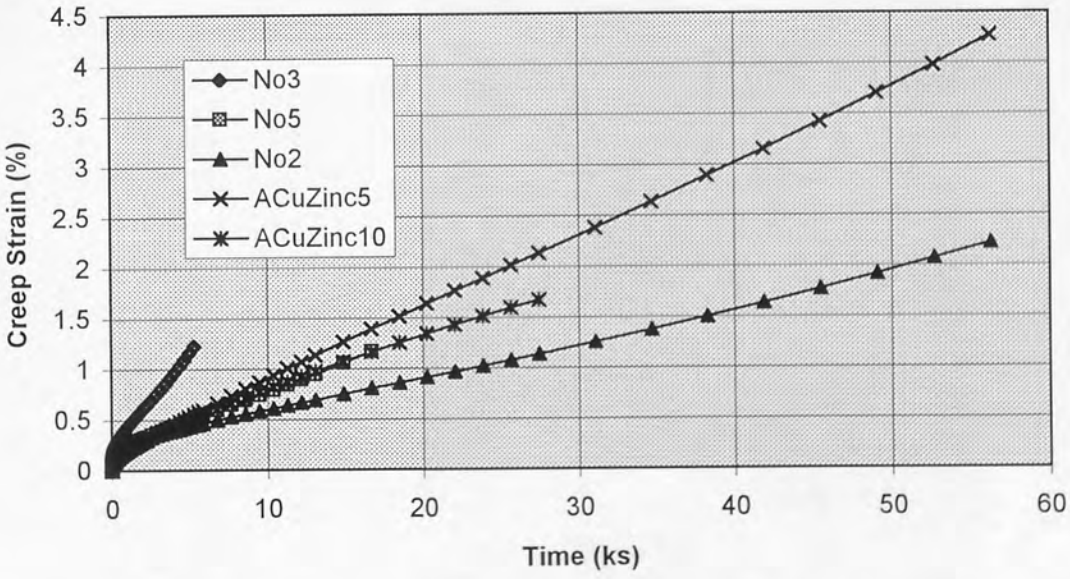

Figure 5.9. Comparison of creep curves for alloys at 40 MPa and 160° C.

5.2.1 Primary Creep of the Experimental Alloys

The values of primary creep contraction were obtained by extrapolating the linear secondary creep portion of the curves back to zero time. The values of primary creep (%) were calculated for all alloys.

The results of the creep experiments revealed that for commercial zinc-based alloys (No3, No5 and No2), the average primary creep (%) decreased with increasing temperature (*Figure 5.10*), e.g. the average primary creep of alloy No3 at 70°C was 0.40% which decreased to 0.21% at the higher temperature of 160°C. The creep results also showed that primary creep was dependent on the applied stress, and generally increased with the increase of stress. At 20 MPa, the average primary creep of these alloys was much lower than at higher stress of 100 MPa. It was observed that the average primary creep of alloy No3 was generally lower than the other two commercial alloys under all testing conditions.

In both ACuZinc5 and ACuZinc10, the primary creep decreased with the increase of temperature, as shown in *Figure 5.10*. Stress had a clear effect on primary creep of ACuZinc alloys, and in general primary creep increased with increase of stress, as it did in commercial alloys. ACuZinc5 had primary creep values higher than those of ACuZinc10 except at the lower stress of 40 MPa and comparatively high test temperatures.

From the results of creep experiments, it was concluded that for all alloys tested, the average primary creep (%) decreased with the increase of temperature, and increased with increasing stress.

Another important finding of these tests was that the primary creep contraction of commercial zinc alloys increased with increasing copper content. From the results, the average values of primary creep contraction for alloys were calculated, and plotted against the copper content of the alloys as shown in *Figure 5.11*, which yielded a linear relationship between primary creep and the copper content within the composition range of commercial zinc alloys, but this was not true for ACuZinc alloys and the average primary creep of ACuZinc5 was higher than that of ACuZinc10.

The mean value of the contribution of primary creep to a certain total creep strain for each alloy was calculated and found to be 0.29, 0.31, 0.32, 0.34 and 0.31% for alloys No3, No5, No2, ACuZinc5 and ACuZinc10, respectively.

5.2.2 Secondary Creep Rate

Secondary creep rates ($\dot{\varepsilon}_s$) of the experimental alloys were calculated from their creep curves. The secondary creep rates of commercial alloys and ACuZinc alloys under different testing conditions were plotted in the form of $\ln \dot{\varepsilon}_s$ (s^{-1}) versus ln stress (σ), as shown in *Figures 5.12, 5.13, 5.14, 5.15 and 5.16*. According to the power law equation ($\dot{\varepsilon}_s = A\sigma^n$), the plot should yield straight line with a constant slope at a constant test temperature. The figures showed a reasonably fair correlation with constant slopes for all alloys tested over much of the stress and temperature range, although small deviations were observed at low stress level in alloys No3 and No5 at 100 °C and 70°C, which were not unusual in the creep experiments. The slopes found for alloys No3, No5, No2, ACuZinc5 and ACuZinc10 showed that the values of the stress exponents were much higher for alloy No3 than alloys No5, No2, ACuZinc5 and ACuZinc10. The values of the slopes yielded the important fact that these values decreased with the increase of copper content in the commercial zinc alloys (No3, No5 and No2). The stress exponents for alloys are given in *Table 5.2*.

Table 5.2 : The Average Stress Exponents (n) of Alloys.

Alloy	Stress Exponent (n)
No3	5.10
No5	4.20
No2	3.80
ACuZinc5	3.70
ACuZinc10	4.00

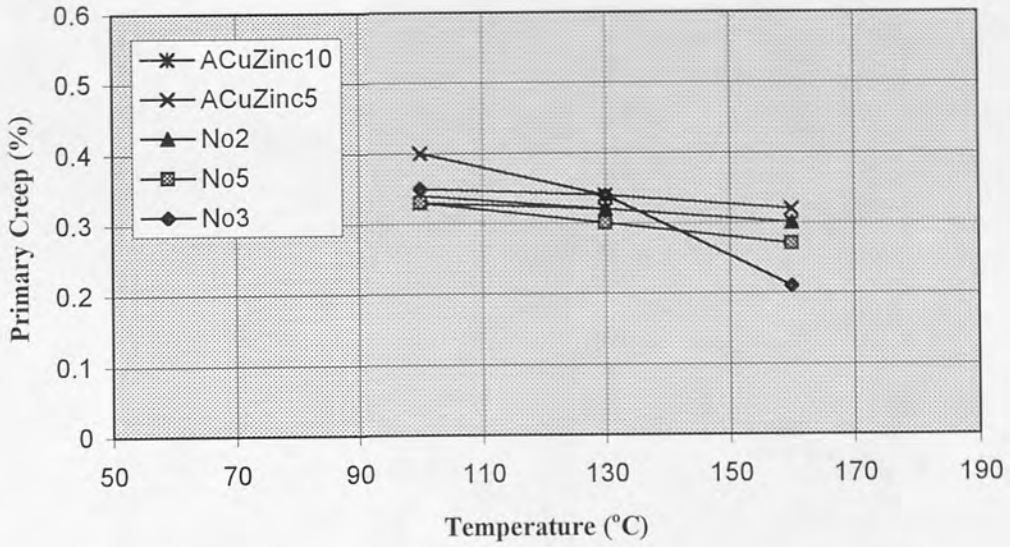

Figure 5.10. Variation of average primary creep contraction of alloys with temperature.

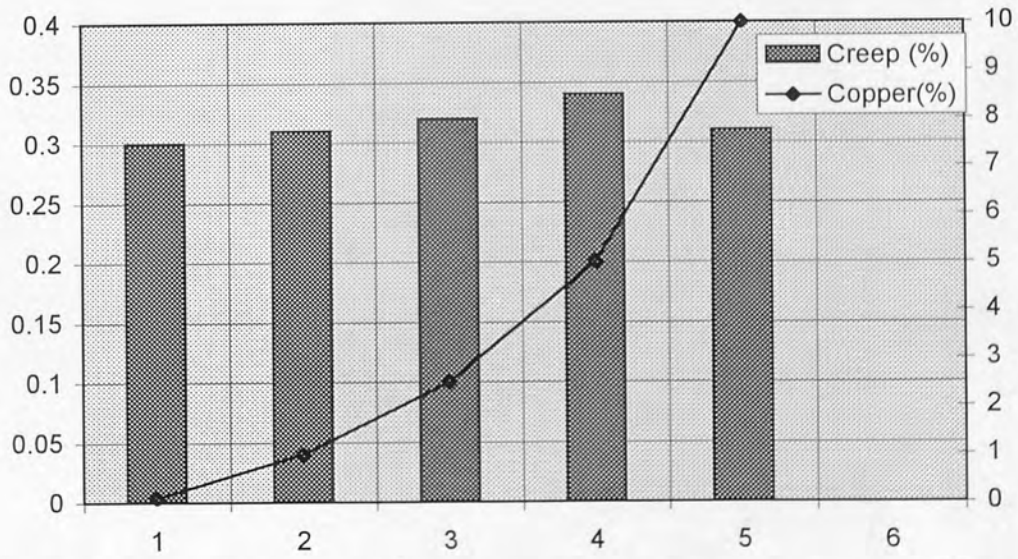

Figure 5.11. Variation of the average primary creep contraction of alloys with increasing Copper content.

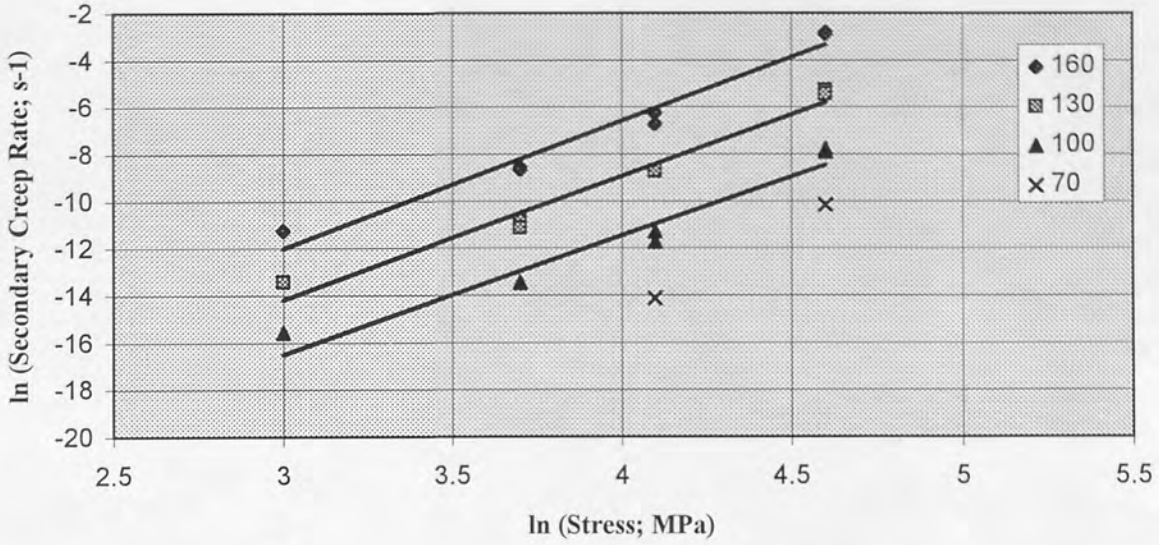

Figure 5.12. Variation of secondary creep rates with applied stress at different temperatures for alloy No3.

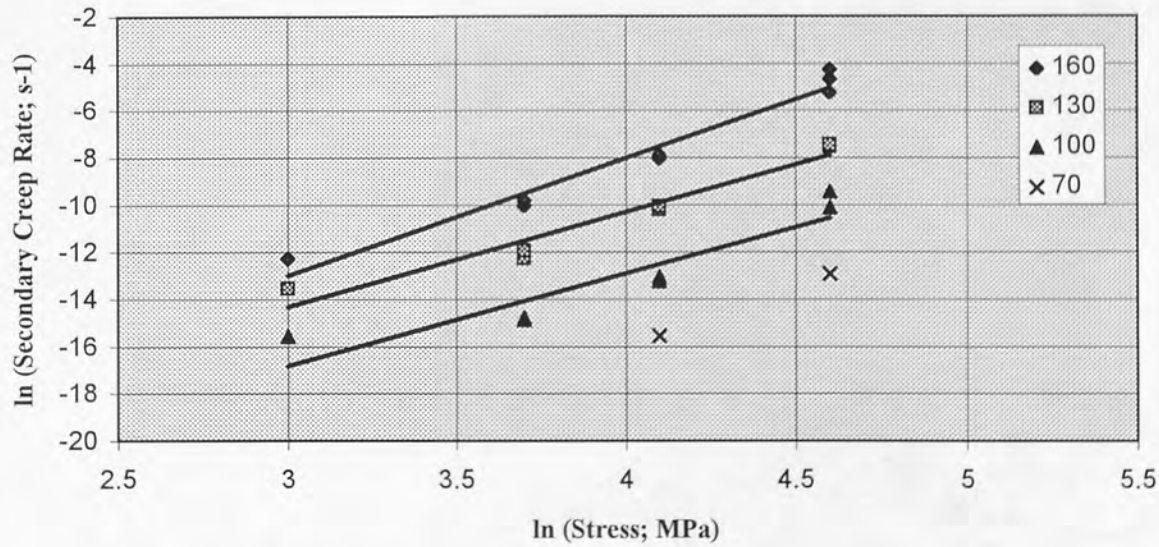

Figure 5.13. Variation of secondary creep rates with applied stress at different temperatures for alloy No5.

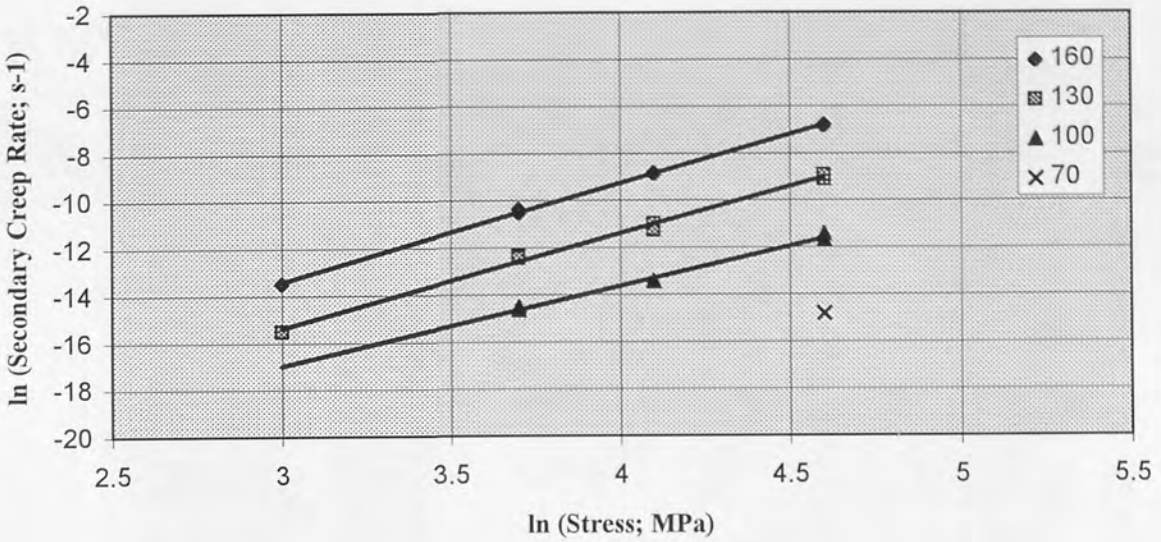

Figure 5.14. Variation of secondary creep rates with applied stress at different temperatures for alloy No2.

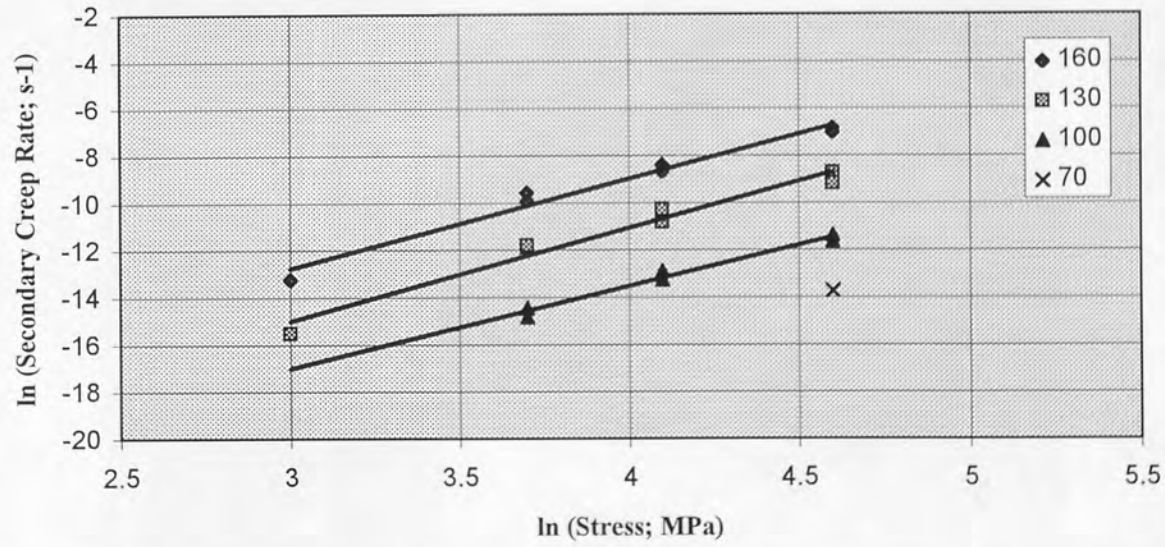

Figure 5.15. Variation of secondary creep rates with applied stress at different temperatures for ACuZinc5.

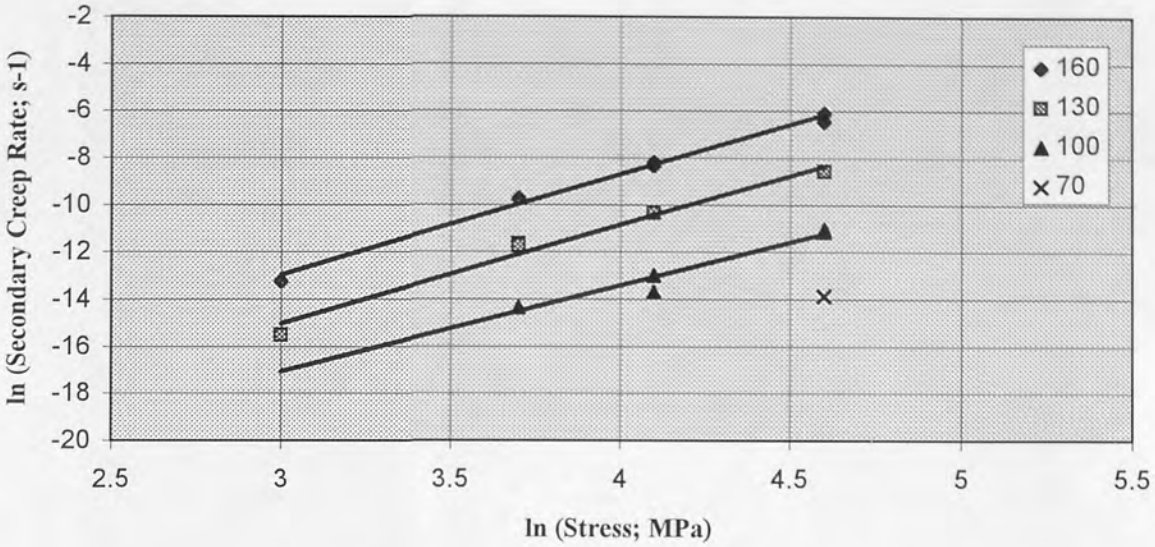

Figure 5.16. Variation of secondary creep rates with applied stress at different temperatures for ACuZinc10.

From these graphs, the secondary creep rates at fixed stresses of 20 MPa, 40 MPa, 60 MPA and 100 MPA for the temperature range of 70°C to 160°C were found. Some inconsistency was observed in secondary creep rates of alloys No2 and No5 at 40 MPa and 100°C. It was noted that at this test condition, alloy No5 had lower secondary creep rate that alloy No2.

From these graphs, the secondary creep rates for a fixed stress of 100 MPa were obtained for alloys and listed in *Table 5.3* for the temperature range of 100 to 160°C.

Table 5.3 : Secondary Creep Rates (s^{-1}) of alloys at 100 MPa.

Temp. (°C)	100	130	160
No3	4.21×10^{-4}	5.07×10^{-3}	6.04×10^{-2}
No5	4.03×10^{-5}	5.38×10^{-4}	5.30×10^{-3}
No2	1.09×10^{-5}	1.32×10^{-4}	1.13×10^{-3}
ACuZinc5	1.14×10^{-5}	1.63×10^{-4}	1.09×10^{-3}
ACuZinc10	1.43×10^{-5}	1.88×10^{-4}	2.22×10^{-3}

5.2.3 Total Creep Contraction

From the creep curves, the times to produce 0.2%, 0.5%, 0.7% and 1% creep strain were obtained. Using the values of times to produce 1% creep strain, the graphs were plotted as ln time (s) versus the reciprocal of the test temperature (K) at different stresses, i.e. 40, 60 and 100 MPa for all the alloys. These plots are shown in *Figures 5.17, 5.18, 5.19, 5.20, 5.21 and 5.22*. According to Arrhenius-type equation, such a plot should yield a straight line of slope (Q_c/R) and therefore the activation energy for creep (Q_c). It was observed that straight lines were obtained for each alloy although deviations were observed at lower stresses and temperatures for alloys No3 and No5. From these slopes of lines, the activation energies for alloys were calculated and listed in *Table 5.4*.

Table 5.4 : The Calculated Activation Energies (Q_c) of Alloys.

Alloy	Activation Energy of Creep (kJ/mole)
No3	103
No5	108
No2	99
ACuZinc5	103
ACuZinc10	107

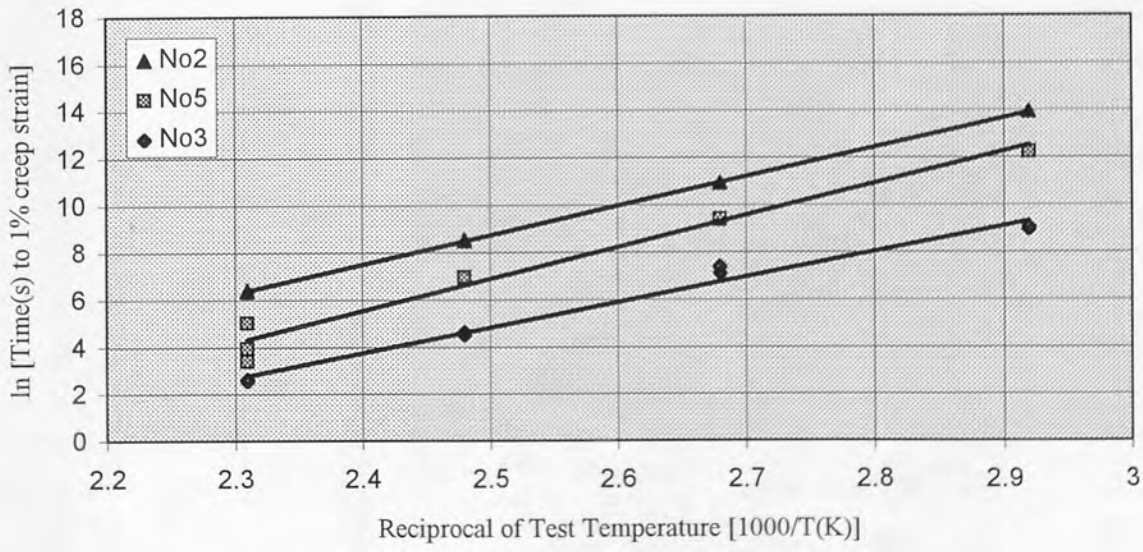

Figure 5.17. Ln time to 1% creep strain versus reciprocal of test temperature at 100 MPa for alloys No3, No5 and No2.

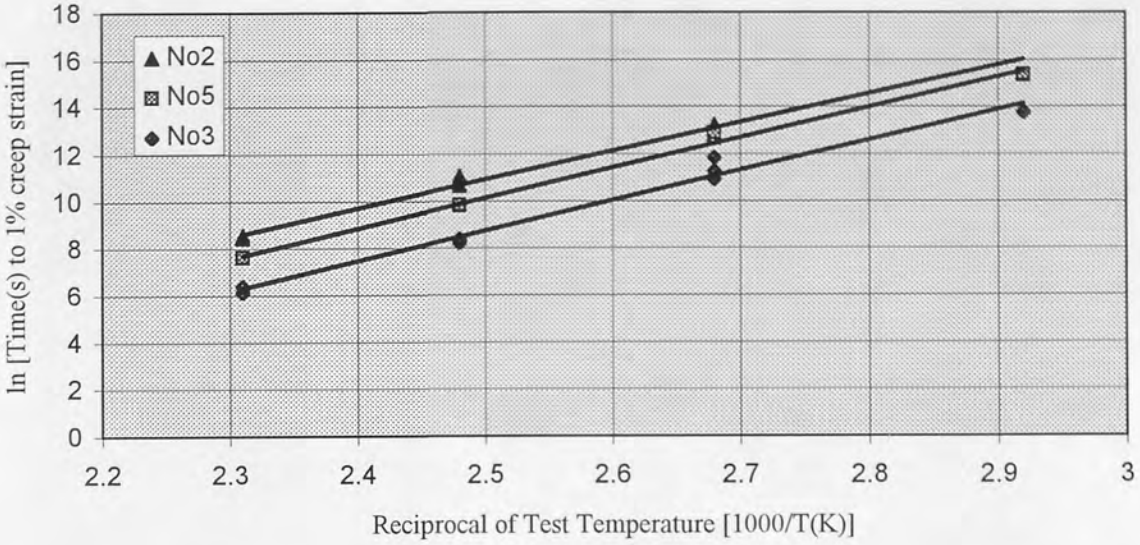

Figure 5.18. Ln time to 1% creep strain versus reciprocal of test temperature at 60 MPa for alloys No3, No5 and No2.

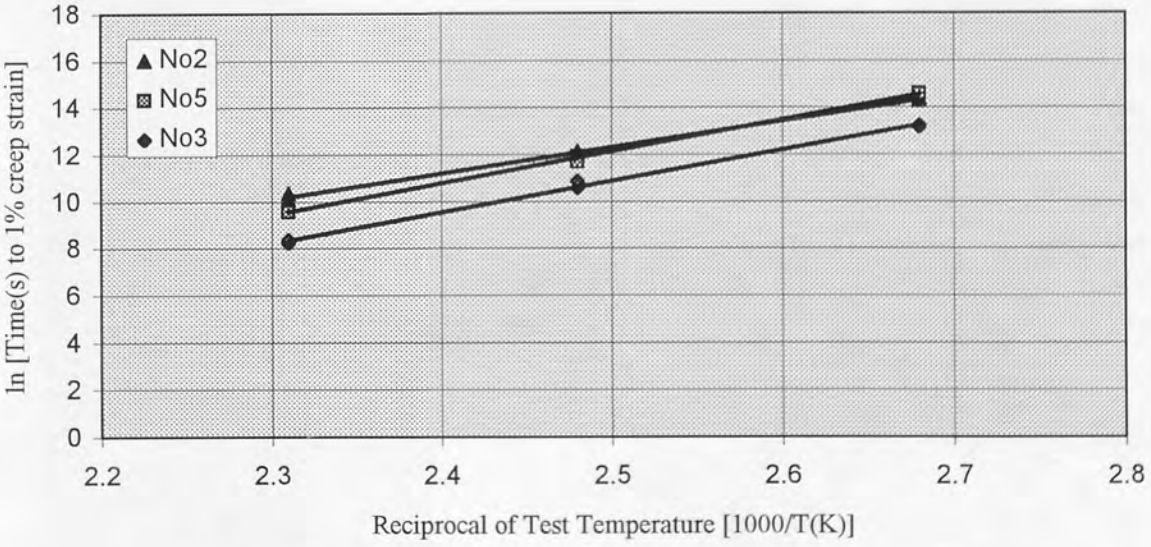

Figure 5.19. Ln time to 1% creep strain versus reciprocal of test temperature at 40 MPa for alloys No3, No5 and No2.

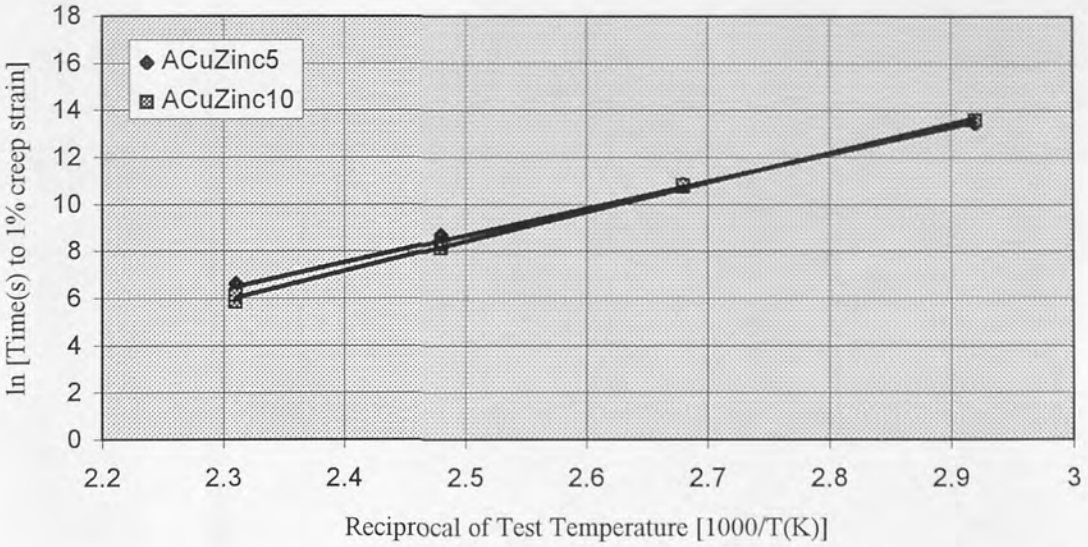

Figure 5.20. Ln time to 1% creep strain versus reciprocal of test temperature at 100 MPa for ACuZinc alloys.

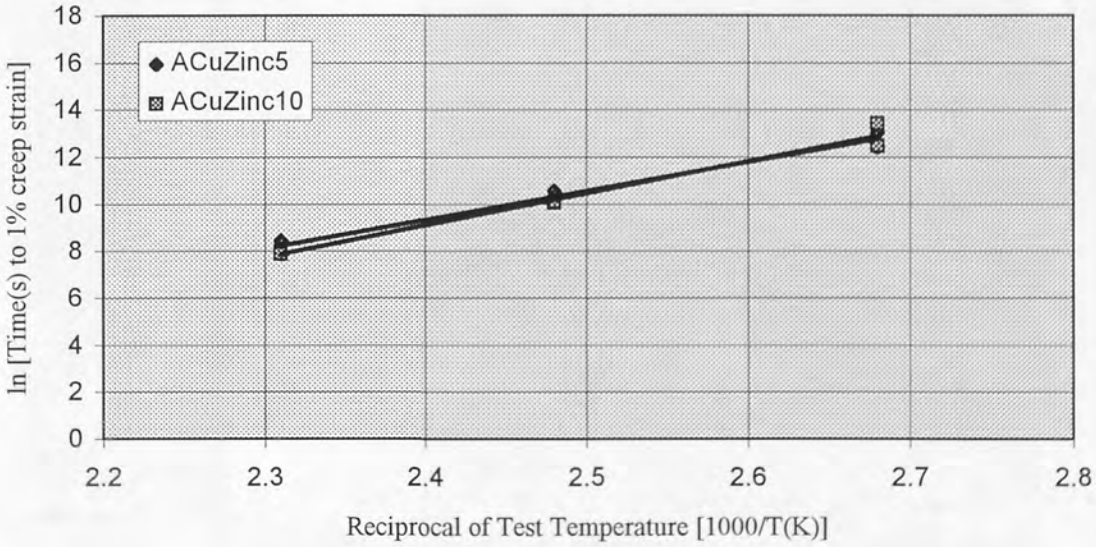

Figure 5.21. Ln time to 1% creep strain versus reciprocal of test temperature at 60 MPa for ACuZinc alloys.

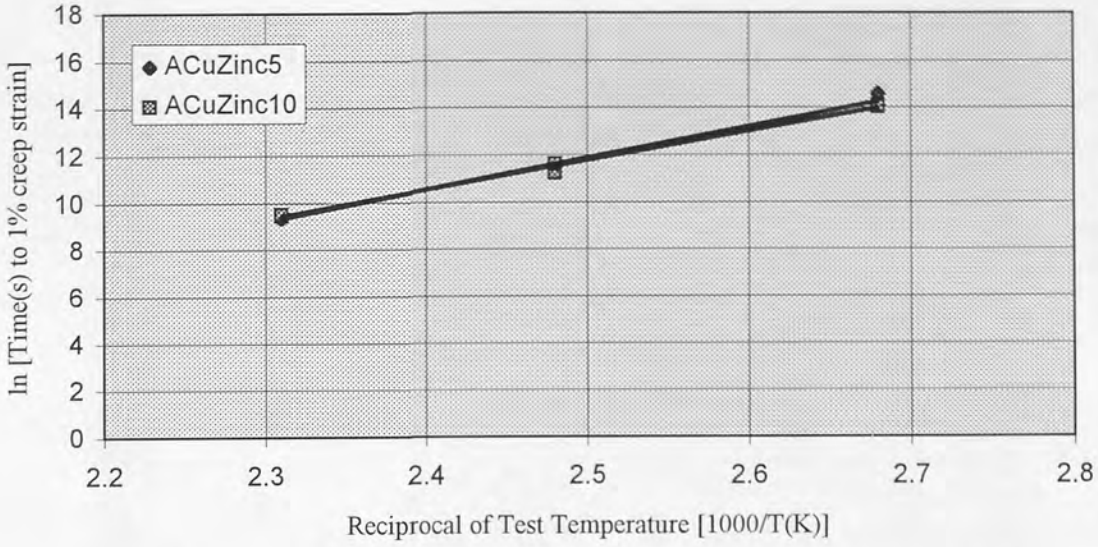

Figure 5.22. Ln time to 1% creep strain versus reciprocal of test temperature at 40 MPa for ACuZinc alloys.

5.3 Results of Load-Relaxation Tests

For all load-relaxation tests of the experimental alloys, the results are given in the form of graphs, plotted as retained load (N) versus time (Mins.) at 80°C, 100°C and 120°C. In all cases, the curves showed that the initial load loss was high, decreasing gradually with time but not ceasing. It was also observed that the amount of load loss increased rapidly with test temperature. Almost all of the relaxation curves approximated to a logarithmic decay of retained load with time although there was some variation in the initial part of the curves. All load-relaxation tests were conducted for a period of about 160 hours, i.e. about 7 days, and this test duration was selected so that relaxation behaviour of alloys may be analysed over a reasonable time period. The load-relaxation test data for alloys at different temperatures is shown in Appendix B.

The comparative load-relaxation curves in the form of retained load (N) versus time (Min.) at 80°C, 100°C and 120°C have been shown in *Figures 5.23, 5.24 and 5.25*, respectively. It can be seen from these comparative graphs that the increase in the test temperature had the least effect on the relaxation of ILZRO16., while showed the great effect on the load- relaxation behaviour of other five alloys because the final relaxed load after about 160 h in alloys No3, No5, No2, ACuZinc5 and ACuZinc10 at 120°C was much less than that of 80°C (*Figures 5.23 and 5.25).*

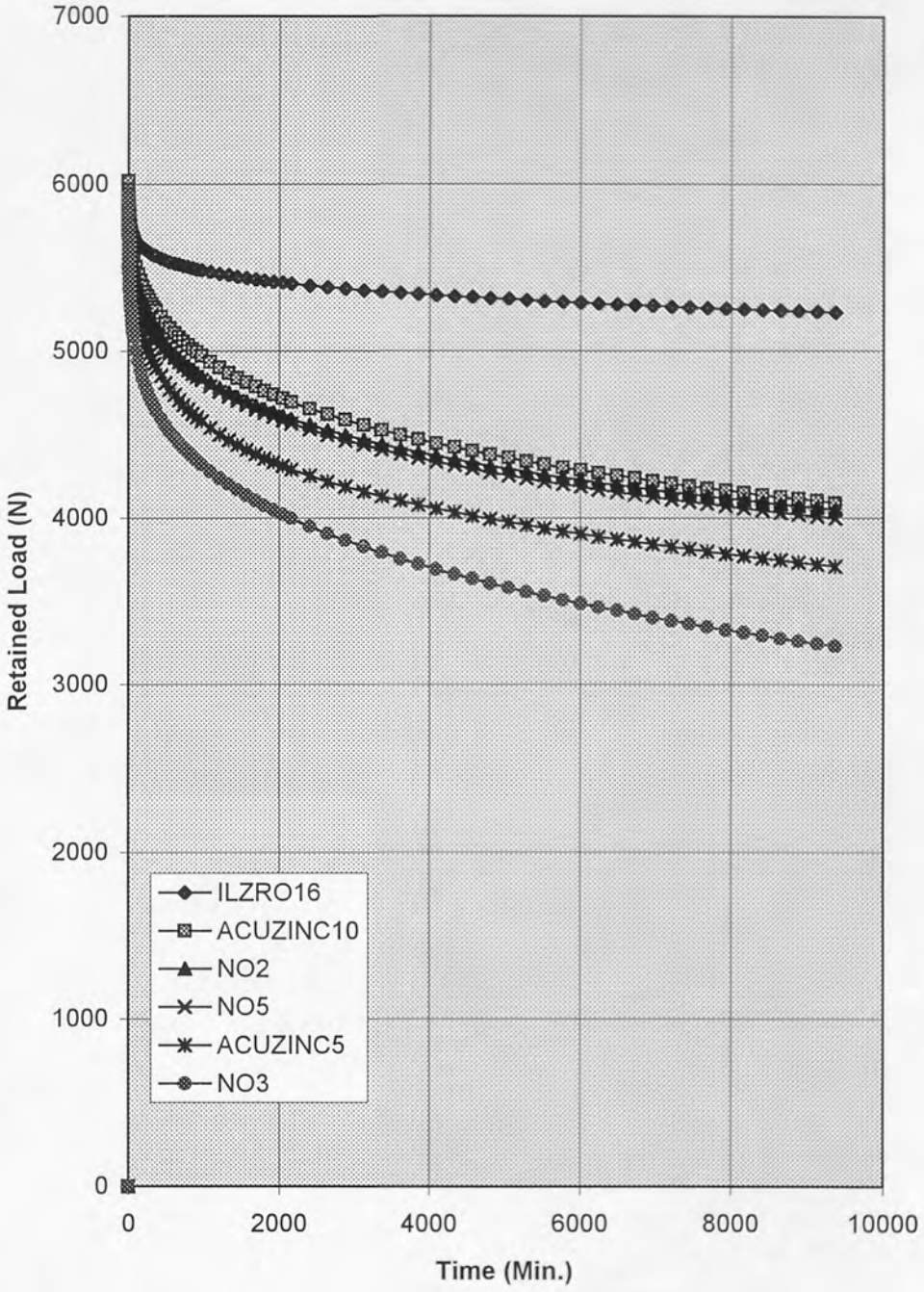

Figure 5.23. Load-Relaxation of ILZRO.16, ACuZinc10, No2, No5, ACuZinc5 and No3 at 80° C.

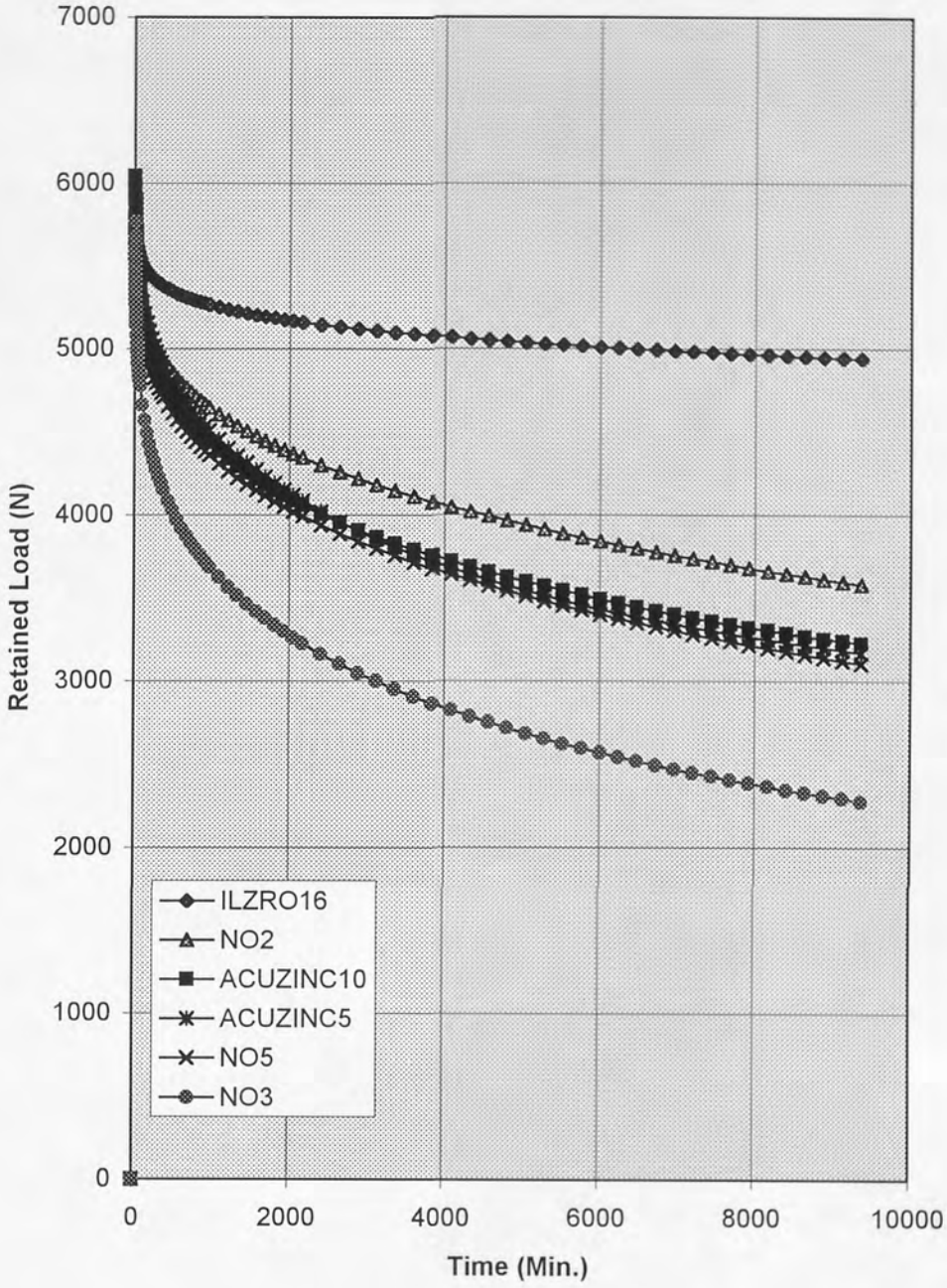

Figure 5.24. Load-Relaxation of ILZRO.16, No2, ACuZinc10, ACuZinc5, No5 and No3 at 100° C.

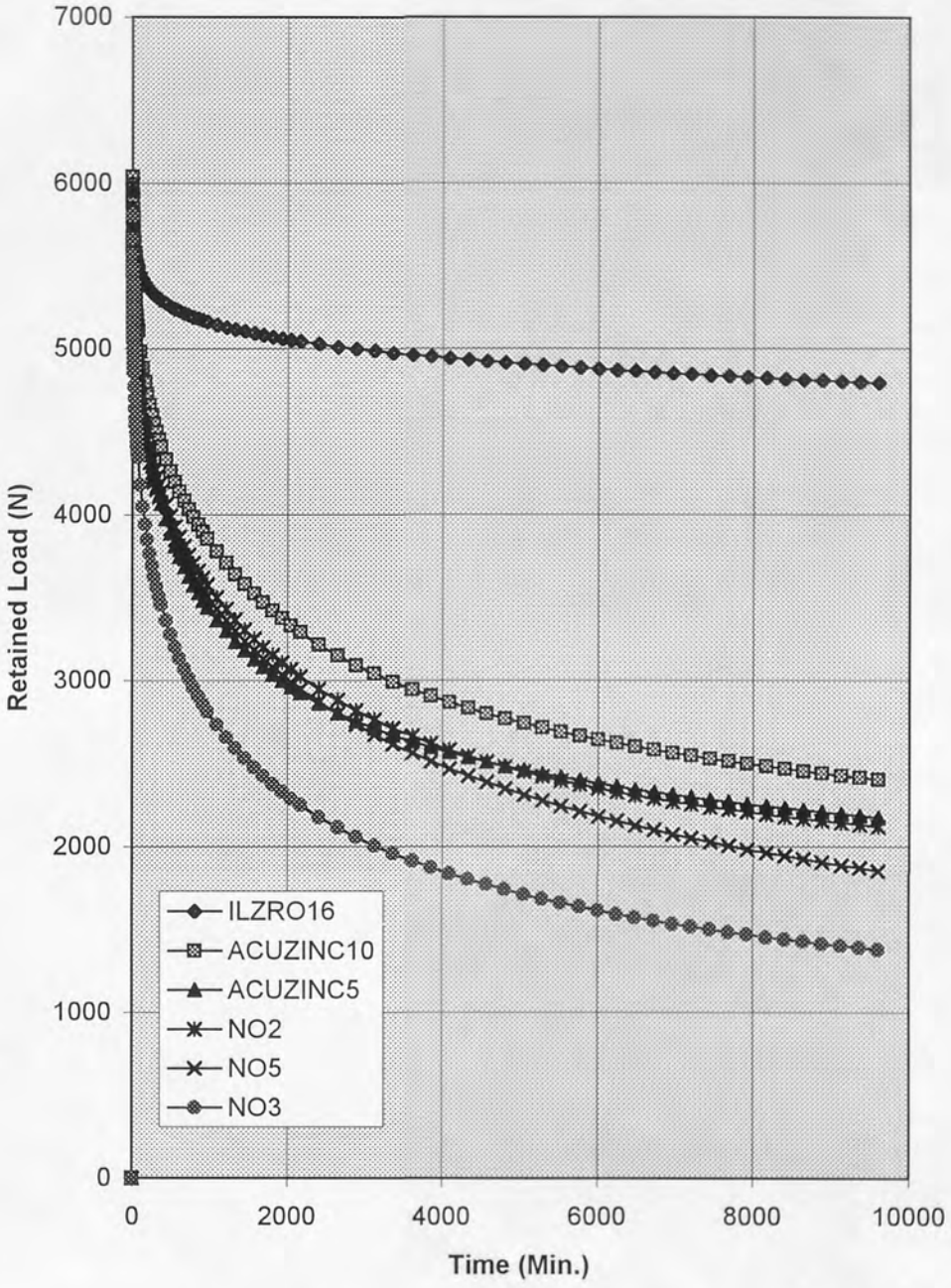

Figure 5.25. Load-Relaxation of ILZRO.16, ACuZinc10, ACuZinc5, No2, No5 and No3 at 120° C.

5.3.1 Results of Commercial Alloys

The results showed clear differences in the comparative resistance to load loss of these commercial alloys. The results revealed that alloy No2 had the best resistance to load loss, with No5 next and No3 worst. From the load-relaxation test data, it was observed that the final relaxed load after about 155 hours recorded at 80°C was 3228 N for alloy No3 as compared to 3996 N for No5 and 4046 N for No2. From these values of relaxed load, it was evident that alloy No2 was markedly superior to No3, but slightly better than No5, and also No5 was much better than No3. At higher temperatures of 100°C and 120°C, these alloys showed the same behaviour. In all results, the initial load loss was high, decreasing gradually with time, but not ceasing. It was observed that the amount of load loss increased rapidly with test temperature, and almost all of the curves approximated to a logarithmic decay of preload with time, although there was some variation in the initial part of the curves.

The results for the commercial alloys proved that at all temperatures, the resistance to load loss increased with increasing copper content. Since alloy No2 had the highest copper content (2.8%), it was therefore more resistant to load loss than alloys No5 and No3. Similarly, No5 was better than No3 due to its higher copper content.

5.3.2 Results of ACuZinc Alloys

From ACuZinc alloys, ACuZinc10 was more resistant than ACuZinc5 under all testing conditions. From comparison graphs, it was clear that at the lowest temperature (80°C), ACuZinc10 had a much higher resistance than ACuZinc5, but at the higher temperatures (100°C and 120°C), the difference was not great, although ACuZinc10 was still slightly better than ACuZinc5.

5.3.3 Results of ILZRO.16

ILZRO.16 had the best resistance to load loss among all six alloys tested under all conditions. The load-relaxation data showed that ILZRO.16 was 22%, 35% and 50% more resistant than ACuZinc10 at 80°C, 100°C and 120°C, respectively. The best resistance of ILZRO.16 might be due to the presence of titanium and chromium content, which increased its strength and resistance to load loss significantly.

5.3.4 The Effect of Short and Long-term Tests

Graphs were drawn to show the variation of retained load with reciprocal temperature at 50, 100 and 150 hours time for all six alloys, as shown in *Figures 5.26, 5.27, 5.28, 5.29, 5.30 and 5.31.* These plots showed that good correlation with constant slopes were obtained over much of the test conditions for all alloys. Although some scattering in the results was also observed, e.g. for alloys No5 and No2 at 100°C, but it was not unusual in these types of tests.

From these plots, the effect of short and long-term load-relaxation tests can be observed. The graphs at 50 h time showed the short-term effects of load-relaxation, while 150 h time graphs demonstrated the long-term effect.

From 50 h time graph, it was observed that ILZRO.16 was the best resistant to load loss, and No3 was the worst, whereas ACuZinc10 and ACuZinc5 were better than No2 and No5. No2 was the best resistant among three commercial alloys, and No5 was better than No3 at this time period. At 100 h and 150 h time, all six alloys showed the same behaviour as observed at 50 h.

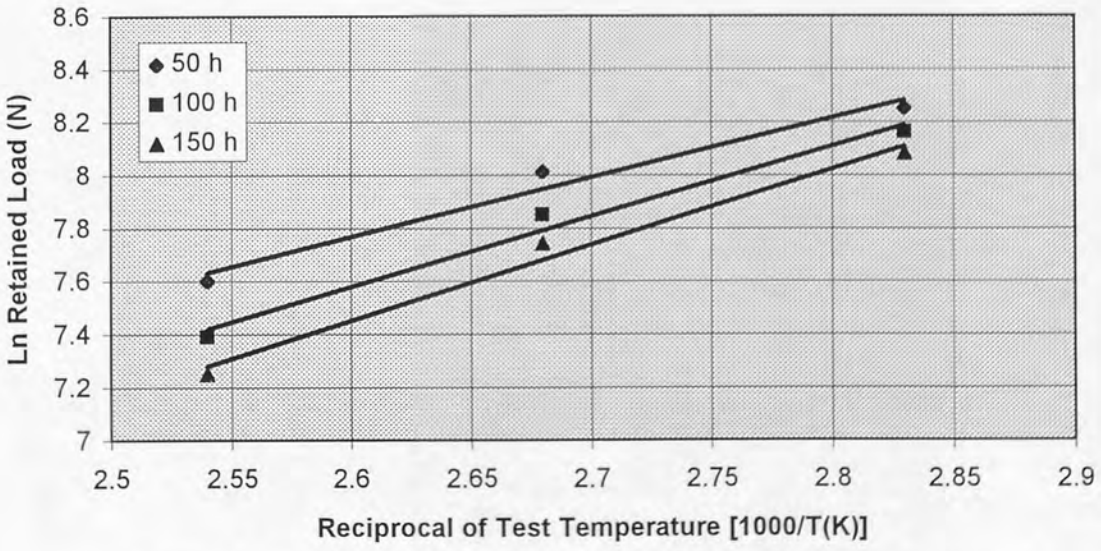

Figure 5.26. Variation of 50, 100 and 150 hours load with reciprocal temperature for alloy No3.

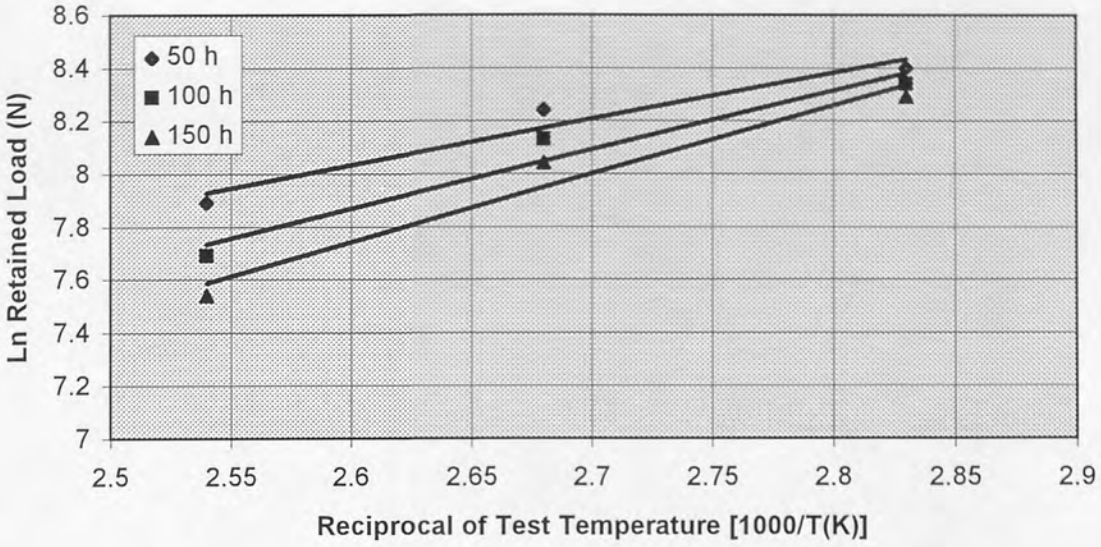

Figure 5.27. Variation of 50, 100 and 150 hours load with reciprocal temperature for alloy No5.

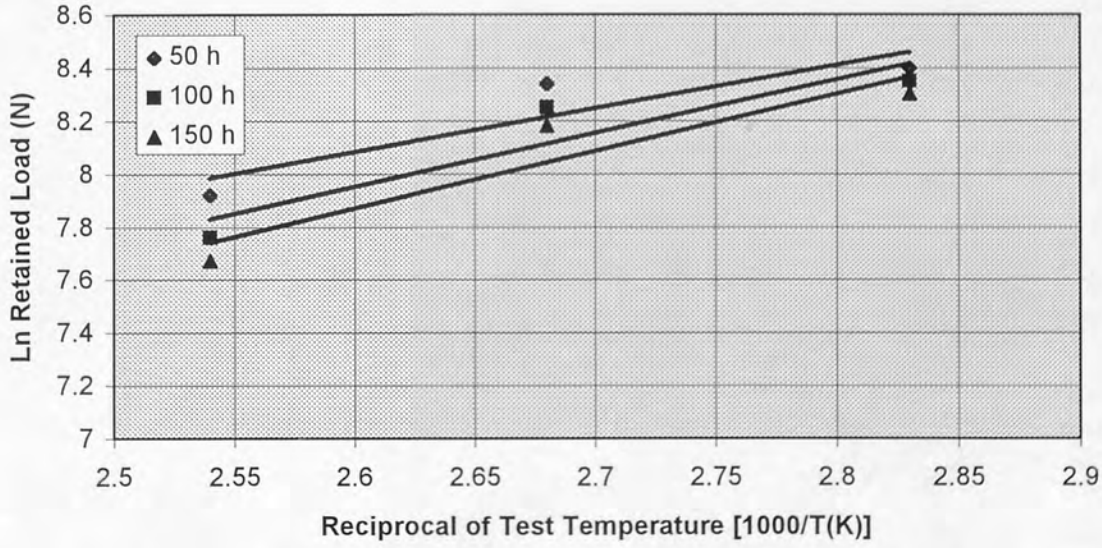

Figure 5.28. Variation of 50, 100 and 150 hours load with reciprocal temperature for alloy No2.

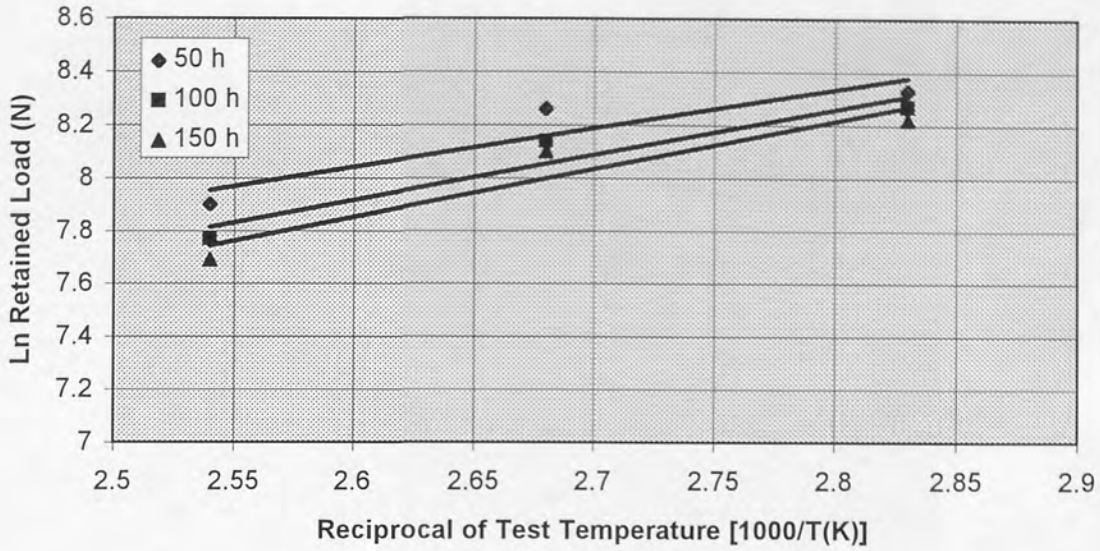

Figure 5.29. Variation of 50, 100 and 150 hours load with reciprocal temperature for ACuZinc5.

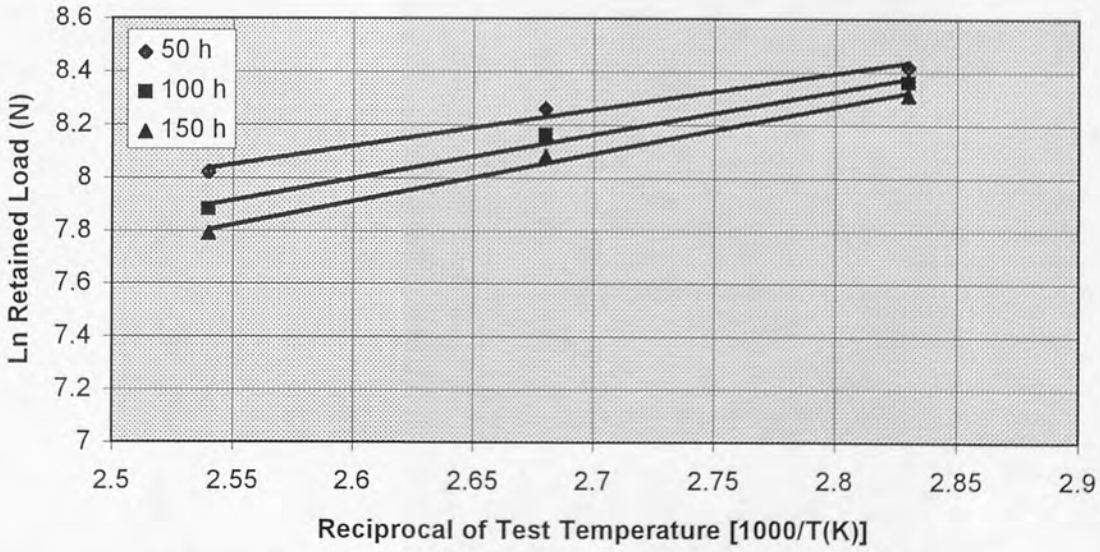

Figure 5.30. Variation of 50, 100 and 150 hours load with reciprocal temperature for ACuZinc10.

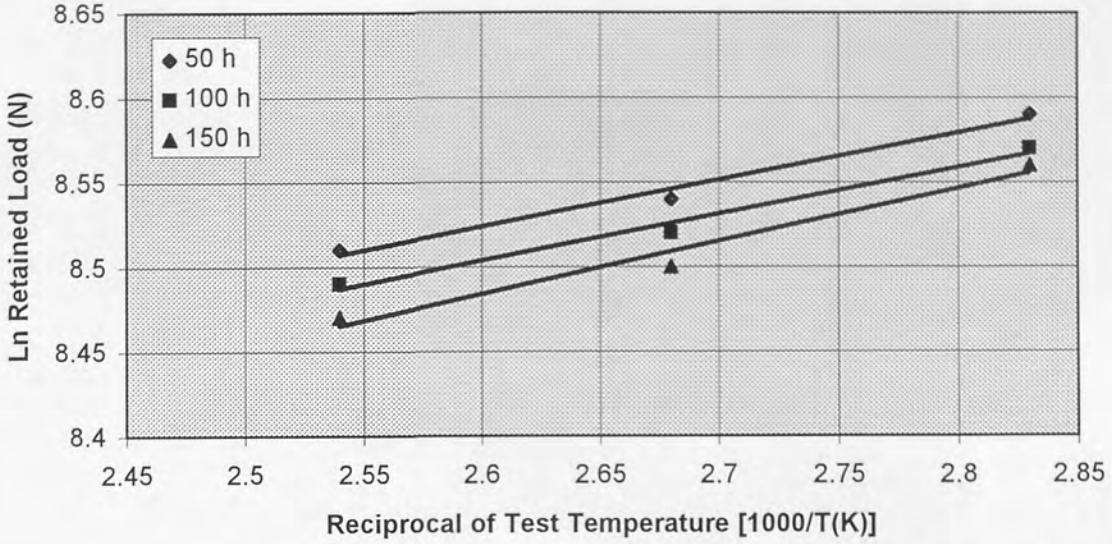

Figure 5.31. Variation of 50, 100 and 150 hours load with reciprocal temperature for ILZRO.16.

5.4 Metallography of the Experimental Alloys

Scanning electron microscopy (SEM) in back-scattered electron imaging mode was used as the general investigation method to study the microstructure of these commercial alloys. The contrast in the electron microscope images depends almost entirely on the average atomic number of the different phases present in the structure of the alloys. Therefore, in the SEM micrographs of these alloys, zinc-rich phases appeared light and aluminium-rich phases dark, since zinc-rich phase had more electron scattering power due to its higher atomic number and produced a greater number of back-scattered electrons than that of the aluminium-rich phase with lower atomic number, although the shade of contrast could be adjusted by varying electronically the sensitivity of the electron detector to the atomic number.

The microstructures of alloys No2, ACuZinc5 and ACuZinc10 were also examined using optical microscopy.

5.4.1 Alloy No3

The as-cast structure of alloy No3 is shown in *Figures 5.32, 5.33 and 5.34* at three different appropriate magnifications. The figures showed that the structure of the alloy was very heterogeneous and hypoeutectic, consisting of a few large and numerous small primary zinc-rich (η) dendrites. These dendritic particles were surrounded by a relatively small volume of lamellar eutectic matrix. The whole structure was fine due to the grain refinement produced by the addition of magnesium. It was also observed that many small rounded dark particles of the Al-rich former β phase were attached to the primary η phase dendrites. The development of these dark, Al-rich particles on the primary zinc-rich η is shown at higher magnification in *Figure 5.33*. It was clear from this figure that this phase was the Al-rich eutectic β phase which had nucleated on the primary phase (η) at high undercoolings during eutectic solidification. β phase is unstable below about the eutectoid temperature of 275°C and decomposes into Zn-rich η and Al-rich α phases. *Figure 5.34* indicates that the β in both the particles and the β constituent of the lamellar matrix had decomposed. In addition, the edges of the primary η dendrites were decorated with small Al-rich particles.

The structure of the alloy No3 after being creep-tested in compression at 100 MPa and 160°C, is shown in *Figures 5.35 to 5.37*. Due to short duration of the test, great changes in the structure of alloy were not expected. However, the primary η dendrites had much larger volume than the eutectic, similar to that observed for the as-cast structure. The figures showed no significant change in the size of primary particles. The lamellae of eutectic matrix were well-developed *(Figure 5.35)*, and were generally smaller than those in the as-cast structure. Small precipitates within the primary particles were observed in both as-cast and creep-tested conditions.

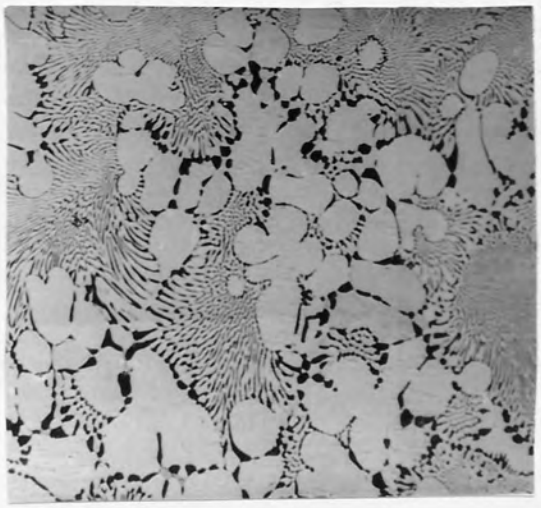

Figure 5.32. As-Cast structure (SEM) of Alloy No3 at low magnification, showing primary η dendrites and eutectic (α + η).

(176×)

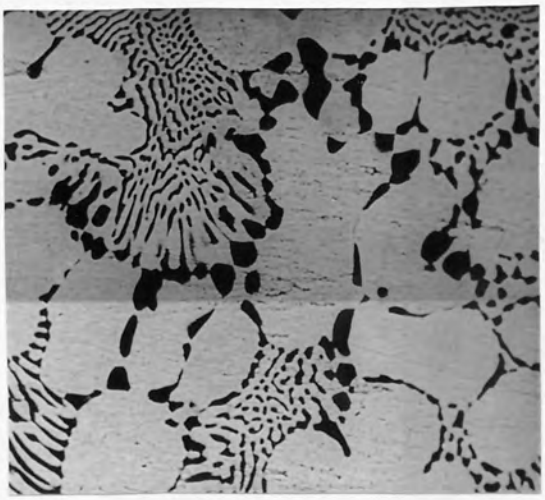

Figure 5.33. SEM. As-Cast structure of of Alloy No3 at medium magnification, showing former β attached to primary η dendrites.

(350×)

Figure 5.34. As-Cast structure (SEM) of Alloy No3 at high magnification.

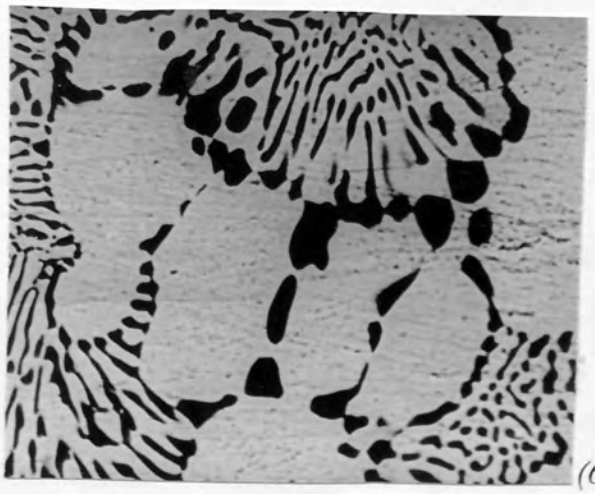

(645×)

Figure 5.35. The structure (SEM) of Alloy No3 tested at 100 MPa and 160°C, at low magnification.

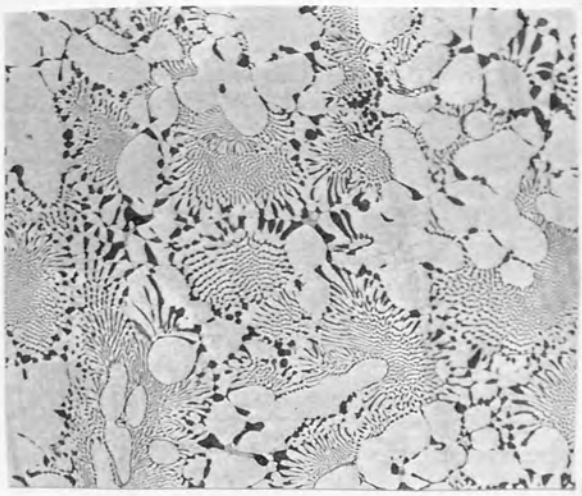

(164×)

Figure 5.36. SEM. Alloy No3 tested at 100 MPa and 160°C, at medium magnification.

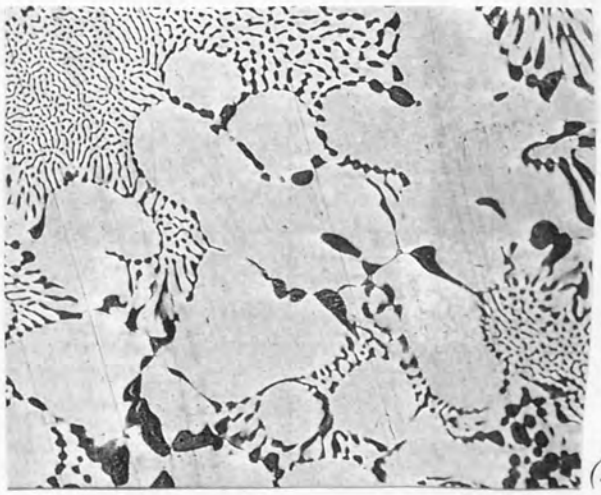

(356×)

Figure 5.37. SEM micrograph of Alloy No3 tested at 100 MPa and 160°C, at high magnification.

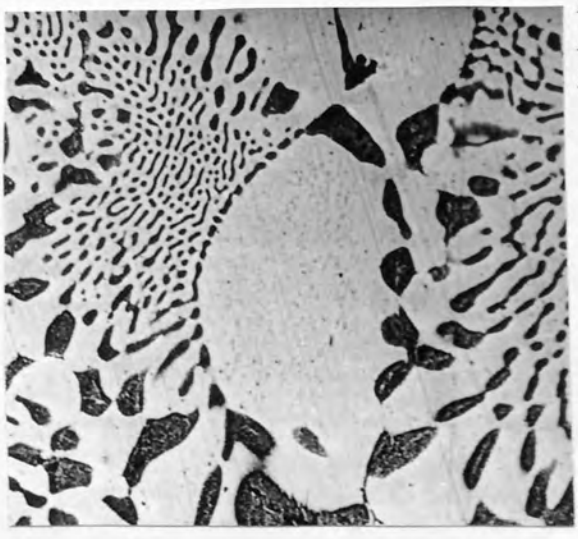

(655×)

5.4.2 Alloy No5

The as-cast structure of alloy No5 is shown in *Figures 5.38 to 5.40* at low to high magnifications, respectively. The scale of the structure was similar to that of alloy No3 with more uniformly distributed primary Zn-rich (η) particles. Like alloy No3, the structure of this alloy also consisted of large and small primary Zn-rich dendrites surrounded by lamellar eutectic matrix. The main difference from the structure of alloy No3 was that the size of primary particles in this case was larger as compared to those of No3, also the primary η dendrites and the η component of the (α + η) eutectic had copper-rich ε-phase precipitates. It was difficult to differentiate these precipitates from zinc (η) particles due to a very small difference in atomic numbers of both zinc and copper. The volume of eutectic matrix was relatively small as compared to primary particles. Many small and dark particles of Al-rich former β phase were observed which were attached to the hypoeutectic η particles (similar to No3). These are shown at higher magnification in *Figure 5.39*. β is unstable below the eutectoid temperature of 275°C and transforms into Zn-rich η and Al-rich α phases.

Figures 5.41 to 5.43 show the structure of alloy No5 after compressive creep testing at 20 MPa and 160°C which represents the alloy structure at the lowest applied stress and the highest test temperature. The volume of eutectic matrix was slightly reduced as compared to the as-cast structure. The micrographs also showed the regular eutectic (α+η) morphology, and it was believed that the higher creep resistance of alloy No5 was due to this regular morphology combined with the strong strengthening effect of the ε-phase precipitates.

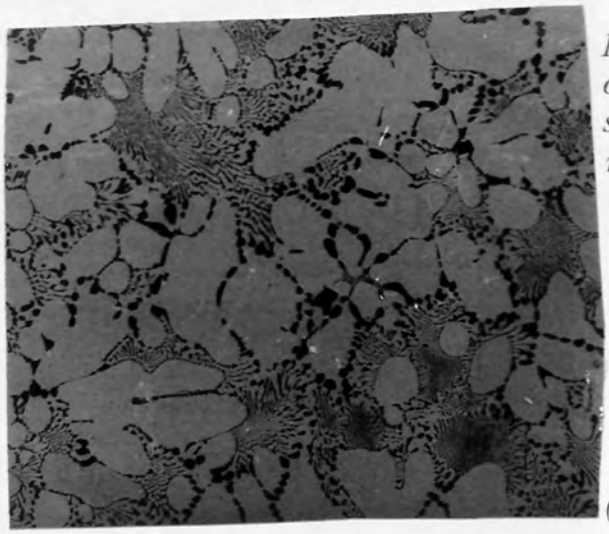

Figure 5.38. As-Cast structure (SEM) of Alloy No5 at low magnification, showing large and small primary η particles and lamellar eutectic.

(152×)

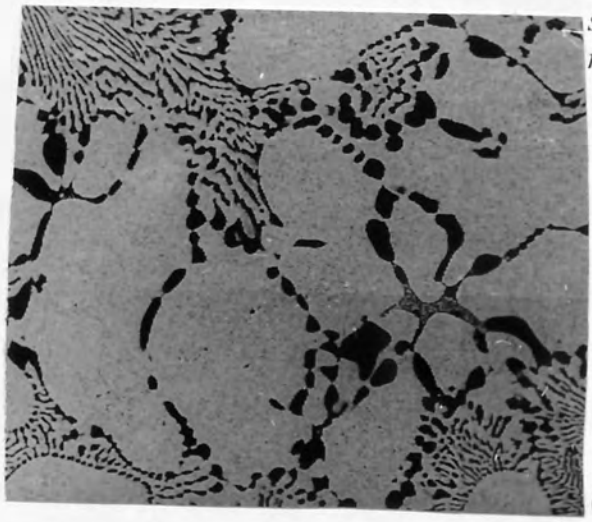

Figure 5.39. SEM. As-Cast structure of Alloy No5 at medium magnification, showing primary η particles with relatively small volume of eutectic.

(308×)

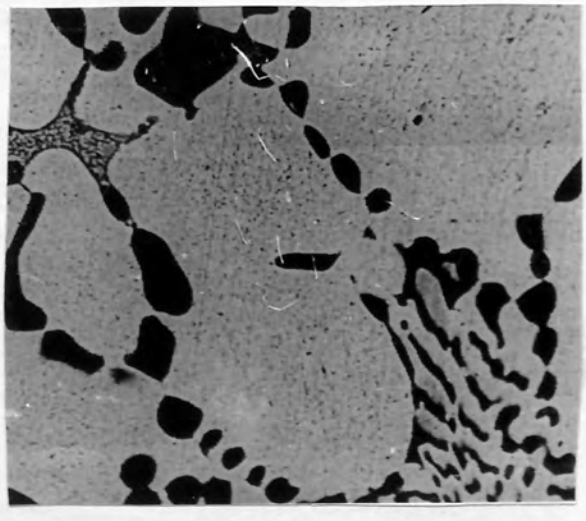

Figure 5.40. SEM. As-Cast structure of Alloy No5 at high magnification, showing primary η particles with Al-rich β phase and eutectic.

(618×)

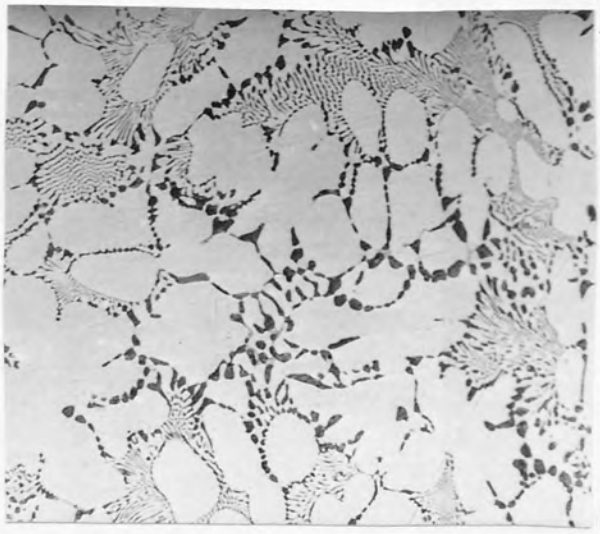

Figure 5.41. SEM micrograph of Alloy No5 tested at 20 MPa and 160°C, at low magnification.

(164×)

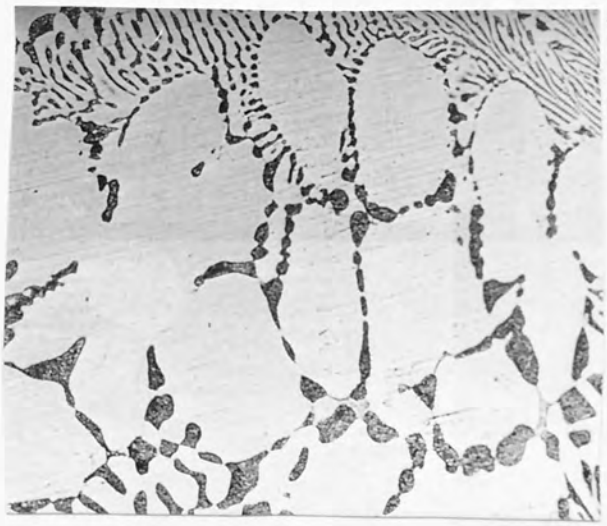

Figure 5.42. SEM. Alloy No5 tested at 20 MPa and 160°C, showing dark particles of Al-rich β phase at medium magnification.

(363×)

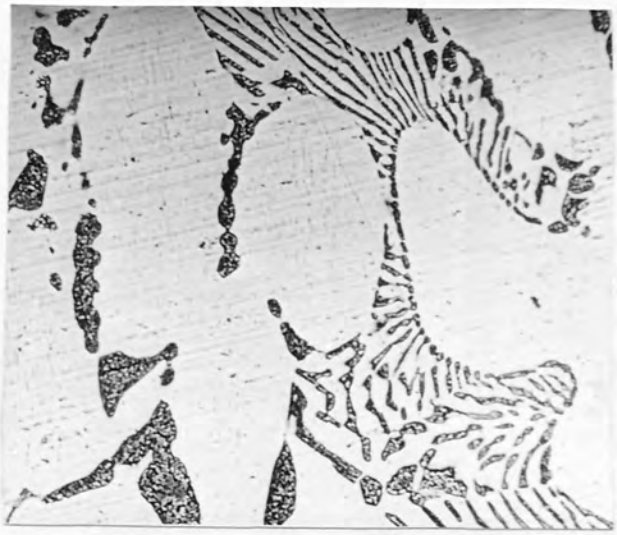

Figure 5.43. SEM micrograph of Alloy No5 tested at 20 MPa and 160°C, at high magnification.

(668×)

5.4.3 Alloy No2

Figures 5.44 to 5.46 show the as-cast structure of No2 at different magnifications. The primary Zn-rich dendrites had more tree-like branches than in No5. The scale of the structure was similar to that of alloy No5. The structure consisted of many large and a few small primary η dendrites surrounded by a relatively small volume of lamellar eutectic matrix. Dark particles of the Al-rich former β phase were associated with hypoeutectic η particles as observed in structures of alloys No3 and No5. Decomposition of the β into Zn-rich η and Al-rich α phases is shown in *Figure 5.45*. Alloy No2 had about 2.8% Cu, and ε-phase precipitates must present in both primary η dendrites and η in the eutectic matrix, however in SEM micrographs it was difficult to distinguish them from zinc due to a very small difference in the atomic numbers of both elements.

The structure of alloy No2 after compressive creep testing (100 MPa and 160°C) is shown in *Figures 5.47 to 5.49*. The structure had primary η dendrites surrounded by a lamellar eutectic matrix. Many small and dark particles of the Al-rich former β phase were associated with primary η particles (*Figures 5.47 and 5.48).* At higher magnification, small precipitates were also observed in primary η dendrites.

The optical micrographs *(Figures 5.50 to 5.52)* of creep-tested (100 MPa and 160°C) samples also showed the primary η dendrites surrounded by lamellar eutectic. The eutectic areas also contained some massive ε-phase particles due to slow cooling during sand-casting process. These ε-phase particles were not detected in the SEM micrographs. It was also visible from SEM and optical micrographs that well-developed lamellar morphology was more dominent in the eutectic structure *(Figures 5.44, 5.45 and 5.52).*

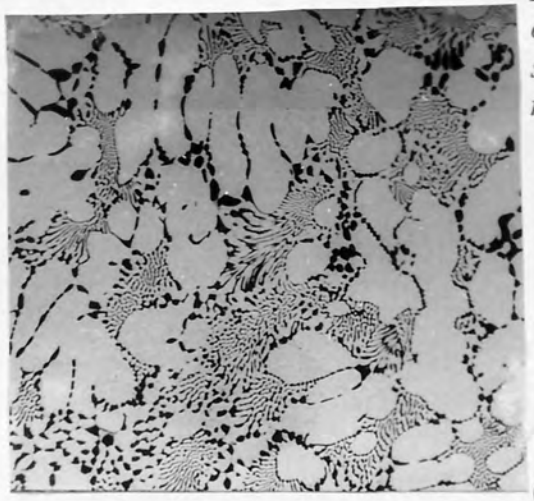

Figure 5.44. As-Cast structure (SEM) of Alloy No2 at low magnification, showing primary η dendrites and regular lamellar eutectic.

(167×)

Figure 5.45. SEM. As-Cast structure of Alloy No2 at medium magnification.

(337×)

Figure 5.46. SEM. As-Cast structure of Alloy No2 at high magnification.

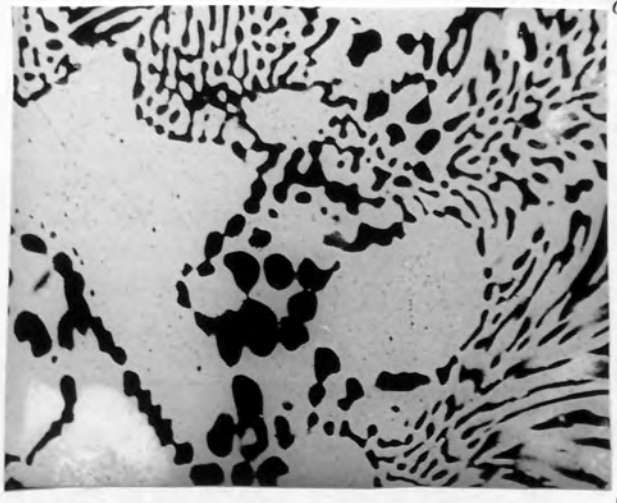

(619×)

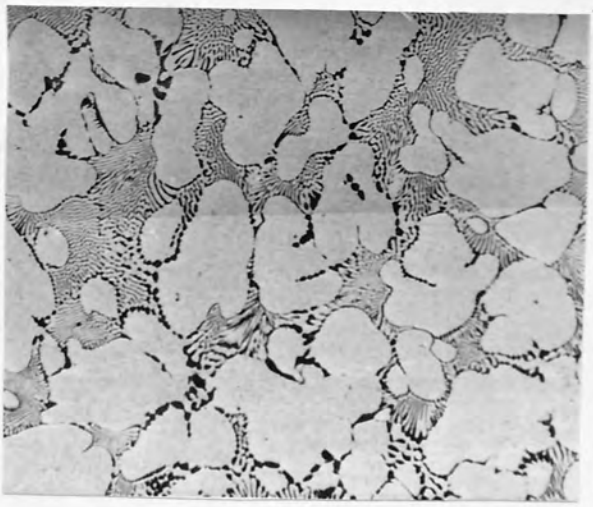

Figure 5.47. The structure (SEM) of Alloy No2 tested at 100 MPa and 160°C, at low magnification.

(162×)

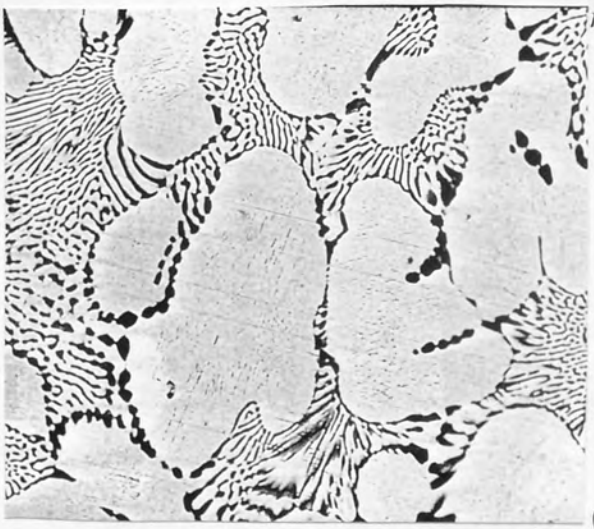

Figure 5.48. SEM. Alloy No2 tested at 100 MPa and 160°C, at medium magnification.

(359×)

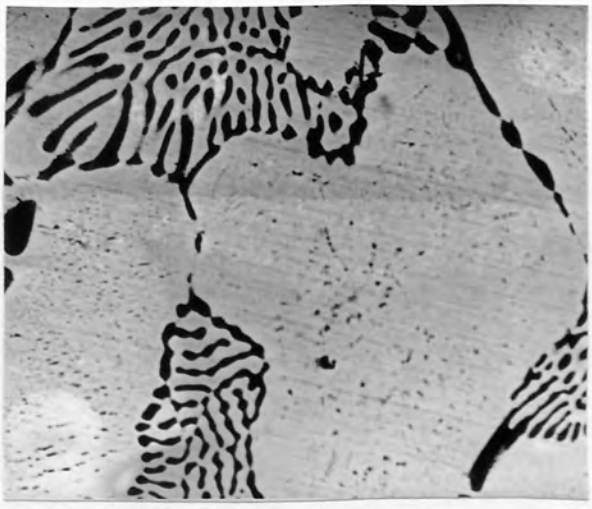

Figure 5.49. SEM micrograph of Alloy No2 tested at 100 MPa and 160°C, at high magnification.

(658×)

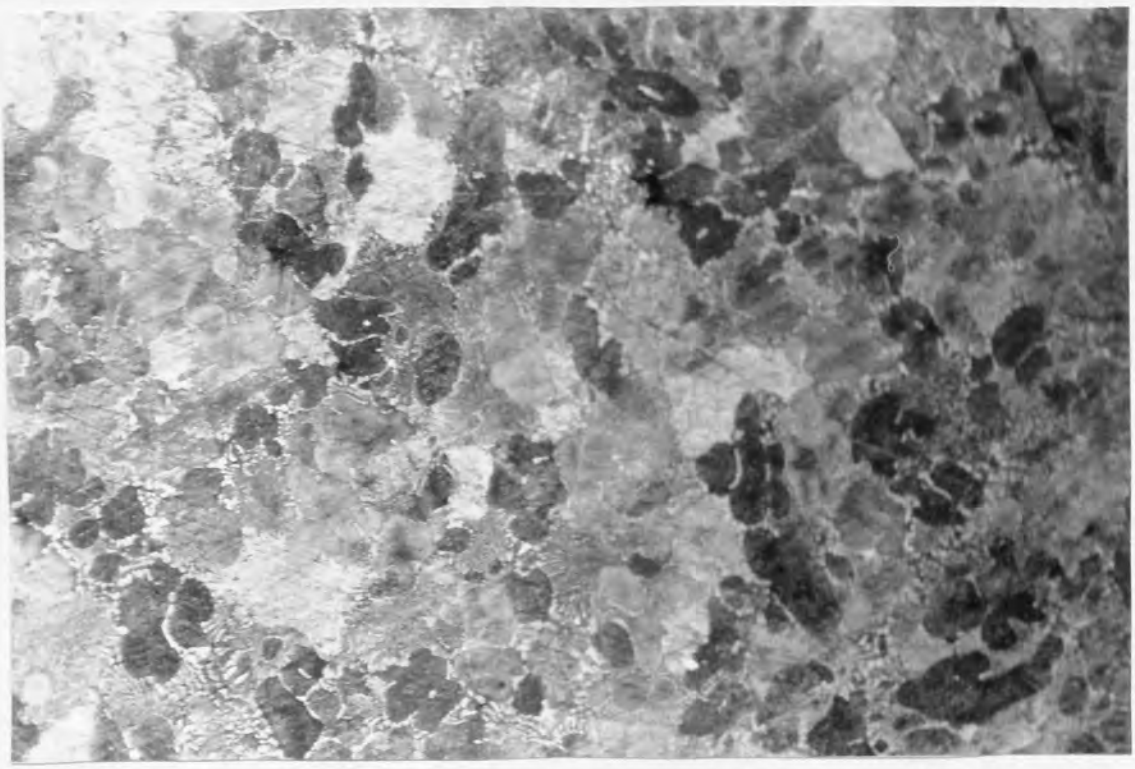

Figure 5.50. Optical micrograph of Alloy No2 tested at 100 MPa and 160°C, at low magnification. (100×)

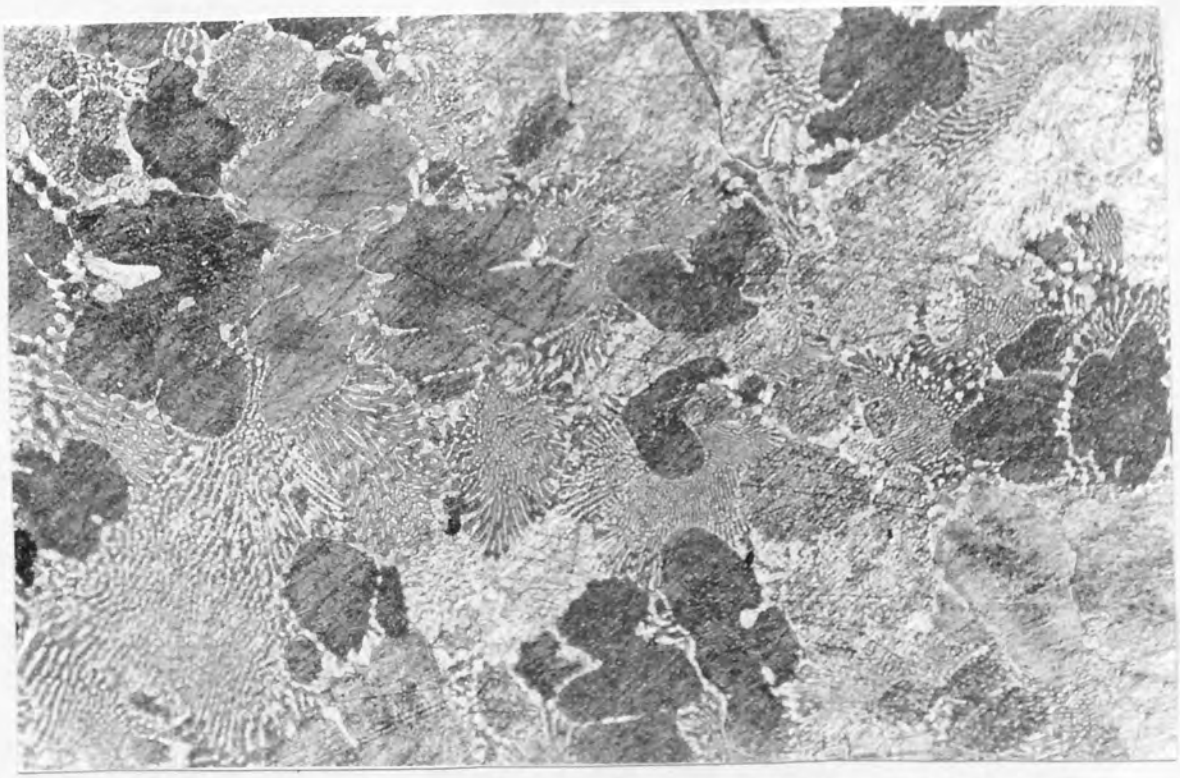

Figure 5.51. Optical Micrograph. Alloy No2 tested at 100 MPa and 160°C at medium magnification, showing primary η dendrites and massive ε-particles in the eutectic. (200×)

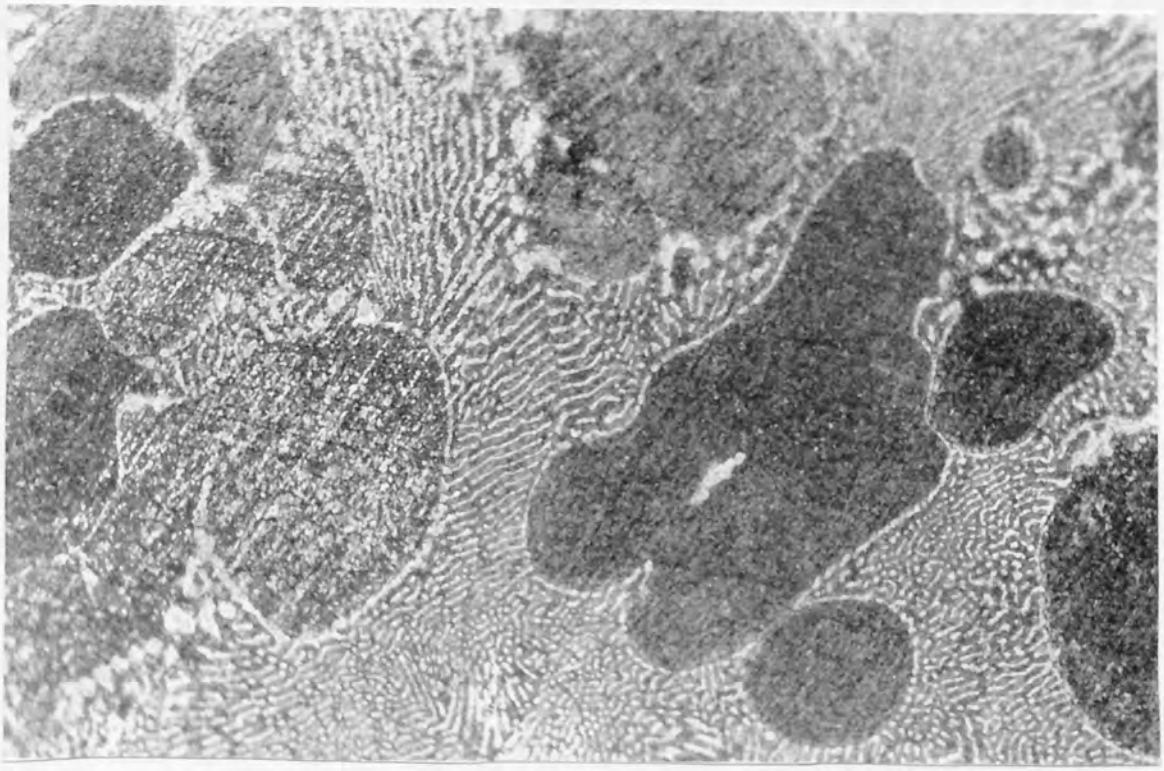

Figure 5.52. Optical micrograph of Alloy No2 tested at 100 MPa and 160°C, at high magnification. (500×)

5.4.4 ACuZinc5

The as-cast structure of ACuZinc5 is shown in *Figures 5.53 to 5.55* at three different magnifications. In contrast to alloys No3, No5 and No2, the structure of ACuZinc5 consisted of primary Cu-rich ε dendrites (small and large) with massive η particles, surrounded by a ternary (α + ε + η) eutectic. The large η particles were more distinct in the optical micrographs. It was observed that eutectic volume was much less as compared to those of alloys No3, No5 and No2.

The primary Cu-rich ε-phase in ACuZinc5 is harder and stronger than the other phases (α and η) and acts as a reinforcement in the matrix. Since tensile strength of alloys is governed by the type of primary phase, the strength and creep properties of ACuZinc5 are enhanced due to the presence of Cu-rich ε-phase which constitutes about 30% of the microstructure of ACuZinc5.

Figures 5.56 to 5.59 show the structure of ACuZinc5 at four magnifications after compressive creep testing at 100 MPa and 160°C. The structure consisted of the primary ε-phase and ternary (α + ε + η) eutectic. The primary ε dendrites showed greater precipitation than the as-cast condition. The structure of lamellar eutectic was also shown at higher magnification *(Figure 5.59)*.

The optical micrographs *(Figures 5.60 to 5.62)* of creep-tested samples, at 100 MPa and 160°C also showed the primary ε dendrites with large and small size zinc-rich (η) particles, surrounded by the ternary (α + ε + η) eutectic. The η particles were due to high zinc contents. The ternary eutectic was heterogeneous and can be seen dictinctly from η and ε-phase particles. Small ε-particles were also visible in interdendritic areas. These optical micrographs also showed that the ternary eutectic had much less volume than the primary ε-dendrites and massive η particles, also some primary ε-particles were nucleated on large η particles.

Figure 5.53. As-Cast structure (SEM) of ACuZinc5 at low magnification, showing primary ε dendrites and ternary eutectic.

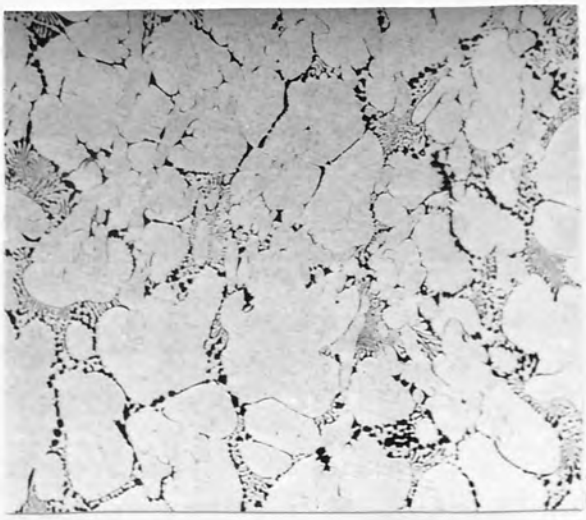

(160×)

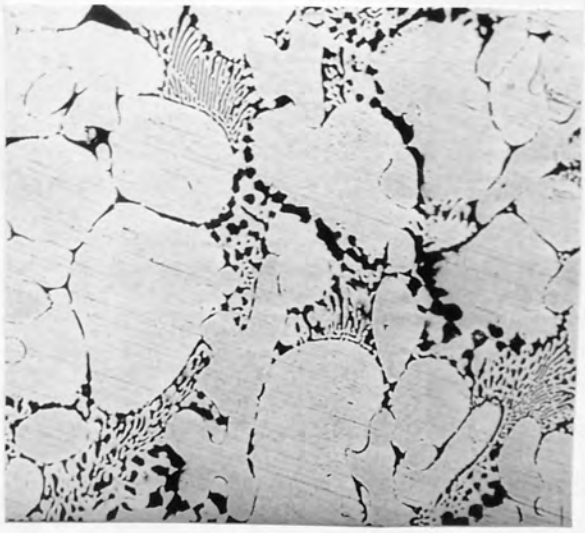

Figure 5.54. SEM. As-Cast structure of ACuZinc5 at medium magnification.

(347×)

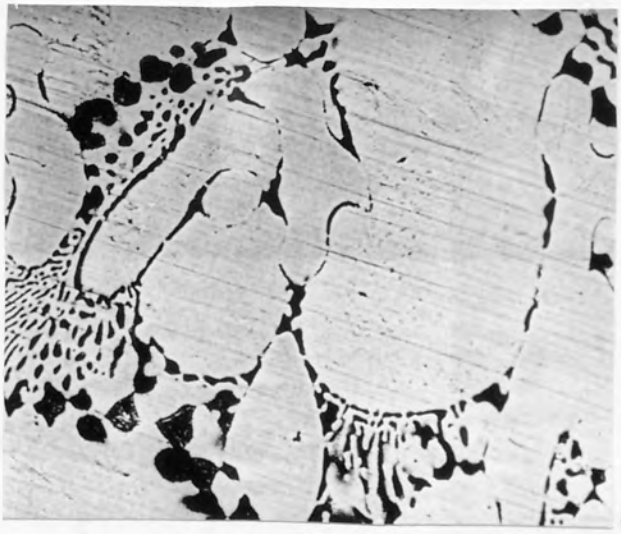

Figure 5.55. SEM. As-Cast structure of ACuZinc5 at high magnification.

(639×)

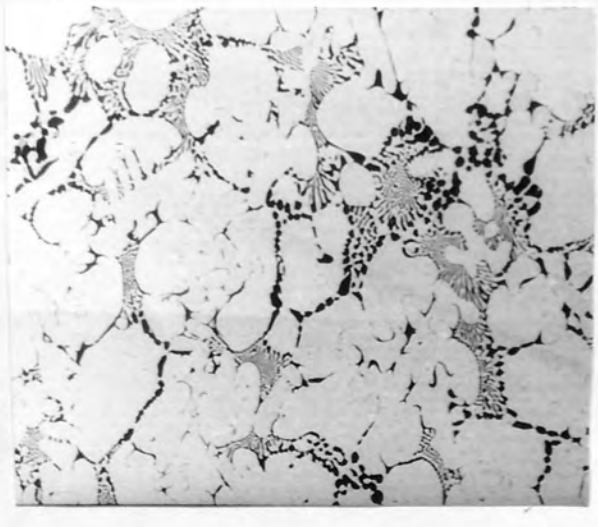

Figure 5.56. The structure (SEM) of ACuZinc5 tested at 100 MPa and 160°C, at low magnification.

(154×)

Figure 5.57. SEM. ACuZinc5 tested at 100 MPa and 160°C, at medium magnification.

(352×)

Figure 5.58. SEM micrograph of ACuZinc5 tested at 100 MPa and 160°C, at high magnification.

(458×)

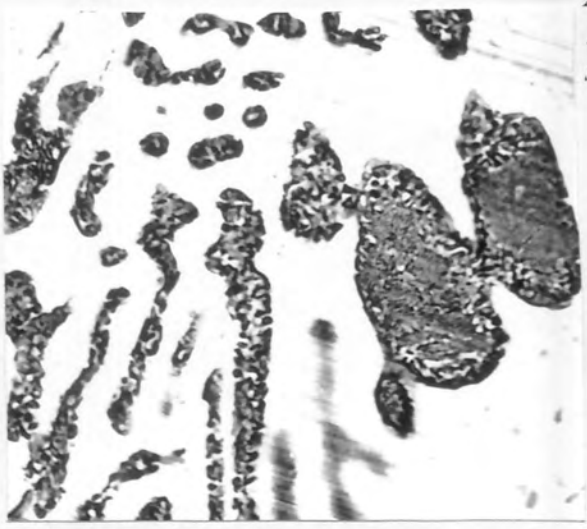

Figure 5.59. SEM micrograph of ACuZinc5 tested at 100 MPa and 160°C at high magnification, showing lamellar eutectic.

(2470×)

Figure 5.60. Optical micrograph of ACuZinc5 tested at 100 MPa and 160°C, at low magnification. (100×)

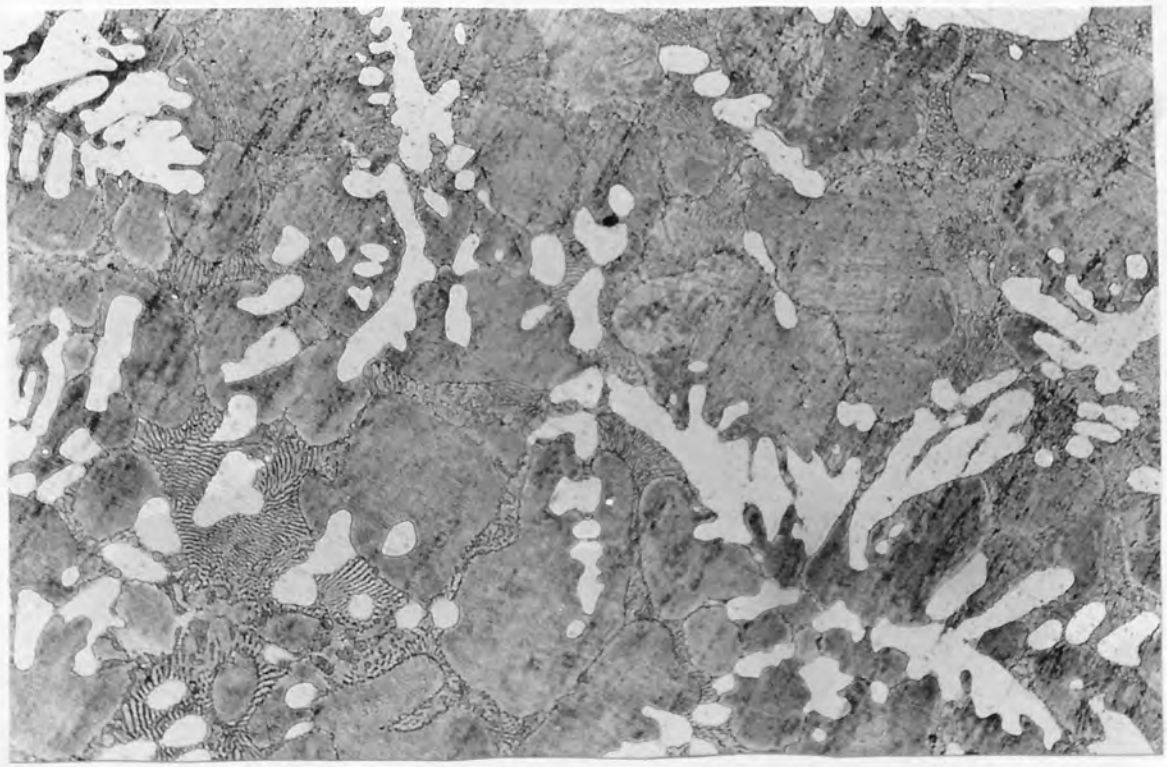

Figure 5.61. Optical Micrograph. ACuZinc5 tested at 100 MPa and 160°C at medium magnification, showing primary ε dendrites and massive η particles with ternary eutectic. (200×)

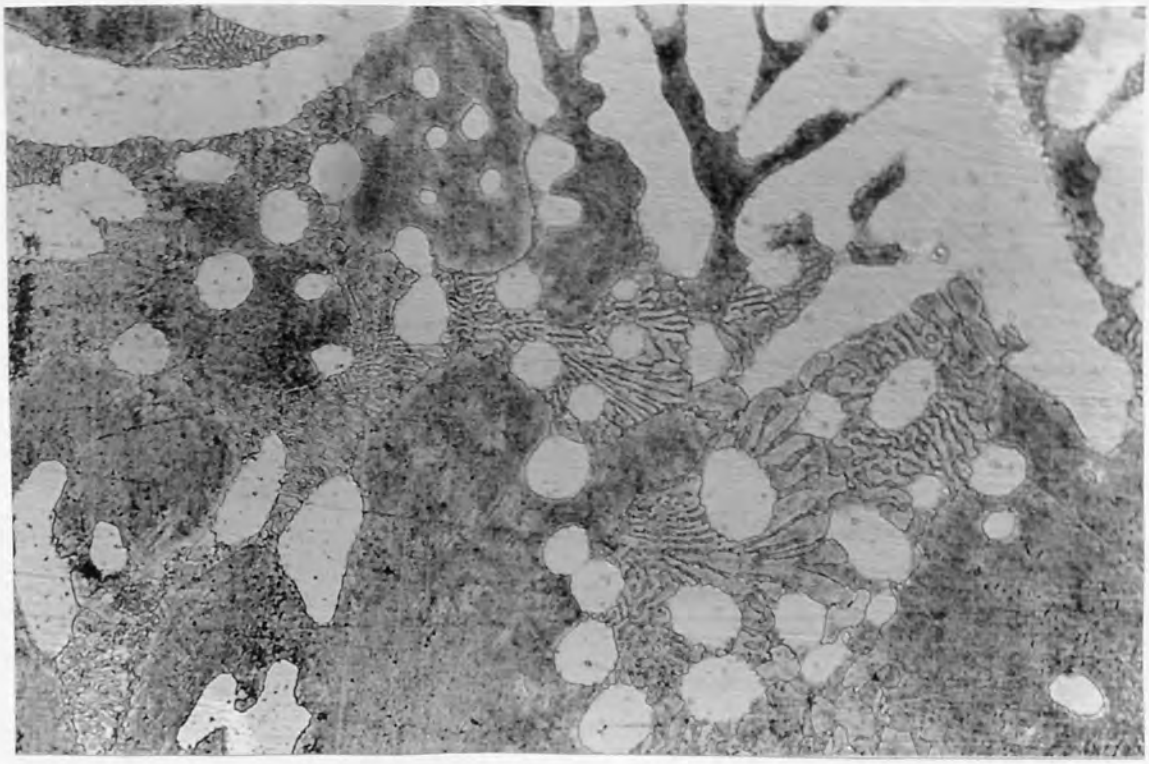

Figure 5.62. Optical micrograph of ACuZinc5 tested at 100 MPa and 160°C, at high magnification. (500×)

5.4.5. ACuZinc10

Figures 5.63 to 5.65 show the as-cast structure of ACuZinc10 at three different magnifications. The structure contained the primary Cu-rich (ε) dendrites which are surrounded by the ternary (α + ε + η) eutectic as observed in the structure of ACuZinc5. In general, the structure was similar to that of ACuZinc5 except the volume fraction of the primary phase was far greater than that of ACuZinc5. This higher volume of primary ε-phase was due to the higher percentage (~10%) of copper in ACuZinc10. It was also observed that the primary ε dendrites had a much larger volume than the eutectic matrix *(Figures 5.63 and 5.64).*

Figures 5.66 to 5.69 show the structure of ACuZinc10 at four different magnifications after creep testing, at 100 MPa and 160°C. The shape of primary ε-dendrites has been changed after the creep test, and the structure had long branch-like dendrites. Also in the eutectic matrix, dark Al-rich particles were seen at lower and higher magnification, and lamellar eutectic matrix was coarsened. The primary ε-dendrites had much greater volume than the ternary eutectic in the stucture *(Figure 5.66),* as observed in the as-cast condition. It was also observed that Al-rich dark particles were decorated around the primary ε-dendrites *(Figures 5.66).*

The optical micrographs of ACuZinc10 *(Figures 5.70 and 5.71)* also showed the primary ε-phase dendrites of different sizes and ternary eutectic. The structure had small size η phase particles only in the ternary eutectic , contrary to the structure of ACuZinc5 which had massive particles of η phase. The microstructure had also greater volume of primary ε-phase dendrites than ACuZinc5, i.e. about 50% of the whole structure. The ternary eutectic had mostly the regular lamellar morphology with some particulate structure. Like ACuZinc5, small discrete ε-phase particles were also observed in the interdendritic areas. The optical micrographs of ACuZinc10 also revealed that that the volume fraction and size of the ε-dendrites increased with increasing copper.

Figure 5.63. As-Cast structure (SEM) of ACuZinc10 at low magnification, showing primary ε dendrites and ternary eutectic.

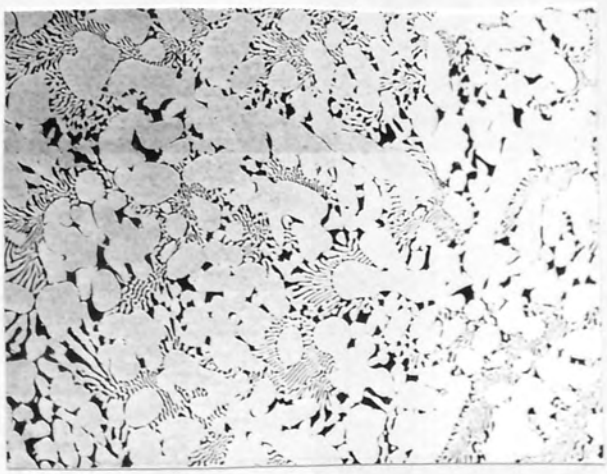

(174×)

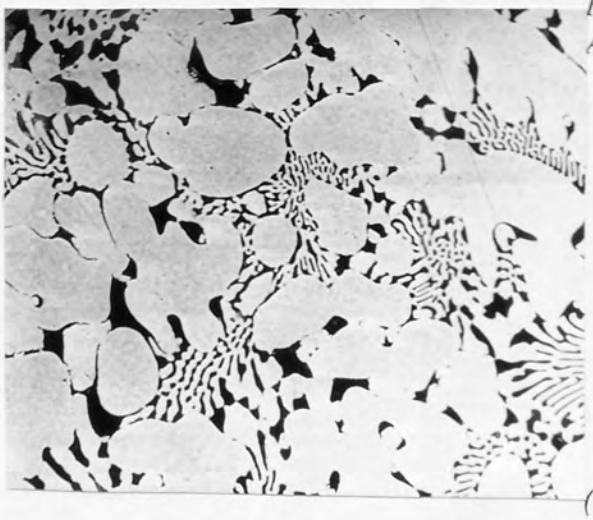

Figure 5.64. SEM. As-Cast structure of ACuZinc10 at medium magnification.

(347×)

Figure 5.65. SEM. As-Cast structure of ACuZinc10 at high magnification.

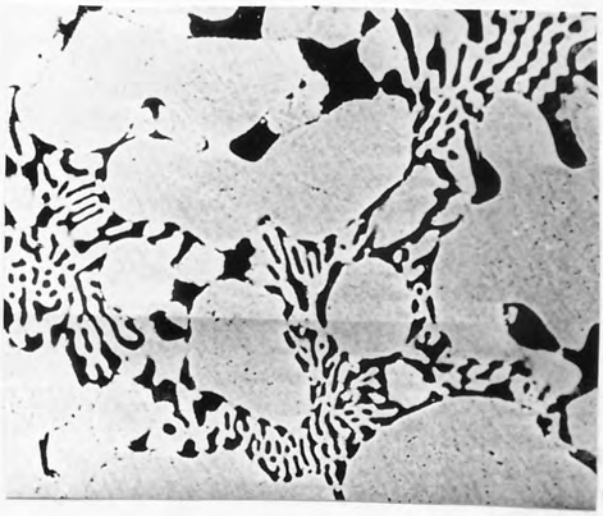

(667×)

Figure 5.66. The structure (SEM) of ACuZinc10 tested at 100 MPa and 160°C, at low magnification.

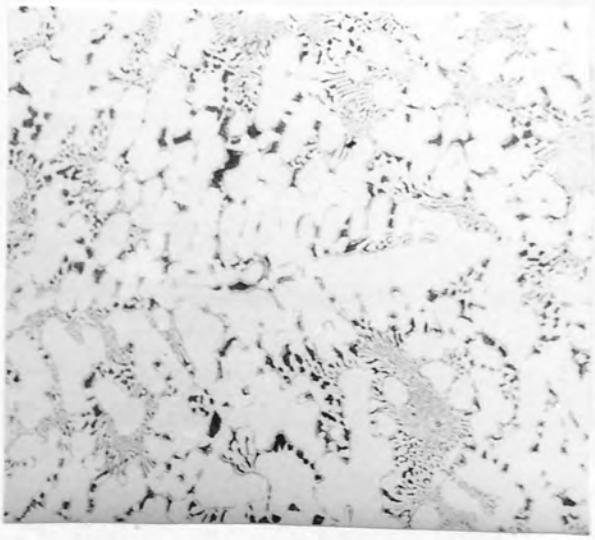

(172×)

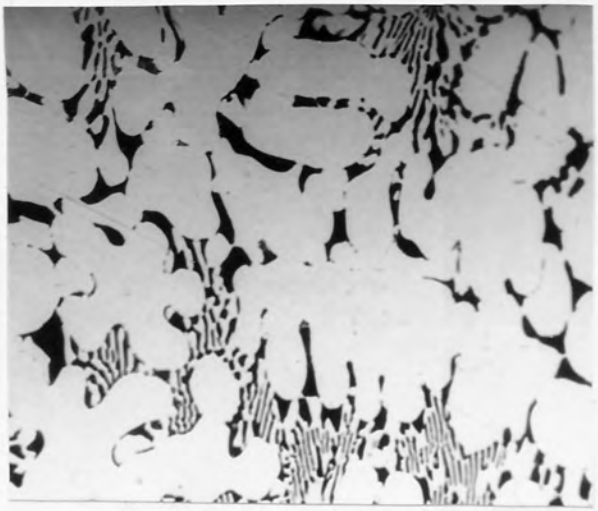

Figure 5.67. SEM. ACuZinc10 tested at 100 MPa and 160°C, at medium magnification.

(368×)

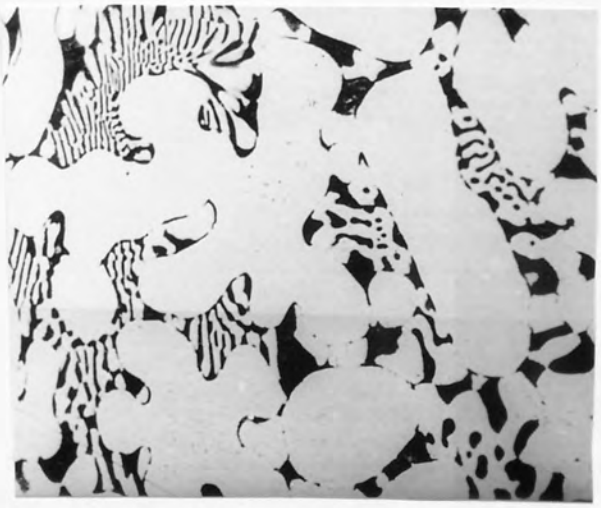

Figure 5.68. SEM micrograph of ACuZinc10 tested at 100 MPa and 160°C, at high magnification.

(458×)

Figure 5.69. SEM micrograph of ACuZinc10 tested at 100 MPa and 160°C at high magnification, showing primary ε dendrites and eutectic.

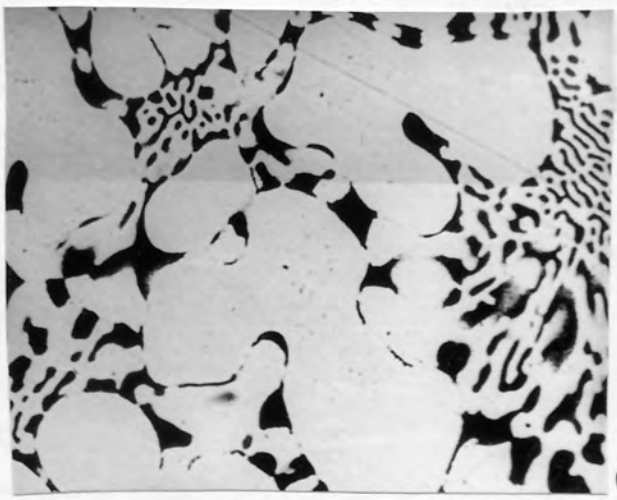

(647×)

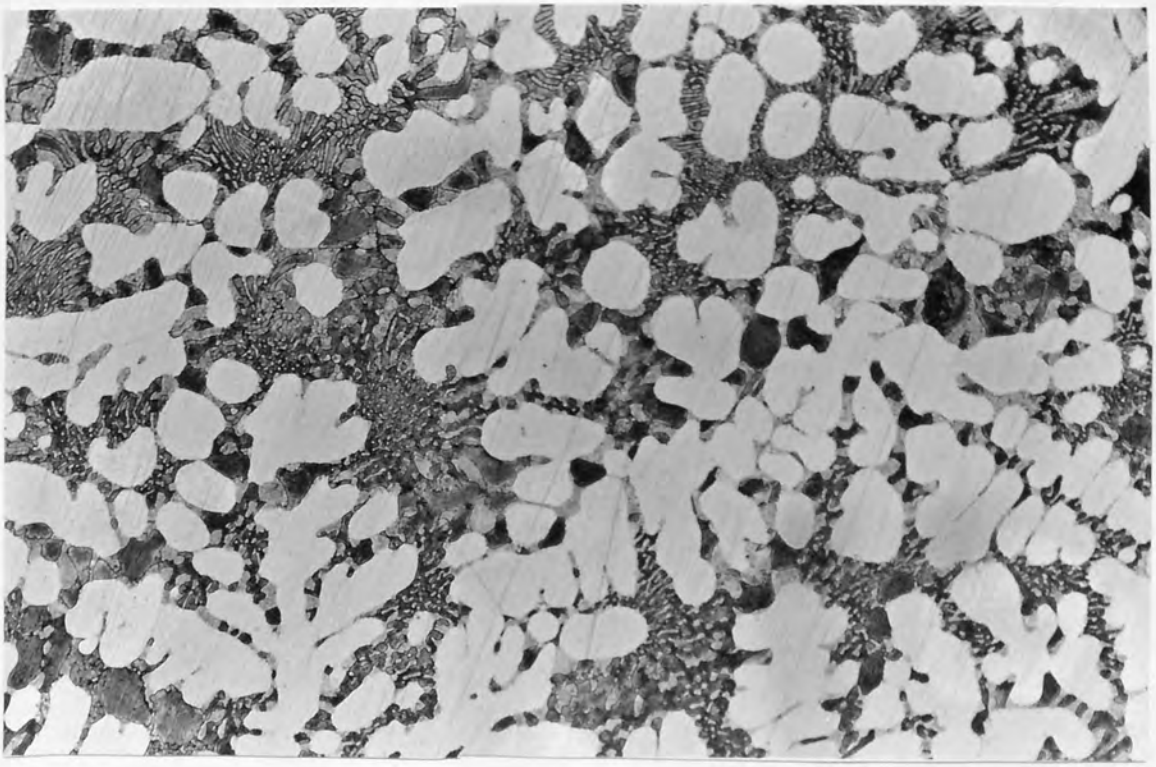

Figure 5.70. Optical Micrograph. ACuZinc10 tested at 100 MPa and 160°C at medium magnification, showing primary ε dendrites and ternary eutectic. (200×)

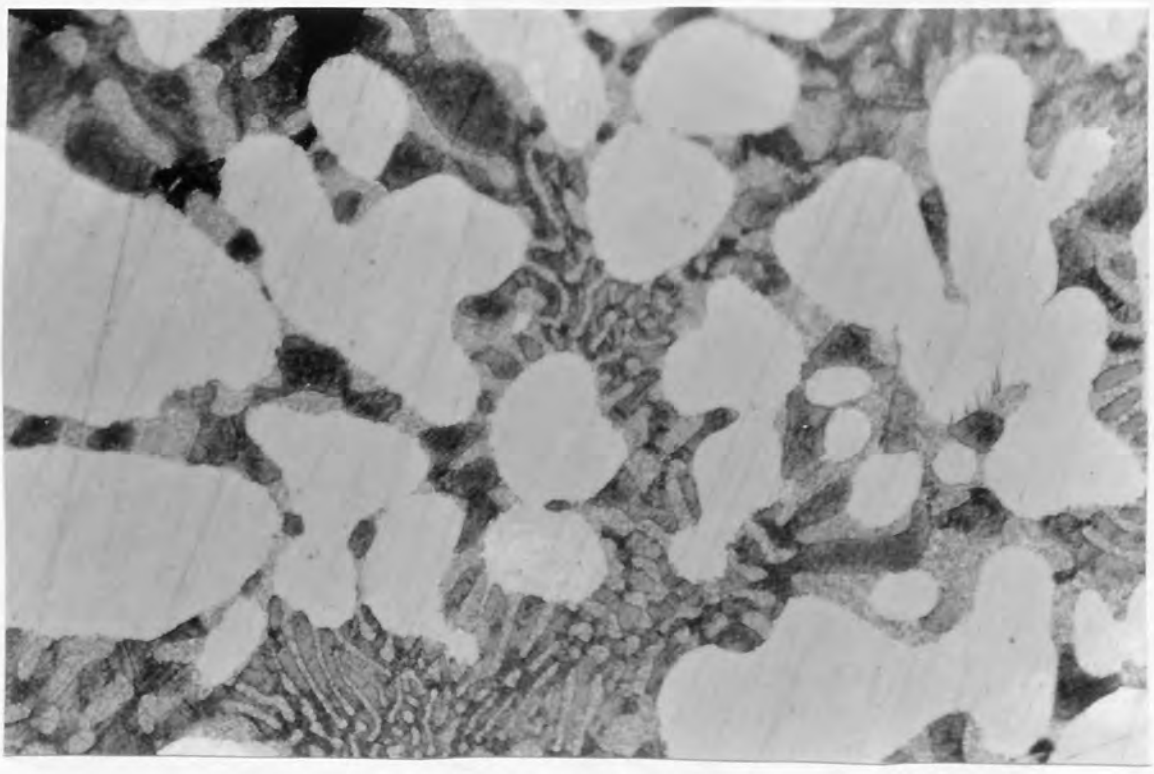

Figure 5.71. Optical micrograph of ACuZinc10 tested at 100 MPa and 160°C, at high magnification. (500×)

CHAPTER 6

6.0 DISCUSSION OF EXPERIMENTAL RESULTS

6.1 Correlation of Creep Data of the Experimental Alloys

For any metal or alloy, simple graphical representations of the creep curves under certain stresses and temperatures are adequate to establish design data of creep such as the time to attain a prescribed creep strain. However, the costs and duration of the tests required to obtain long-term design data are large. It is therefore essential for many practical and theoretical purposes to seek mathematical relationships which would satisfactorily correlate the creep data obtained from a limited number of relatively short duration experiments and allow a quantitative assessment of the creep behaviour of a material under different conditions.

Although primary creep, and in some cases both the primary and the steady-state stages of creep at high temperatures have been used[15] to establish such relationships, many empirical or semi-empirical mathematical relationships suggested in the literature are based on the secondary creep rate data since steady-state creep behaviour is considered as the most important characterisation of creep behaviour of materials[12,22,128] and offers numerous advantages. Therefore, secondary creep rates are generally used for detailed creep analysis of materials. However, the relative importance of the primary, secondary and tertiary creep regions may vary significantly with variations in testing conditions, i.e. stress, temperature and/or metallurgical structure.

The time to attain a particular creep strain (e.g. 1 %) is also an important parameter to be considered when materials data are required for quality assurance or for design purposes, actual measurements must therefore be made of the time to attain particular creep strains, say 0.5 %, 1 % or of the time to fracture under the appropriate test conditions.

As far as the metallurgical structure of alloys is concerned, the present investigation showed that generally the primary creep contraction (%) of alloys No3, No5 and No2 increased with increasing copper content (*Figure 5.11*). This figure showed that there was no great difference in the primary creep contraction of these alloys. In both ACuZinc5 and ACuZinc10 alloys, the primary creep decreased with increase of copper (*Figure 5.11*). Therefore, these results revealed that the primary creep contraction of the alloys increased with an addition of copper up to 5%, but further copper addition did not produce any further increase in the primary creep, as shown for ACuZinc10 in

Figure5.11. The primary creep contraction of alloys was also found to increase with increasing applied stress (*Figures 6.1 to 6.5)* except ACuZinc5 and ACuZinc10 at 20 MPa showed a different behaviour as seen in *Figures 6.4 and 6.5.* The primary creep contraction of ILZRO.16 was found to be higher than other alloys under similar testing conditions.

According to Sully[5], one major difference between the results of compression and tensile creep tests is the extent of deformation in the initial or primary creep stage. It has been proved by simultaneous tensile and compression creep tests on a complex nickel-chromium and an aluminium-copper alloy that the initial or primary creep deformation was larger in the compression than in the tension creep test. [5,128]

When the primary creep contractions (%) for alloy No3 of the current investigation were compared with those of the previous tensile creep tests[84] on the same alloy, it was revealed that in general, the primary creep contraction (%) was greater for compression tests at nearly similar test conditions which verified the observations of Sully. A comparison of primary creep deformation (%) for alloy No3 in compression (current research) and tensile tests[84] has been shown in *Table 6.1.*

Table 6.1: Comparison of Primary Creep (%) for Alloy No3 in Tensile[84] and Compression Tests.

Stress (MPa)	Temp. (°C)	Tensile Test Primary Creep (%)	Compression Test Primary Creep (%)
100	60	0.163	-
100	70	-	0.72
60	60	0.106	-
60	70	-	0.32
40	60	0.101	-
40	70	-	0.13
60	90	0.230	-
60	100	-	0.51
40	90	0.135	-
40	100	-	0.24
41	120	0.25	-
40	130	-	0.23
21	120	0	-
20	130	-	0.17
40	150	0.157	-
40	160	-	0.26
20	150	0.11	-
20	160	-	0.11

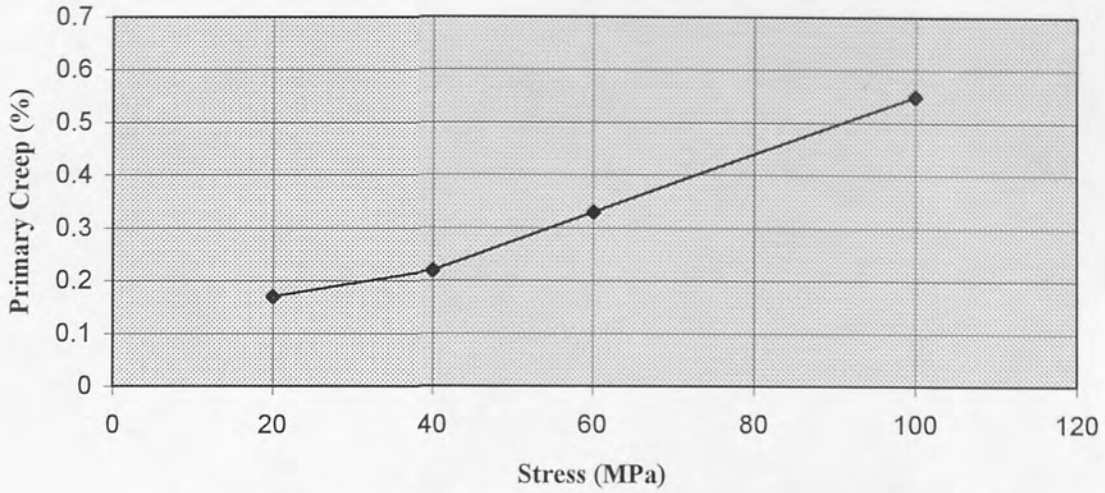

Figure 6.1. Variation of primary creep with applied stress for alloy No3 at 130° C.

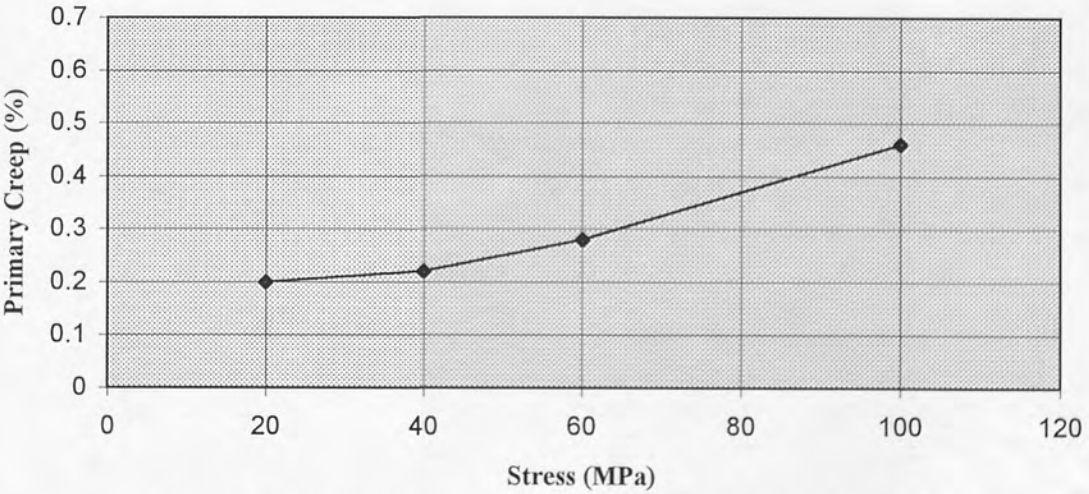

Figure 6.2. Variation of primary creep with applied stress for alloy No5 at 130° C.

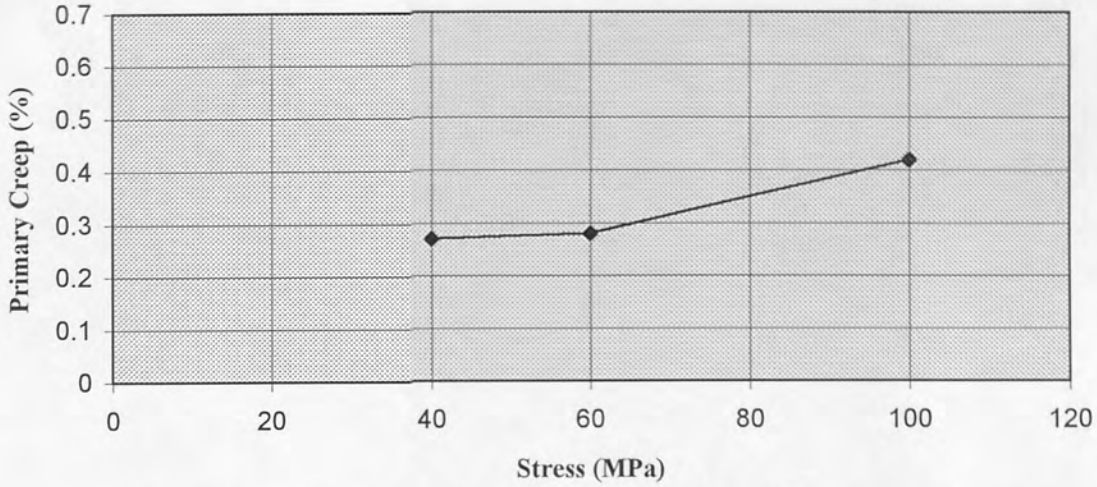

Figure 6.3. Variation of primary creep with applied stress for alloy No2 at 130° C.

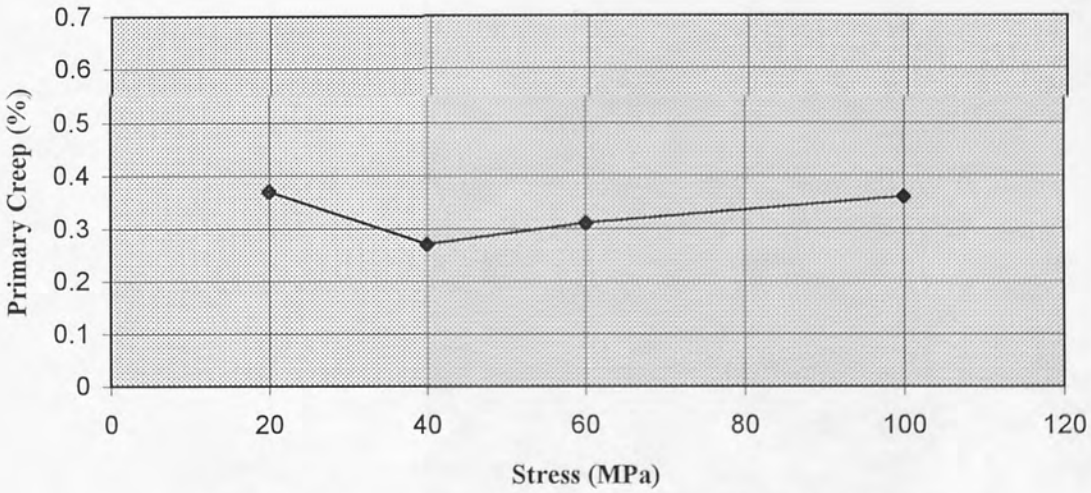

Figure 6.4. Variation of primary creep with applied stress for ACuZinc5 at 160° C.

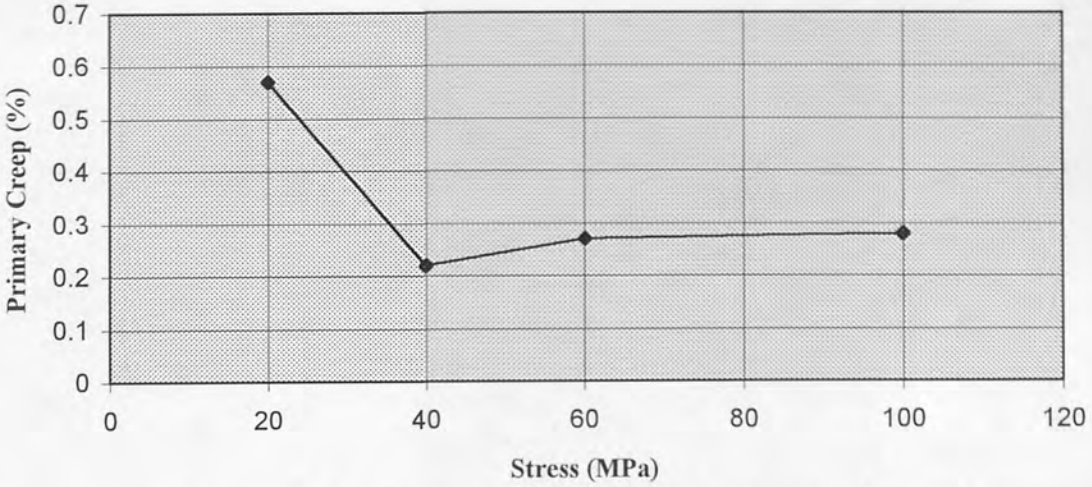

Figure 6.5. Variation of primary creep with applied stress for ACuZinc10 at 160° C.

On the other hand, for alloy No3 which showed the least amount of primary creep contraction of all, durations of the secondary creep regions of the tests were comparatively short, and in some tests, a creep strain of 1% was reached in the tertiary creep region.

Since the creep specimen used during this investigation had L/D < 3, where L is the length and D is the diameter of the specimen, some specimens showed barrelling at higher stresses and temperatures, e.g. the specimen of alloy No3 at 100 MPa and 160°C barrelled after about 8 % of total creep strain.

A knowledge of the variation of creep properties in a material with temperature and with stress is of extreme practical importance, since without knowledge of the relation between creep and these variables, it is impossible to use the results of the creep tests to predict the creep behaviour at stresses and temperatures other than those at which the tests are carried out.

Several empirical relationships between creep rate or creep strain, stress and temperature have been suggested[13,15,18,21,25] for the purpose of predicting creep behaviour of different materials.

A linear relationship was obtained between the logarithm of applied stress and the logarithm of time to attain 1% creep strain in *Figures 6.6, 6.7, 6.8, 6.9 and 6.10* for

alloys No3, No5, No2, ACuZinc5 and ACuZinc10, respectively which indicated that the times to a given creep strain were a simple power law function of the applied stress, and implied that the creep rate of zinc alloys could be correlated by the following expression:[129]

$$\dot{\varepsilon}_S = B\sigma^n \exp(-Q/RT) \qquad (6.1)$$

where B is a constant, σ the nominal stress, n the stress exponent, Q an effective activation energy for creep, R the universal gas constant and T is the absolute test temperature.

Equation 6.1 is known as Dorn-Weertman equation.[3] This relation was derived from Norton's power law[21] *(Equation 2.20). Equation 6.1* was used in the form of *Equation 2.30* by Murphy et al[93] to correlate the experimental creep data of gravity-cast zinc alloys of near-eutectoid composition. Later, Murphy and Durman[89,130] used *Equation 2.30* to correlate the total creep elongation (up to 1%) of zinc-rich alloys No3, ZA.8 and ZA.27 with the testing conditions where n = 3.5 and Q = 106 kJ/mole for all three alloys tested. *Equation 2.30* was as follows: [130]

$$f(\varepsilon) = A\, t\, \sigma^n \exp(-Q/RT)$$

where A is a constant which takes into account the effects of composition and metallurgical structure, t the creep time and f (ε) is an undefined function of the creep strain ε, and when A, σ, n, Q and T are constant, f (ε) represents the shape of the creep strain versus time curve.

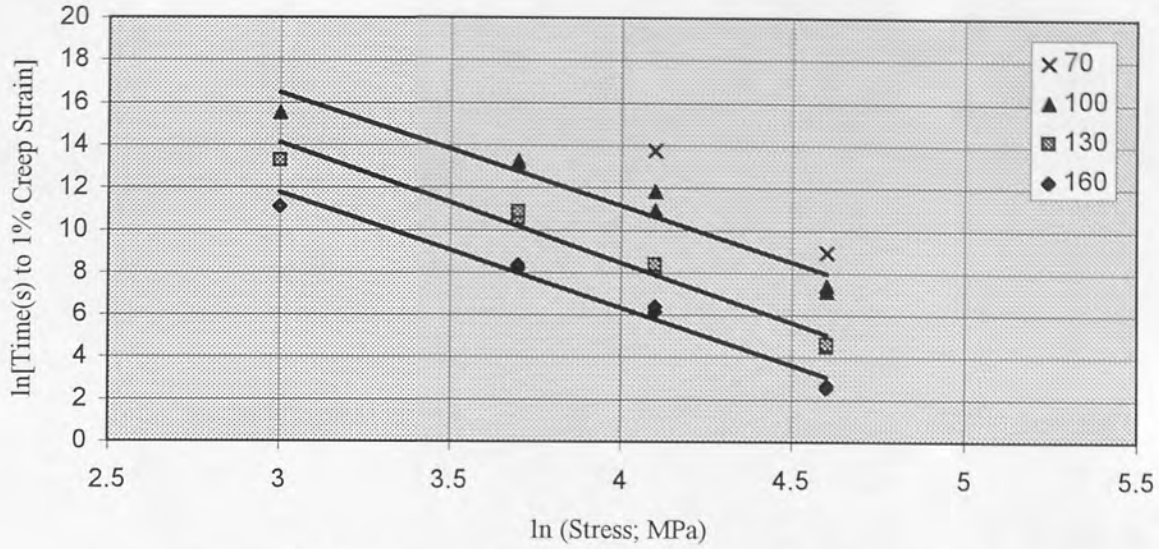

Figure 6.6. Variation of time to 1% creep strain with applied stress at different temperatures for alloy No3.

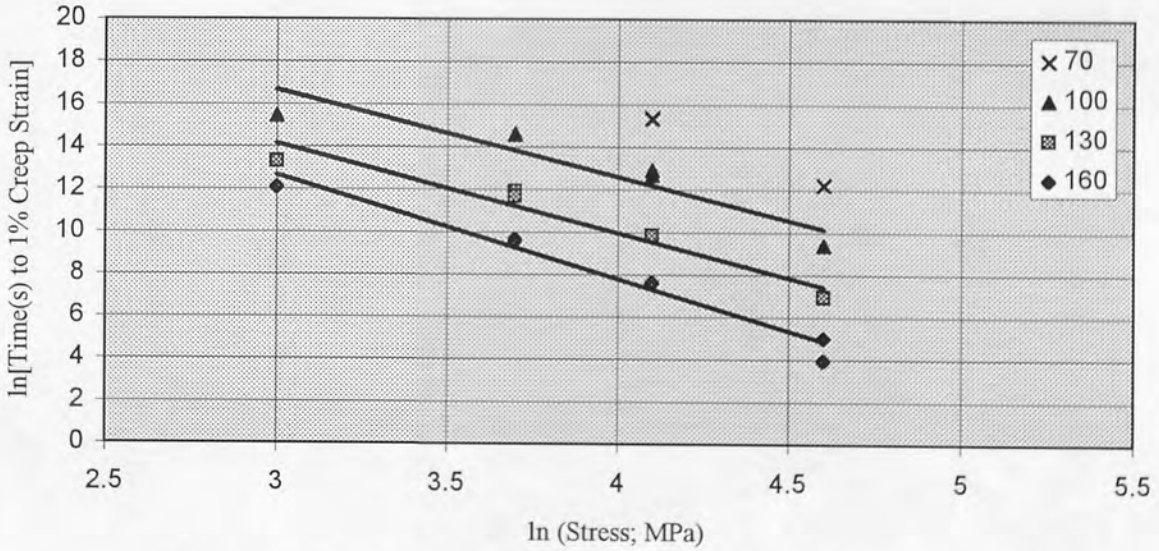

Figure 6.7. Variation of time to 1% creep strain with applied stress at different temperatures for alloy No5.

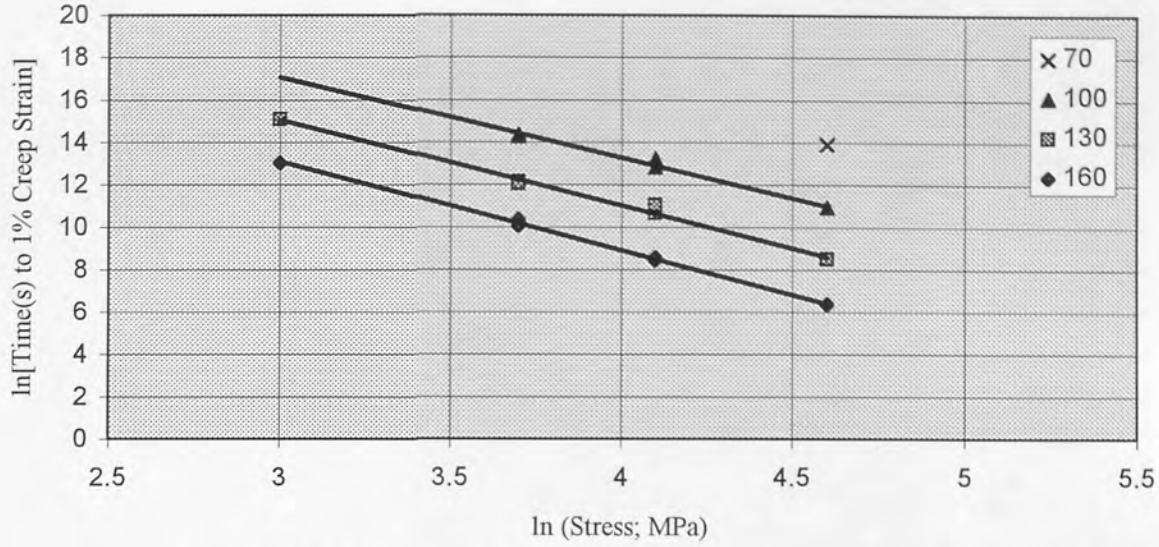

Figure 6.8. Variation of time to 1% creep strain with applied stress at different temperatures for alloy No2.

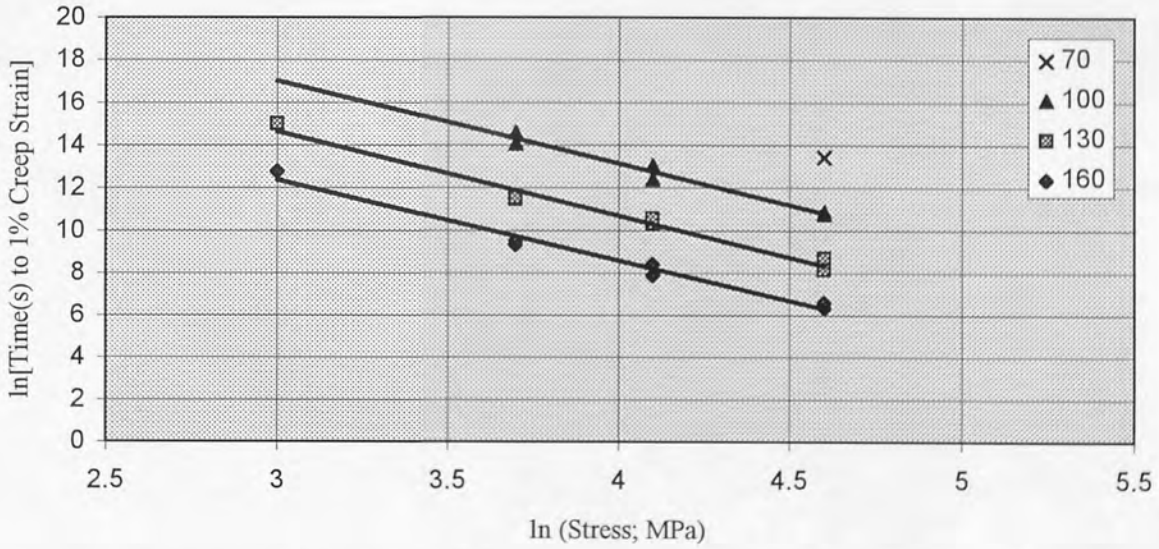

Figure 6.9. Variation of time to 1% creep strain with applied stress at different temperatures for ACuZinc5.

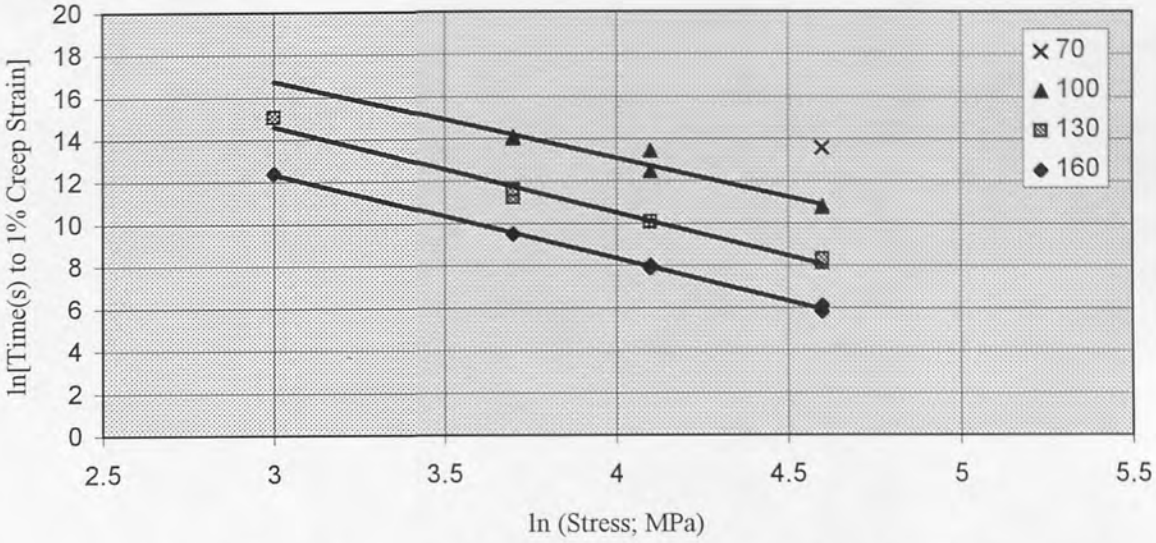

Figure 6.10. Variation of time to 1% creep strain with applied stress at different temperatures for ACuZinc10.

Murphy et al [130] derived the following relationship from *Equation 2.30* for a fixed creep strain by taking logarithms and rearranging:

$$\ln t = C' - n (\ln \sigma) + Q/RT \qquad (6.2)$$

where C' is a new constant which incorporates A and ε.

The approximate linearity of the plots for the alloys *(Figs. 6.6 to 6.10)* showed that the total creep contraction (up to 1%) can be related to the applied stress, temperature and the time of these tests by using the *Equation 6.2.*

If this final relationship is obeyed for the zinc alloys studied here, a plot of ln secondary creep rate (s^{-1}) to any fixed creep strain against ln stress (MPa) at constant temperature should be linear with a slope of (-n) with an intercept ($C' + Q/RT$), or a plot of ln time (s) to any fixed creep strain versus 1/T at constant stress should be linear with a slope of Q/R, and an intercept of $[C' - n(\ln \sigma)]$.

Such plots, as shown in *Figures 5.12 to 5.16*, plotted as ln secondary creep rate to 1% strain versus ln stress were in fact all linear with constant slopes over the majority of temperatures and stresses used, indicating a mean stress exponent (n) of 4.2 for all experimental alloys.

The plots of ln time to 1% creep strain versus 1/T at constant stresses shown in *Figures 5.17 to 5.22* for all five alloys were also linear with a good correlation of the data, indicating mean activation energy for creep (Q) of 104 kJ/mole for alloys. The value of activation energy (Q) is very close to that obtained in the tensile creep experiments on zinc-based alloys No3, ZA.8 and ZA.27 by Durman.[84]

Therefore, it was obvious that all the above linear plots were in accordance with the form of the single equation used, and thus the creep behaviour of the alloys could be related to the testing conditions by this single relationship over all stress and temperature ranges. Once the values of n and Q are known, the constant C', which is a characteristic for each alloy and the chosen % strain, can be calculated from the intercept ($C' + Q/RT$). Such a parametric plot therefore, should allow the total creep strain to be calculated for any combination of temperature, applied stress and time.

However, a considerable degree of extrapolation is required to obtain C' in this way. Instead, C' is obtained and correlation of the data is given more clearly by a parametric plot of $[(Q/RT) - n \ln \sigma]$ against ln time to a given % contraction, which should give linear plots of 'unit slope' and intercept C' along the ln time ordinate. The differences in creep behaviour between the alloys are derived solely from differences in the values of this constant (C').

The plots of ln time to attain 0.2, 0.5, 0.7 and 1 % creep contraction versus the above creep parameter for alloys No3, No5, No2, ACuZinc5 and ACuZinc10 are shown in *Figures 6.11, 6.12, 6.13, 6.14 and 6.15,* respectively, using the unsmoothed original experimental data from individual creep curves (Appendix A) and excluding the data at 40 MPa and 70°C, and 20 MPa at 100°C for alloys No2, ACuZinc5 and ACuZinc10 due to very small amount of total creep strain achieved during these tests. These graphs show that although there is a great deal of scatter in the 0.2 % plots, where differences between individual creep tests are significant, a very good correlation of the data is obtained in general by the parametric plots for 0.5, 0.7 and 1% total creep contraction, indicating that this parameter may be used to estimate the creep behaviour of the experimental alloys with high confidence. The values of the the creep constants (C') were obtained from these plots for all alloys and % contractions, and are listed in *Table 6.2.*

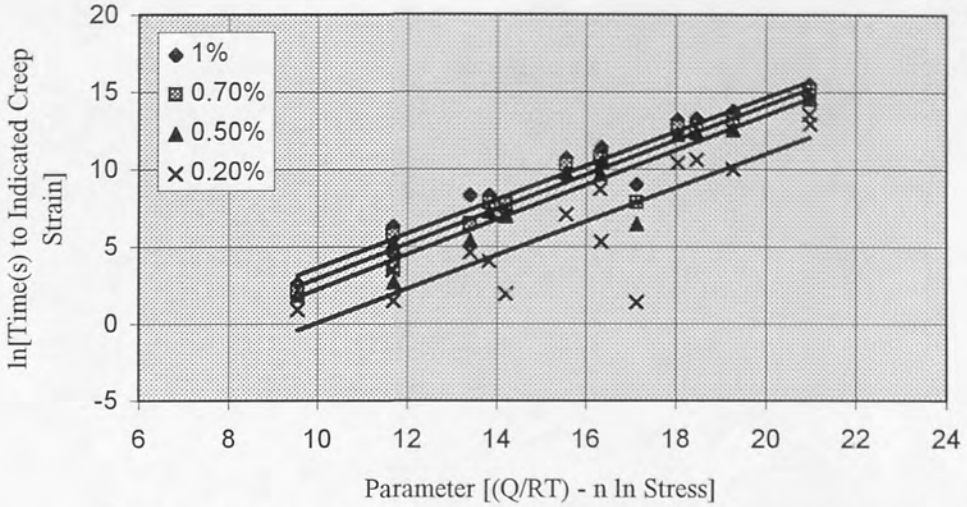

Figure 6.11. Ln [times(s)] to various creep strains versus creep parameter for alloy No3.

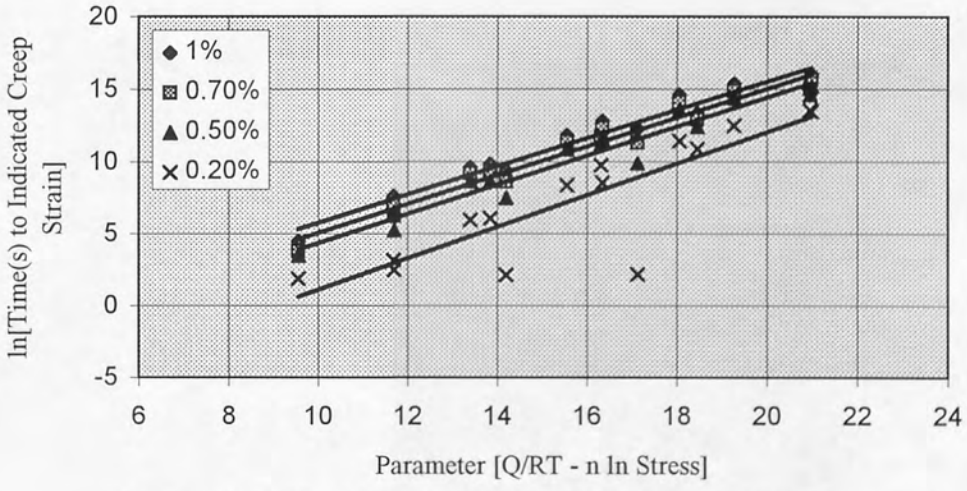

Figure 6.12. Ln [times(s)] to various creep strains versus creep parameter for alloy No5.

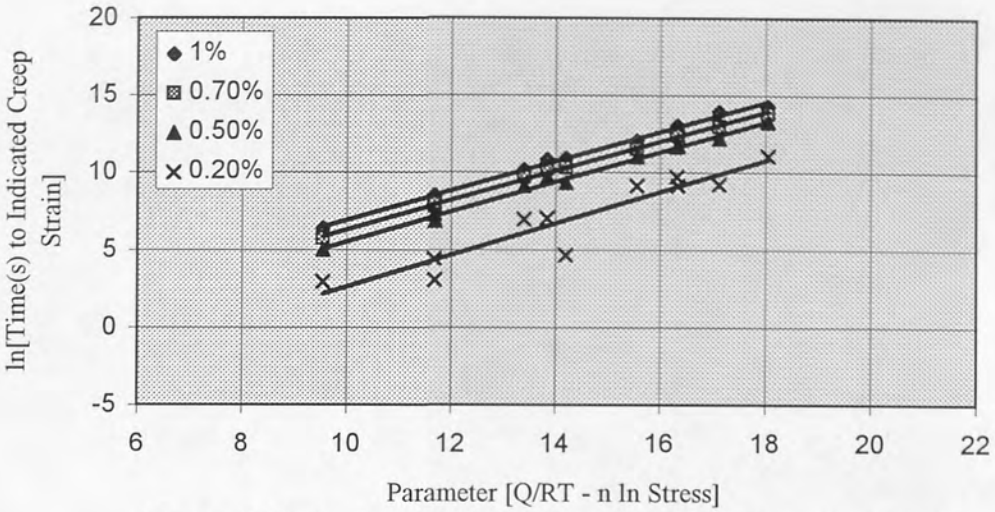

Figure 6.13. Ln [times(s) to various creep strains versus creep parameter for alloy No2.

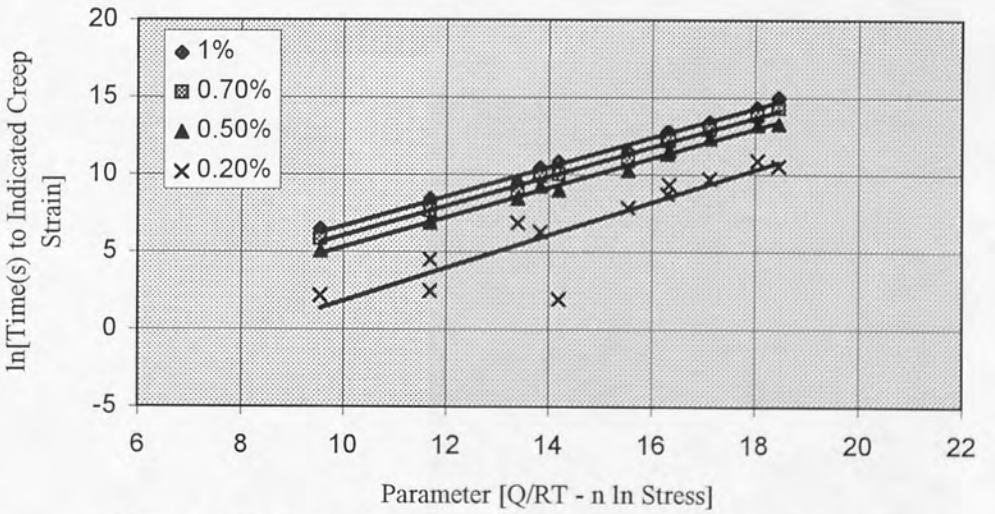

Figure 6.14. Ln [times(s)] to various creep strains versus creep parameter for ACuZinc5.

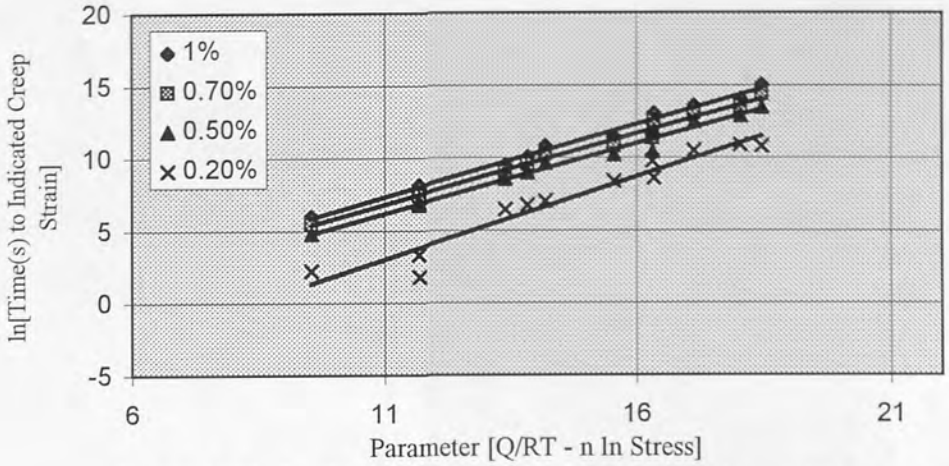

Figure 6.15. Ln [times(s)] to various creep strains versus creep parameter for ACuZinc10.

In order to compare the relative creep performance of the alloys for the same amount of creep contraction, the parametric plots for creep contractions of 0.2, 0.5, 0.7 and 1% were plotted in *Figures 6.16, 6.17, 6.18 and 6.19,* respectively. From these figures, it is clear that alloy No2 has a substantially better creep performance than alloys No3 and No5 for all strain levels, also it is slightly better than ACuZinc5 and ACuZinc10 for all creep strains used (0.2 to 1.0 %).

For general use of the *Equation 6.2,* values of the creep constant C' in *Table 6.2* were plotted against the selected % contractions as C' versus ln (% creep contraction) in *Figures 6.20 and 6.21* for the commercial zinc-rich and ACuZinc alloys, respectively. These plots yielded a linear relationship, with a fair correlation of the data, so that the value of C' can be calculated from the plot easily for any given % contraction and using the *Equation 6.2,* such data can be used to calculate the permissible combinations of stress, temperature and creep life for any total creep strain within the range of 0.2 to 1.0 %. Although deviations were observed at the lowest strain level (0.2 %) for all experimental alloys, such deviations are not unusual at low strains.

Table 6.2. The values of the creep constants C′ for alloys No3, No5, No2, ACuZinc5 and ACuZinc10.

Alloy	Strain (%)	Creep Constant (C′)
No3	0.2	-10.81
	0.5	-9.04
	0.7	-8.24
	1.0	-7.32
No5	0.2	-9.80
	0.5	-5.82
	0.7	-4.85
	1.0	-3.98
No2	0.2	-7.68
	0.5	-4.20
	0.7	-3.26
	1.0	-2.66
ACuZinc5	0.2	-8.75
	0.5	-4.23
	0.7	-3.47
	1.0	-2.82
ACuZinc10	0.2	-9.54
	0.5	-4.42
	0.7	-3.93
	1.0	-3.63

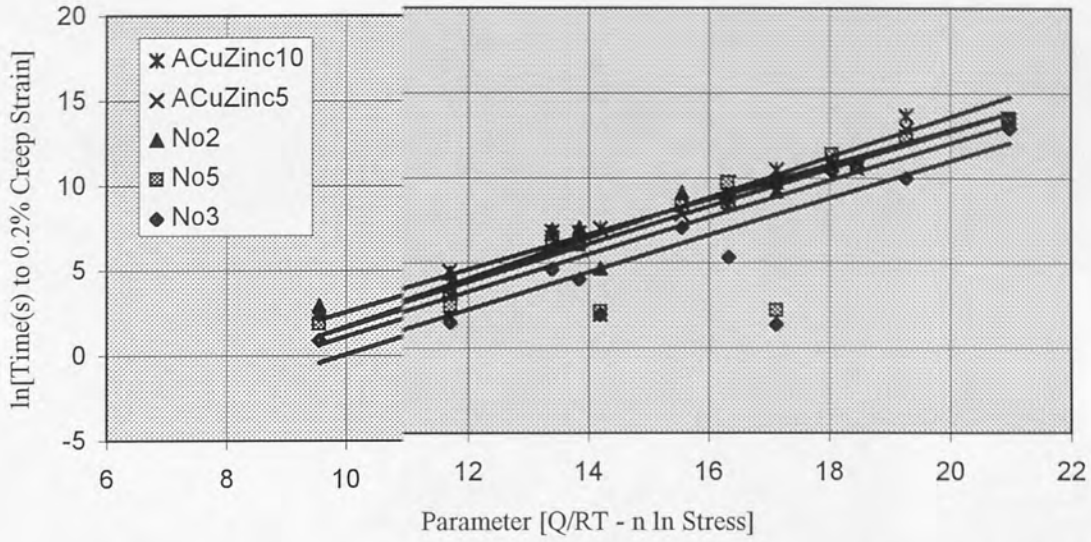

Figure 6.16. Ln [times(s)] to 0.2% creep strain versus creep parameter for experimental alloys.

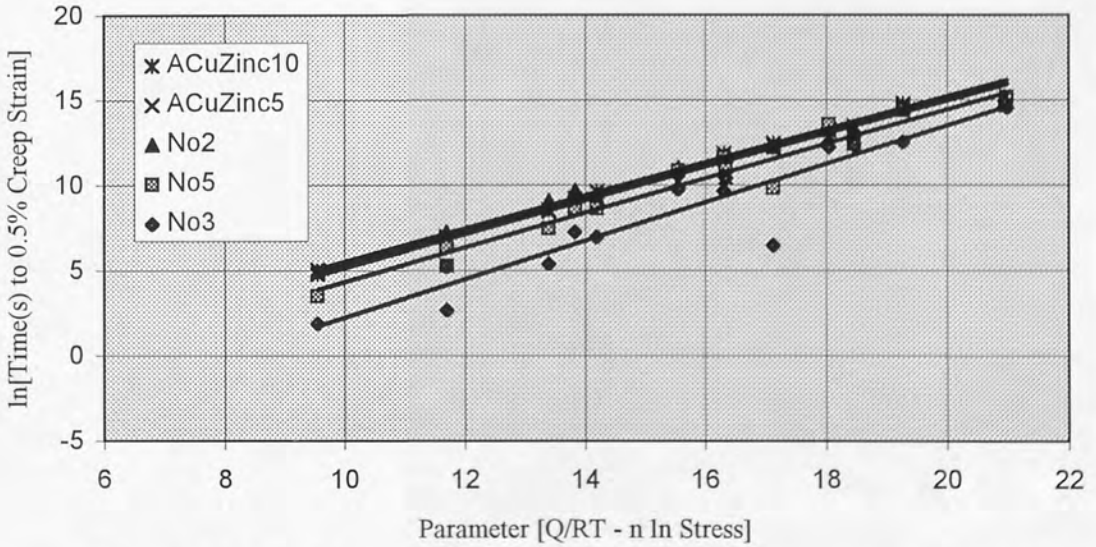

Figure 6.17. Ln [times(s)] to 0.5% creep strain versus creep parameter for experimental alloys.

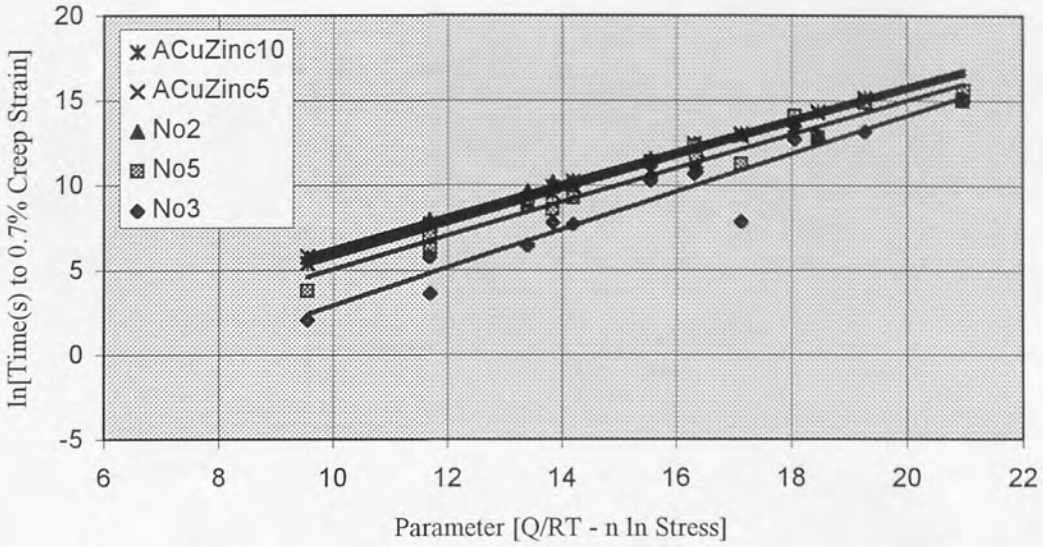

Figure 6.18. Ln [times(s)] to 0.7% creep strain versus creep parameter for experimental alloys.

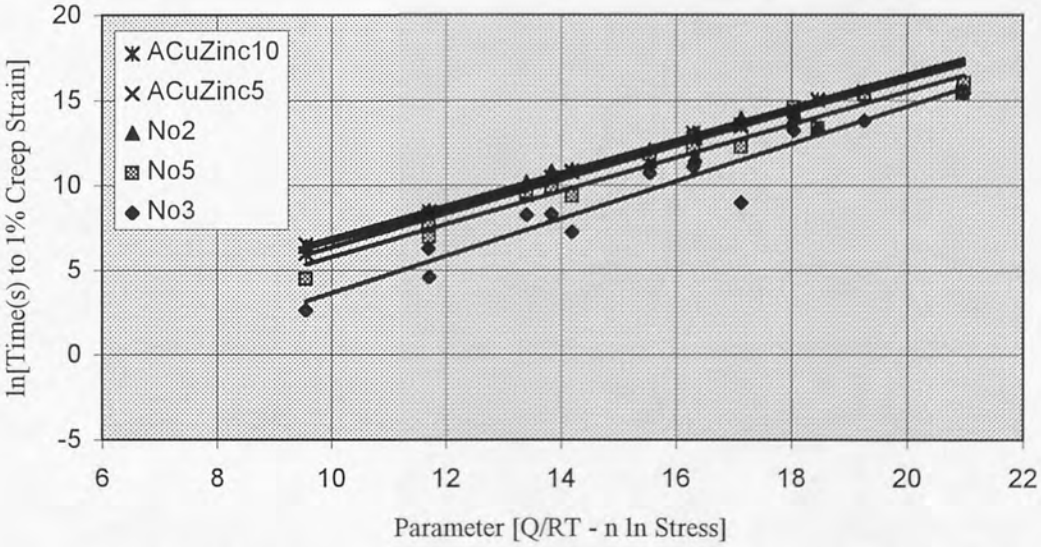

Figure 6.19. Ln [times(s)] to 1% creep strain versus creep parameter for experimental alloys.

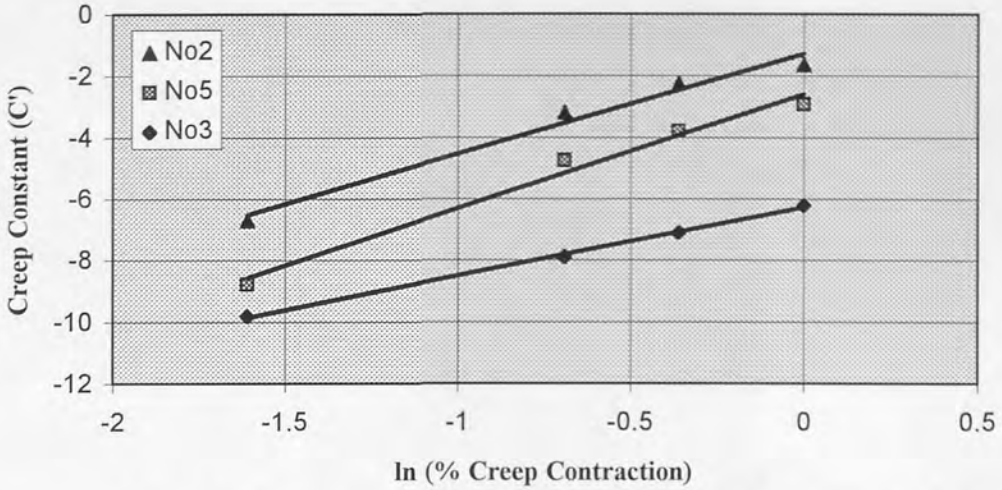

Figure 6.20. Variation of constant C' with creep contractions for alloys No3, No5 and No2.

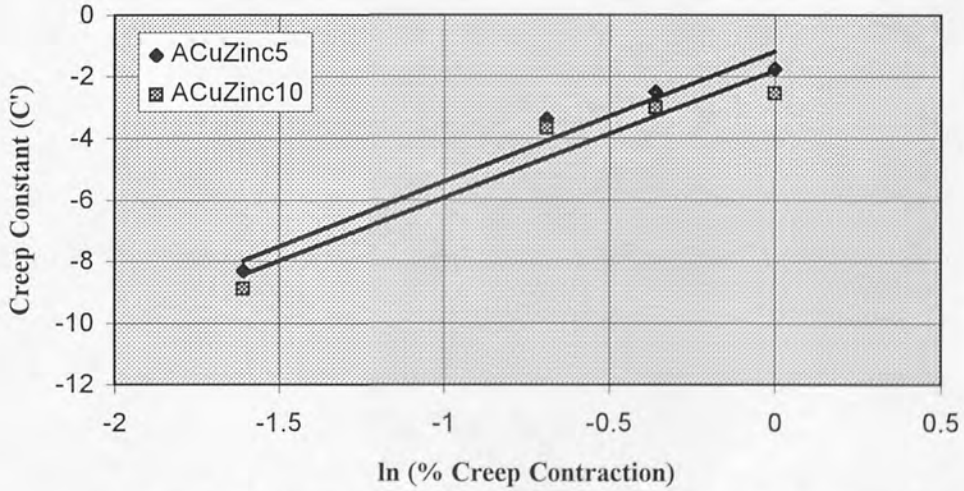

Figure 6.21. Variation of constant C' with creep contractions for ACuZinc5 and ACuZinc10.

After finding the values of the stress exponent (n), the activation energy (Q) and creep constant (C'), the maximum continuous design stresses which produce 0.2%, 0.5%, 0.7% or 1.0% creep strains in 100,000 hours (11.4 years) at different test temperatures were calculated. The service life of 100,000 hours was used on the basis of ASME Boiler Code, which is also used by the zinc industry, where the maximum design stress based on creep is that which produces a strain of 0.1% in 10,000 hours.[83] These values of design stresses are listed in *Table 6.3,* also the results of the calculations are plotted as a family of curves in *Figures 6.22, 6.23, 6.24, 6.25 and 6.26* for the alloys No3, No5, No2, ACuZinc5 and ACuZinc10, respectively which enable the total creep strain within

the range of 0.2 to 1.0% to be determined from any combination of stress and temperature for service lives of 100,000 hours (11.4 years).

Design stresses at lower temperatures for alloy No3, shown in *Table 6.3* are close to those found in tensile creep experiments[130] for the same alloy (No3) within the applicability range of the equation used. However, these stresses were higher than those calculated in tensile creep tests for alloy No3 at comparatively higher temperatures at all strains (0.2-1%), e.g. at 100°C, the design stress required to produce 1% strain in tensile creep was 2.70 MPa, whereas it was 4.72 MPa for compression creep test during the current research.

One major cause may be be due to the coarse-grained structure of the specimens used in the compressive creep tests as compared to tensile creep tests where fine-grained specimens were used. Keeping in view that the ratio of the volume of the boundaries to the volume of the crystals for a given specimen depends upon the crystal size and, it is obvious that for a fine-grained material, this ratio will be greater than it would be for a coarse-grained material which has smaller total boundary volume. Therefore, the boundaries are considered more important in determining the properties of a fine-grainedmaterial than of a coarse-grained material. At high temperatures ($T \geq 0.5\ T_m$), viscous behaviour of the boundary region is primarily considered responsible for creep in a material. On the other hand, at low temperatures, the boundary is much stronger in relation to the crystal. At high temperatures, a coarse-grained material will therefore be inherently more creep-resistant than a fine-grained material, whereas at low temperatures, the reverse would be expected to occur. [128] The experimental results during the current work strongly support this argument.

The design stresses found for ACuZinc5 were slightly higher than those of ACuZinc10 under all testing conditions, which exhibited different behaviour from those of tensile creep tests[79,80] on these alloys because in those tests ACuZinc10 showed better creep resistance than ACuZinc5 under all testing conditions. However, both ACuZinc alloys were more creep resistant than ZA.8 and ZA.27 previously tested for tensile creep[130] under comparable testing conditions.

On the basis of calculated design stresses, it was found that alloy No2 had slightly better creep performance than ACuZinc5 and ACuZinc10 at all strain levels. At 160°C, the

design stress required for ACuZinc5 to produce 1 % strain was found to be 4.56 MPa for service life of 100,000 hours (11.4 years) as compared to 4.73 MPa for alloy No2. This showed that the design stress for alloy No2 was only about 3 % more than that of ACuZinc5 at 160°C. Similarly, the design stress required to achieve 1% creep strain at 160°C for ACuZinc10 was 3.75 MPa showing lower creep strength than alloy No2.

An important conclusion can be drawn from these results that the copper content in these experimental alloys up to about 3 % (alloy No2) increased the creep strength at all strains (up to 1.0 %) and increasing the copper beyond 3% did not assist much in increasing the creep resistance of alloys, as shown in *Table 6.3* for ACuZinc5 and ACuZinc10. It was also experienced that increasing the copper content beyond 5 % did not improve the creep resistance of these zinc-rich alloys at all which can be seen from the results of ACuZinc10. This is contrary to the results obtained from the tensile creep tests[79,80] for ACuZinc5 and ACuZinc10.

The values of allowable design stresses obtained at all strain levels for service life of 100,000 hours for alloys No2 and ACuZinc5 are very close to each other under similar testing conditions, as shown in *Table 6.3*.

Unfortunately no other data on the kinetics of compressive creep of these alloys are available for comparison with the present results. However, alloy No3 is the only experimental alloy for which long-term actual tensile creep data are available in the literature[83] *(Figure 2.6)*. From *Figure 2.6,* it can be observed that the experimental data of alloy No3 at 25°C indicates an allowable design stress of 30 and 25.8 MPa to produce 0.5% total creep strain in five and ten years, respectively. The allowable design stresses (in compressive creep) for the same amount of creep strain (0.5%) in the same period at 25°C is estimated by the empirical equation *(Equation 6.2)* as 28.6 and 24.2 MPa, respectively which are slightly lower than those found in long-term tensile creep tests. This close agreement of design stresses indicates that the empirical equation can be used to determine the design stresses for long-term service lives of the alloys.

Table 6.3. Maximum continuous design stresses (MPa) to produce % strain in 100,000 hours.

Temperature (°C)		70	100	130	160
No3	0.2 %	4.13	2.06	1.13	0.68
	0.5 %	6.31	3.14	1.73	1.04
	0.7 %	7.62	3.79	2.09	1.25
	1.0 %	9.49	4.72	2.60	1.56
No5	0.2 %	5.26	2.62	1.44	0.86
	0.5 %	13.85	6.90	3.80	2.28
	0.7 %	17.16	8.54	4.71	2.82
	1.0 %	21.02	10.46	5.77	3.46
No2	0.2 %	8.71	4.33	2.39	1.43
	0.5 %	19.94	9.93	5.47	3.28
	0.7 %	24.94	12.42	6.85	4.10
	1.0 %	28.78	14.32	7.90	4.73
ACuZinc5	0.2 %	6.75	3.36	1.85	1.11
	0.5 %	19.80	9.86	5.43	3.26
	0.7 %	23.73	11.81	6.51	3.90
	1.0 %	27.70	13.79	7.60	4.56
ACuZinc10	0.2 %	5.59	2.78	1.54	0.92
	0.5 %	18.92	9.42	5.19	3.11
	0.7 %	21.27	10.59	5.84	3.50
	1.0 %	22.79	11.34	6.25	3.75

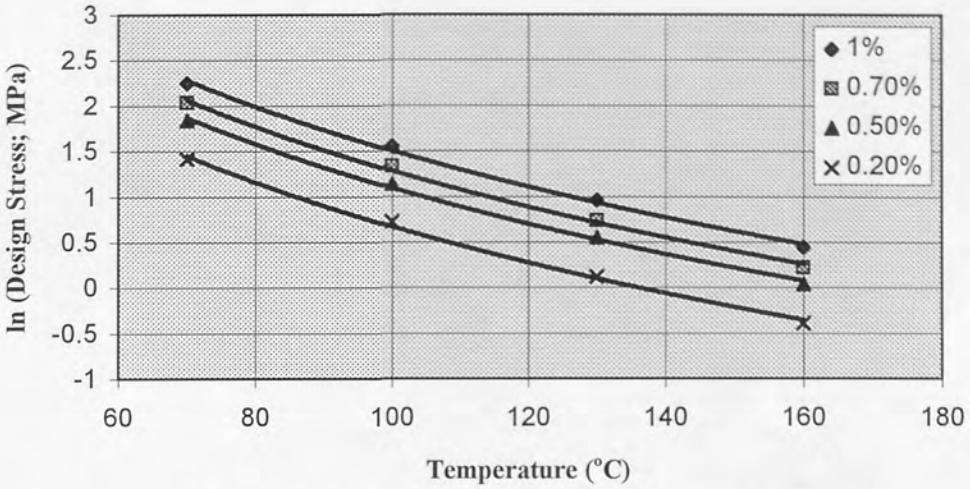

Figure 6.22. Maximum design stresses for indicated allowable creep strains in 100,000 hours (11.4 years) design life for alloy No3.

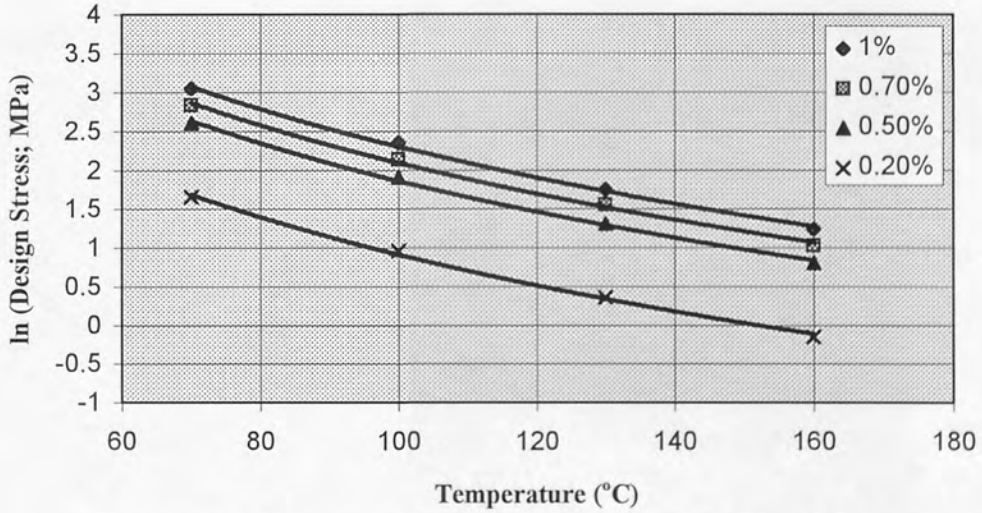

Figure 6.23. Maximum design stresses for indicated allowable creep strains in 100,000 hours (11.4 years) design life for alloy No5.

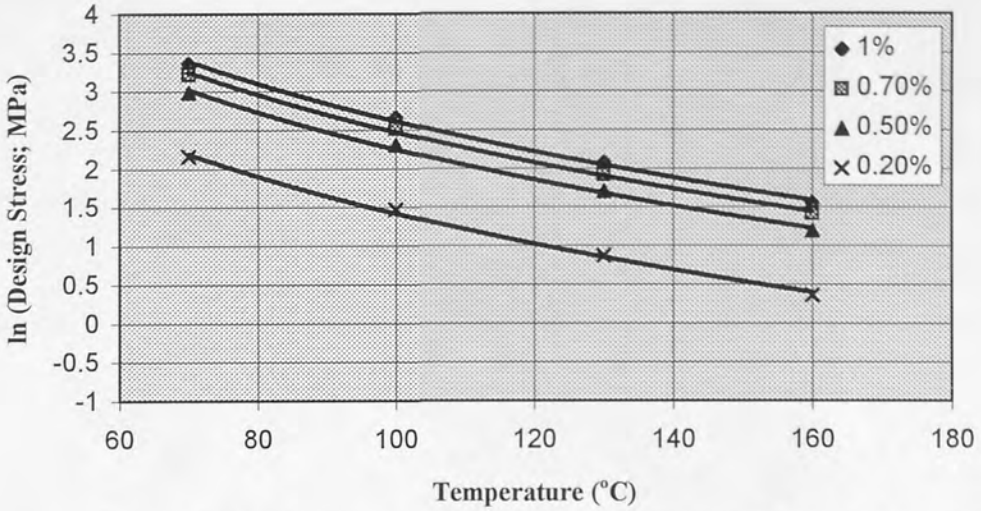

Figure 6.24. Maximum design stresses for indicated allowable creep strains in 100,000 hours (11.4 years) design life for alloy No2.

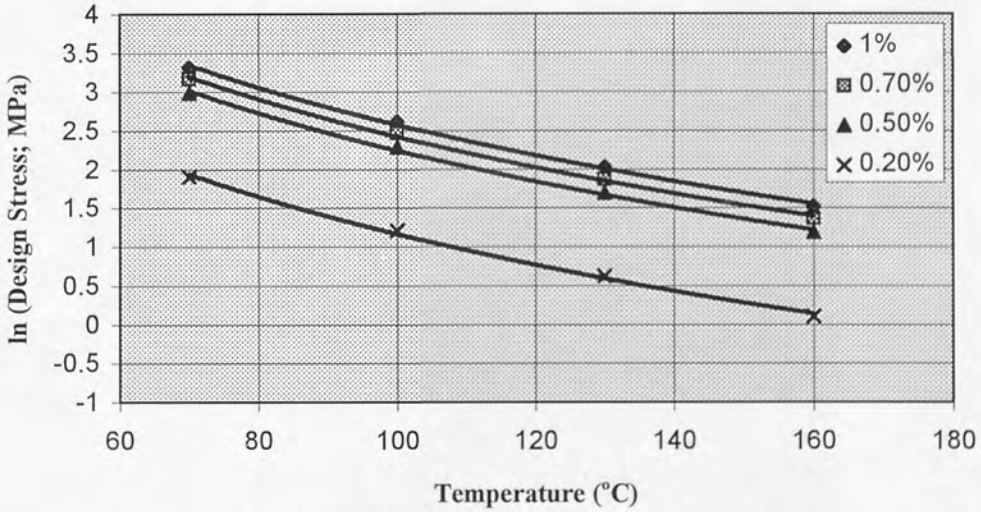

Figure 6.25. Maximum design stresses for indicated allowable creep strains in 100,000 hours (11.4 years) design life for ACuZinc5.

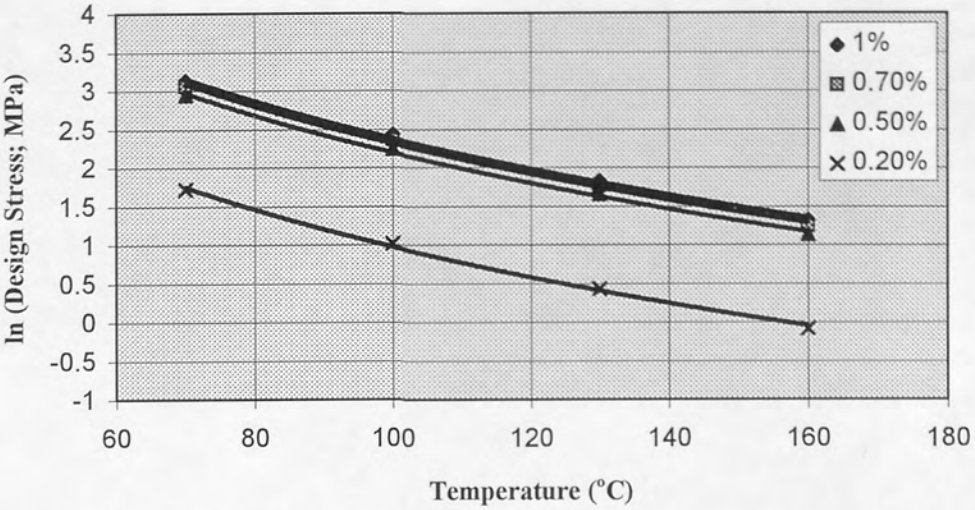

Figure 6.26. Maximum design stresses for indicated allowable creep strains in 100,000 hours (11.4 years) design life for ACuZinc10.

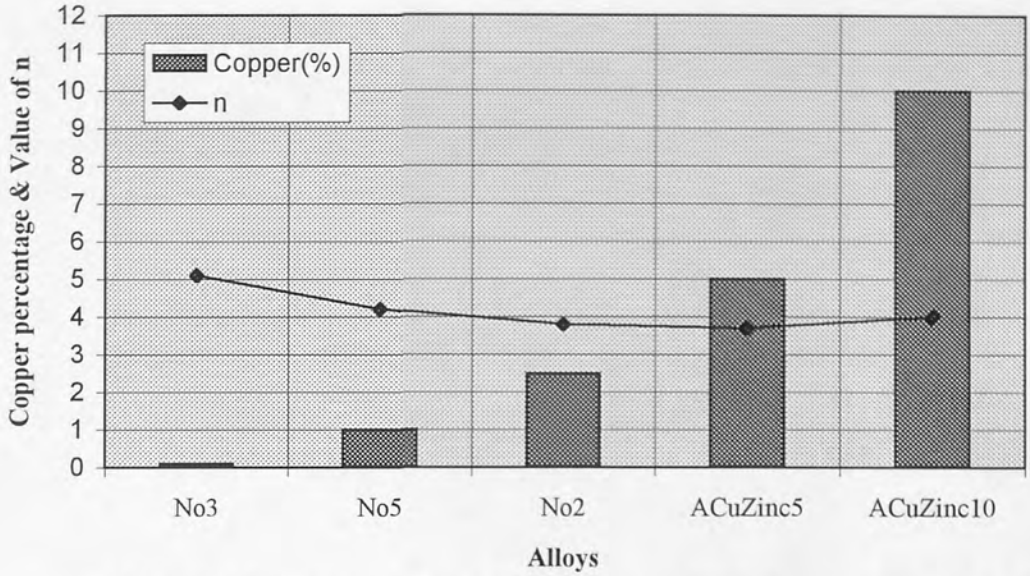

Figure 6.27. Variation of the stress exponent (n) with copper content of alloys.

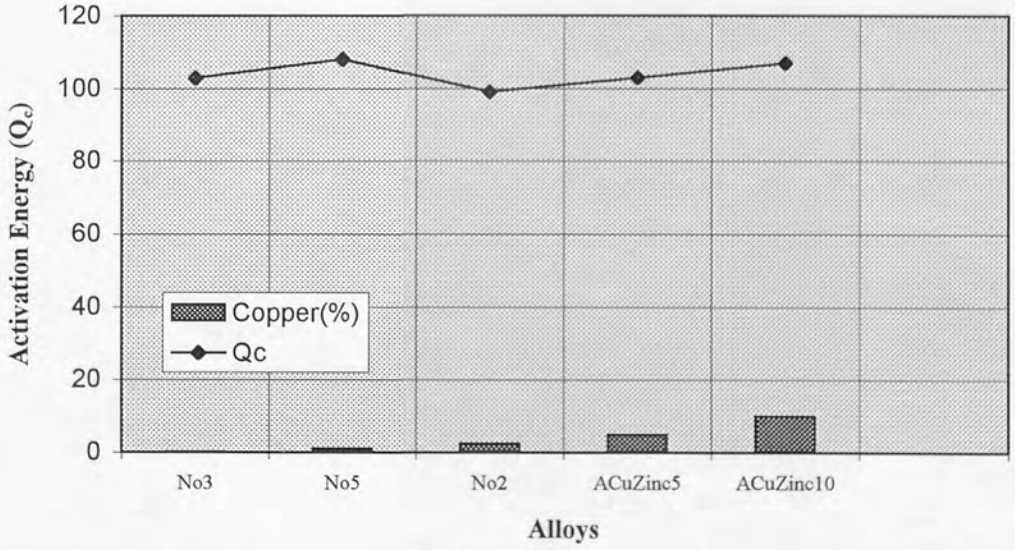

Figure 6.28. Variation of activation energy with copper content of alloys.

6.2 Theoretical and Metallographic Considerations

The relative importance of the primary, secondary and tertiary stages of creep can change significantly with variations in stress and/or temperature. The exact type of creep behaviour exhibited by the metals or alloys depends on the conditions of stress and temperature during the test. As a result, at high stresses, a creep strain of say 1% may be observed in the primary stage, but only in the tertiary stage at low stresses.

Although the time required to attain a specified strain (0.5%, 1%) is considered as an essential requirement for many engineering design procedures, the secondary creep rate is also an important parameter because it provides the most definitive characterisation of creep processes. It is therefore widely used as a measure of relative creep resistance of metals and alloys, and researchers have given a considerable attention on the experimental determination and theoretical interpretation of the ways in which secondary creep rates vary with stress, temperature and material parameters.

A comparison of the secondary creep rates for experimental alloys *(Figures 5.12 to 5.16)* showed that alloy No2 had generally much lower secondary creep rate than those of commercial alloy No5 which in turn was better than alloy No3 over all testing temperatures and stresses. It was also found that alloy No2 had a slightly lower secondary creep rate than ACuZinc5 and ACuZinc10 under most testing conditions. Both ACuZinc alloys had generally lower secondary creep rates than alloys No3 and No5. It was also observed that although alloy No3 had the least primary creep, due to its higher secondary creep rates, it was much inferior to other experimental alloys. The experimental results showed that total creep performance of ILZRO.16 was substantially better than the commercial and ACuZinc alloys. It was observed that times to 1% creep strain were much higher (3-5 times) than alloys No2, ACuZinc5 and ACuZinc10, at 100 MPa and 160°C. The secondary creep rates for ILZRO.16 were also much lower than other alloys under similar testing conditions. Therefore, on the basis of available results, it was evident that ILZRO.16 had much higher creep resistance than all other experimental alloys.

Stress & Temperature Dependence of the Creep Rate:

The stress exponents (n) and the activation energies for creep (Q_c) were determined for all alloys on the basis of secondary creep rates and times to 1% creep strain. The values of stress exponents and activation energies of alloys have been given in *Tables 5.2 and 5.4*, respectively. It can be seen from the *Table 5.2* that values of the stress exponents are within the range of 3.7 ~ 5.1, which are in agreement with those given by other

investigators[98] for Zn-Al alloys. However, these values are higher than those reported by some other researchers for tensile creep tests.[93,130,131] These values of n were found to decrease with the increase of the copper content in the alloys tested, but the copper content above 5% increased the value of n, and can be observed from the value of n for ACuZinc10 *(Figure 6.27)*. However, there is no real difference in the values of n for alloys within the experimental error with possible exception of alloy No3. It was also observed that generally the value of n decreased with the decrease in test temperature for all experimental alloys. The values are also in close agreement with those determined for the polycrystalline zinc.[132,133]

The activation energies for creep *(Table 5.4)* have been found to be within the range of 99 ~ 108 kJ/mole and very close to those obtained by Durman[84] for zinc alloys No3, ZA.8 and ZA.27. The values also showed that an increase in copper content had a mixed effect on the activation energy with no definite trend, as shown in *Figure 6.28* and it may be that all were the same within the experimental error. These values of activation energies are much higher than that for grain boundary self-diffusion in pure zinc, about 61 kJ/mole.[134] However, the values are in excellent agreement with those of previously found for zinc-based alloys[93,130,131], and those for self-diffusion in plycrystalline zinc (91-110 kJ/mole) reported by different researchers.[132,135,136]

The activation energies for creep in polycrystalline zinc are discrete and vary from 54 to 159 kJ/mole.[18,66,132,133,137-140,141] However, the activation energies reported by the majority of researchers were between 88 and 109 kJ/mole within the temperature and stress ranges studied during the current investigation. The only major deviation has been observed by Cottrell and Aytekin[35] for polycrystalline zinc in the temperature range of 95-120°C. They found the activation energy of 54 kJ/mole, which was much less than the activation energies of creep reported by other workers. This discrepancy is not clearly understood, but according to Tegart and Sherby[132], a possible explanation is that Cottrell and Aytekin determined the activation energies of zinc over a small range of temperature, i.e. 95-120°C, and a small error in determination of creep rates would have resulted in a large error in the values of Q_c.

Therefore, it may be concluded that the calculated activation energies for creep in the experimental alloys are in the same range as those determined by various workers for creep and self-diffusion in polycrystalline zinc.

6.2.1 Rate-Controlling Mechanisms

A satisfactory procedure of identifying the rate-controlling or dominant creep mechanism may be offered by comparing the calculated values of the stress exponent (n) and the activation energy (Q_c) with the values of these parameters predicted theoretically for different creep processes. Another important consideration for dominent creep mechanism is the analysis of microstructure of the alloys. The values of the stress exponents are within the range of 3.0 - 5.5, indicating Weertman's dislocation climb as the most likely mechanism.[142]

According to Garofalo[13], in many cases, for alloys the activation energy for creep is nearly equal to the activation energy for diffusion of one of the elements, usually the one having the lowest diffusivity that is zinc in the experimental Zn-Al alloys. The similar values of activation energy for creep and self-diffusion in zinc suggest that the creep rate in the experimental alloys is diffusion-controlled in the zinc-rich phase for these high temperature creep tests ($T \geq 0.5T_m$).

The main difference of dislocation creep mechanisms at high temperature from those at low temperature is the rate-controlling process, because in climb processes at high temperature, the creep rate is controlled by the diffusion of vacancies between dislocations[8] instead of the activated glide of the dislocation itself at lower temperatures.

Based on the climb of dislocations over second-phase particles, Ansell and Weertman proposed a model, predicting a stress exponent of 4. This value is in close agreement with the stress exponent values obtained for the alloys No5, No2, ACuZinc5 and ACuZinc10. Since these alloys have copper content of 1-10%, copper-rich ε-phase therefore acts as a second phase and its precipitates block the movement of dislocations. Therefore, on the basis of the values of n and Q_c, it is reasonable to conclude that the creep in alloy No3 is controlled by dislocation climb process, whereas in alloy No5, No2, ACuZinc5 and ACuZinc10, the creep controlling mechanism is climb of dislocations over second-phase (ε) particles.

Since the creep tests were conducted in the high temperature range ($T \geq 0.5T_m$), the vacancies play an important role in the climb motion of edge dislocations. According to this mechanism, the relation between secondary creep rate and stress can be expressed by power laws, whereas value of the stress exponent in h.c.p. metals is between 4 and 6.

[22] The climb-controlled creep model proposed by Weertman[20] has reasonable agreement with some previous experimental results.[20,21]

The results of creep tests obtained during the current investigation on zinc-rich alloys clearly obey the power law creep because, (i) the test temperature is between 0.5 and 0.63 T_m, (ii) the activation energy for creep (Q_c) is within the range of the activation energy for self-diffusion (Q_{sd}) under the testing conditions used, and (iii) the physical mechanism responsible for creep is generally climb-controlled.

6.2.2 Specific Alloys

6.2.2.1 Alloy No3

The composition of alloy No3 shows that it consists mainly of zinc with a small amount of aluminium and some impurities. Therefore, it has the least complex microstructure consisting largely of zinc-rich primary η dendrites surrounded by a relatively small volume of lamellar eutectic matrix of α and η, after cooling to room temperature.

The comparison of creep results of alloy No3 with those of other zinc-4 % aluminium alloys, i.e. No5 and No2 showed that alloy No3 had significantly higher creep rates than No5 and No2 under all testing conditions. At higher temperatures, alloy No3 had much lower overall creep resistance than alloys No5 and No2 (by a factor of about 2-40). It has already been proved[84] that the creep strength of the primary η particles in alloy No3 is lower than that of the eutectic, therefore the lower overall creep resistance of this alloy is mainly due to the primary η particles having comparatively greater volume than eutectic in the microstructure.

The solid solubility of aluminium (in equilibrium) in zinc is 1.1% at 382°C (eutectic temperature) and decreases to a very small value at room temperature, whereas the excess aluminium is removed by precipitation of aluminium as a phase (α) in zinc-rich matrix upon solidification.

According to a previous investigation on tensile creep of Zn-Al alloys[84], the creep strength of a pressure die-cast zinc-based alloy with no aluminium was higher than that of alloy No3, and it was concluded that the creep resistance of zinc was further reduced by the precipitation of aluminium as a phase in the zinc matrix. This trend has also been observed in zinc alloys with small amounts of aluminium (0.2 and 0.4 %). It has been reported[84] that these alloys had better superplasticity than a series of binary Zn-Al

alloys including the Zn-Al eutectoid alloy at low temperatures, but they did not exhibit superplasticity at the high temperature of 250°C. This behaviour was expected due to the fact that in low aluminium zinc alloys, all the aluminium dissolved in the zinc solid solution at 250°C because the solubility of aluminium in zinc is 0.42 % at 227°C. [111] However, sand-cast alloy No3 showed a better overall creep performance in compression (current research) than the pressure diecast alloy without aluminium previously investigated[84] for tensile creep.

In the sand-cast case, the matrix of zinc is weak and has low creep resistance, whereas the eutectic of α plates has a good lamellar structure and should provide a high resistance to creep.

One key indicator of the dominent creep mechanism is the stress exponent, n. The mean value of the stress exponent, n, for alloy No3 determined from the gradient of the $\log\varepsilon_s/\log\sigma$ relationship, is 5.1. According to Evans and Wilshire[22], the value of n varies between 4 and 6 for h.c.p. metals. Tegart[143] has reported the values of the stress exponent of 5.5 and 4.7 for polycrystalline zinc, whereas Flinn and Munson[133] has given the values of 4.7 and 4.0 for zinc. Bird et al[142] have also given the value of n up to 5.5 for h.c.p. metals. This suggests that the creep behaviour of alloy No3 is similar to the polycrystalline zinc.

However, it has been reported[25] that upon alloying the value of n decreases, and therefore this value of n seems adequate for alloy No3. The value of the stress exponent shows the important relation between stress and the steady-state creep rate. Sherby and Burke[53] have illustrated the variation of the steady-state creep rate over a wide range of stress for a typical polycrystal metal at higher temperatures (above 0.5 T_m), as shown in *Figure 6.29*. The figure has been divided into three different ranges (I, II and III) according to the relations between stress and the steady-state creep rate. Since during the current investigation, the test temperature range was kept from 0.50 to 0.63 T_m (high temperature range), Range II of *Figure 6.29* may be used to analyse the behaviour of alloy No3.

At high test temperatures, it is believed that the creep process is controlled by dislocation climb involving an equilibrium vacancy concentration in Range II. [53] This mechanism has been verified by some other researchers.[21,22]

The other key indicator of the dominent controlling mechanism is the activation energy for creep. The value of activation energy for alloy No3 determined from the experimental data is 103 kJ/mole, which is in good agreement with those for self-diffusion in zinc (91-110 kJ/mole) reported in the literature.[132,135,136] Since the calculated activation energy for creep (Q_c) of alloy No3 is in the same range as those found for creep and self-diffusion in zinc, the creep rate is therefore considered as controlled by dislocation climb.

This correlation between the activation energies is also in accordance with the results obtained for pure metals and solid solutions in high temperature creep regions[53], and the most likely creep mechanism in such cases is that of dislocation climb proposed by Weertman[16], based on the climb of edge dislocations. The stress exponent predicted for this process is 4.5[16] ~ 5.[24] This type of creep beehaviour has been observed in Class II type alloys[22,53] (Class I according to Evans and Wilshire[22]).

According to Mohamed and Lagdon[24], this type of alloy has the following characteristics:

(i) The creep behaviour of the alloys in this class is similar to that of pure metals.

(ii) The stress exponent (n) is close to 5.

(iii) An instantaneous strain occurs on application of the load at the start of the test.

(iv) The creep curve shows normal primary creep.

(v) A regular array of sub-grains is formed during creep process.

The experimental creep data of alloy No3 shows the similar characteristic features as given above for Class II type alloys, and therefore it can be concluded that creep in the alloy No3 is controlled by dislocation climb mechanism through the diffusive motion of vacancies to or from the climbing dislocations. According to this mechanism, strain is accumulated by dislocation glide but the creep rate is assumed to be controlled by the rate at which climb processes allow rearrangement and annihilation of dislocations to occur.

Another possibility was the presence of Nabarro-Herring creep mechanism in alloy No3, but for this type of creep process, n should be unity[22,31,142], and the applied stress is normally low[22] ($\sigma \approx 10^6$ N/m^2)[11]. Another requirement for this type of creep process is that either the test piece should be very small or consist of very fine material. Also, the

microstrucure of this alloy did not show the slip bands. On this basis, Nabarro-Herring creep mechanism can not be applied to explain the creep behaviour of alloy No3.

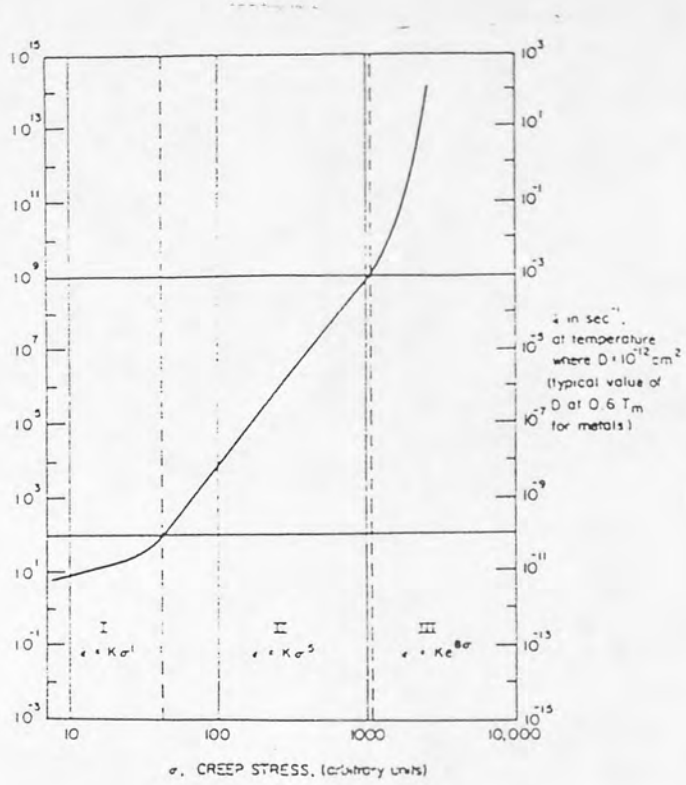

Figure 6.29. Creep stress versus diffusion-compensated steady state creep rate for a typical polycrystalline metal. Range II is controlled by dislocation climb involving an equilibrium vacancy concentration.

6.2.2.2 Alloy No5

As far as creep in this alloy is concerned, comparison of the creep results of No5 and No3 showed an important fact that the overall creep resistance of the alloy No5 was much higher (about 3-10 times) than alloy No3 under different testing conditions. The overall better creep strength of alloy No5 is believed to be due to the addition of copper content.

The scale of the structure in alloy No5 was similar to that of alloy No3. It consisted of large and small primary η dendrites surrounded by lamellar eutectic matrix. The dendrites and the η component of the $(\alpha + \eta)$ matrix contained ε-phase precipitates which can be observed in transmission electron micrographs at higher magnifications.[84] Copper is used to harden and strengthen the binary zinc alloys. The small precipitates of

ε-phase present in the zinc matrix play an important role in the overall creep performance of this alloy. As seen from the *Figures 5.12 and 5.13*, the secondary creep rates for alloy No5 were much lower than those of No3. The times to 1% creep strain were also much longer for No5.

A regular lamellar eutectic (α + η) morphology combined with the strong strengthening effect of ε-phase must be primarily responsible for the higher creep resistance of alloy No5 as compared to alloy No3. The similar effects of copper additions on the creep properties of zinc-based alloys have been observed by some other workers. [84,94,144]

Copper levels up to 1% have shown no real problems with stability of dimensions on prolonged ageing because in an earlier work[145], zinc alloy ZA12 (1% Cu) exhibited very little expansion on ageing due to the lower level of copper. It is therefore expected that alloy No5 with 0.85% copper will not show significant dimensional instability on prolonged ageing.

Superior creep strength of the lamellar eutectic in alloy No5 is based on the precipitation-hardening due to the presence of small ε-precipitates in the matrix and η-dendrites. The role of these second-phase particles during creep process is that they act as obstacles to dislocation movement, and therefore reduce the creep rate of the alloy. A moving dislocation attempts to cut through or bow between the particles, or to by-pass them through climb and cross-slip when encountering particles on the glide plane. The reduction of creep rate ultimately increases the creep strength of alloy No5. This process has been explained in *Figure 6.30.* The dislocations are forced between adjacent particles, leaving a dislocation loop around each particle. The required stress will decrease as the spacing d between the particles increases.

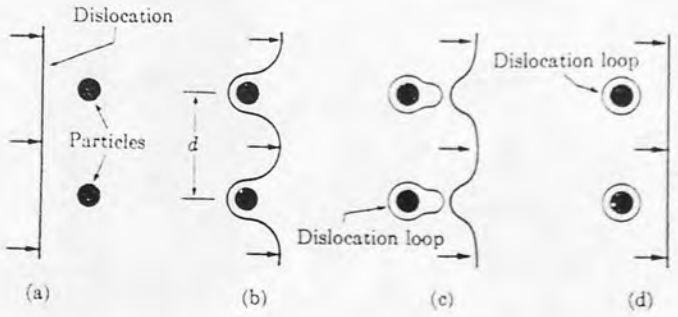

Figure 6.30. A dislocation line being forced through second-phase particles lying in its slip plane.

There are two general types of high temperature creep theories for materials hardened by second-phase particles:

(i) those assuming a rate-controlling mechanism such as climb over second-phase particles, and (ii) those assuming that the creep process is controlled by recovery creep.

On the basis of the climb model, the effect of second-phase particles on steady-state creep was first studied by Ansell and Weertman.[146] The model suggested by them was somewhat similar to that presented for steady-state creep in pure metals and depends on the climb of dislocations. In this particular model, they considered two different processes depending on the low and high stress levels. At low stresses, they proposed that dislocation segments climb over the particles with no pile-up or bowing of dislocations at the particles. The expression for creep rate is given by:

$$\dot{\varepsilon} = \frac{\pi\sigma b^3 D}{2kTh^2}$$

where σ is the applied stress, b the Burgers vector, D the self-diffusion coefficient, k the Boltzmann's constant, T the absolute temperature and h is the particle size.

At stresses greater than the Orowen stress, $\mu b/\lambda$, where μ is the shear modulus and λ the interparticle spacing, they considered the dislocations moved past the particles by bowing out and pinching off loops around the particles until the back stress exerted by the loops around the particles prevented new dislocations from bowing out between the particles. The creep rate is then governed by climb of the first pinched off loop around the particles through the diffusion of vacancies away from or towards the dislocation line. After climbing to the top of the particle, the pinched off loop then meets the dislocations of opposite sign and is annihilated. This process gives an expression for the steady-state creep rate as:

$$\dot{\varepsilon} = \frac{2\pi\sigma^4\lambda^2 D}{h\mu^3 kT}$$

This equation shows that the stress/creep rate relation obeys a fourth power law which is very close to the stress exponent (n) value, determined from the $\ln\dot{\varepsilon}/\ln\sigma$ plot for the alloy No5, i.e. 4.2.

Recovery creep theories in materials hardened by a second phase are essentially the same as those suggested for pure metals and solid solutions (section 2.3.1.4), except that second-phase particles reduce the rate of recovery and this, in turn, reduces the creep rate. According to Lagneborg[147], the model could account for very large stress-dependence of creep rate, and the values of the stress exponents may vary from 5 to 11.

Considering the structural details, the value of the stress exponent and the activation energy for creep, which was found to be in the range of activation energy for self-diffusion in zinc, it may be concluded that in alloy No5, the rate-controlling mechanism of creep over a reasonable stress and temperature range is the climb of dislocations over ε-phase particles.

6.2.2.3 Alloy No2

Alloy No2 had the highest strength and creep resistance of the Zn-4% aluminium alloy family. The experimental results showed that the overall creep performance of this alloy was significantly better than alloys No3 and No5 (about 2-40 times). The superior creep resistance of this alloy was due to its higher copper content than other two alloys, as this was the only significant difference between alloys No2 and No5.

The microstructure of this alloy consisted mainly of primary η dendrites of different sizes surrounded by decomposed β particles, together with a lamellar eutectic matrix. Both primary η dendrites and eutectic matrix, also of η, contained ε-phase (copper-rich) precipitates. Since this alloy has a higher copper content (about 3%) than alloy No3, the η matrix must contain a much higher density of ε-precipitates after cooling to room temperature. Since cooling is slow during sand-casting, some ε as massive particles must be present in eutectic areas, as can be seen in optical micrographs. Decomposition of β phase was similar to that of alloy No5 with lamellar and particulate mixtures of η and α phases (*Figures 5.45, 5.46 and 5.52)*, but due to the higher copper content of the alloy, a regular lamellar morphology was more dominant. The creep resistance of these phases is expected to be much higher due to the lamellar morphology of the eutectic, as discussed for alloy No3.

It has been found[145] that copper additions increase the strength and creep resistance of zinc alloys. In binary alloys, copper also affects the phase transformations that take place

in the alloys and results in the formation of new phases. This can result in a loss of dimensional stability of the alloys on ageing.

The results of compressive creep tests during the current investigation were different from those of some previous tensile creep tests[95,96] on zinc-rich alloys having copper content more than 1%. According to those results, a copper content of more than 1% did not improve the creep resistance of the zinc-rich alloys. However, an investigation by Savaskan and Murphy[93,98], on the creep behaviour of three zinc alloys having 3 and 4 % copper, showed the opposite results because the alloy with 4 % copper had higher creep resistance than that of the alloy with 3 % copper.

The structural morphology of the eutectic also plays an important role in affecting the creep properties of the alloys.[144] Alloy No2 having a regular eutectic morphology with the strengthening effect of the small ε-precipitates in zinc matrix therefore showed the superior creep strength. It has higher creep resistance than No5 mainly due to more regular eutectic morphology and greater volume of eutectic matrix, and this is in accordance with the current experimental observations. As in alloy No5, the ε-phase particles reduce the creep rate by blocking the dislocation movement. The average value of the stress exponent obtained from $\ln\varepsilon_s/\ln\sigma$ plot for alloy No2 was 3.8 which was very close to the value of n given for the climb of dislocations over second-phase particles as a rate-controlling creep mechanism. The activation energy for creep (Q_c) was also found to be in the range of self-diffusion in zinc.

Ansell and Weertman were the first who developed a theory based on the climb model for high temperature creep of alloys hardened by a second phase. The detail of this theory has been given in section 6.2.2.2.

It has been observed[118] that ε-phase is not a stable phase at low temperatures, and according to the well-established ternary aluminium-copper-zinc diagrams, it undergoes a four phase reaction below 275°C with α-phase to form stable copper and zinc-rich T′ and η phases, respectively. It has been shown[84] that only partial transformation of ε precipitates to T′ phase occurred in a zinc-rich alloy ZA.8 after a creep testing of long duration (~ 40 days) at 150°C. At low temperatures, due to the low diffusivity of zinc in aluminium matrix, time to complete the final four phase reaction may however need a period in excess of several years. [84,148]

6.2.2.4 ACuZinc5 & ACuZinc10

Both ACuZinc alloys are considered as high-copper zinc-based alloys. In contrast to the three other experimental zinc alloys, the structure of ACuZinc5 and ACuZinc10 consisted of primary copper-rich ε dendrites surrounded by a ternary ($\alpha + \varepsilon + \eta$) eutectic. In addition to the primary ε, ACuZinc5 also contained distinct η dendrites. The microstructure of ACuZinc5 and ACuZinc10 has been explained in sections 5.3.4 and 5.3.5, respectively. The structure of both ACuZinc alloys, shown by optical micrographs was similar to that given by a previous investigation on these alloys.[149]

Compared with the previous alloys, the analysis of creep behaviour of the alloys ACuZinc5 and ACuZinc10, with respect to its metallography, is more complicated due to their multi-phase structure. From optical micrographs of ACuZinc5, it was observed that this alloy contains a considerable amount of large, η phase masses in addition to the ε-phase dendrites. It is therefore located in the transient zone between the η phase and the ε-phase groups of alloys. ACuZinc10 contains more ε-phase dendrites, but η-phase only in the ternary eutectic. However, the volume fraction of ε in ACuZinc10 is far greater than the volume fraction in ACuZinc5 due to the higher copper content. The ε-phase is harder and stronger than the other phases and it is supposed that this phase is also creep-resistant. ε acts as a reinforcement in the matrix, and hence their superior properties. The ternary eutectic is heterogeneous, and distinct from primary ε and η dendrites.

Researchers[90,92] have shown that copper additions enhance the strength and creep resistance of zinc-rich alloys, but at the expense of reduced elongation. After the investigation of a large number of zinc-based alloys having copper content from 1-15 %, it was concluded[145] that alloys which had copper up to 1 %, showed no real problem with dimensional stability on prolonged ageing. However, when copper exceeded 1 %, the alloy attained higher strength or better bearing properties, and due to the excess copper, both the amount of ε-phase and the amount of copper dissolved in the zinc was increased which enhanced the growth on ageing. The long-term expansion is caused by two distinct processes, i.e. (i) a long-term reaction between copper-rich ε-phase and α (aluminium-rich)- phase to produce the stable T′ and η (zinc-rich) phases, and (ii) the structure cell of zinc is expanded due to the excess copper or a contraction from the precipitation of the excess aluminium.

The reaction between ε-phase and α-phase has been explained by Murphy[118] in a detailed investigation on the structure and properties of various ternary Zn-Al alloys. However, the structural changes occurred due to copper have not been studied in detail during this work, and it can not be said certainly that all above-mentioned reactions took place in both ACuZinc alloys during the current creep tests.

The creep resistance of both ACuZinc alloys was found to be substantially higher than that of zinc alloys No3 and No5 at all stress/temperature combinations used during the current creep experiments. ACuZinc alloys consistently showed lower secondary creep rates than commercial alloys No3 and No5, and times to 0.5 %, 0.7 % and 1.0 % strain were also longer for ACuZinc alloys.

Many researchers have studied the effect of copper additions on the tensile creep properties of zinc-rich alloys. The results of these investigations have been discussed in detail in section 2.7. There is a great difference in results of different workers.

Savaskan and Murphy[97,98] investigated the tensile creep behaviour of gravity-cast zinc alloys containing 3 and 4 % copper, over a range of stress and temperature. These tests revealed that the alloy with 4 % copper showed much lower creep rates than with 3 % copper in the as-cast condition, and it was concluded that the superior creep resistance of this alloy was due to the overall copper content. In contrast to the findings of Savaskan and Murphy, ACuZinc5 was found to be more creep resistant in compression than ACuZinc10 over the majority of test temperatures and stresses, i.e. ACuZinc5 has comparatively lower secondary creep rates, longer times to 1 % creep strain, and higher continuous design stresses calculated at different allowable strains (up to 1 %). The current creep tests also revealed that although the creep resistance of ACuZinc5 and ACuZinc10 was better than zinc alloys No3 and No5 under all testing conditions, alloy No2 having about 3 % copper was more creep resistant than both ACuZinc alloys at all temperatures and stresses.

An important conclusion can be drawn from all these results that copper content of more than about 3 % in these zinc-rich alloys did not improve the creep resistance in compression as was expected because alloy No2 had the best creep strength among all the alloys tested. These results do not agree with those of tensile creep tests [97,98] conducted on zinc alloys having high copper content. Higher creep resistance of alloy

No2 than ACuZinc alloys may be due to, (i) the discrete particles formed in the copper-rich liquid when the eutectic solidification took place, are not beneficial in improving the creep resistance of these alloys since no further benefit in creep performance was obtained by increasing the copper content of the alloy No2 to that of the alloys ACuZinc5 and ACuZinc10. It was also observed that zinc alloy ZA.8 (1% Cu) had substantially better overall creep performance than ZA.27 (2.18% Cu) under all testing conditions, [84] and (ii) in both ACuZinc5 and ACuZinc10, ε is a major primary c.p.h. phase which is not much precipitation-hardened with zinc (may be equal to alloy No5), but alloy No2 having copper-saturated η as a primary phase with strong precipitation hardening by ε, may well have more creep strength than both ACuZinc alloys (*Figure2.15).* Although both ACuZinc5 and ACuZinc10 have regular eutectic morphology, the massive primary dendrites of ε if less creep-resistant in compression, may not assist in increasing the creep strength of ACuZinc alloys, and may well reduce it.

The values of the stress exponent (n) obtained during these tests for ACuZinc5 and ACuZinc10 are 3.7 and 4.0, respectively. The values of n are within the range $3.0 \leq n \leq 5.5$, given by Weertman for his dislocation climb creep mechanism in h.c.p. metals.[25,142] It was also verified by Evans and Wilshire[22] that the values of n considerably greater than unity were obtained under high-temperature creep conditions. The values of activation energy for creep (Q_c) obtained from the creep data are 103 and 107 kJ/mole for ACuZinc5 and ACuZinc10, respectively. These values of Q_c are very close to that obtained for zinc, i.e. 109 kJ/mole in two different studies above $0.45T_m$.[141] These values of activation energy for ACuZinc5 and ACuZinc10 are also within the range of activation energies for self-diffusion in zinc. This close agreement of both types of activation energy suggests that the rate-controlling process for these high temperature tests might be similar to that for volume self-diffusion. The values of Q_c are also in close agreement with those found by Tegart and Sherby[132] for zinc in the temperature range 0.5-0.6 T_m which is similar to the temperature range of the current creep tests. However, the activation energy obtained by them at high temperatures (0.8-1.0 T_m) was very high, i.e. 159 kJ/mole, suggesting different creep process in zinc at temperatures higher than about 0.6 T_m. It was also observed that the activation energies calculated for both ACuZinc alloys are very close to each other at different stresses which means that the experimental observations for both alloys can be

represented by a power law equation because the activation energy is nearly independent of the applied stress.

According to Landon et al[150], at test temperatures above about 0.5 T_m, creep of polycrystalline materials is accompanied with subgrain formation and tilting suggesting that the rate-controlling mechanism for high temperature creep might depend on the rate at which the dislocations climb.

Considering the structural details, the values of the stress exponent obtained from the plots of ln ε_s/ln σ for both ACuZinc alloys which are in close agreement with that observed in the creep deformation of materials hardened by second-phase particles, and the activation energies for creep are within the range of lattice-diffusion in zinc, it may be concluded that the rate-controlling mechanism over a reasonable stress and temperature range is the climb of dislocations over ε-phase (second-phase) particles for both ACuZinc5 and ACuZinc10. The theory for high temperature creep of alloys hardened by a second-phase particles based on the climb model, proposed by Ansell and Weertman has been explained earlier. The second-phase particles produce non-homogeneous structure as shown in optical micrographs of both ACuZinc alloys. In both ACuZinc alloys, the dislocation movement was impeded by the ε-phase particles which reduces the creep rate.

6.3 Analysis of Load-Relaxation Tests

6.3.1 Comparison of Results of Commercial Alloys and ACuZinc Alloys

When the results of load-relaxation tests for ACuZinc alloys were compared with those of commercial alloys, it was observed that ACuZinc10 was more resistant than alloys No3, No5 and No2 at 80°C. Although ACuZinc5 had better resistance than No3, but alloys No2 and No5 were stronger than ACuZinc5. ACuZinc10 was slightly better than No2 and No5, but both ACuZinc5 and ACuZinc10 showed much higher resistance than No3. At 80°C, ACuZinc5 and ACuZinc10 were 13 % and 21 % stronger than No3, respectively.

At 100°C, alloy No2 was more resistant than ACuZinc5 and ACuZinc10, but both ACuZinc alloys were more resistant than No5 and No3. ACuZinc10 and ACuZinc5 were slightly better than No5, whereas alloy No3 had much lower resistance than ACuZinc alloys. At 100°C, ACuZinc10 had 29 % higher resistance than No3, while

ACuZinc5 was 28 % stronger than No3. At comparatively higher test temperature of 120°C, both ACuZinc alloys became more resistant than alloys No3, No5 and No2. The comparative graphs clearly showed that ACuZinc10 was much better than commercial zinc-based alloys. ACuZinc5 was slightly better than No2 and No5, but markedly superior to No3.

The results of load-relaxation tests at 120°C revealed that at higher temperatures, the resistance to load loss increased in alloys having higher copper content, i.e. ACuZinc alloys. Therefore, on the basis of the results of these tests, an important conclusion can be drawn that ACuZinc alloys are suitable for those higher temperature applications where load-relaxation is an important design parameter. The comparative load-relaxation graphs in the form of retained load (N) versus time (Mins.) at 80, 100 and 120°C have been shown in *Figures 5.38, 5.39 and 5.40*, respectively.

To check the effect of short and long-term load-relaxation tests, graphs were drawn to show the variation of retained load with reciprocal temperature at 50, 100 and 150 h time for all six experimental alloys, as shown in *Figures 6.31, 6.32 and 6.33*, respectively. From 50 h time graph, it was observed that ILZRO.16 was the most resistant to load loss, and No3 was the worst, whereas ACuZinc10 and ACuZinc5 were better than the alloys No2 and No5. No2 was the most resistant among three commercial alloys, whereas No5 was better than No3 at this time period. At time periods of 100 h and 150 h, all six alloys showed the same behaviour as observed at 50 h.

When the results of load-relaxation tests for sand-cast alloys No3, No5 and No2 from the current investigation were compared with those of the previous relaxation tests[124] on the same alloys in pressure die-cast form, at 80°C, it was observed that the relaxation of load was much less than those of the previous load-relaxation experiments. The comparison of retained loads from both studies after 50 and 100 hours at 80°C for these zinc-rich alloys have been shown in *Figures 6.34 and 6.35*. The figures showed a great difference between the results of both investigations. The much higher retained loads of the current test data are principally due to the sand-casting method used for the production of the present alloys, although different engagement lengths, design and size of the specimen may also have played a part.

Another comparison of the retained loads (N) for alloys No3 and No5 at 80°C obtained during the current relaxation tests and a previous investigation by Murphy and Goodwin[125] on pressure die castings also showed a big difference between the data from these studies (*Figure 6.36).* The sand-cast castings again showed superior resistance to load-relaxation, but the pressure die castings were more resistant to relaxation than those from the earlier investigation, due to differences in sample and load cell geometries.

6.3.2 The Effect of Copper Content on Load-Relaxation Behaviour of Alloys

To show the effect of copper content on load-relaxation behaviour of alloys, the variation of the retained load against the copper content at three different temperatures was plotted at 50, 100 and 150 hours, as shown in *Figures 6.37, 6.38 and 6.39*, respectively.

It was observed that at 80°C and 100°C, the resistance of alloys was increased up to the addition of about 3 % copper (alloy No2), but beyond this limit, the addition of copper content generally did not affect the resistance of alloys. However, at higher temperature (120°C), the copper addition of more than 3 % markedly increased the resistance of alloys, particularly when about 10% copper was added, as shown in *Figures 6.37 to 6.39*.

It is a well-known fact that load-relaxation is a phenomenon which is closely related to creep and follows the same mechanisms as creep. It is therefore reasonable to analyse the results of load-relaxation in the light of general creep theories.

Considering all these observations, it may be concluded that higher copper contents in ACuZinc5 and ACuZinc10 contribute greatly to their relaxation strength at higher temperatures, either in the form of a solid solution or ε-phase precipitates which play an important role in preventing the dislocation movement, and therefore reducing the relaxation rate.

Copper influences the precipitation properties of alloys by increasing the precipitate volume and thus gives a certain strengthening. Another well-known effect of copper additions to these alloys is a reduced tendency to intercrystalline weakness due to a copper-stimulated precipitation within the grains.

6.3.3 Comparison of Creep and Load-Relaxation Results

One purpose of the current research was to determine if there is any correspondence between the creep and load-relaxation characteristics of the experimental alloys. Although a few disagreements between the creep and relaxation results were observed, the two types of tests showed roughly the same grading of the alloys. The only major variation in results of both types of tests was recorded for ACuZinc5 and ACuZinc10.

6.3.3.1 ILZRO.16

The results of both types of tests showed that ILZRO.16 was the best among the experimental alloys under all testing conditions. ILZRO.16 showed better creep and relaxation properties, especially at elevated temperatures. The superior resistance to creep and load-relaxation of ILZRO.16 was considered as due to titanium and chromium content, but the reasons for this are not known.

6.3.3.2 Alloys No3, No5 and No2

This group of zinc alloys (Zn-4% Al) showed almost the same grading in both types of experiments. It has been observed that alloy No2 showed the best resistance to creep and relaxation, alloy No5 was inferior to No2 and alloy No3 was the worst in this group of zinc alloys. However, there are some minor disagreements between creep and load-relaxation data. The comparative creep curves showed that under all testing conditions, alloy No3 had much lower resistance than No5 and No2, and although alloys No5 and No2 showed similar strains initially but there was a difference for prolonged test periods, as can be seen in *Figures 6.40 to 6.42.*

If load-relaxation curves are compared with the creep curves, it can be observed that at higher temperature (120°C), alloy No2 relaxed slightly more slowly than did No5, showing better overall resistance to relaxation than No5 although relaxation curves of both alloys were similar up to about first 33 hours of test *(Figure. 5.25)*. Alloy No3 relaxed more quickly than alloys No5 and No2 at 120°C, as can be seen in *Figure 5.25.* At lower temperatures (80°C and 100°C), all three alloys relaxed in the similar manner as at 120°C, as shown in *Figures 5.23 and 5.24.*

Therefore, the comparative data of creep and load-relaxation for alloys No3, No5 and No2 clearly showed that these alloys had the same grading in both types of tests although some minor disagreements were observed from the experimental results.

6.3.3.3 ACuZinc Alloys

This group of experimental alloys exhibited quite different behaviour in both types of tests. The experimental results showed that generally ACuZinc5 was more creep-resistant than ACuZinc10 under most of the testing conditions, as can be seen from secondary creep rates, times to 1% creep strain and design stresses calculated at different temperatures for both ACuZinc alloys although at lower stresses, ACuZinc10 showed slightly better creep resistance than ACuZinc5 *(Figures 6.43 to 6.45)*.

In contrast to the results of creep tests, ACuZinc10 showed more resistance to load-relaxation than ACuZinc5 under all testing conditions, as shown in *Figures 5.23 to 5.25*. It is very clear from these figures that ACuZinc10 relaxed more slowly than did ACuZinc5 although the difference in relative relaxation strengths of alloys was more pronounced at lower temperature than at higher temperature.

The differences between the creep and load-relaxation results of ACuZinc alloys were not understood because there was no difference in composition, casting method and testing procedure for both alloys. However the relaxation tests were carried out at lower temperatures and for longer times than the creep tests, and changes in creep mechanism can not be ruled out.

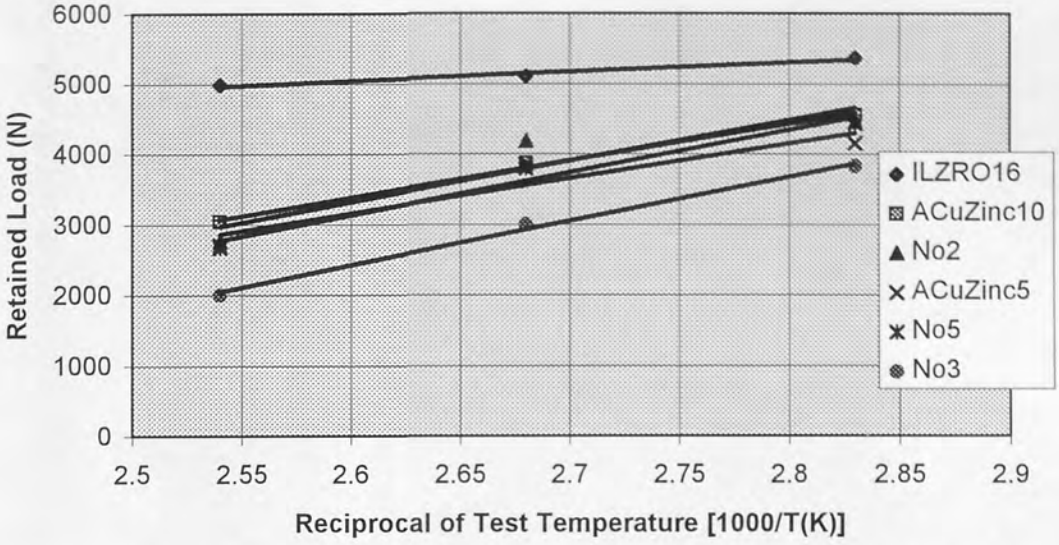

Figure 6.31. Variation of 50 hour load with reciprocal temperature for alloys ILZRO.16, ACuZinc10, No2, ACuZinc5, No5 and No3.

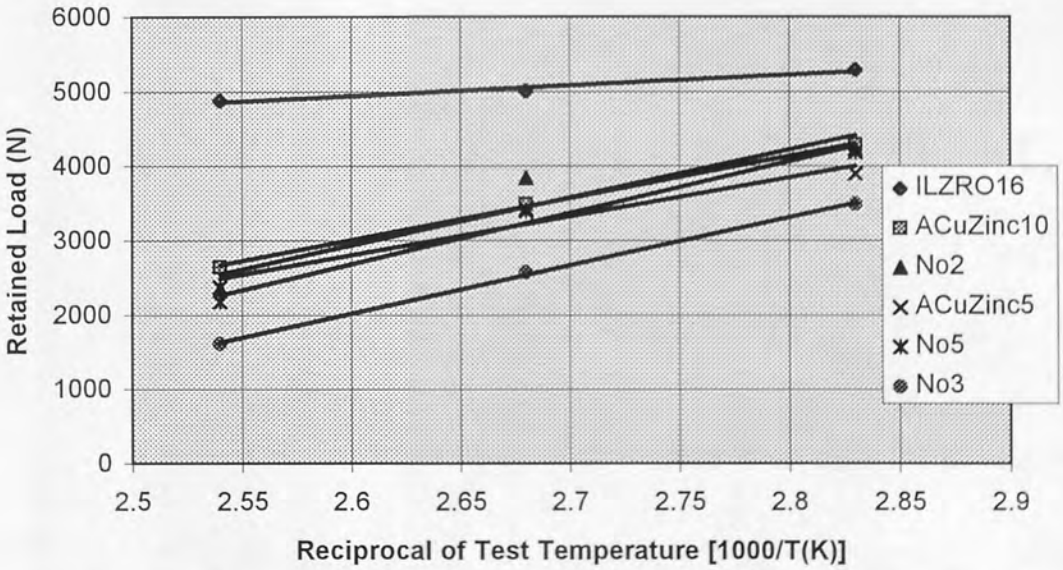

Figure 6.32. Variation of 100 hour load with reciprocal temperature for alloys ILZRO.16, ACuZinc10, No2, ACuZinc5, No5 and No3.

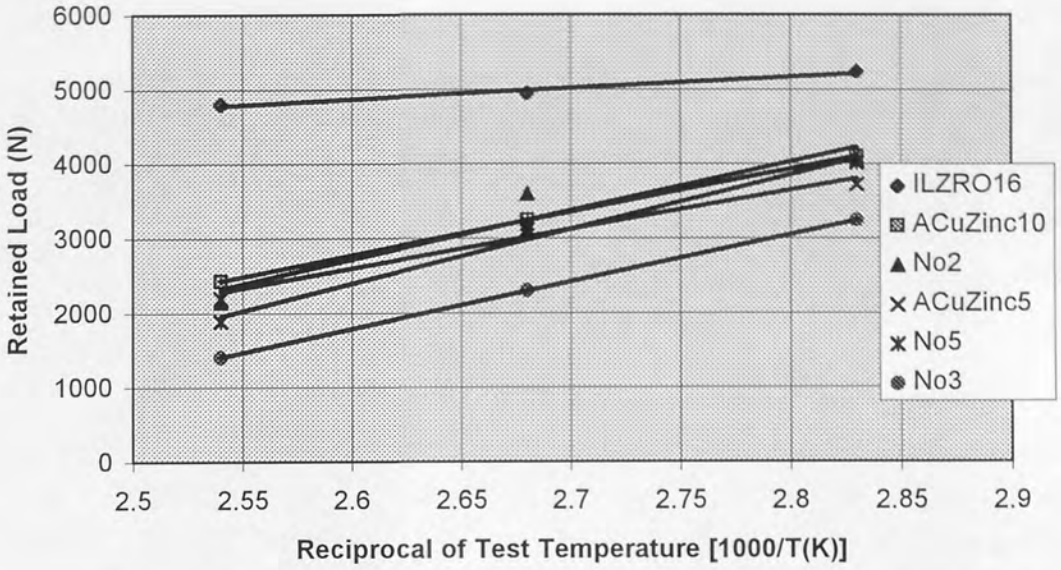

Figure 6.33. Variation of 150 hour load with reciprocal temperature for alloys ILZRO16, ACuZinc10, No2, ACuZinc5, No5 and No3.

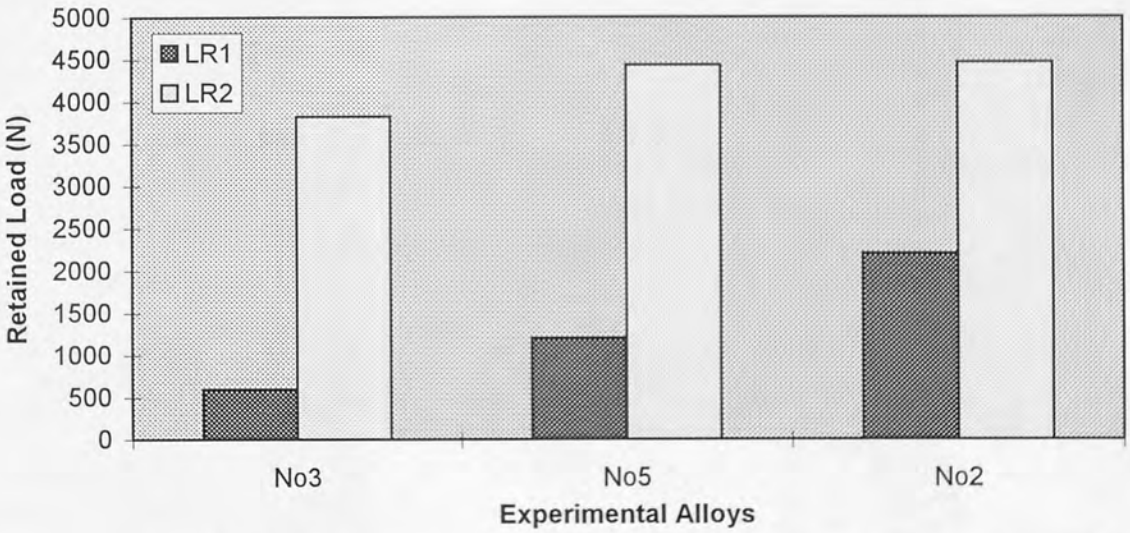

Figure 6.34. A comparison of the variation of mean 50 h retained loads at 80° C for alloys No3, No5 and No2. LR1 = Load relaxation results from Ref. 124, LR2 = Results of the current research.

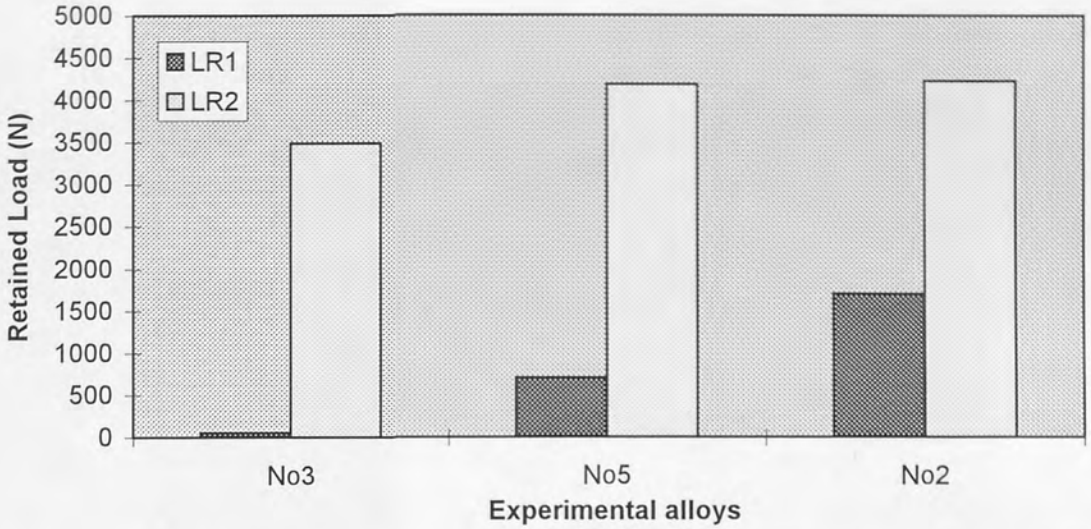

Figure 6.35. A comparison of the variation of mean 100 h retained loads at 80° C for alloys No3, No5 and No2. LR1 = Load relaxation results from Ref. 124, LR2 = Results of the current research.

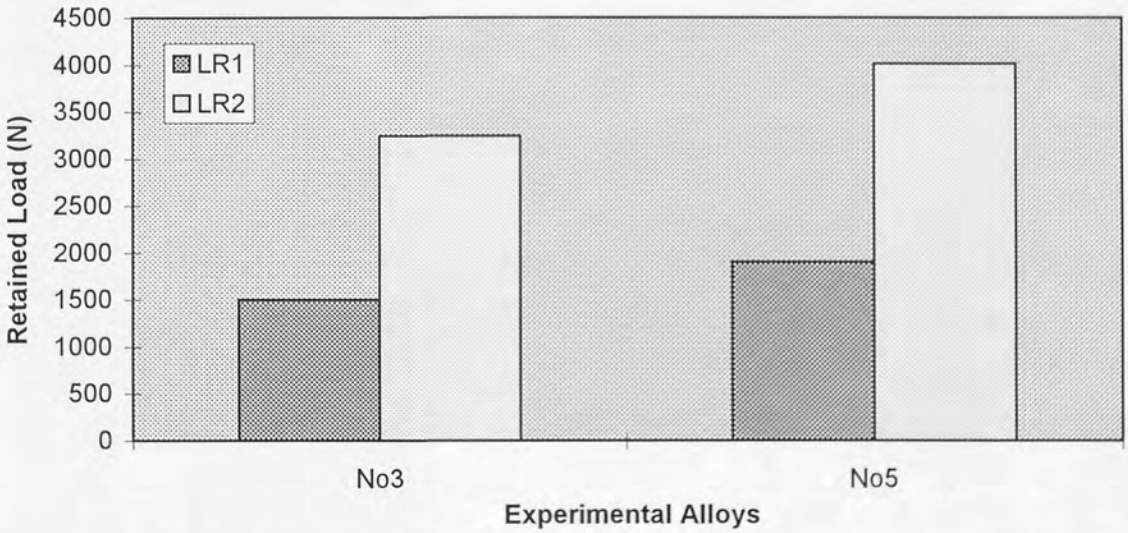

Figure 6.36. A comparison of the variation of mean 150 h retained loads at 80° C for alloys No3 and No5. LR1 = Load relaxation results from Ref. 125, LR2 = Results of the current research.

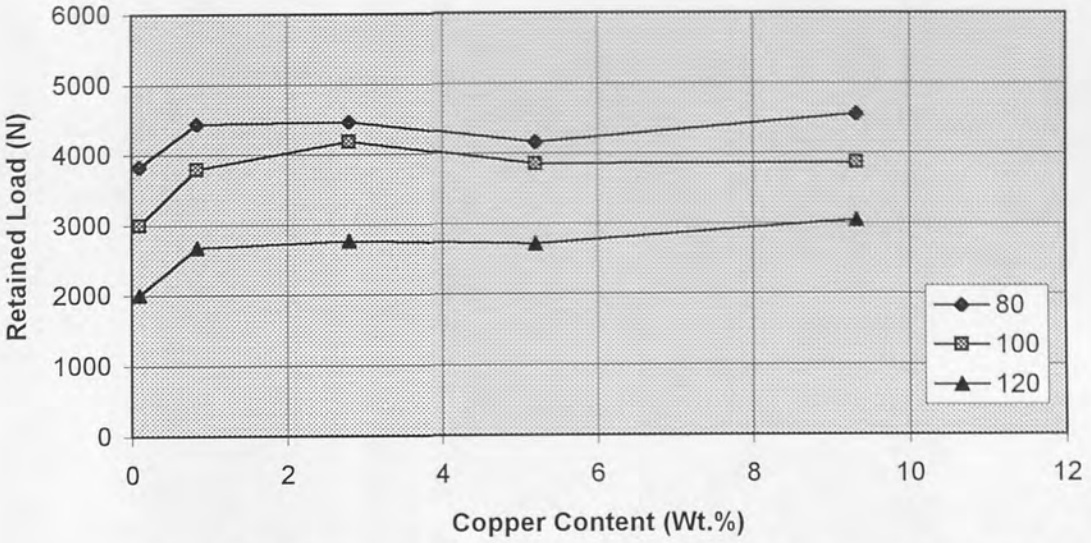

Figure 6.37. Variation of 50 hour load with copper content for alloys No3, No5, No2, ACuZinc5 and ACuZinc10 at 80, 100 and 120° C.

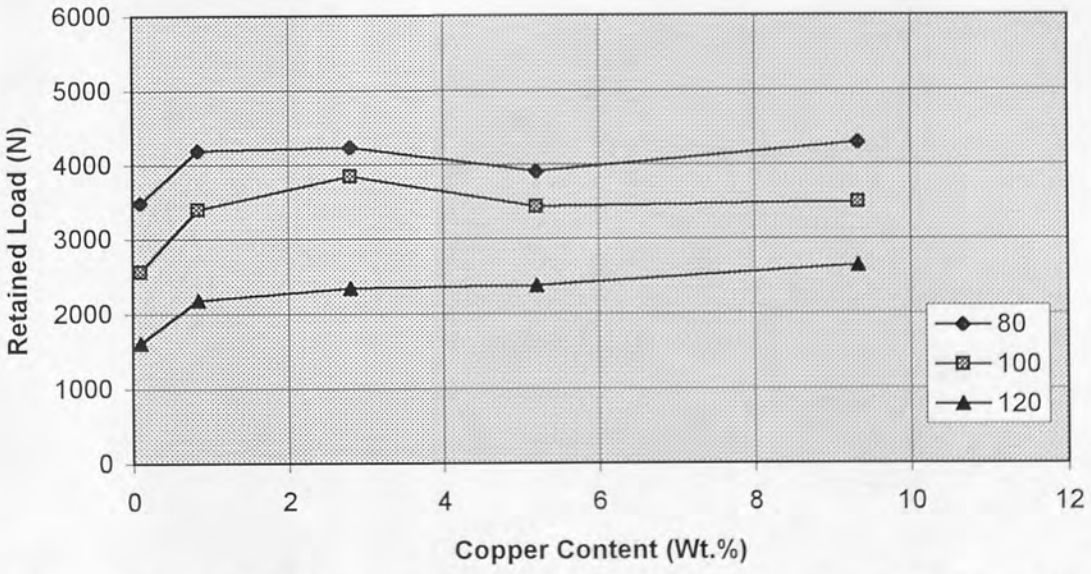

Figure 6.38. Variation of 100 hour load with copper content for alloys No3, No5, No2, ACuZinc5 and ACuZinc10 at 80, 100 and 120° C.

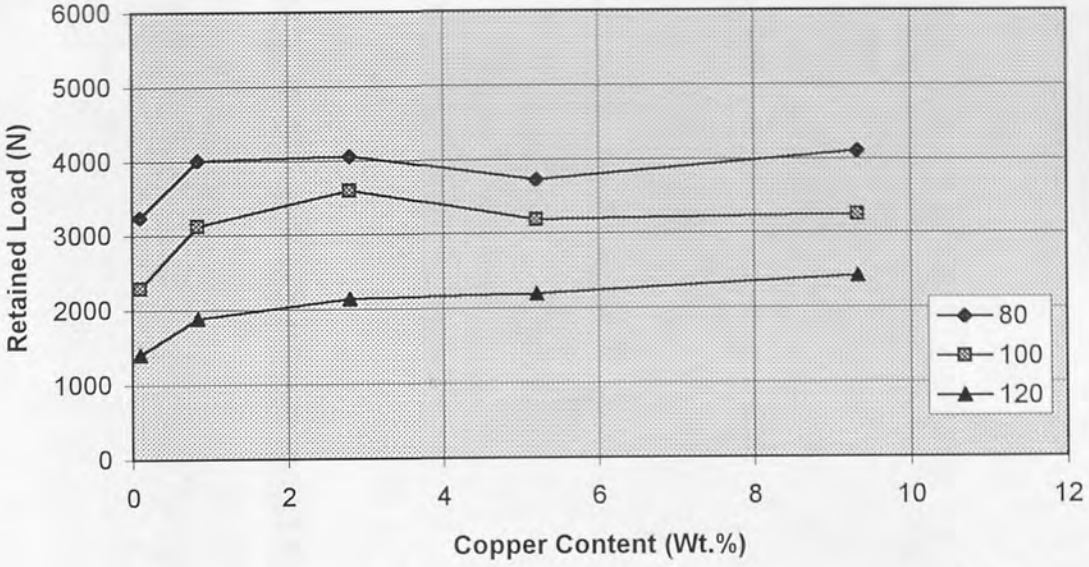

Figure 6.39. Variation of 150 hour load with copper content for alloys No3, No5, No2, ACuZinc5 and ACuZinc10 at 80, 100 and 120° C.

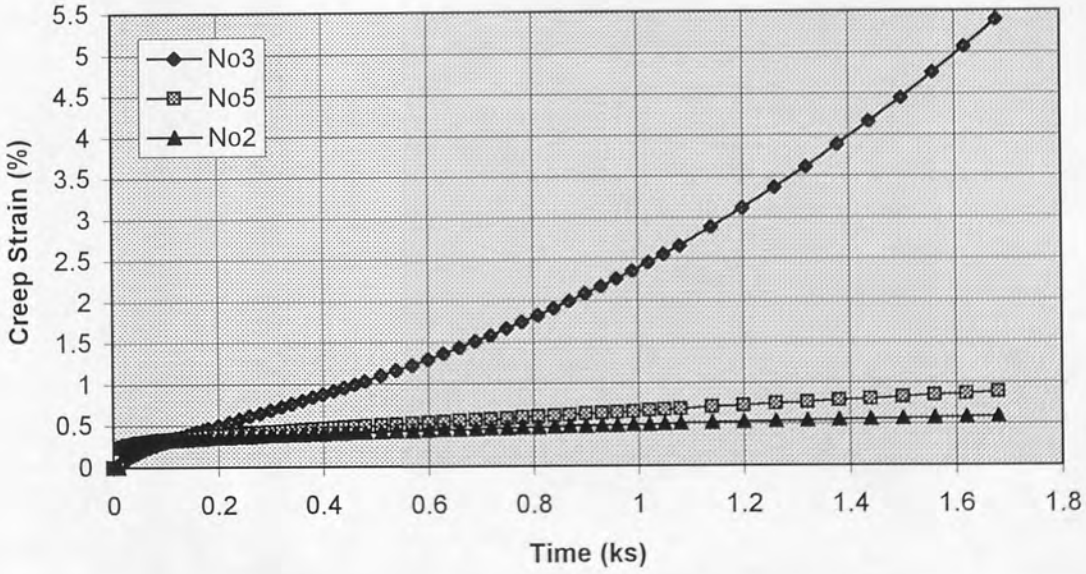

Figure 6.40. Comparison of creep curves for alloys at 60 MPa and 160° C.

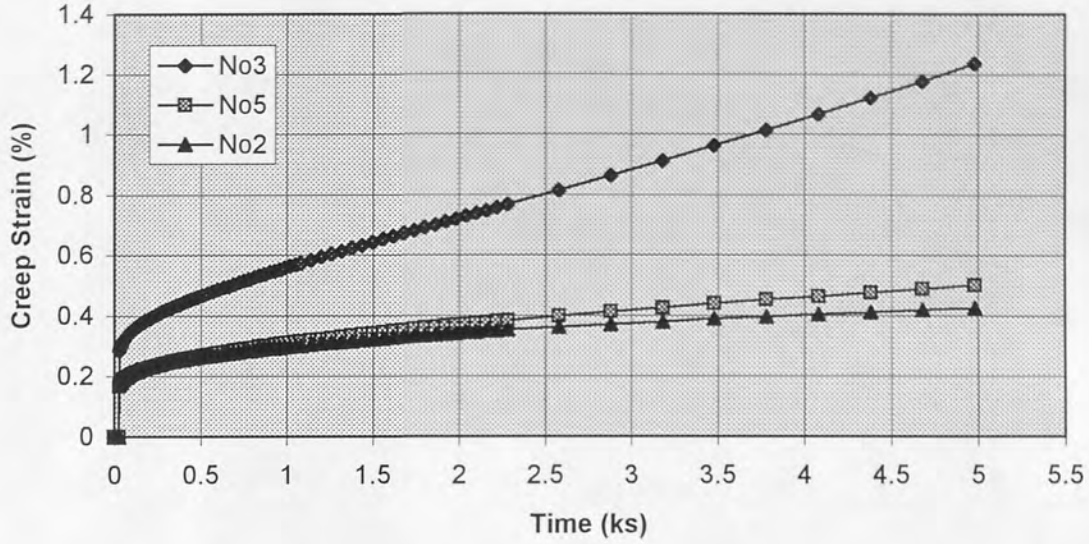

Figure 6.41. Comparison of creep curves for alloys at 60 MPa and 130° C.

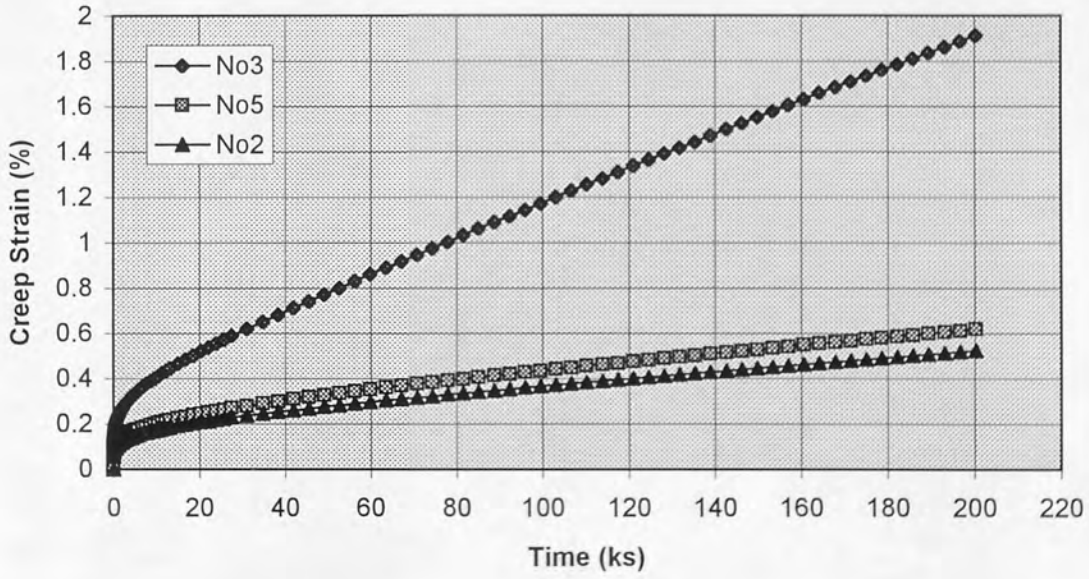

Figure 6.42. Comparison of creep curves for alloys at 60 MPa and 100° C.

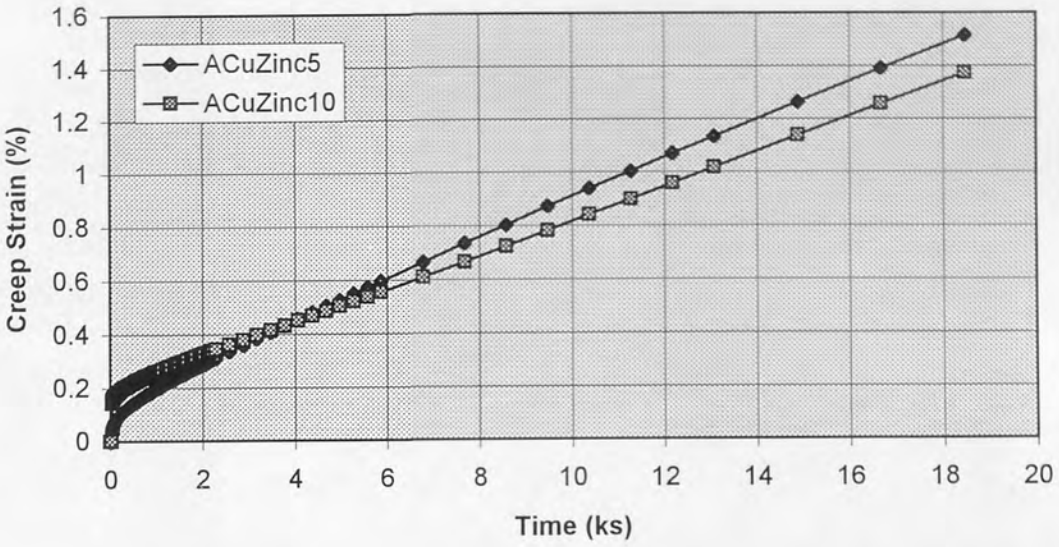

Figure 6.43. Comparison of creep curves for alloys at 40 MPa and 160° C.

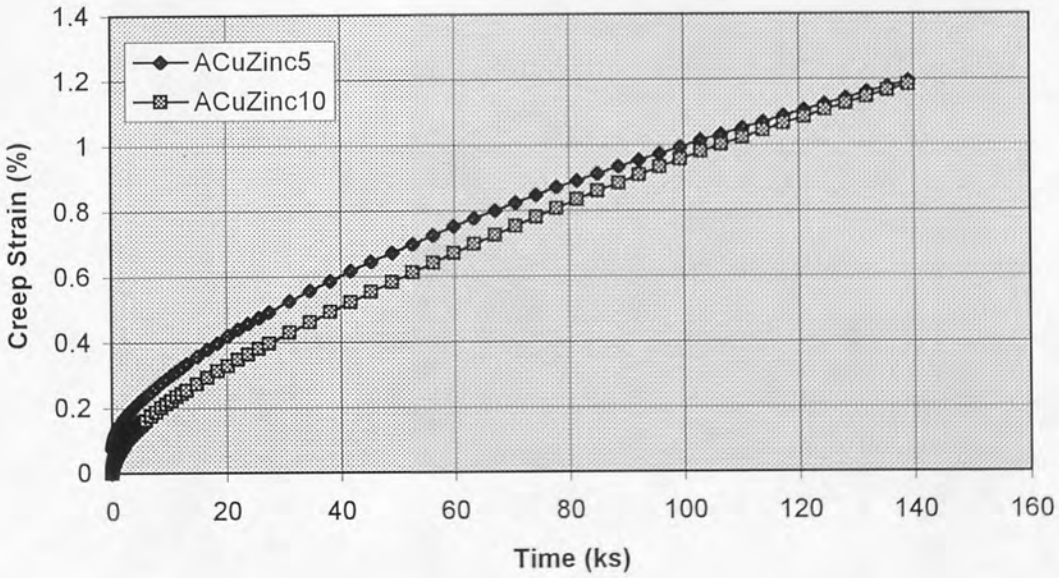

Figure 6.44. Comparison of creep curves for alloys at 40 MPa and 130° C.

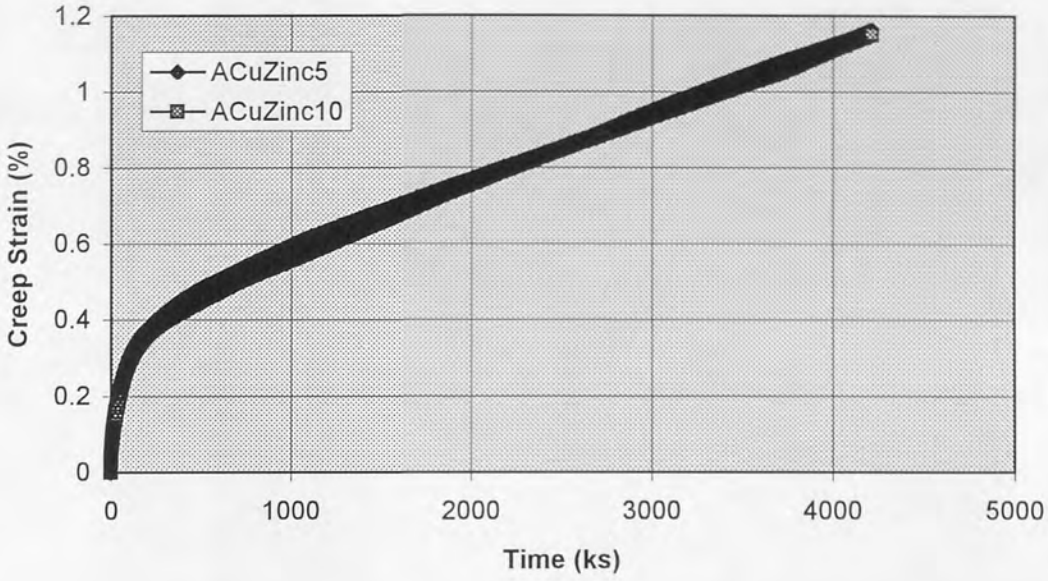

Figure 6.45. Comparison of creep curves for alloys at 20 MPa and 130 ° C.

6.4 Correlation of Load-Relaxation Data of the Experimental Alloys

Load-relaxation data for the sand-cast zinc alloys during the current investigation was obtained from a limited number of tests of relatively short duration. This data has little further use unless some mathematical relationships are used to correlate it satisfactorily and allowing a quantitative analysis of the relaxation behaviour of alloys under different testing conditions.

For this purpose, numerous mathematical relationships suggested in the literature are based on various elements, such as constant total strain in the specimen, data of creep tests, logarithmic creep equations, time-hardening theory, strain-hardening theory and internal stress. [6,121,151-155]

However, recently Murphy[156] has derived the following general relation between the retained load (N), time t (Mins.) and test temperature T (K) to analyse the load-relaxation data of zinc-rich die cast alloys:

$$\ln L = \alpha[Q/RT - \ln B - \ln t] \qquad (6.3)$$

where L is the load after time t, Q is an activation energy for load-relaxation, R is the universal gas constant, and α and B are constants.

This relationship was derived on the basis of an empirical Arrhenius-type equation[130] which described the kinetics of tensile creep in the secondary region.

Using the experimental relaxation data, mean load-relaxation curves were plotted on a linear and on a power law basis, in *Figures 6.46, 6.47, 6.48, 6.49, 6.50, 6.51, 6.52, 6.53, 6.54, 6.55, 6.56 and 6.57* for castings of alloys No3, No5, No2, ACuZinc5, ACuZinc10 and ILZRO.16, respectively. All these plots showed a good power law correlation at different temperatures for test times in excess of 1000 minutes. The values of power law constants at different temperatures are given in *Table 6.4*, and the mean values of power law constants are shown in *Table 6.5*. The values of α and A generally increased with the increase of temperature. The mean values of α for commercial alloys No3, No5 and No2 showed a decrease with the increase of copper content. The similar trend has been observed for ACuZinc alloys. The plots of ln retained load versus 1/T at a fixed time (t) should give a straight line relationship with slope ($\alpha Q/R$) and intercept $-\alpha(\ln B + \ln t)$.

Table 6.4. The values of power law constants for alloys at different test temperatures.

Alloy	Temp. (°C)	A	α
No3	80	11078	0.133
No3	100	17509	0.221
No3	120	26146	0.320
No5	80	8781	0.085
No5	100	13153	0.156
No5	120	27247	0.290
No2	80	8565	0.081
No2	100	10847	0.119
No2	120	18916	0.239
ACuZinc5	80	8833	0.094
ACuZinc5	100	14337	0.164
ACuZinc5	120	13822	0.202
ACuZinc10	80	9282	0.089
ACuZinc10	100	12334	0.145
ACuZinc10	120	16751	0.212
ILZRO.16	80	6354	0.021
ILZRO.16	100	6418	0.028
ILZRO.16	120	6488	0.033

Table 6.5. The mean values of power law constants for alloys.

Alloy	A	α
No3	18244	0.225
No5	16394	0.177
No2	12776	0.146
ACuZinc5	12331	0.153
ACuZinc10	12789	0.149
ILZRO.16	6420	0.027

From the relaxation curves, the retained loads after 50, 100 and 150 hours were obtained and plotted against reciprocal temperature, as shown in *Figures 5.26, 5.27, 5.28*, 5.29, 5.30 and 5.31 for alloys No3, No5, No2, ACuZinc5, ACuZinc10 and ILZRO.16, respectively. The plots gave a fair straight line relationship for all three time periods, although some curvature is visible in almost all lines. The values of slopes and intercepts obtained from the plots, and the mean values of α from *Table 6.5* were used to calculate the activation energy Q and the constant ln B. Although the time in *Figures 5.26 to 5.31* is given in hours, the constant ln B was computed from time in minutes. The calculated values of the activation energy are within the range of those given for self-diffusion in zinc by other researchers.[132,135,136] The mean values of Q increased for commercial zinc alloys No3, No5 and No2 with the copper content. The mean values of Q for ACuZinc5 and ACuZinc10 are very close to each other.

The values of ln B were also calculated from the power-law data in *Table 6.4*, since $\ln A = \alpha[Q/RT - \ln B]$. The average values of ln B obtained by this method for each alloy are very close to those averages obtained from the reciprocal temperature data. The mean values of ln B from both averages were calculated for alloys. The mean values of Q, ln B and B are listed in *Table 6.6.* The values of these constants are quite different for alloys No3, No5 and No2, but for ACuZinc5 and ACuZinc10, there is only small difference of values was observed.

After finding the values of α, Q and ln B, the retained loads (N) were calculated for alloys by using the general equation for load-relaxation (*Equation 6.3*) at 20°C, 80°C, 100°C and 120°C after 30,000 h of service time, as shown in *Table 6.7*. The calculated values of retained loads (N) showed that ILZRO.16 had the best resistance to relaxation under all testing conditions. From commercial alloys, No2 was the best resistant to relaxation, then No5 and No3 was the worst at all temperatures. It was also observed

that ACuZinc10 was more resistant to relaxation than ACuZinc5 under all testing conditions.

Table 6.6. Constants for General Equation of Load Relaxation for alloys derived from the experimental data.

Alloy	mean Q (kJ/mol)	mean ln B
No3	95	-12.615
No5	103	-20.975
No2	110	-28.750
ACuZinc5	91	-32.085
ACuZinc10	90	-34.265
ILZRO.16	87	-290.590

Table 6.7. Maximum calculated retained loads (N) for alloys after 30,000 h of service time at different temperatures.

Alloy	50°C	80°C	100°C	120°C
No3	1915	974	659	464
No5	2842	1595	1144	848
No2	3214	1934	1442	1108
ACuZinc5	2671	1720	1333	1061
ACuZinc10	2845	1860	1457	1169
ILZRO.16	4863	4508	4314	4147

ACuZinc5 showed better resistance than commercial alloys No3 under all testing conditions and No5 at higher temperatures (≥ 80°C). At lower temperature (50°C), ACuZinc5 was less resistant than alloy No5. It had lower resistance than alloy No2 at all temperatures. ACuZinc10 showed lower resistance than No2 at lower temperatures, but at higher temperatures (≥ 100°C), it had higher relaxation strength than alloy No2.

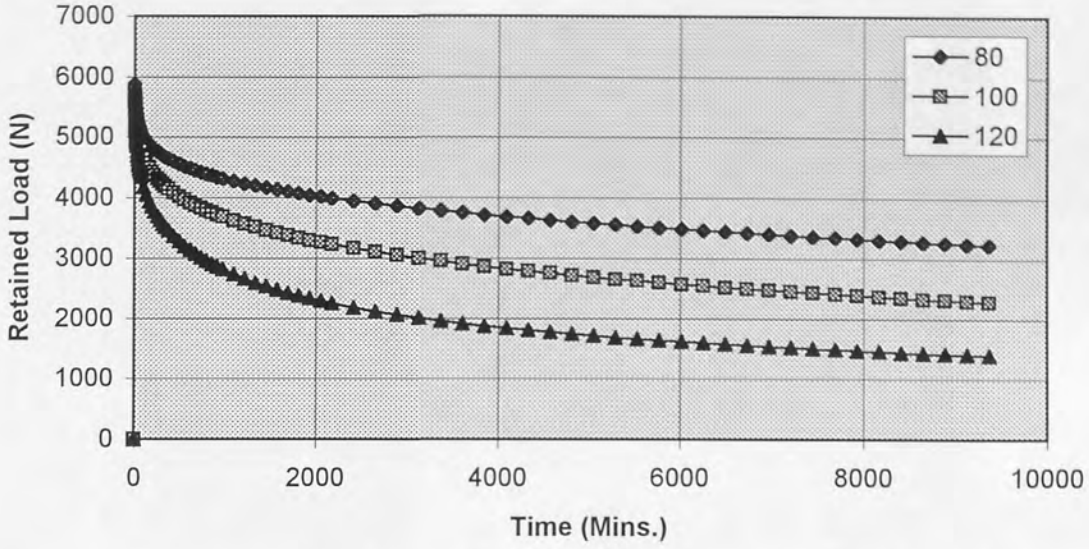

Figure 6.46. Mean load-relaxation curves (linear plot) for alloy No3 at 80, 100 and 120° C.

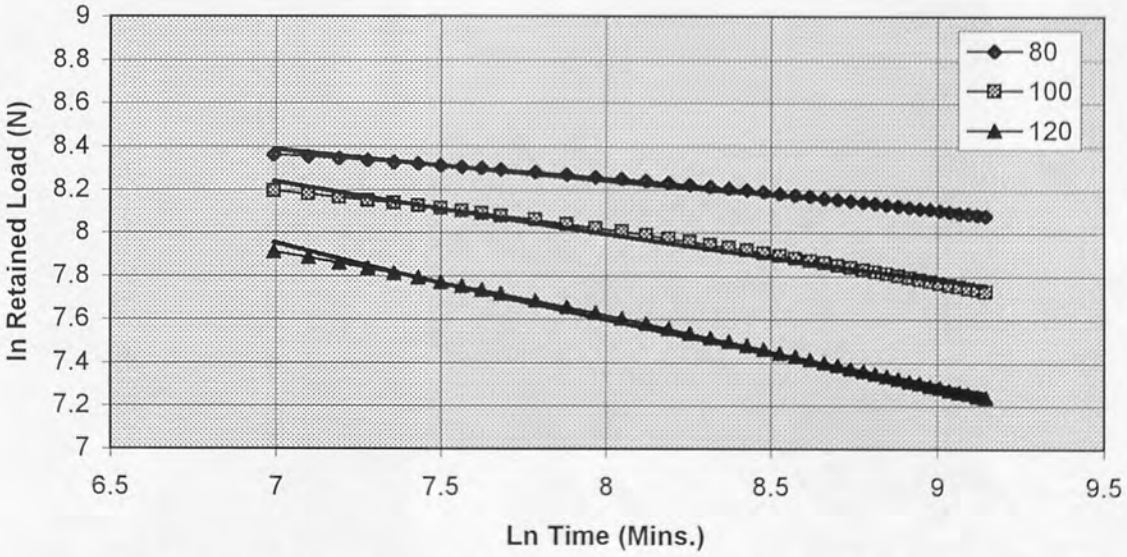

Figure 6.47. Mean load-relaxation curves (power law plots) for alloy No3 at 80, 100 and 120° C.

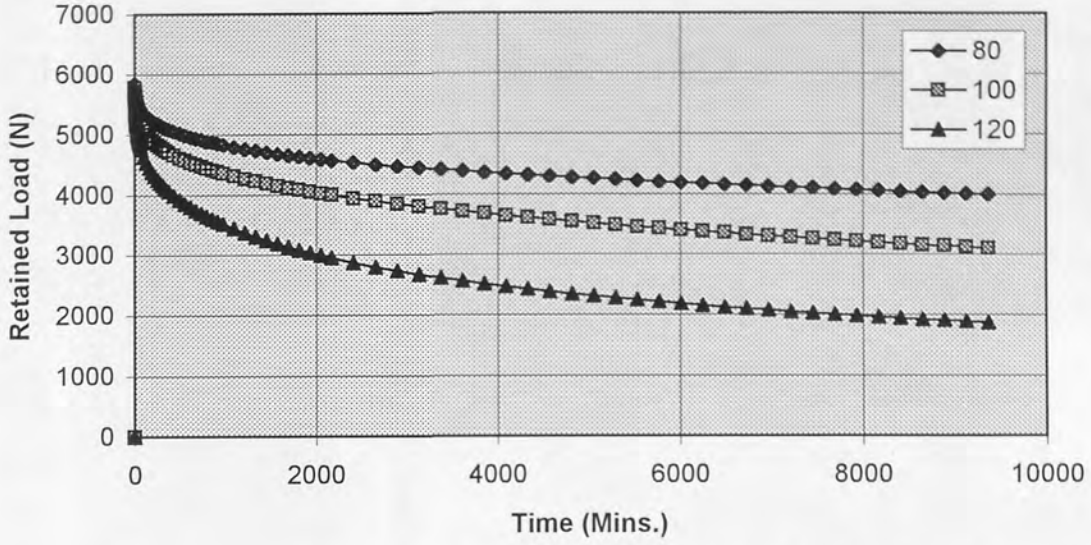

Figure 6.48. Mean load-relaxation curves (linear plot) for alloy No5 at 80, 100 and 120° C.

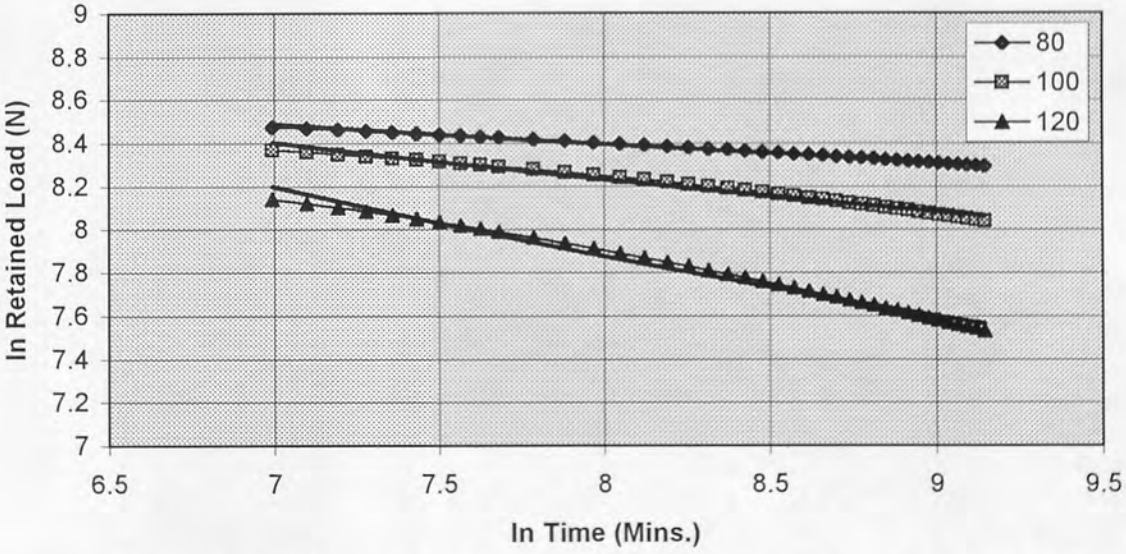

Figure 6.49. Mean load relaxation curves (power law plots) for alloy No5 at 80, 100 and 120° C.

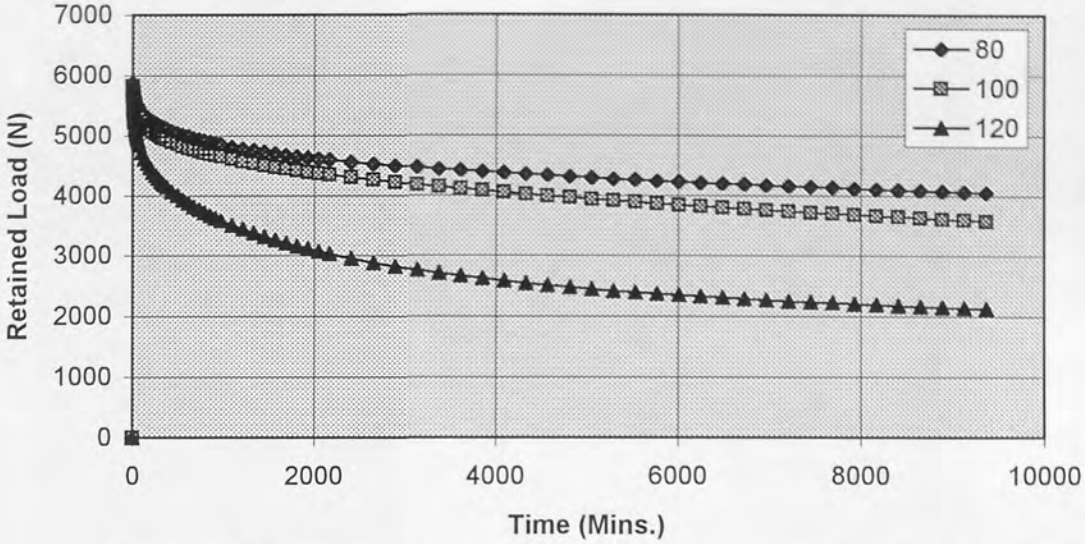

Figure 6.50. Mean load-relaxation curves (linear plot) for alloy No2 at 80, 100 and 120° C.

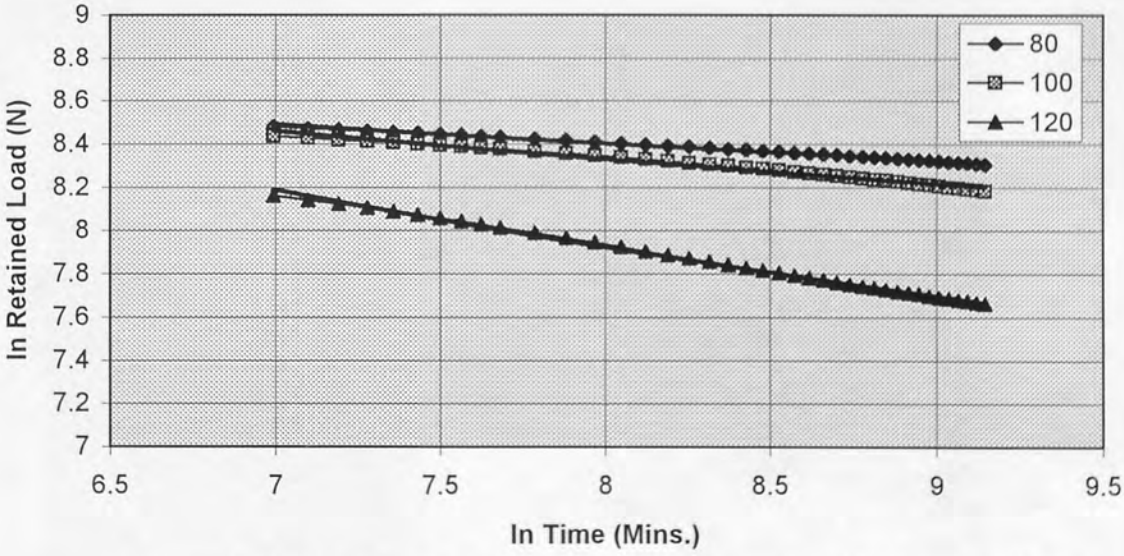

Figure 6.51. Mean load relaxation curves (power law plot) for alloy No2 at 80, 100 and 120° C.

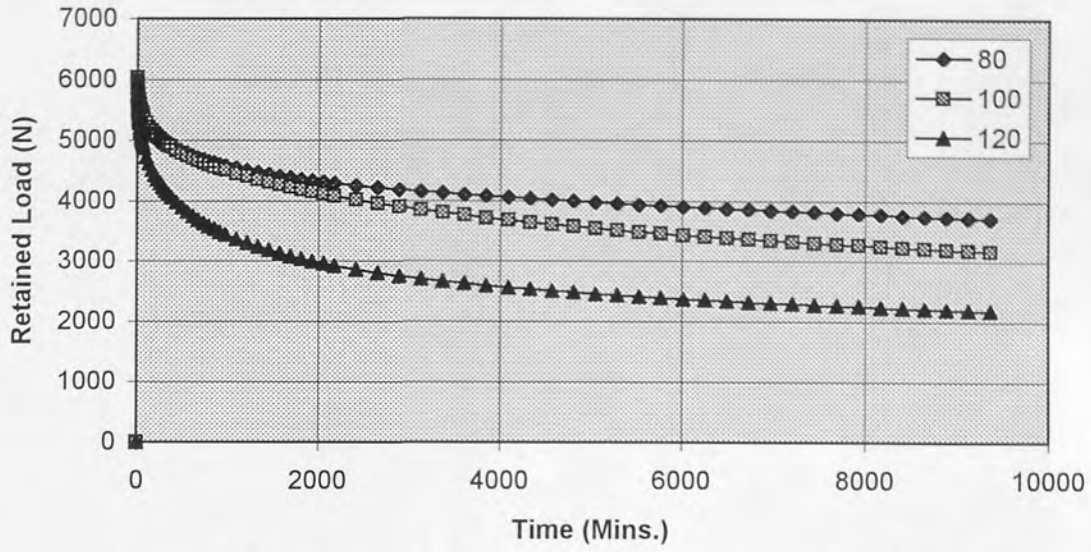

Figure 6.52. Mean load-relaxation curves (linear plot) for ACuZinc5 at 80, 100 and 120° C.

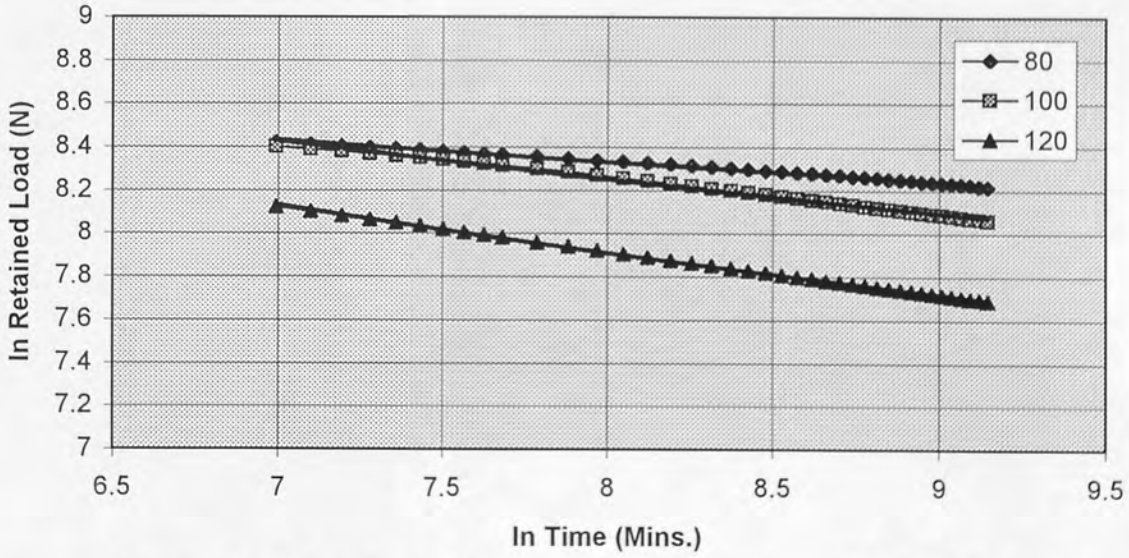

Figure 6.53. Mean load-relaxation curves (power law plots) for ACuZinc5 at 80, 100 and 120° C.

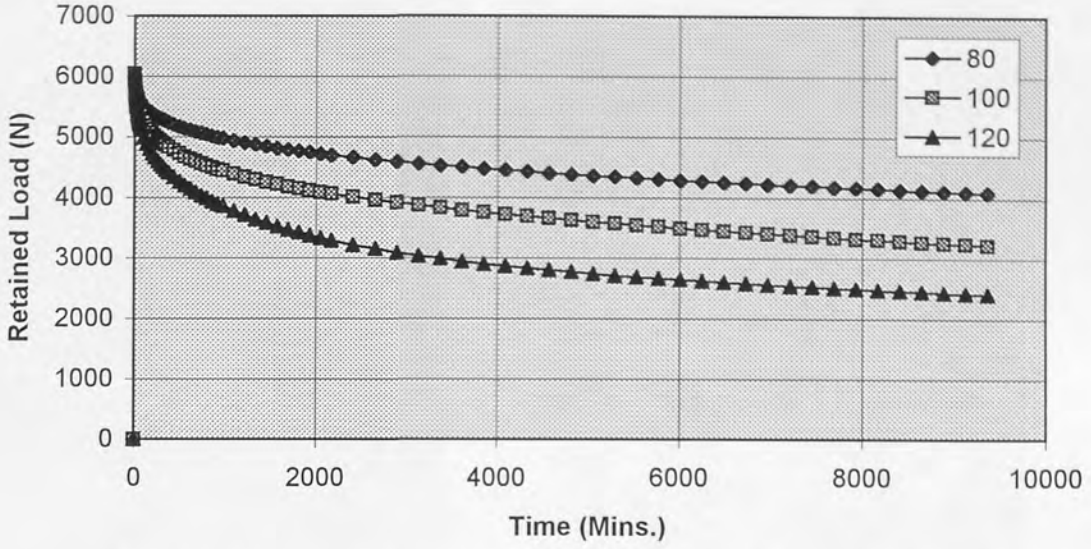

Figure 6.54. Mean load-relaxation curves (linear plot) for ACuZinc10 at 80, 100 and 120° C.

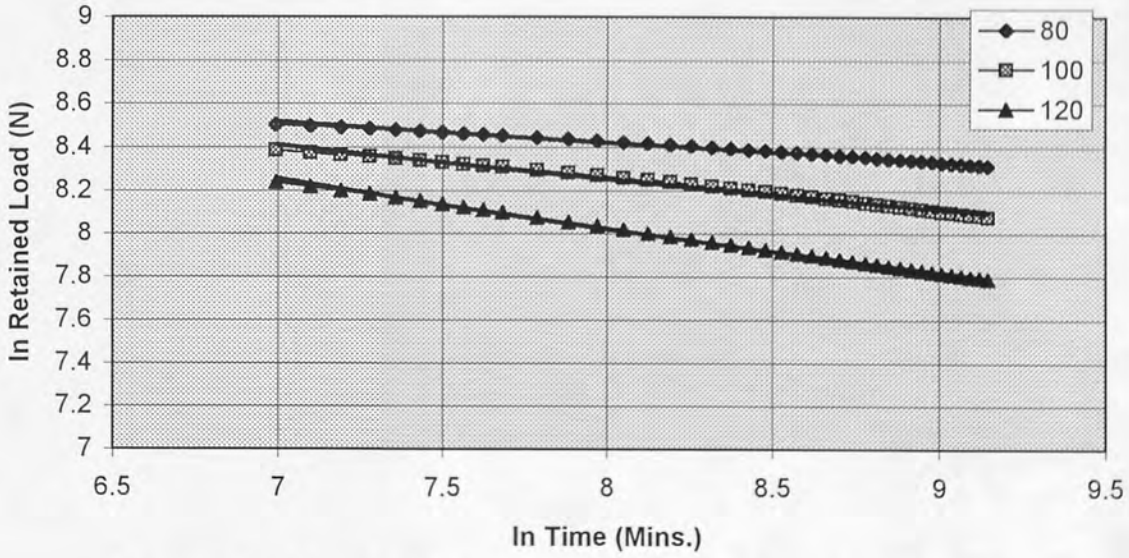

Figure 6.55. Mean load relaxation curves (power law plot) for ACuZinc10 at 80, 100 and 120° C.

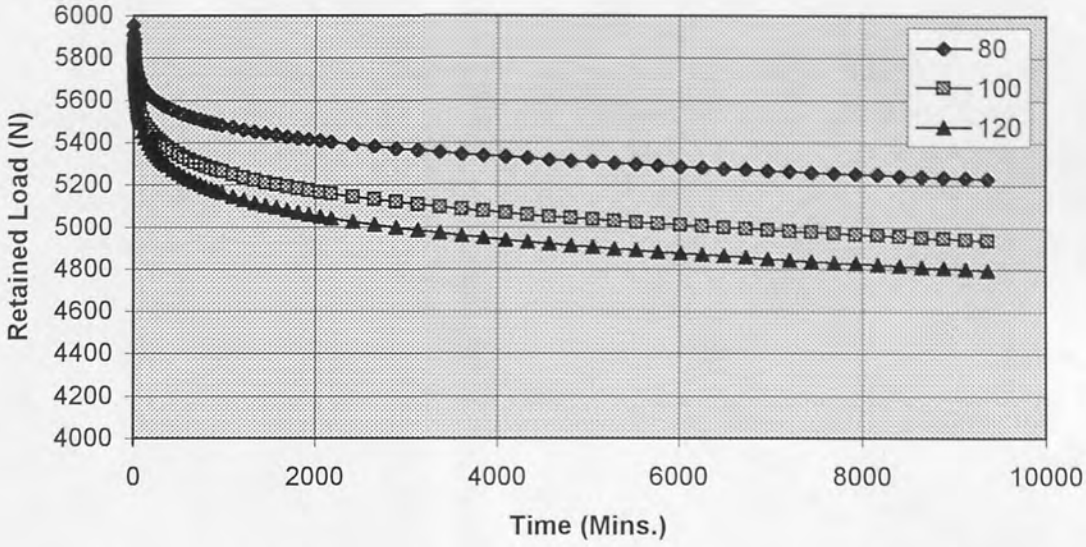

Figure 6.56. Mean load-relaxation curves (linear plot) for ILZRO.16 at 80, 100 and 120° C.

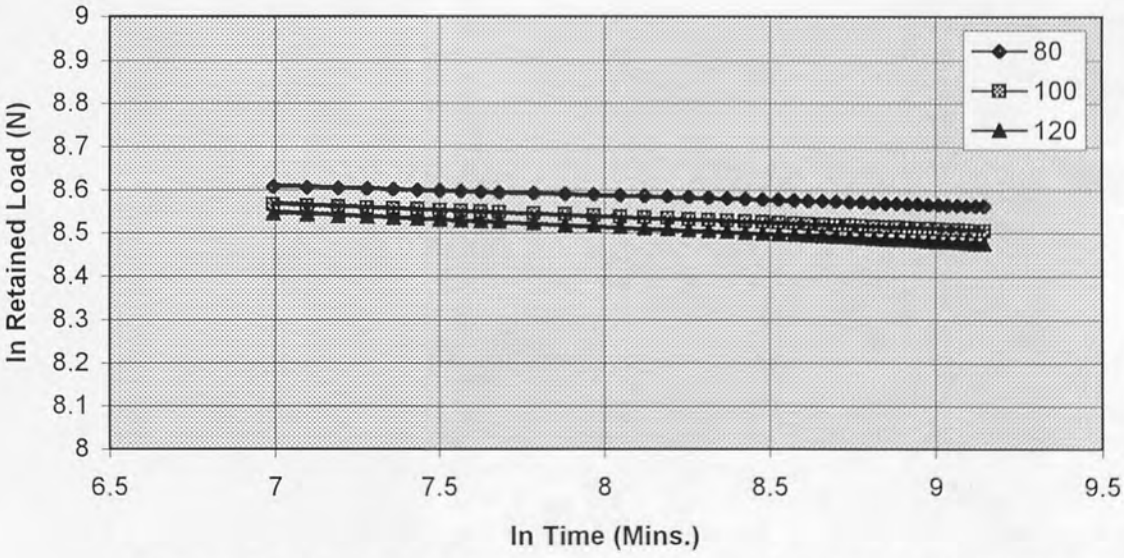

Figure 6.57. Mean load-relaxation curves (power law plot) for ILZRO.16 at 80, 100 and 120° C.

CHAPTER 7

7.0 CONCLUSIONS

1. The primary creep contraction of the alloys was generally found to increase with increasing copper content, but in a non-linear fashion.

2. The secondary creep rates of the alloy No2 were found to be substantially lower than those of the commercial alloys No3 and No5, and slightly lower than those of ACuZinc5 and ACuZinc10. The secondary creep rates of ACuZinc10 were slightly higher than those of ACuZinc5, and lower than those of the alloys No3 and No5.

3. The total creep contraction of the experimental alloys was shown to be correlated by a simple creep equation of the form:

$$f(\varepsilon) = A\, t\, \sigma^n \exp(-Q/RT)$$

where ε is the strain after time t, at temperature T (K), Q is the activation energy, R the gas constant, and A and n are constants.

4. The activation energies for creep (Q_c) of all experimental alloys were found to be in the range of activation energies for lattice self-diffusion in pure zinc, suggesting that the creep rate was being controlled by diffusion in the zinc-rich phase. The stress exponents (n) were in accordance with those of well-established rate-controlling mechanisms, i.e. dislocation climb for alloy No3 and dislocation climb over second phase particles for alloys No5, No2, ACuZinc5 and ACuZinc10.

5. Based on the above creep equation, continuous design stresses were calculated which showed that the alloy No2 had a substantially better total creep resistance than the other Zn-4 % Al alloys No3 and No5, for allowable creep strains up to 1.0 %. Similarly, alloy No5 had much better creep strength than alloy No3 over all allowable strains. Both ACuZinc alloys were inferior in creep strength to alloy No2, but superior to the commercial alloys No3 and No5. ACuZinc5 had a slightly better creep resistance than ACuZinc10 over all strains.

6. During load-relaxation tests, for all alloys the initial load loss was high, decreasing gradually with time, but not ceasing. The degree of load loss increased rapidly with test

temperature, and almost all of the relaxation curves approximated to a logarithmic decay of load with time.

7. The resistance to load loss generally increased with increasing copper content, particularly at higher temperatures.

8. The load-relaxation data could be correlated well using a general load relaxation equation derived by Murphy. This general equation has the form:

$$\ln L = \alpha[Q/RT - \ln B - \ln t]$$

where L is the load retained after time t, at temperature T (K), α and B are constants, Q the activation energy and R is Boltzman's constant.

9. The mean values of α decreased with the increase of copper content for both commercial and ACuZinc alloys, whereas the values of activation energy for load relaxation although similar to those obtained in compressive creep tests, increased with copper content for commercial alloys and decreased for ACuZinc alloys.

10. On the basis of short and long-term relaxation testing, ILZRO.16 showed the best resistance to load loss. Alloy No2 was the most resistant among three Zn-4% Al alloys family, and No5 was better than No3 at all test temperatures. Both ACuZinc alloys had higher resistance than alloys No3, No5 and No2 under all conditions. ACuZinc10 was superior in relaxation strength to ACuZinc5 under all testing conditions.

11. The current load-relaxation results of alloys No3, No5 and No2 showed that sand-casting produced much greater resistance to load-relaxation than hot-chamber pressure diecastings.

12. Although a few minor disagreements between the creep and load relaxation results were observed, ILZRO.16, No3, No5 and No2 showed a similar relative performance in both types of tests. However the performances of ACuZinc5 and ACuZinc10 were transposed in the creep and load-relaxation experiments. This reversal may be due to the lower temperature and longer times of the load- relaxation tests, the effect of a more complex stress system, or to small structural changes during testing.

CHAPTER 8

8.0 SUGGESTIONS FOR FURTHER WORK

1. ILZRO.16 has been creep tested at only the highest stress and higher temperatures. Further creep experiments under other conditions are required to find the creep behaviour, and to accomplish the controlling mechanism for this alloy.

2. All zinc alloys were tested for compressive creep only. It will be interesting to test these alloys for tensile creep, and to compare the results of both types of processes.

3. The microstructure of the alloys was investigated by scanning electron microscopy (SEM). To study more details of the structure, TEM work would be very useful to understand the creep mechanisms involved in the alloys more clearly. Further SEM work on creep tested samples under different conditions would also be beneficial.

4. ACuZinc5 and ACuZinc10 are newer high copper zinc alloys. Both alloys were creep tested under different conditions. In this study, it has been attempted to establish the complete creep characterisation of these alloys. This investigation will be helpful in increasing the popularity and use of these alloys for different applications, especially at elevated temperatures. However, further creep testing and microstructure study is required to establish the creep-controlling mechanisms operating in both ACuZinc alloys.

5. All of the experimental alloys were tested in the temperature range of 0.5 T_m to 0.63 T_m, further creep testing is therefore required at temperatures lower than 0.5 T_m and higher than 0.63 T_m to find the creep behaviour of the alloys completely at low and high temperatures.

6. The alloys were tested for load relaxation at three different temperatures. Further load relaxation experiments are essential to acquire more relaxation data for complete understanding of the relaxation behaviour of the alloys.

7. The general load relaxation equation used to calculate the retained loads at different temperatures for alloys can not be considered as 100% accurate, it is therefore needed

to formulate a more accurate equation which could be used to detect the load relaxation strength of the alloys.

8. The compressive creep and load-relaxation tests on pressure diecastings of the zinc alloys are also important as a further research work. The results of these tests may be compared with those obtained from the current investigation on the same sand-cast alloys.

REFERENCES

1. **Conrad H.** Experimental Evaluation of Creep and Stress Rupture. *Editor : Dorn J.E., McGraw-Hill Book Company, Inc., New York, 1961.*

2. **Dowling N.E.** Mechanical Behaviour of Materials. *Prentice-Hall Int., Inc., New Jersey, 1993.*

3. **Carter G.F.** Principles of Physical and Chemical Metallurgy. *American Society for Metals, Ohio, 1979.*

4. **Tweeddale J.G.** Materials Technology. *Vol. 1, Butterworths & Co. (Publishers) Ltd., London, 1973.*

5. **Sully A.H.** Creep Testing in Compression for Simple Creep Assessment. *Product Engineering, Vol. 24, 150-153, 1953.*

6. **Oding I.A., Ivanova V.S., Burdukskii V.V. and Geminov, V.N.** Creep and Stress Relaxation in Metals. *English Editor : Kennedy a.j. 1st Edition, Oliver and Boyd, London, 1965.*

7. **Reed-Hill R.E.** Physical Metallurgy Principles, *2nd Edition, D. Van Nostrand Co., New York, 1973.*

8. **Weertman J. and Weertman J.R.** Physical Metallurgy, Part II. *Editors : Cahn R.W. and Haasen P., North-Holland Physics Publishing, Amsterdam, 1983.*

9. **Gittus J.** Creep, Viscoelasticity and Creep Fracture in Solids. *Applied Science Publishers Ltd., London, 1975.*

10. **Higgins R.A.** Engineering Metallurgy. *6th Edition, Published by: Edward Arnold, 1993.*

11. **Smallman R.E.** Modern Physical Metallurgy. *3rd Edition, Butterworth & Co. (Publishers) Ltd., Scotland, 1970.*

12. **Greenfield P.** Creep of Metals at High Temperatures, *Mills & Boon Ltd., London, 1972.*

13. **Garofalo F.** Fundamentals of Creep and Creep-Rupture in Metals. *The MacMillan Company, New York, 1965.*

14. **Lagneborg R.** Creep and Fatigue in High Temperature Alloys. *Editor : Bressers J., Applied Science Publishers Ltd., London, 1981.*

15. **Ahmadieh A. and Mukherjee A.K.** Stress-Temperature-Time Correlation for High Temperature Creep Curves. *Mat. Sci. & Eng., Vol. 21, 115-124, 1975.*

16. **Weertman J.** Theory of Steady State Creep Based on Dislocation Climb. *J. Applied Physics, Vol. 26, 1213-1217, 1955.*

17. **Mott N.F.** A Theory of Work-Hardening of Metals-II: Flow Without Slip-Lines, Recovery and Creep. *Phil. Mag., Vol. 44, 742-765, 1953.*

18. **Mukherjee A.K., Bird J.E. and Dorn J.E.** Experimental Correlations for High Temperature Creep. *Trans. ASM, Vol. 62, 155-179, 1969.*

19. **Crossland I.G. and Jones R.B.** Dislocation Creep in Magnesium. *Met. Sci. J., Vol. 6, 162-166, 1972.*

20. **Weertman J.** Steady State Creep Through Dislocation Climb. *J. Applied Physics, Vol. 28, 362-364, 1957.*

21. **Lagneborg R.** Dislocation Mechanisms in Creep. *Int. Metall. Rev., Vol. 17, 130-146, 1972.*

22. **Evans R.W. and Wilshire B.** Creep of Metals and Alloys. *The Inst. of Metals, London, 1985.*

23. **Weertman J.** Creep of Indium, Lead and Some Other Alloys with Various Metals. *Trans. Metall. Soc., AIME, Vol. 218, 207-218, 1960.*

24. **Mohamed F.A. and Langdon T.G.** The Transition from Dislocation Climb to Viscous Glide in Creep of Solid Solution Alloys. *Acta Metall., Vol. 22, 779-788, 1974.*

25. **Takeuchi S. and Argon A.S.** Steady-State Creep of Single-Phase Crystalline Matter at High Temperature. *J. Mat. Sci., Vol. 11, 1542-1566, 1976.*

26. **Murty K.L., Mohamed F.A. and Dorn J.E.** Viscous Glide, Dislocation Climb and Newtonian Viscous Deformation Mechanisms of High Temperature Creep in Al-3Mg. *Acta Metall., Vol. 20, 1009-1018, 1972.*

27. **Nam S.W., Lee D.H. and Hong K.T.** Effects of Grain Size on the Transition Behaviour of an Al-Mg Solid Solution Alloy in the Power Law Creep Regime. *Proc. of the 5th Int. Conf. on Creep of Materials, Lake Buena Vista, Florida, 18-21 May, 1992.*

28. **Jones B.L. and Sellars C.M.** The Creep of Copper, Copper-10 at% Nickel and Copper-10 at% Gold. *Met. Sci. J., Vol. 4, 96-102, 1970.*

29. **Nix W.D. and Barrett C.R.** A Model for Steady State Creep Based on the Motion of Jogged Screw Dislocations. *Acta Metall., Vol. 13, 1247-1258, 1965.*

30. **Nix W.D.** On the Jogged Screw Dislocation Model for Steady State Creep. *Acta Metall., Vol. 15, 1079-1081, 1967.*

31. **Weertman J.** Dislocation Climb Theory of Steady State Creep. *Trans. ASM, Vol. 61, 681-694, 1968.*

32. **Malu M. and Tien J.K.** A Theory for Steady-State Creep Based on the

Motion of Interstitial Type Jogs. *Acta Metall., Vol. 22, 145-151, 1974.*

33. **Bailey R.W.** Note on the Softening of Strain-Hardened Metals and Its Relation to Creep. *J. Inst. of Metals, Vol. 35, 27-40, 1926.*

34. **Orowan E.** The Creep of Metals. *J. West Scotland Iron and Steel Inst., Vol. 54, 45-83, 1946-47.*

35. **Cottrell A.H. and Aytekin V.** The Flow of Zinc under Constant Stress. *J. Inst. of Metals, Vol. 77, 389-422, 1950.*

36. **McLean D.** The Physics of High Temperature Creep in Metals. *Reports on Progress in Physics, Vol. 29, 1-33, 1969.*

37. **Lagneborg R.** Development and Refinement of the Recovery Creep Theory. *Met. Sci. J., Vol. 3, 161-168, 1969.*

38. **Lagneborg R.** A Modified Recovery Creep Model and its Evaluation. *Met. Sci. J., Vol. 6, 127-133, 1972.*

39. **Nabarro F.R.N.** Deformation of Crystals by the Motion of Single Ions. *Report of a Conference on the Strength of Solids. Phy. Soc., 75-90, London, 1948.*

40. **Herring C.** Diffusional Viscosity of a Polycrystalline Solid. *J. Applied Physics, Vol. 21, 437-445, 1950.*

41. **Coble R.L.** A Model for Boundary Diffusion Controlled Creep in Poly - crystalline Materials. *J. Applied Physics, Vol. 34, 1679-1682, 1963.*

42. **Burton B. and Greenwood G.W.** Analysis of Coble Creep in Cylindrical and Cubic Crystals. *Mat. Sci. & Technology, Vol. 1, 1029-1032, Dec. 1985.*

43. **Conrad H.** The Role of Grain Boundaries in Creep and Stress Rupture. *Editor: Dorn J.E., McGraw-Hill Book Company, Inc., New York, 1961.*

44. **Hanson D. and Wheeler M.A.** The Deformation of Metals under Prolonged Loading. Part1.- The Flow and Fracture of Aluminium. *J. Inst. of Metals, Vol. 45, 229-257, 1931.*

45. **McLean D. and Farmer M.H.** The Relation During Creep between Grain Boundary Sliding, Sub-Crystal Size, and Extension. *J. Inst. of Metals, Vol. 85, 41-50, 1956-57.*

46. **Gifkins R.C.** The Measurement of Grain-Boundary Sliding in Polycrystalline Specimens. *Met. Sci. J., Vol. 7, 15-19, 1973.*

47. **Fazan B., Sherby O.D. and Dorn J.E.** Some Observations on Grain Boundary Shearing During Creep. *Trans. AIME, Vol. 200, 919-922, 1954.*

48. **Gibbs G.B.** The Sliding Conribution to the Total Strain of a Polycrystalline Aggregate. *Met. Sci., Vol. 11, 65-67, 1977.*

49. **Suery M. and Mukherjee A.K.** Creep Behaviour of Crystalline Solids. Editors : Wilshire B. and Evans R.W., *Pineridge Press, Swansea, 1985.*

50. **Shariat D., Vastava R.B. and Langelo T.G.** An Evaluation of the Roles of Inter-crystalline and Interphase Boundary Sliding in Two-Phase Superplastic Alloys. *Acta Metall., Vol. 30, 285-296, 1982.*

51. **Valiev R.Z. and Kaibyshev O.A.** Mechanism of Superplastic Deformation in a Magnesium Alloy. *Phy. Stat. Sol., Vol. 9, 65-76, 1977.*

52. **Jones R.B.** Diffusion Creep in Polycrystalline Magnesium. *Nature, Vol. 207, 70, 1965.*

53. **Sherby O.D. and Burke P.M.** Mechanical Behaviour of Crystalline Solids at Elevated Temperatures. *Prog. Mat. Sci., Vol. 13, 325-390, 1966-67.*

54. **Luo A. and Jacobson D.L.** Creep Behaviour of a Tungsten-3.6w/o Rhenium-0.33w/o Zirconium Carbide at Ultrahigh Temperatures. *Proc. of the 5th Int. Conf. on Creep of Materials, Lake Buena Vista, Florida, 18-21 May, 1992.*

55. **Tegart W.J.McG.** Activation Energies for High Temperature Creep of Polycrystalline Magnesium. *Acta Metall., Vol. 9, 614-617, 1961.*

56. **Garofalo F.** An Empirical Relation Defining the Stress Dependence of Minimum Creep Rate in Metals. *Trans. AIME, Vol. 227, 351-356, 1963.*

57. **Jones R.B. and Harris, J.E.** Creep Deformation of Polycrystalline Magnesium. Joint Int. Conf. on Creep. *The Inst. of Mech. Eng., London, 1963.*

58. **Price A.T., Hall H.A. and Greenough A.P.** The Surface Energy and Self Diffusion Coefficient of Solid Iron Above 1350^{o}C. *Acta Metall., Vol. 12, 49-58, 1964.*

59. **Lawly A., Coll J.A. and Cahn R.W.** Influence of Crystallographic Order on Creep of Iron-Aluminium Solid Solutions. *Trans. AIME, Vol. 218, 166-176, 1960.*

60. **Blum W. and Reppich B.** Creep Behaviour of Crystalline Solids. *Editors : Wilshire B. and Evans R.W., Pineridge Press, Swansea, 1985.*

61. **Haung H.I.L., Sherby O.D. and Dorn J.E.** Activation Energy for High Temperature Creep of High Purity Aluminium. *Trans. AIME, Vol. 206, 1385-1388, 1956.*

62. **Tietz T.E. and Dorn J.E.** Creep of Copper at Intermediate Temperatures. *Trans. AIME, Vol. 206, 156-162, 1956.*

63. **Sherby O.D., Lytton J.L. and Dorn J.E.** Activation Energies for Creep of High -Purity Aluminium. *Acta Metall., Vol. 5, 219-227, 1957.*

64. **Garofalo F., Richmond O., Domis W.F. and Gemmingen F.V.** Strain-Time, Rate-Stress and Rate-Temperature Relations During Large Deformations in Creep. *Joint Int. Conf. on Creep. The Inst. of Mech. Eng., London, 1963.*

65. **Howard E.M., Barmore W.C., Mote J.D. and Dorn J.E.** On the Thermally-Activated Mechanism of Prismatic Slip in the Silver-Aluminium Hexagonal Intermediate Phase. *Trans. AIME, Vol. 227, 1061-1068, 1963.*

66. **Poirier J.P.** Is Power-Law Creep Diffusion-Controlled? *Acta Metall., Vol. 26, 629-637, 1978.*

67. **Jaffe N. and Dorn J.E.** Effect of Stress on the Creep Rate of High-Purity Aluminium in the Cross-Slip Region. *Trans. AIME, Vol. 224, 1167-1173, 1962.*

68. **Conrad H.** Thermally Activated Deformation of Metals. *J. of Metals, Vol. 16, No. 7, 582-588, July 1964.*

69. **Friedel J.** Dislocations. *Addison Wesley, Reading, 1964.*

70. **Wachtman J.B.J.** Creep and Recovery. *American Society for Metals, Cleveland, 1957.*

71. **Brinson G. and Argent B.B.** The Creep of Niobium. *J. Inst. of Metals, Vol. 91, 293-298, 1962-63.*

72. **Davies P.W., Dennison J.P. and Evans R.W.** The High-Temperature Creep and Fracture of Polycrystalline Gold. *J. Inst. Metals, Vol. 92, 409-412, 1963-64.*

73. **Evans W.J. and Wilshire B.** Transient and Steady-State Creep Behaviour of Nickel, Zinc, and Iron. *Trans. Met. Soc. AIME, Vol. 242, 1303-1307, 1968.*

74. **Davies P.W., Evans W.J., Williams K.R. and Wilshire B.** An Equation To Represent Strain/Time Relationships During High Temperature Creep. *Scripta Metall., Vol. 3, 671-674, 1969.*

75. **Evans W.J. and Wilshire B.** The High Temperature Creep and Fracture Behaviour of 70-30 Alpha-Brass. *Met. Trans., Vol. 1, 2133-2139, 1970.*

76. **Evans R.W., Parker J.D. and Wilshire B.** Recent Advances in Creep and Fracture of Engineering Materials and Structures. *Editors : Wilshire B. and Owen D.R.T., Pineridge Press, Swansea, 1982.*

77. **Evans R.W., Beden I. and Wilshire B.** Proc. 2nd. Int. Conf. on Creep and Fracture of Engineering Materials and Structures. *Editors : Wilshire B. and Owen D.R.T., Pineridge Press, Swansea, 1984.*

78. **Evans R.W. and Wilshire B.** Proc. 3rd. Int. Conf. on Creep and Fracture of Engineering Materials and Structures. *Editors : Wilshire B. and* Evans R.W., *Pineridge Press, Swansea, 1987.*

79. **Hanna M.D. and Rashid M.S.** ACuZinc: Improved Zinc Alloys for Die Casting Applications. *SAE Technical Paper Series, International Congress and Exposition, Detroit, Michigan, March 1-5, 1993.*

80. **Rashid M.S. and Hanna M.D.** ACuZinc: Creep Resistant Zinc Die Casting Alloys. *Trans. NADCA, 1993.*

81. **Apelian D., Paliwal M. and Herrschart D.C.** Casting with Zinc Alloys. *J. Metals, Vol. 33, 12-20, Nov. 1981.*

82. **Calayag T. and Ferres D.** High Performance High Aluminium Zinc Alloys for Low Speed Bearings and Bushings. *SAE Technical Paper Series, Earthmoving Industry Conf., Peoria, Illinois, April 19-21, 1982.*

83. Engineering Properties of Zinc Alloys. *Published by Int. Lead Zinc Research Organisation Inc., 3rd Ed., New York, 1989.*

84. **Durman M.** The Creep Behaviour of Pressure Die Cast Zinc-Aluminium Based Alloys. *Ph.D. Thesis, The University of Aston in Birmingham, 1989.*

85. **Machler M.** Zinc Alloy enhances Strength and Creep Resistance. *Advanced Materials & Processes, Vol. 150, 25-26, Oct. 1996.*

86. **Balliett R.W.** Mechanical Properties of Creep Resistant Zinc Die-Casting Alloys. *Paper No. G575-OB, 8th SDCH Int. Die-Casting Exposition and Congress, Detroit, Michigan, March 17-20, 1975.*

87. **Rennhack E.H. and Conard G.P.** Creep Deformation of Rolled Zn-Ti Alloys. *Trans. Metall. Soc. AIME, Vol. 236, 1441-1444, 1966.*

88. **Rennhack E.H. and Conard G.P.** Structural Aspects of Fibering in Rolled Zn-Ti Alloys and their Relation to Creep. *Trans. Metall. Soc. AIME, Vol. 236, 694-698, 1966.*

89. **Murphy S., Hill J. and Durman M.** Creep Behaviour of Commercial Pressure Die Cast Zinc Alloys. *Presented at 12th Int. Pressure Diecaster Conf., Florence, Italy, 1987.*

90. **Loong C.A.** Temperature and Ageing and Thickness Effects on Die-Casting Alloys. *Proc. 25th CIM Conf., 157-170, Toronto, Canada, 1986.*

91. **Hanna M.D., Carter J.T. and Rashid M.S.** Sliding Wear and Friction Characteristics of Six Zn-Based Die-Casting Alloys. *To be Published in the 11th Int. Conf. on Wear of Metals, April 1997.*

92. **Gervais E., Levert H. and Bess M.** Development of a Family of Zinc Based Foundry Alloys. *Presented at the 84th Casting Congress and Exposition, and Published in the Transactions of the American Foundrymen's Society, St. Louis, Missouri, U.S.A., April 21-25, Vol. 88, 1980.*

93. **Murphy S., Savaskan T. and Hill J.** The Creep Kinetics of Zinc-Aluminium

Based Alloys. *Presented at 24th Ann. Conf. Of Metallurgists, CIM, Vancouver, Canada, 1985.*

94. **Naziri H. and Pearce R.** The Influence of Copper Additions on the Superplastic Forming Behaviour of the Zn-Al Eutectoid. *Inst. J.Mech. Sci., Vol. 12, 513-521, 1970.*

95. **Nuttall K.** Effect of Some Ternary Additions on the Mechanical Properties of the Zn-Al Eutectoid Alloy. *J. Inst. Metals, Vol. 101, 329-333, 1973.*

96. **Mulvania L.E., Weltzin R.D. and Talcott P.A.** A Superplastic Zn-Al Alloy with Creep Resistance. *Met. Eng. Quarterly, Vol. 14, 55-60, 1974.*

97. **Savaskan T.** The Structure and Properties of Zinc-Aluminium Based Bearing Alloys. *Ph.D. Thesis, The University of Aston in Birmingham, 1980.*

98. **Savaskan T. and Murphy S.** Creep Behaviuor of Zn-Al-Cu Bearing Alloys. *Z. Metallkunde, Vol. 74, 76-82, 1983.*

99. **Murray J.L.** The Al-Zn System. *Bulletin of Alloy Phase Diagrams, Vol. 4, No. 1, 55-73, 1983.*

100. **Hanson D. and Gayler M.L.V.** Further Study of the Alloys of Aluminium and Zinc. *J. Inst. Metals, Vol. 27, 267-306, 1922.*

101. **Tanabe T.** Studies in the Aluminium-Zinc System. *J. Inst. Metals, Vol. 32, 415-453, 1924.*

102. **Isihara T.** On the Equilibrium Diagram of the Aluminium-Zinc System. *J. Inst. Metals, Vol. 33, 73-90, 1925.*

103. **Owen E.A. and Pickup L.** X-ray Study of Aluminium-Zinc Alloys at Elevated Temperatures. *Phil. Mag., Vol. 20, 761-777, 1935.*

104. **Ellwood E.C.** An X-ray Study of the Constitution of Aluminium-Zinc Alloys of High Purity Above 275°C, with a Description of a New High Temperature X-ray Camera. *J. Inst. Metals, Vol. 66, 87-96, 1940.*

105. **Ellwood E.C.** The Solid Solutions of Zinc in Aluminium. *J. Inst. Metals, Vol. 80, 217-224, 1951-52.*

106. **Fink W.L. and Willey L.A.** Equilibrium Relations in Aluminium-Zinc Alloys of High Purity, II. *Trans. Amer. Inst. Min. Met. Eng., Vol. 122, 244-265, 1936.*

107. **Gayler M.L.V. and Sutherland E.G.** The Constitution of Aluminium-Zinc Alloys of High Purity, the Nature of the Thermal Change at 443°C. *J. Inst. Metals, Vol. 63, 123-147, 1938.*

108. **Hansen M. and Anderko K.** Constitution of Binary Alloys. *2nd. Ed.,*

McGraw Hill Book Company Inc., USA, 1958.

109. **Presnyakov A.A., Gorban Yu A. and Chervyakova V.V.** The Aluminium-Zinc Phase Diagram. *Russian Journal of Physical Chemistry, Vol. 35, No. 6, 632-633, 1961.*

110. **Goldak G.R. and Parr J.G.** A High Temperature X-ray Diffractometer Study of the Zinc-Aluminium System in the Region 40-75 wt. % Zinc. *J. Inst. Metals, Vol. 92, 230-233, 1963-64.*

111. **Mondolfo L.F.** Aluminium Alloys - Structure and Properties. *Butterworth, London, 1976.*

112. **Greaves R.H. and Wrighton H.** Practical Microscopical Metallography. 4th. Ed., *Chapman & Hall, London, 1957.*

113. **Pearson W.B.** A Handbook of the Lattice Spacings and Structures of Metals and alloys. *Vol. 2, Pergamon Press, London, 1967.*

114. **Metal's Handbook.** Phase Diagrams of Binary Alloy Systems. *8th. Ed., Vol. 8, American Society for Metals, Ohio, 1973.*

115. **Fletcher A.J. and Thomas D.L.** Solid State Transformations in Certain Copper-Aluminium-Zinc Alloys. *J. Inst. Metals, Vol. 98, 188-192, 1970.*

116. **Willey L.A.** Aluminium- Copper-Zinc. *Metals Handbook, 8th Edition, Vol. 8, 390-391, American Society for Metals, Ohio, 1973.*

117. **Strawbridge D.J., Hulme-Rothery W. and Little A.T.** The Constitution of Aluminium- Copper-Magnesium-Zinc Alloys at 460°C. *J. Inst. Metals, Vol. 74, 191-225, 1947-48.*

118. **Murphy S.** Solid-Phase Reactions in the Low-Copper Part of the Al-Cu-Zn System. *Z. Metallkunde, Vol. 71, 96-102, 1980.*

119. **Murphy S.** The Structure of the T' Phase in the System Al-Cu-Zn. *Met. Sci., Vol. 9, 163-168, 1975.*

120. Stress Relaxation Testing. Editor: Fox a., *ASTM Special Technical Publication 676, A Symposium Sponsored by ASTM, Kansas City, Mo., 24-25 May, 1979.*

121. **Johnson A.E.** Creep and Relaxation of Metals at High Temperatures. *Engineering, Vol. 168, 237-239, 1949.*

122. **Henderson J. and Ferguson F.R.** Creep Relaxation in Components. *NEL Report No. 625, Glasgow, Nov. 1976.*

123. **Solberg J.K. and Thon H.** Stress Relaxation and Creep of Some Aluminium Alloys. *Mat. Sci. & Eng., Vol. 75, 105-116, 1985.*

124. **Murphy S. and Haines C.W.** Preload Relaxation of Threaded Fasteners in Zinc Alloy Pressure Die Castings. *Advances in Science, Technology and Applications of Zn-Al Alloys, Edited by: Villasenor G.T., Zhu Y.H. and PinaC., Mexico, 1994.*

125. **Murphy S. and Goodwin F.E.** Preload Relaxation of Steel Fasteners in Zinc Alloy Pressure Die Castings - Some Engineering Solutions. *SAE Technical Paper Series, International Congress and Exposition, Detroit, Michigan, Feb. 26-29, 1996.*

126. Casting Processes. *Published by the Open University, U.K., 1979.*

127. **Bownes F.F.** Sand Casting, Castings. *Editor: Beadle J.D., 1971.*

128. **Sully A.H.** Metallic Creep. *Butterworths Scientific Publications, London, 1949.*

129. **Whittenberger J.D., Arzt E. and Luton J.** 1400 and 1500 K Compressive Creep Properties of an NiAl-AlN Composite. *Scripta Metall., Vol. 26, 1925-1930, 1992.*

130. **Murphy S., Durman M. and Hill J.** Kinetics of Creep in Pressure Diecast Commercial Zinc-Aluminium Alloys. *Z. Metallkunde, Vol. 79, 243-247, 1988.*

131. **Durman M. and Murphy S.** An Improved Parametric Method for the Correlation of Creep Data from Commercial Pressure-Diecast Zinc-Based Alloys. *Z. Metallkunde, Vol. 82, 129-134, 1991.*

132. **Tegart W.J.M. and Sherby O.D.** Activation Energies for High Temperature Creep of Polycrystalline Zinc. *Phil. Mag., Vol. 5, 1287-1296, 1958.*

133. **Flinn J.E. and Munson D.E.** Stress-Dependence of the Transition Behaviour in Multi-Mechanism Creep Reactions : with Special Reference to Zinc. *Phil. Mag., Vol. 11, 861-870, 1967.*

134. **Wajda E.S.** Grain Boundary Self-Diffusion in Zinc. *Acta Metall., Vol. 2, 184-187, 1954.*

135. **Sirn G.A., Wajda E.S. and Huntington N.B.** Self-Diffusion in Zinc. *Acta Metall., Vol. 1, 515-518, 1953.*

136. **Hilliard J.E., Averbach B.L. and Cohen M.** Self and Inter Diffusion in Aluminium-Zinc Alloys. *Acta Metall., Vol. 7, 86-92, 1959.*

137. **Dorn J.E.** Some Fundamental Experiments on High Temperature Creep. J. Mechanics & Physics of Solids. *Vol. 3, 85-116, 1954.*

138. **Gilman J.J.** Plastic Anisotropy of Zinc Monocrystals. *Trans. Metall. Soc. AIME, Vol. 226, 1326-1336, Oct. 1956.*

139. **Davies P.W. and Williams K.R.** The Creep and Fracture of Polycrystalline Zinc over the Temperature Range 348-470 K. *Met. Sci., Vol. 9, 149-154, 1975.*

140. **Sherby O.D. and Weertman J.** Diffusion-Controlled Dislocation Creep : A Defense. *Acta Metall., Vol. 27, 387-400, 1979.*

141. **Sherby O.D., Orr R.L. and Dorn J.E.** Creep Correlations of Metals at Elevated Temperatures. *Trans. AIME, J. Metals, Vol. 200, 71-80, 1954.*

142. **Bird J.E., Mukherjee A.K. and Dorn J.E.** Proc. An Int. Conf. on Quantitative Relation between Properties and Microstructure. *Editors : Brandon D.G. and Rosen A., Israel Universities Press, Jerusalem, 1969.*

143. **Tegart W.J.M.** Activation Energies for High Temperature Creep of Polycrystalline Magnesium. *Acta Metall., Vol. 9, 614-617, 1961.*

144. **Durman M. and Murphy S.** Advances in Science, Technology and Applications of Zn-Al Alloys. *Editors : Villasenor G.T., Zhu Y.H. and Pina C., Mexico, 1994.*

145. **Mykura N., Zhu Y.H. and Murphy S.** Solid-State Reactions in Zn-Al Based Alloys. *Canadian Metall. Quarterly, Vol. 25, No. 2, 151-159, 1986.*

146. **Ansell G.S. and Weertman J.** Creep of a Dispersion-Hardened Aluminium Alloy. *Trans. Metall. Soc. AIME, Vol. 215, 838-843, 1959.*

147. **Lagneborg R.** Recovery Creep in Materials Hardened by a Second Phase. *J. Mat. Sci., Vol. 3, 596-602, 1968.*

148. **Durman M. and Murphy S.** Precipitation of Metastable ε-Phase in a Hypereutectic Zinc-Aluminium Alloy Containing Copper. *Acta Metall. Mater., Vol. 39, 2235-2242, 1991.*

149. **Rashid M.S. and Hanna M.D.** The Influence of Composition and Microstructure on the Strength of Zinc Alloys. *GMR-7574, ASM Int. Chapter, 1992.*

150. **Landon P.R., Lytton J.L., Shepard L.A. and Dorn J.E.** The Activation Energies for Creep of Polycrystalline Copper and Nickel. *Trans. ASM, Vol. 51, 900-910, 1959.*

151. **Gupta I. and Li J.C.M.** Stress Relaxation, Internal Stress, and Work Hardening in some BCC Metals and Alloys. *Metall. Trans., Vol. 1, 2323-2330, Aug. 1970.*

152. **Yamada H. and Li C.Y.** Stress Relaxation and Mechanical Equation of State in Austenitic Stainless Steels. *Metall. Trans., Vol. 4, 2133-2136, Sept. 1973.*

153. **Henderson J.** Complex Stress Relaxation of Metals at Elevated Temperatures. *Metals Technology, Vol. 1, 338-342, July 1974.*

154. **Attermo R. and Lagneborg R.** Stress Relaxation of electrical conductor Aluminium. *Metals Technology, Vol. 1, 462-467, Oct. 1974.*

155. **Woodford D.A.** Trans. 6th Int. Conf. on Creep & Fatigue-Design and Life Assessment at High Temperature. *The Inst. Mech. Eng., London, 1996.*

156. **Murphy S.** Torque Relaxation in Zinc Diecastings. *Project Report, Project ZM 414, June 1996.*

APPENDICES

APPENDIX A

CREEP TEST DATA OF THE ALLOYS No3, No5, No2, ACuZinc5, ACuZinc10 AND ILZRO.16

Creep Test Data of Alloy No3 at 160°C.

Stress (MPa)	Primary Creep %	Secondary Creep Rate (1/s)	Time to 0.2% Creep Strain (ks)	Time to 0.5% Creep Strain (ks)	Time to 0.7% Creep Strain (ks)	Time to 1.0% Creep Strain (s)
100	0	0.0604	-	0.005	0.008	0.014
100	0.27	0.0559	-	0.008	0.008	0.013
60	0.11	0.00191	-	0.200	0.307	0.463
60	0.28	0.00121	0.010	0.170	0.340	0.593
40	0.23	0.000189	-	1.410	2.430	3.730
40	0.26	0.000174	0.100	1.380	2.580	4.230
20	0.11	0.0000128	9.050	33.000	47.300	67.000
20	0.26	0.0000109	3.100	22.300	41.200	66.900

Creep Test Data of Alloy No3 at 130°C.

Stress (MPa)	Primary Creep %	Secondary Creep Rate (1/s)	Time to 0.2% Creep Strain (ks)	Time to 0.5% Creep Strain (ks)	Time to 0.7% Creep Strain (ks)	Time to 1.0% Creep Strain (s)
100	0.55	0.00507	-	0.019	0.040	0.090
100	0.55	0.00428	0.005	0.010	0.035	0.101
60	0.39	0.000163	-	0.675	1.860	3.730
60	0.27	0.000164	-	1.410	2.625	4.400
40	0.23	0.0000193	-	13.980	24.780	38.280
40	0.21	0.0000143	1.740	20.000	34.000	52.400
20	0.17	0.00000146	41.800	232.600	369.400	574.600

Creep Test Data of Alloy No3 at 100°C.

Stress (MPa)	Primary Creep %	Secondary Creep Rate (1/s)	Time to 0.2% Creep Strain (s)	Time to 0.5% Creep Strain (s)	Time to 0.7% Creep Strain (s)	Time to 1.0% Creep Strain (s)
100	0.48	0.000421	-	0.150	0.510	1.230
100	0.41	0.000363	0.008	0.290	0.780	1.620
60	0.51	0.00000358	-	12.180	55.860	138.040
60	0.29	0.0000121	0.090	16.795	33.770	54.675
60	0.40	0.00000782	0.500	18.400	41.200	77.800
40	0.24	0.00000138	-	191.280	328.080	556.680
40	0.18	0.00000143	31.000	216.200	351.500	529.400
30	0.22	0.000000419	81.500	666.400	1150.600	1888.600
20	0.06	0.000000173	769.000	2576.200	3659.800	5427.400

Creep Test Data of Alloy No3 at 70°C.

Stress (MPa)	Primary Creep %	Secondary Creep Rate (1/s)	Time to 0.2% Creep Strain (ks)	Time to 0.5% Creep Strain (ks)	Time to 0.7% Creep Strain (ks)	Time to 1.0% Creep Strain (s)
100	0.72	0.0000382	0.003	0.60	2.50	7.68
100	0.59	0.000061	0.005	0.66	2.70	8.50
60	0.32	0.000000724	22.08	272.28	527.88	949.08
40	0.13	0.000000017	419.80	2054.20	-	-

Creep Test Data of Alloy No5 at 160°C.

Stress (MPa)	Primary Creep %	Secondary Creep Rate (1/s)	Time to 0.2% Creep Strain (ks)	Time to 0.5% Creep Strain (ks)	Time to 0.7% Creep Strain (ks)	Time to 1.0% Creep Strain (s)
100	0.23	0.00530	0.010	0.055	0.095	0.150
100	0.50	0.00953	0.003	0.010	0.024	0.052
100	0.64	0.01430	-	0.006	0.014	0.030
60	0.32	0.000328	0.013	0.525	1.140	1.995
60	0.26	0.000370	0.034	0.645	1.200	2.040
40	0.23	0.0000441	0.090	5.950	10.230	15.440
40	0.22	0.0000549	0.690	5.130	8.700	14.000
20	0.15	0.00000480	-	72.300	114.000	176.000

Creep Test Data of Alloy No5 at 130°C.

Stress (MPa)	Primary Creep %	Secondary Creep Rate (1/s)	Time to 0.2% Creep Strain (ks)	Time to 0.5% Creep Strain (ks)	Time to 0.7% Creep Strain (ks)	Time to 1.0% Creep Strain (s)
100	0.53	0.000538	0.011	0.16	0.48	1.05
100	0.39	0.000584	0.013	0.221	0.516	1.035
60	0.32	0.0000372	0.08	4.98	10.38	18.17
60	0.24	0.0000433	0.78	5.88	10.83	18.48
40	0.25	0.00000468	1.53	52.83	94.08	149.88
40	0.19	0.0000066	6.78	47.28	77.88	117.7
20	0.2	0.0000013	52.70	232.70	380.2	601.60

Creep Test Data of Alloy No5 at 100°C.

Stress (MPa)	Primary Creep %	Secondary Creep Rate (1/s)	Time to 0.2% Creep Strain (ks)	Time to 0.5% Creep Strain (ks)	Time to 0.7% Creep Strain (ks)	Time to 1.0% Creep Strain (s)
100	0.53	0.0000403	0.007	1.08	4.53	11.78
100	0.41	0.0000789	0.01	2.33	5.88	12.00
60	0.32	0.00000213	0.75	81.80	178.90	313.68
60	0.25	0.0000018	9.50	134.90	247.00	401.90
40	0.25	0.000000347	74.60	731.30	1278.50	2173.10
40	0.2	0.000000375	103.00	790.60	1318.00	2115.40
20	0.13	0.000000173	481.00	2209.08	3242.20	5103.40

Creep Test Data of Alloy No5 at 70°C.

Stress (MPa)	Primary Creep %	Secondary Creep Rate (1/s)	Time to 0.2% Creep Strain (ks)	Time to 0.5% Creep Strain (ks)	Time to 0.7% Creep Strain (ks)	Time to 1.0% Creep Strain (s)
100	0.51	0.00000244	0.009	18.500	77.800	204.200
60	0.22	0.000000177	239.800	1634.900	2752.680	4487.800
60	0.19	0.000000175	275.800	1813.000	2947.080	4700.200
40	0.14	0.000000096	419.800	2054.200	-	-

Creep Test Data of Alloy No2 at 160°C.

Stress (MPa)	Primary Creep %	Secondary Creep Rate (1/s)	Time to 0.2% Creep Strain (ks)	Time to 0.5% Creep Strain (ks)	Time to 0.7% Creep Strain (ks)	Time to 1.0% Creep Strain (s)
100	0.40	0.00108	0.028	0.130	0.290	0.570
100	0.32	0.00113	0.010	0.160	0.324	0.600
60	0.35	0.000138	-	1.035	2.540	4.680
60	0.24	0.000146	0.150	1.790	3.165	5.240
40	0.21	0.0000262	1.920	10.880	18.360	31.100
40	0.27	0.0000315	-	6.870	13.220	23.400
20	0.34	0.0000014	16.680	121.080	248.800	457.600

Creep Test Data of Alloy No2 at 130°C.

Stress (MPa)	Primary Creep %	Secondary Creep Rate (1/s)	Time to 0.2% Creep Strain (ks)	Time to 0.5% Creep Strain (ks)	Time to 0.7% Creep Strain (ks)	Time to 1.0% Creep Strain (s)
100	0.47	0.000109	0.012	0.690	2.160	4.900
100	0.34	0.000132	0.030	1.200	2.620	5.000
60	0.35	0.0000167	-	8.650	20.600	41.900
60	0.20	0.0000129	2.280	23.900	38.500	62.100
40	0.21	0.00000424	9.390	67.220	114.070	186.150
40	0.34	0.000004	9.480	52.680	92.280	167.880
20	0.38	0.000000183	63.4	776.2	1766200	3548200

Creep Test Data of Alloy No2 at 100°C.

Stress (MPa)	Primary Creep %	Secondary Creep Rate (1/s)	Time to 0.2% Creep Strain (ks)	Time to 0.5% Creep Strain (ks)	Time to 0.7% Creep Strain (ks)	Time to 1.0% Creep Strain (s)
100	0.56	0.0000081	0.010	6.330	20.280	54.480
100	0.33	0.0000109	0.200	15.780	34.000	55.100
60	0.45	0.00000148	0.140	49.080	167.880	369.480
60	0.24	0.00000142	18.400	185.800	322.600	549.100
40	0.21	0.000000498	74.280	592.680	989.900	1589.880
40	0.25	0.000000439	58.000	581.800	1042.600	1749.400

Creep Test Data of Alloy No2 at 70°C.

Stress (MPa)	Primary Creep %	Secondary Creep Rate (%/s)	Time to 0.2% Creep Strain (s)	Time to 0.5% Creep Strain (s)	Time to 0.7% Creep Strain (s)	Time to 1.0% Creep Strain (s)
100	0.69	0.00000043	0.007	59.800	236.200	945.400
100	0.28	0.00000060	20.280	344.300	643.080	1114.700

Creep Test Data of ACuZinc5 at 160°C.

Stress (MPa)	Primary Creep %	Secondary Creep Rate (1/s)	Time to 0.2% Creep Strain (ks)	Time to 0.5% Creep Strain (ks)	Time to 0.7% Creep Strain (ks)	Time to 1.0% Creep Strain (s)
100	0.38	0.001090	0.009	0.110	0.275	0.570
100	0.33	0.000892	0.009	0.200	0.405	0.750
60	0.41	0.000224	-	0.480	1.320	2.600
60	0.21	0.000170	0.170	1.680	2.880	4.600
40	0.20	0.0000700	1.050	4.680	7.330	11.280
40	0.34	0.0000491	0.810	4.670	7.810	13.260
20	0.37	0.0000018	11.200	82.800	185.800	350.500

Creep Test Data of ACuZinc5 at 130°C.

Stress (MPa)	Primary Creep %	Secondary Creep Rate (1/s)	Time to 0.2% Creep Strain (ks)	Time to 0.5% Creep Strain (ks)	Time to 0.7% Creep Strain (ks)	Time to 1.0% Creep Strain (s)
100	0.44	0.000163	0.009	0.570	1.620	3.480
100	0.40	0.000101	0.015	1.320	3.030	5.900
60	0.36	0.0000341	0.017	6.780	15.780	30.130
60	0.23	0.0000199	1.050	13.200	23.500	39.000
40	0.34	0.00000703	1.320	27.480	51.750	94.080
40	0.29	0.00000742	3.780	27.890	52.750	100.180
20	0.41	0.000000182	38.200	574.600	1588.000	3272.800

Creep Test Data of ACuZinc5 at 100°C.

Stress (MPa)	Primary Creep %	Secondary Creep Rate (1/s)	Time to 0.2% Creep Strain (ks)	Time to 0.5% Creep Strain (ks)	Time to 0.7% Creep Strain (ks)	Time to 1.0% Creep Strain (s)
100	0.46	0.00001140	0.010	8.580	22.080	47.280
100	0.53	0.00000878	-	6.780	21.180	52.700
60	0.39	0.00000252	2.040	45.480	122.880	243.480
60	0.25	0.00000170	10.300	153.400	270.400	449.200
40	0.34	0.000000528	13.090	329.880	679.560	1262.280
40	0.24	0.000000360	95.800	740.200	1285.600	2135.280
20	-	-	3982.000	-	-	-

Creep Test Data of ACuZinc5 at 70°C.

Stress (MPa)	Primary Creep %	Secondary Creep Rate (1/s)	Time to 0.2% Creep Strain (ks)	Time to 0.5% Creep Strain (ks)	Time to 0.7% Creep Strain (ks)	Time to 1.0% Creep Strain (s)
100	0.27	0.0000011	16.6	223.6	401.9	679

Creep Test Data of ACuZinc10 at 160°C.

Stress (MPa)	Primary Creep %	Secondary Creep Rate (1/s)	Time to 0.2% Creep Strain (ks)	Time to 0.5% Creep Strain (ks)	Time to 0.7% Creep Strain (ks)	Time to 1.0% Creep Strain (s)
100	0.27	0.00222	0.009	0.100	0.190	0.340
100	0.28	0.00160	0.009	0.140	0.262	0.460
60	0.27	0.000242	0.020	0.930	1.740	2.925
60	0.28	0.000278	0.035	0.780	1.500	2.580
40	0.21	0.0000584	0.300	4.980	8.300	12.850
40	0.22	0.0000572	0.960	5.130	8.500	13.450
20	0.57	0.00000178	5.500	32.800	85.000	243.400

Creep Test Data of ACuZinc10 at 130°C.

Stress (MPa)	Primary Creep %	Secondary Creep Rate (1/s)	Time to 0.2% Creep Strain (ks)	Time to 0.5% Creep Strain (ks)	Time to 0.7% Creep Strain (ks)	Time to 1.0% Creep Strain (s)
100	0.35	0.000188	0.008	0.840	1.860	3.480
100	0.48	0.000191				3.330
100	0.33	0.000171	0.004	0.105	2.210	4.000
60	0.27	0.0000317	0.160	7.180	13.270	22.980
60	0.24	0.0000320	0.156	8.580	14.380	23.880
40	0.39	0.00000859	0.080	13.980	35.100	73.870
40	0.19	0.00000781	8.580	38.900	63.500	106.680
20	0.38	0.000000183	49.000	704.200	1701.400	3400.600

Creep Test Data of ACuZinc10 at 100°C.

Stress (MPa)	Primary Creep %	Secondary Creep Rate (1/s)	Time to 0.2% Creep Strain (ks)	Time to 0.5% Creep Strain (ks)	Time to 0.7% Creep Strain (ks)	Time to 1.0% Creep Strain (s)
100	0.33	0.0000143	-	12.180	25.680	46.250
100	0.20	0.0000162	2.250	18.350	30.770	49.400
60	0.42	0.00000233	0.047	47.300	121.000	254.200
60	0.26	0.00000111	34.600	236.280	398.200	675.480
40	0.31	0.000000589	31.080	329.880	639.480	1211.880
40	0.25	0.000000581	74.200	448.600	783.700	1316.700
20	-	-	866.200	-	-	-

Creep Test Data of ACuZinc10 at 70°C.

Stress (MPa)	Primary Creep %	Secondary Creep Rate (1/s)	Time to 0.2% Creep Strain (ks)	Time to 0.5% Creep Strain (ks)	Time to 0.7% Creep Strain (ks)	Time to 1.0% Creep Strain (s)
100	0.27	0.000000944	36.400	257.800	455.800	783.400

Creep Test Data of ILZRO.16 at 160°C.

Stress (MPa)	Primary Creep %	Secondary Creep Rate (1/s)	Time to 0.2% Creep Strain (ks)	Time to 0.5% Creep Strain (ks)	Time to 0.7% Creep Strain (ks)	Time to 1.0% Creep Strain (s)
100	0.83	0.0000857	-	0.010	0.150	1.860

Creep Test Data of ILZRO.16 at 130°C.

Stress (MPa)	Primary Creep %	Secondary Creep Rate (1/s)	Time to 0.2% Creep Strain (ks)	Time to 0.5% Creep Strain (ks)	Time to 0.7% Creep Strain (ks)	Time to 1.0% Creep Strain (s)
100	0.40	0.000000943	0.015	121.000	311.800	643.000

APPENDIX B

LOAD-RELAXATION TEST DATA OF THE ALLOYS No3, No5, No2, ACuZinc5, ACuZinc10 AND ILZRO.16

Load-Relaxation Data at 80°C.

Time (Mins.)	Alloy No3	ACuZinc5	Alloy No5	ACuZinc10	Alloy No2	ILZRO.16
0	-217	10	-223	-220	6	7
0.5	-210	11	140	-219	6	7
1	-219	11	125	-222	6	7
1.5	5741	11	117	3364	7	7
2	5835	10	6040	6107	5240	6
2.5	5749	6030	5954	6020	5914	4062
3	5694	5900	5910	5983	5861	5974
3.5	5653	5855	5881	5959	5828	5910
4	5619	5826	5859	5941	5804	5882
4.5	5592	5805	5842	5926	5786	5864
5	5568	5788	5826	5913	5770	5852
5.5	5548	5773	5813	5902	5757	5842
6	5529	5760	5801	5892	5745	5833
6.5	5513	5749	5790	5883	5734	5827
7	5497	5738	5780	5875	5725	5821
7.5	5483	5728	5771	5867	5715	5816
8	5470	5719	5763	5860	5707	5811
8.5	5457	5711	5755	5854	5699	5807
9	5446	5703	5747	5847	5692	5802
9.5	5434	5695	5740	5841	5685	5797
10	5424	5688	5734	5836	5679	5795
11	5404	5676	5721	5825	5666	5789
12	5387	5664	5710	5816	5655	5784
13	5371	5653	5700	5808	5645	5779
14	5356	5643	5691	5799	5635	5774
15	5341	5633	5681	5792	5626	5770
16	5328	5624	5673	5784	5618	5765
17	5316	5615	5666	5777	5610	5762
18	5304	5606	5658	5771	5602	5758
19	5293	5598	5651	5764	5595	5756
20	5282	5592	5644	5758	5588	5752
25	5235	5558	5614	5732	5557	5740
30	5196	5529	5588	5709	5531	5729
35	5163	5503	5566	5689	5509	5719
40	5133	5481	5546	5671	5489	5711
45	5107	5461	5528	5655	5470	5704
50	5083	5442	5512	5640	5454	5697
55	5061	5424	5497	5626	5438	5692
60	5041	5407	5483	5614	5424	5686
65	5022	5392	5470	5601	5410	5681
70	5005	5378	5458	5590	5398	5676
100	4919	5303	5396	5534	5333	5653
130	4854	5243	5347	5489	5281	5636
160	4800	5192	5307	5451	5238	5622
190	4754	5148	5271	5418	5200	5609
220	4713	5109	5240	5388	5167	5599
250	4677	5073	5211	5362	5136	5590
280	4644	5040	5184	5338	5107	5582
310	4614	5010	5160	5315	5082	5574
340	4586	4982	5137	5294	5058	5567
370	4560	4956	5116	5274	5035	5561
430	4514	4908	5076	5237	4994	5549
490	4471	4867	5041	5204	4957	5539

550	4434	4828	5008	5174	4923	5530
610	4398	4793	4979	5146	4894	5522
670	4366	4760	4951	5120	4865	5514
730	4336	4731	4926	5095	4838	5507
790	4307	4703	4901	5072	4813	5501
850	4281	4676	4879	5050	4790	5495
910	4255	4651	4857	5029	4768	5489
970	4231	4628	4837	5009	4747	5484
1090	4187	4584	4799	4972	4708	5474
1210	4145	4544	4766	4937	4673	5464
1330	4108	4508	4734	4907	4640	5457
1450	4073	4475	4703	4877	4610	5449
1570	4040	4444	4676	4849	4581	5441
1690	4007	4415	4650	4822	4554	5435
1810	3977	4388	4625	4797	4529	5428
1930	3949	4362	4602	4774	4506	5422
2050	3922	4337	4581	4751	4484	5417
2170	3895	4314	4560	4730	4463	5411
2410	3847	4272	4521	4689	4424	5401
2650	3801	4233	4484	4652	4387	5392
2890	3759	4197	4451	4618	4353	5384
3130	3719	4163	4421	4585	4321	5376
3370	3681	4132	4391	4555	4292	5369
3610	3645	4102	4365	4526	4264	5362
3850	3611	4075	4339	4499	4238	5356
4090	3579	4049	4314	4473	4213	5350
4330	3549	4024	4291	4450	4189	5344
4570	3519	4000	4269	4426	4167	5339
4810	3490	3977	4247	4404	4145	5333
5050	3463	3955	4227	4382	4124	5328
5290	3436	3934	4207	4362	4104	5323
5530	3411	3913	4188	4342	4085	5318
5770	3386	3893	4171	4324	4067	5314
6010	3363	3874	4156	4305	4049	5309
6250	3340	3857	4139	4288	4032	5305
6490	3318	3838	4122	4271	4015	5301
6730	3295	3820	4106	4255	3999	5297
6970	3275	3801	4088	4237	3983	5292
7210	3255	3784	4072	4220	3967	5288
7450	3234	3769	4059	4206	3952	5285
7690	3214	3752	4044	4190	3938	5282
7930	3195	3737	4030	4176	3924	5278
8170	3178	3721	4015	4162	3910	5275
8410	3160	3705	4001	4149	3896	5271
8650	3142	3690	3988	4136	3883	5269
8890	3125	3677	3976	4124	3870	5266
9130	3107	3663	3964	4110	3857	5263
9370	3092	3648	3951	4098	3844	5260
9610	3075	3635	3939	4086	3832	5257
9850						

Load-Relaxation Data at 100°C.

Time (Mins.)	Alloy No3	Alloy No5	ACuZinc5	Alloy No2	ACuZinc10	ILZRO.16
0	-225	-149	-80	26	-202	29
0.5	-225	-148	-80	27	-199	32
1	-225	-149	-80	26	3804	31
1.5	2741	5392	-81	29	6064	6089
2	5866	5925	2426	4098	5989	5932
2.5	5734	5854	6259	5898	5941	5893
3	5659	5812	6180	5812	5905	5869
3.5	5603	5780	6134	5765	5876	5853
4	5560	5756	6100	5731	5850	5841
4.5	5524	5734	6075	5705	5828	5830
5	5493	5717	6053	5682	5808	5820
5.5	5466	5701	6034	5663	5790	5813
6	5442	5688	6017	5647	5774	5806
6.5	5420	5675	6002	5633	5758	5800
7	5399	5664	5988	5619	5743	5794
7.5	5381	5653	5974	5606	5730	5789
8	5363	5644	5963	5595	5718	5784
8.5	5347	5635	5952	5584	5705	5780
9	5332	5626	5941	5573	5693	5775
9.5	5318	5618	5931	5565	5682	5770
10	5305	5610	5922	5556	5671	5766
11	5279	5596	5904	5541	5651	5760
12	5256	5583	5886	5524	5632	5753
13	5235	5571	5872	5510	5615	5747
14	5215	5559	5858	5497	5598	5741
15	5197	5549	5844	5485	5582	5736
16	5179	5539	5832	5473	5568	5731
17	5162	5530	5819	5462	5554	5727
18	5147	5521	5808	5451	5540	5722
19	5132	5513	5798	5442	5527	5718
20	5118	5506	5788	5433	5514	5714
25	5055	5470	5742	5390	5458	5696
30	5003	5441	5704	5356	5411	5681
35	4958	5415	5669	5325	5368	5669
40	4918	5393	5639	5298	5330	5658
45	4882	5374	5611	5274	5297	5647
50	4850	5356	5586	5252	5265	5638
55	4820	5340	5564	5231	5235	5630
60	4792	5324	5542	5212	5208	5623
65	4767	5310	5522	5194	5183	5615
70	4743	5297	5503	5178	5159	5608
100	4622	5228	5408	5094	5038	5576
130	4529	5176	5332	5028	4944	5551
160	4452	5132	5269	4972	4866	5531
190	4387	5094	5214	4926	4799	5513
220	4330	5060	5166	4885	4739	5498
250	4281	5031	5123	4848	4687	5486
280	4234	5003	5082	4814	4639	5474
310	4192	4978	5046	4782	4596	5464
340	4152	4954	5011	4753	4555	5454
370	4115	4932	4980	4725	4516	5445
430	4049	4892	4920	4674	4447	5429
490	3990	4857	4869	4629	4386	5414

550	3937	4823	4821	4588	4330	5401
610	3888	4793	4777	4549	4280	5389
670	3843	4764	4736	4515	4233	5379
730	3801	4738	4697	4482	4190	5369
790	3763	4713	4661	4451	4151	5360
850	3726	4689	4626	4421	4113	5351
910	3692	4666	4593	4394	4079	5343
970	3659	4645	4562	4368	4046	5336
1090	3599	4603	4502	4318	3985	5322
1210	3542	4568	4447	4271	3930	5309
1330	3494	4533	4396	4231	3879	5296
1450	3445	4501	4348	4189	3834	5286
1570	3402	4471	4302	4153	3792	5276
1690	3363	4441	4259	4118	3751	5267
1810	3323	4413	4216	4084	3717	5259
1930	3286	4387	4177	4051	3681	5251
2050	3251	4362	4138	4020	3647	5243
2170	3218	4338	4101	3990	3615	5235
2410	3155	4293	4031	3933	3556	5222
2650	3097	4252	3966	3880	3501	5210
2890	3044	4213	3906	3830	3450	5198
3130	2997	4176	3850	3785	3404	5187
3370	2951	4141	3798	3741	3364	5178
3610	2907	4109	3751	3698	3323	5169
3850	2867	4077	3705	3658	3285	5159
4090	2826	4048	3662	3619	3248	5151
4330	2789	4021	3622	3583	3211	5142
4570	2757	3994	3584	3550	3179	5134
4810	2724	3969	3549	3516	3150	5128
5050	2692	3944	3516	3484	3119	5121
5290	2661	3919	3484	3453	3090	5114
5530	2632	3896	3454	3423	3062	5107
5770	2604	3874	3425	3395	3036	5102
6010	2577	3852	3397	3367	3010	5096
6250	2551	3830	3372	3341	2985	5090
6490	2526	3810	3347	3316	2962	5084
6730	2502	3790	3324	3292	2939	5079
6970	2479	3770	3301	3268	2918	5073
7210	2457	3753	3280	3244	2897	5069
7450	2436	3734	3259	3222	2878	5064
7690	2416	3716	3240	3200	2859	5059
7930	2395	3698	3221	3179	2841	5055
8170	2376	3682	3203	3159	2824	5050
8410	2354	3665	3185	3138	2808	5046
8650	2336	3650	3169	3119	2790	5041
8890	2320	3633	3152	3101	2775	5035
9130	2303	3617	3136	3082	2765	5032
9370	2286	3602	3121	3065	2751	5028
9610	2269	3588	3107	3047	2739	5025
9850						

Load-Relaxation Data at 120°C.

Time (Mins.)	Alloy No3	Alloy No5	Alloy No2	ACuZinc5	ACuZinc10	ILZRO.16
0	-186	-207	-91	49	-155	-68
0.5	-186	-207	-87	5803	-154	-68
1	-182	-207	-90	5887	-155	-68
1.5	5687	-207	-92	5791	-155	-68
2	5804	5560	5914	5728	5215	-69
2.5	5675	5818	5735	5681	6050	65
3	5588	5720	5657	5643	5983	5894
3.5	5521	5657	5605	5610	5942	5815
4	5467	5610	5566	5581	5911	5775
4.5	5424	5573	5535	5556	5884	5748
5	5385	5542	5506	5532	5863	5728
5.5	5351	5515	5483	5511	5842	5712
6	5321	5491	5462	5491	5826	5698
6.5	5293	5470	5442	5472	5811	5687
7	5267	5451	5425	5455	5796	5676
7.5	5242	5433	5406	5439	5783	5666
8	5221	5416	5392	5423	5771	5657
8.5	5200	5401	5377	5408	5758	5648
9	5180	5387	5363	5394	5748	5641
9.5	5161	5373	5350	5381	5738	5633
10	5144	5360	5338	5367	5727	5627
11	5111	5337	5315	5343	5709	5614
12	5080	5314	5294	5320	5691	5604
13	5053	5294	5275	5298	5676	5593
14	5026	5276	5256	5278	5660	5583
15	5002	5259	5238	5259	5646	5576
16	4979	5242	5223	5241	5633	5567
17	4958	5227	5208	5224	5620	5560
18	4937	5212	5192	5207	5608	5553
19	4918	5199	5178	5192	5596	5545
20	4899	5185	5165	5176	5585	5540
25	4817	5127	5106	5108	5536	5512
30	4748	5079	5056	5050	5494	5490
35	4688	5037	5012	4998	5457	5471
40	4635	5000	4973	4952	5424	5455
45	4587	4966	4937	4910	5394	5439
50	4543	4935	4905	4872	5367	5427
55	4503	4907	4876	4837	5342	5416
60	4467	4881	4848	4802	5318	5404
65	4432	4857	4822	4771	5295	5394
70	4399	4833	4797	4741	5274	5386
100	4234	4715	4673	4588	5167	5339
130	4104	4620	4574	4465	5081	5307
160	3995	4540	4491	4360	5011	5281
190	3902	4470	4420	4268	4948	5258
220	3818	4408	4357	4186	4891	5239
250	3745	4351	4300	4110	4842	5223
280	3677	4299	4247	4041	4796	5207
310	3614	4251	4199	3977	4753	5194
340	3557	4206	4154	3917	4713	5182
370	3503	4164	4112	3861	4676	5171
430	3406	4087	4035	3760	4607	5150
490	3319	4017	3966	3669	4544	5131

550	3240	3953	3902	3588	4487	5116
610	3168	3894	3843	3515	4436	5101
670	3102	3839	3789	3448	4386	5088
730	3041	3787	3738	3387	4340	5076
790	2985	3739	3690	3331	4297	5064
850	2932	3694	3644	3280	4255	5054
910	2883	3651	3602	3231	4216	5042
970	2836	3609	3561	3186	4179	5033
1090	2751	3531	3484	3103	4109	5015
1210	2674	3461	3416	3030	4045	4999
1330	2605	3395	3353	2963	3984	4984
1450	2540	3334	3294	2903	3929	4972
1570	2482	3278	3238	2848	3876	4959
1690	2429	3224	3186	2797	3826	4948
1810	2379	3173	3139	2751	3778	4936
1930	2332	3124	3093	2708	3734	4927
2050	2289	3078	3050	2668	3693	4917
2170	2248	3034	3009	2631	3654	4907
2410	2172	2952	2934	2565	3582	4891
2650	2105	2877	2865	2506	3518	4874
2890	2045	2808	2801	2454	3458	4859
3130	1991	2745	2745	2409	3405	4847
3370	1941	2686	2692	2367	3356	4834
3610	1894	2631	2643	2329	3310	4821
3850	1856	2579	2597	2295	3269	4811
4090	1814	2530	2555	2263	3232	4799
4330	1777	2485	2517	2234	3196	4790
4570	1743	2444	2482	2207	3162	4781
4810	1711	2403	2450	2181	3130	4771
5050	1681	2364	2419	2158	3101	4763
5290	1654	2328	2390	2136	3073	4756
5530	1627	2293	2364	2115	3046	4748
5770	1603	2259	2339	2095	3022	4740
6010	1580	2227	2315	2077	2998	4733
6250	1558	2197	2293	2060	2975	4726
6490	1540	2168	2272	2043	2954	4720
6730	1518	2140	2252	2028	2933	4713
6970	1499	2113	2232	2013	2913	4707
7210	1481	2087	2215	1999	2895	4700
7450	1464	2062	2198	1985	2876	4693
7690	1448	2039	2183	1972	2859	4688
7930	1432	2016	2168	1960	2841	4682
8170	1416	1993	2153	1948	2825	4678
8410	1402	1972	2139	1937	2809	4671
8650	1389	1951	2126	1925	2795	4665
8890	1377	1932	2113	1915	2780	4660
9130	1364	1913	2101	1905	2765	4656
9370	1352	1894	2090	1895	2751	4650
9610	1339	1875	2078	1885	2738	4646
9850						